Engineering of particles for inhalation

Pitchayajittipong, Chonladda

Award date:
2008

Awarding institution:
University of Bath

Engineering of Particles for Inhalation

Chonladda Pitchayajittipong

A thesis submitted for the degree of Doctor of Philosophy

University of Bath

Department of Pharmacy and Pharmacology

December 2008

แด่ คุณพ่อและคุณแม่

To my father & mother

Acknowledgements

I have greatly enjoyed the past four years here at Bath and I would like to express thanks to all the people who have contributed in some way to this thesis.

Firstly, I am deeply indebted to Professor Robert Price, my supervisor, for his support, enthusiasm and inspiration. Furthermore, I would like to thank Dr Jag Shur for his support, advice and proof-reading. Thanks to all of my friends in the Pharmaceutical Surface Science Research Group: Amandeep, Harsh, Richard, Haggis, Ana and Andrea. Thanks to Rod, Steven, Kevin, Jo, Don, and Ade for keeping equipment and computers running. I also acknowledge my English teacher, Jane, who guides me about academic writing.

A special thank to the Thai Government Scholarship for supporting me all financial affairs since I have started my PhD study in the United Kingdom. I would gratefully thank to all of my colleagues at Pharmacy department from my work place, Ubonratchathani University, to give me a chance for enlarging my knowledge and experiences.

Thanks to all teachers, friends from schools, Khon Kean University and Chulalongkorn University which were all academic institutes that I had studied. I would like to thank all people who supported me to have a first great experience at Otago University, New Zealand, for three month project during my final year of bachelor degree. A special thank to all my friends in Thailand especially for Areerat, Keeratiporn, Siranee, Paichittee, Suwattiya, and Nitinan, in UK particularly for Supaporn, or wherever they might be at the moment.

Finally, and most importantly, I would like to show gratitude to my parents, my two brothers and two sisters for being with me all the time in my life. I would like to add my special thanks to my sister, Jinladda, for encouraging me to come to study abroad and advising me to have all excellent experiences in my life. Without you all in my family, the following pages would have never been written. Thanks for your never-ending love and support.

Scientific Publications

Pitchayajittipong, C., Shur, J., and Price, R. *De novo* engineering of crystalline combination inhalation particles of a long-acting β_2-agonist and corticosteroid. Pharmaceutical Research, (Submitted 2008).

Pitchayajittipong, C., Shur, J., Kaerger, J.S., Price, R. Effect of processing of active pharmaceutical ingredients on the performance of dry powder inhalers. Pharmaceutical Research (Submitted 2008).

Pitchayajittipong, C., Shur, J., Kaerger, J.S., Price, R. Characterisation and functionality of anhydrous inhalation lactose. Journal of Pharmaceutical Sciences (Submitted 2008).

Pitchayajittipong, C., Shur, J., and Price, R. Engineering of large hollow porous for inhaled drug delivery. Journal of Pharmaceutical Sciences (Submitted 2008).

Pitchayajittipong, C., Shur, J., Kaerger, J.S., Price, R. Quantification of force balance of combination dry powder inhaler formulations using atomic force microscopy. Journal of Pharmaceutical Sciences (Submitted, 2008).

Abstract

Current pharmaceutical engineering for the manufacture of binary and combined dry powder inhaler (DPI) dosage forms relies on destructive strategies such as micronisation to generate respirable drug particles. Such processes are inefficient and difficult to control to produce particles of defined quality and functionality for inhaled drug delivery, which can affect drug product performance throughout the shelf-life of the product. Furthermore, owing to current pharmaceutical manufacturing practises of combined inhalation products, these products are subject to greater variability in dose delivery of each active, which may be perpetuated as a function of product storage conditions and limit clinical efficacy of the drug product. Hence, there is a requirement of processes that may enable production of binary and combination DPI products that will allow actives to be delivered more efficiently and independently of dose variations. The aim, therefore, of this study was to develop the solution atomisation and crystallisation by sonication (SAX) process for engineering of single and combination drug particles with suitable physicochemical properties for delivery to the lungs.

The SAX process consists of key stages, which include, solution atomisation to produce aerosol droplets, generation of highly supersaturated droplets by evaporation of carrier solvent from aerosol droplet, collection of droplets in a crystallisation vessel containing appropriate non-solvent and the application of ultrasonic waves to the crystallisation vessel. Atomisation of a 1.5% w/v solution of budesonide in dichloromethane resulted in particles with defined surface geometry, which were formulated in binary dry powder inhaler (DPI) formulations and assessed using the next generation impactor. The percentage fine particle fraction (%FPF) of the SAX budesonide particles was significantly ($p<0.05$) greater than micronised budesonide, which was related to smaller contact area of the SAX particles that result in lower adhesion and therefore, greater fine drug particle aerosolisation. In contrast, atomisation of a 3% w/v solution of budesonide resulted in hollow/porous particles of budesonide that possessed a volume median diameter of 10 µm, which owing to their lower density behaved aerodynamically as micronised budesonide particles.

Crystalline particles containing both fluticasone propionate (FP) and salmeterol xinafoate (SX) were prepared upon atomisation of a solution consisting of FP and SX. FP and SX were dissolved in an appropriate solvent with a 10:1 ratio. Particle size analysis of SAX FP/SX suggested a monomodal particle size distribution presenting a

median equivalent volume diameter of 4.68 ± 0.01 µm. Chemical analysis of the SAX processed FP/SX showed that both materials were present in the correct ratio. The %FPF of micronised FP/SX formulation was 7.88 ± 0.46 % for FP and 6.70 ± 0.53 % for SX. In comparison, the formulation of SAX processed FP/SX particles showed significantly ($p<0.05$) greater %FPF of FP (10.68 ± 0.32 %) and SX (11.96 ± 1.09 %). Stage-by-stage analysis suggested that the SAX-processed FP/SX formulations were deposited on stages 2–5 consistently in the correct ratio, whereas the micronised FP/SX formulation resulted in greater FP deposition than SX into the lower stages of the NGI on aerosolisation. Following storage at 25˚C/75% RH and 40˚C/75 % RH for four weeks, the %FPF of FP and SX from combination formulations of micronised FP/SX had significantly ($p<0.05$) decreased, whereas the %FPF of either active from SAX FP/SX formulations showed no significant change.

In addition, crystalline particles containing both budesonide (Bud) and formoterol fumarate dihydrate (FFD) were prepared upon atomisation of a solution consisting of Bud and FFD. Both drugs were dissolved in an appropriate solvent in the ratio 36:1 of Bud:FFD. The %FPF of Bud and FFD from SAX-produced Bud/FFD formulation was significantly ($p<0.05$) greater than micronised Bud/FFD formulation. The combination particles of Bud/FFD engineered from SAX process were successfully deposited consistently on to the lower stages of NGI in comparison with combined micronised particles. However, following storage of the formulations at 25˚C/75% RH and 40˚C/75% RH for four weeks, the %FPF of Bud from combination formulations of micronised and SAX Bud/FFD had significantly ($p<0.05$) decreased, whereas the %FPF of FFD from micronised Bud/FFD formulations showed no significant change. In contrast, the %FPF of FFD following aerosolisation of the SAX Bud/FFD formulation after storage decreased significantly ($p<0.05$). This may be related to the fact that performance of both actives in the SAX preparation are affected by one another, therefore, changes in one active may affect the delivery of the other after storage.

In conclusion, these data demonstrate that the SAX process has been successfully deployed for the fabrication of particles with desired physicochemical properties for pulmonary drug delivery. Furthermore, the SAX process may be utilised to produce individual particulates of two active ingredients, which will allow the delivery of combination medicaments effectively and independently of dose variation. This approach presents itself as novel means to produce inhaled combination dosage forms.

Contents

List of Abbreviations

a^*	Absorption coefficient
a	Polarisability
A^*	Amplitude of the wave
$\overset{\circ}{A}$	Angstrom
ACI	Andersen cascade impactor
API	Active pharmaceutical ingredient
A_s	Area produced by the separation of two surfaces
ASES	Aerosol solvent extraction system
Bud	Budesonide
c	Actual concentration
c^*	Equilibrium saturated concentration
$^{\circ}$C	Degree centigrade
C_{50}	Impactor stage cut-off diameter
C_{ae}	Cunningham slip correction factor
c_{solute}	Concentration of solute
cAMP	Cyclic adenosine monophosphate
CFC	Chlorofluorocarbon
cm	Centimetre
CO_2	Carbon dioxide
COPD	Chronic obstructive pulmonary disease
CV	Coefficient of variation
d	Particle diameter
d_{10}	Cumulative diameter that accounts for 10% of all volume
d_{50}	Cumulative diameter that accounts for 50% of all volume
d_{90}	Cumulative diameter that accounts for 90% of all volume
dm/dt	Change in mass to time ratio
d_p	Distance between the planes of the crystal
DPI	Dry powder inhaler
DSC	Differential scanning calorimetry
DVS	Dynamic vapour sorption

D & C	Device and capsules
ED	Emitted dose
f	Frequency of the wave
F	Vibration frequency
F_c	Capillary force
F_{EL}	Electrostatic force
FFD	Formoterol fumarate dihydrate
FP	Fluticasone propionate
FPF_{ED}	Fine particle fraction of emitted dose
FPD	Fine particle dose
F_{VDW}	van der Waals forces
F_w	Force of attraction
g	Gram
g	acceleration due to gravity
GAS	Gaseous anti-solvent
h	Planck's constant
H	Hamaker constant
HFA	Hydrofluoroalkane
HPLC	High performance liquid chromatography
HPMC	Hydroxypropyl methylcellulose
I	Intensity of the wave
I_0	Intensity at the source
ICS	Inhaled corticosteroid
J	Rate of nucleation
k	Boltzmann constant
kHz	Kilohertz
kV	Kilovolt
l	Pre-set distance
L	Litre
LABA	Long-acting B_2-agonist
m	Metre
mA	Milliampere
m_{drug}	Mass of drug
mg	Milligram

min	Minute
ml	Millilitre
mm	Millimetre
mM	Millimolar
MMAD	Mass Median Aerodynamic Diameter
mmHg	Milimetres of mercury
mN	Millinewton
MOC	Micro orifice collector
MP & T	Mouthpiece and throat
MSLI	Multi-stage Liquid Impinger
n	The order of reflection
n_n	Number of circular nozzles
NGI	Next Generation Impactor
nm	Nanometre
P_a	Acoustic pressure
PBC	Periodic bond chain
P_c	Critical pressure
PCA	Precipitation by compressed anti-solvent
P_h	Ambient hydrostatic pressure
PGSS	Precipitation from gas saturated solution
pMDI	Pressurised metered dose inhaler
PS	Pre-separator
q	Electrical charge
Q	Volumetric air flow rate
r	Radius
r_{crit}	Critical radius
R	Airway radius
R^2	Coefficient of determination
RESS	Rapid expansion of supercritical solution
RH	Relative humidity
rpm	Rotations per minute
s	Separation distance
S	Supersaturation ratio
S	Stage

SABA	Short-acting B_2-agonist
SAX	Solution atomisation and crystallisation by sonication
SC CO_2	Supercritical carbondioxide
SD	Standard deviation
SEDS	Solution enhanced dispersion by SCF
SEM	Scanning electron microscopy
Stk	Stokes' number
SX	Salmeterol xinafoate
SCF	Supercritical fluid
St_{50}	Stoke number that gives a 50% change of particle deposition
t	Time
T_c	Critical temperature
T_g	Glass transition temperature
v	Number of atoms per unit volume of a particle
V	Air velocity
V_m	Molecular volume
V_p	Particle volume
V_s	Velocity of sound in the liquid
V_t	Terminal velocity
W	Watts
W_a	Work of adhesion
W_c	Work of cohesion
W_n	Nozzle diameter
$\bar{x}$	Mean
XRPD	X-ray powder diffraction
α	Alpha form
α	Contact angles between sphere and water
β	Beta form
β	Contact angles between a surface and water
γ	Surface tension
γ_L	Surface tension of water
γ^x	Surface free energy of material x

γ^{xy}	Interfacial free energy of the contacting surfaces
Δc	Concentration driving force
ΔG	Gibbs free energy
ΔG_s	Surface excess free energy
ΔG_v	Volume excess free energy
ΔU	Potential difference arising from the difference in work functions
ε	Permittivity
η	Air viscosity
θ	Angle
λ	Wavelength
$\lambda_{1,2}^{d}$	The constant of dispersion
µg	Microgram
µl	Microlitre
µm	Micrometre
π	Pi
ρ_a	Density of air
ρ_f	Density of the fluid
ρ_p	Particle density
σ	Relative supersaturation
% v/v	Percentage volume per volume
% w/v	Percentage weight per volume
% w/w	Percentage weight per weight

Chapter 1: Introduction

1.1 Respiratory Medicine

1.1.1 Structure of the Human Respiratory Tract

The human respiratory tract starts from the nose and ends in the peripheral regions of the lung at the respiratory bronchioles and alveoli (Gurney, 1991). The respiratory tract comprises a series of bifurcating airways (Figure 1.1). The trachea, which is connected to the oral and nasal cavities by the oropharynx, divides into right and left main bronchi, which in turn bifurcate into narrower and shorter bronchi and bronchioles. The dichotomous branching of the airways from the bronchi to the bronchioles undergoes over 32 bifurcations (Gurney, 1991). The trachea, bronchi and bronchioles are all together known as the conducting airways, and their major function is to lead inspired air to the gas exchanging regions of the lung. The respiratory bronchioles and alveoli are the site of gas exchange, where the whole of the cardiac output supplies capillaries in the peripheral regions of the lungs via the pulmonary artery. The entire respiratory tract is lined with a continuous sheet of epithelial cells, which vary in type and function throughout the tracheobronchial tree (Jeffery, 1997). The main role of the epithelial cells is to separate the external environment from the internal environment of the sub-epithelial airway structures. This is achieved by mucus secretion and by the specialised tight junctions between the epithelial cells that limit the penetration of inhaled substances through intercellular channels into the sub-epithelial areas (Knowles and Boucher, 2002).

In addition to being a portal for the exchange of oxygen and carbon dioxide between inhaled and exhaled air, the lungs have evolved to protect the peripheral regions from deposition of airbone particles through a number of different mechanisms (Lippmann, Yeates et al., 1980). With the movement of large volumes of air via the lungs, the respiratory tract is unavoidably exposed to a large amount of airborne particles. The human lung effectively filters over a billion particles each and every day (Lippmann, Yeates et al., 1980). These airborne particles include and are not limited to pollen grains, fungal spores, viruses, bacteria, diesel particulates and pet dander (Bascom, Bromberg et al., 1996). The efficient protection against particulate material is as a

result of the physical structure of the lung, and the internal surface coating of the bronchi and bronchioles with mucus as well as beating cilia hairs, which constantly expel entrapped particles from the respiratory tract (Gurney, 1991; Boucher, 1994).

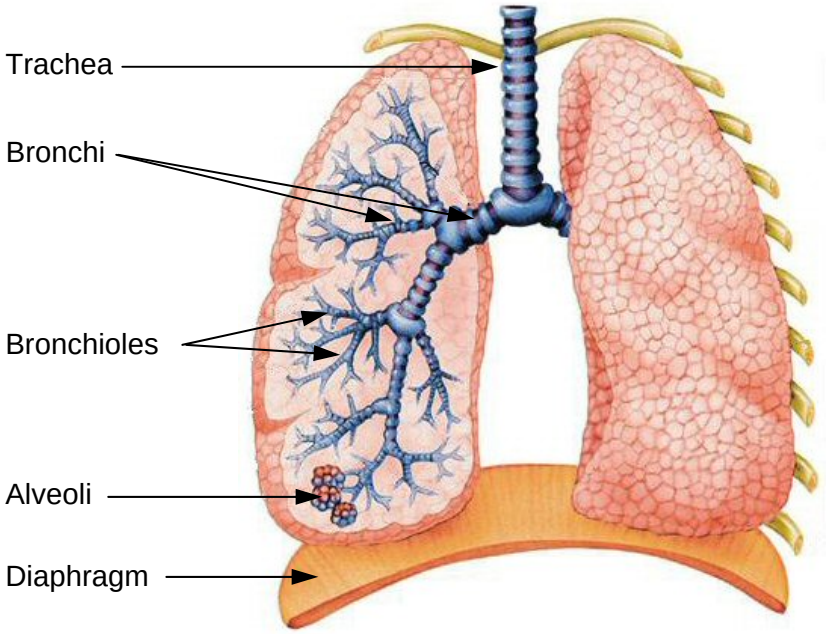

Figure 1.1: Structure of the human respiratory tract adapted from http://www.oup.co.uk/oxed/children/oise/pictures/humans/lungs/

1.1.2 Asthma and Chronic Obstructive Pulmonary Disease (COPD)

Asthma and chronic obstructive pulmonary disease (COPD) are both common diseases, and their incidence is increasing globally, placing an increasing burden on health services in industrialised and developing countries (Mannino and Buist, 2007; Barnes, 2007; Pearce, it-Khaled et al., 2007). Such diseases are characterised by airway obstruction, which is variable and reversible in asthma but is progressive and largely irreversible in COPD (Barnes, Chung et al., 1998; Barnes, Shapiro et al., 2003). Furthermore, both diseases are characterised by chronic inflammation of the respiratory tract, which is mediated by increasing expression of multiple inflammatory proteins, enzymes and receptors (Barnes, 2008). As the intensity of the inflammation increases in both diseases, there are exacerbations (Barnes, 2008).

1.1.2.1 Asthma

A series of factors combines to produce increasing airway inflammation and airway hyper-responsiveness and, when these features reach a sufficient level, bronchoconstriction and asthma symptoms are triggered (Holgate, Davies et al., 2007). Typically, the inhalation of an allergen in an asthmatic can result in an episode of asthma. Asthmatics have high levels of the antibody immunoglobulin E (IgE), which binds to receptors on inflammatory cells, most notably mast cells (Holgate, 2008). The interaction of the inhaled allergen and IgE results in the activation of mast cells, releasing pre-formed mediators such as histamine, prostaglandins and leukotrienes, which cause the smooth muscle of the airways to contract, thereby producing bronchoconstriction (Holgate, 2007).

The inflammatory response in asthma is highly complex involving inflammatory cells such as mast cells, eosinophils, B-lymphocytes, and T-lymphocytes (Holgate, 2008). These inflammatory mediators regulate the response of other mediators and have a number of effects resulting in contraction of airway smooth muscle, increase of vascular permeability and stimulation of airway mucus secretion (Holgate, 2008). Hence, the wall of the airway in asthma is thickened by edema, and cellular infiltration, thereby increasing smooth muscle mass and glands. With increasing severity of the disease, remodelling of the airways leads to fibrosis of the airway wall, fixed narrowing of the airway and reduced response to therapy (Holgate and Polosao, 2008).

1.1.2.2 Chronic Obstructive Pulmonary Disease (COPD)

The global initiative on obstructive lung disease (GOLD) defines COPD as a disease state characterised by airflow limitation that is not fully reversible. The airflow limitation is usually progressive and this limitation is associated with an abnormal inflammatory response of the lungs to noxious particles and gases (Pauwels, Buist et al., 2001). This definition encompasses the idea that COPD is a chronic inflammatory disease, which is characterised by acceleration in the normal decline of lung function seen with age (Pauwels and Rabe, 2004). Amongst other inflammatory mediators, the key inflammatory cells that play a pivotal role in COPD include neutrophils, macrophages, B-lymphocytes and T-lymphocytes.

In developed countries, cigarette smoking is by far the commonest cause of COPD accounting for >95% of cases, but there are several other risk factors, including air pollution, poor diet and occupational exposure (Barnes, Shapiro et al., 2003). Cigarette smoke extract can activate macrophages, which secrete many inflammatory proteins that orchestrate the inflammatory response in COPD (Barnes, Shapiro et al., 2003). Inflammatory mediators attract inflammatory cells such as neutrophils, which secrete proteases that contribute to alveolar destruction and mucus hyper-secretion (Barnes, Shapiro et al., 2003). Furthermore, macrophages generate reactive oxygen species and nitric oxide, which together with peroxynitrate may contribute to steroid therapy resistance in COPD (Barnes, 2004).

COPD includes chronic obstructive bronchiolitis with fibrosis, obstruction of the small airways, emphysema with enlargement of airspaces, destruction of lung parenchyma, loss of elasticity, and closure of small airways (Barnes, Shapiro et al., 2003). All of these features are induced by smoking. The slowly progressive airflow limitations in COPD eventually lead to disability and premature death.

1.1.2.3 Differences between Asthma and COPD

Although there are some overlaps in the features of asthma and COPD, they are separate disorders with different aetiologies, pathologies, natural history and responses to treatment (Barnes, 2008). In asthma, airway inflammation and hyper-reactivity are the key factors giving rise to bronchial muscle contraction and airway obstruction. In COPD, structural changes arising from alveolar destruction by emphysema result in a loss of elastic recoil and collapse of small airways on expiration contributing to airway obstruction.

There are marked differences in the pattern of inflammation that occurs in asthma and COPD (Barnes, Shapiro et al., 2003). The inflammatory cells recruited and mediators released in both disease conditions are different, which poses distinct consequences of inflammation and differing response to therapy (Barnes, 2008). The inflammation observed in asthma is mainly located in the larger conducting airways, and small airways can also be affected in more severe forms of the disease. In contrast, inflammation in COPD is located in the peripheral regions of the lung and small airways (Tiddens, 2004). These differences in disease may partly reflect the distribution of inhaled agents such as allergens in asthma and tobacco smoke in COPD.

1.1.3 Treatment of Asthma and COPD

Asthma and COPD are both characterised by airflow limitation and chronic inflammation. Hence, the most effective treatment for reducing airway constriction and inflammation is to deploy medicaments that target these aspects of the disease pathophysiology. The first-line treatments in both asthma and COPD are bronchodilators (short and long acting β_2-agonists) and anti-inflammatory therapy (inhaled corticosteroids), which are employed to aid bronchodilation and reduce inflammation, respectively (Greening, Ind et al., 1994; Matz, Emmett et al., 2001).

1.1.3.1 Bronchodilators

Bronchodilator drugs (relievers) are used to relieve symptoms of bronchoconstriction (Barnes, 2002). These drug agents are typically β_2-agonists, which stimulate β-adrenoceptors in the smooth muscle of the airway, producing smooth-muscle relaxation and bronchodilatation (Holgate and Polosao, 2008). The short-acting β_2-agonists (SABA) include salbutamol and terbutaline, which have a duration of action of 3-4 hours with an onset of action of 15 minutes (Biddiscombe, Melchor et al., 1987). In contrast, the long-acting β_2-agonists, including salmeterol xinafoate (SX) and formoterol fumarate dihydrate (FFD), have a duration of action of more than 12 hours and are helpful in controlling chronic asthma (Cazzola, Testi et al., 2002).

Other agents that are able to induce bronchodilation in asthma and COPD include anti-cholinergic agents, which produce bronchodilation by blocking the bronchoconstrictor effect of vagal nerve stimulation on bronchial smooth muscle (Barnes, Shapiro et al., 2003). The short-acting anti-cholinergic agents such as ipratropium bromide take about 1 hour to reach their maximum effect and have a duration of action of about 4-6 hours (Pauwels, Buist et al., 2001). However, longer acting anti-cholinergic agents are in development. Tiotropium is a long-acting anti-cholinergic drug which has greater affinity and a slower rate of dissolution from muscarinic receptors than iprotropium with a once daily dosage regimen (Cazzola, Ando et al., 2007).

Theophylline is also capable of bronchodilation. Theophyllines increase cyclic adenosine monophosphate (cAMP) stimulation of β_2-adrenoceptors by inhibiting the metabolism of cAMP by the enzyme phosphodiesterase (Cazzola, Ando et al., 2007).

However, the high incidence of side-effects has been prohibitive to its use in mainstream therapy.

1.1.3.2 Anti-Inflammatory Drugs

Inhaled corticosteroids (ICS), such as budesonide (Bud), fluticasone propionate (FP) and mometasone furoate, are the mainstay of asthma and COPD treatment. They reduce airway inflammation which is the underlying pathophysiological process in both diseases (Barnes, 2002). ICS therapy responsiveness is usually high in asthma. Corticosteroids suppress inflammation by inducing the recruitment of nuclear enzyme histone deacetylase 2 (HDAC2), which suppresses the expression of genes of various inflammatory mediators (Barnes, 2004). By contrast, patients with COPD respond poorly to ICS therapy, which fails to suppress inflammation (Barnes, 2008). This has been reported to be related to the decrease of activity and expression of HDAC2 in the inflammatory cells and peripheral lungs of COPD patients (Barnes, 2008). However, low concentrations of theophylline have been able to restore HDAC2 activity *in vitro* and reverse corticosteroid resistance in COPD (Barnes, 2008).

1.1.3.3 Combination Inhalation Therapy

It has been demonstrated that addition of a long-acting β_2-agonist (LABA) to an ICS is superior to ICS alone in achieving asthma control (Matz, Emmett et al., 2001). Data have shown that when FP and SX are combined, there is an increased clinical benefit if compared to the individual drug components used separately (Nelson, Chapman et al., 2003). For patients with more severe COPD, the study has suggested that using a combination of Bud and FFD improves the overall exacerbation rate when compared with β_2-agonist alone (Campbell and Szafranski, 2002). In addition, a 3-year retrospective study of COPD patients managed in primary care concluded that regular use of FP in combination with SX is associated with significantly greater survival of COPD patients (Calverley, Pauwels et al., 2003).

The explanation for the superior clinical effect of combination inhalation therapy over that of treatment with the individual medicaments has been related to complementary efficacy of both LABA and ICS when co-administered (Zetterstrom, Buhl et al., 2001). However, the superior clinical efficacy of combined inhalation therapy may also be due

to synergistic interactions of ICS (FP) and LABA (SX) at the receptor, molecular and cellular level (Nelson, Chapman et al., 2003).

Inhalers combining a LABA and an ICS are now available. One such combination is a combination of FP with SX in Advair®/Seretide® inhaler (GlaxoSmithKline, UK) and the other is Bud with FFD in Symbicort® (AstraZeneca, UK).

1.2 Pulmonary Drug Delivery

The use of the inhalant route allows easy accessibility to the respiratory tract as anti-asthma drugs and other medication can be administered directly to their site of action in the lungs (Byron and Patton, 1994). Therefore, this route of drug delivery has become the primary route of administration in the therapy of a number of respiratory disorders. Advantages of inhalation drug therapy include these facts: small amounts of drug are sufficient to prevent or treat symptoms; adverse reactions are usually much less than those produced by systemic administration; and there is rapid and predictable onset of action (Byron and Patton, 1994). The pulmonary epithelium provides an excellent absorptive surface for aerosolised compounds and may be more suitable for selected compounds than the gastrointestinal tract. In addition, the exceedingly large surface area (143 m^2) of the lungs and slow mucociliary clearance from the lung periphery render this a viable route of administration for systemically acting agents (Lalor and Hickey, 1996).

The target site of drug delivery systems for inhalation depends on the condition being treated. The respiratory bronchioles and alveoli would potentially be a target site of drug absorption for systemic circulation and can be targeted by formulations designed for the treatment of non-respiratory disease (Patton, 1996). Local respiratory diseases treated by inhalation therapy such as asthma and COPD are diseases that affect the conducting airways (Bryon and Patton, 1994), so therapeutic drugs for these conditions are targeted directly to the site of action within the lungs (Virchow, Crompton et al., 2008).

1.2.1 Particle Deposition in the Lungs

An inhaled drug particle must deposit at the site of action to have a pharmacological effect (Byron and Patton, 1994). How and where particles deposit in the lung is highly dependant on the aerodynamic particle size and three main deposition mechanisms: Inertial impaction, sedimentation and diffusion. Other deposition mechanisms include interception and electrostatic precipitation (Heyder, Gebhart et al., 1986; Lalor and Hickey, 1996). Deposition may occur by a number of these mechanisms, which are dependant upon a variety of variables (Martonen and Katz, 1993). These mechanisms are described below.

1.2.1.1 Inertial Impaction

The predominant mechanism of particle deposition in the lungs is inertial impaction and this mechanism occurs mainly in the upper and conducting airways (Asgharian and Anjilvel, 1994). As an inhaled airstream changes direction on passing through the repeated bifurcations and bends of the respiratory tract, a particle suspended in the airflow may not lose its inertia and relax into the new direction of the airflow, thereby impacting on the respiration surface (Martonen, Katz et al., 1992). Deposition by inertial impaction is highly dependant on the material density and size of the suspended particles. The probability of impaction for a particle travelling in an airway is related to its Stokes' number (Stk), a dimensionless parameter that can be calculated using Equation 1.1.

$$Stk = \frac{\rho_p d^2 V}{18\eta R} \qquad \text{Equation 1.1}$$

where ρ_p is the particle density, d is the particle diameter, V is the air velocity, η is the air viscosity and R is the airway radius. From this equation, the higher the value of Stokes' number, the more readily particles will deposit by inertial impaction (Morrison, 1974; Martonen and Katz, 1993; Crowder, Rosati et al., 2002).

1.2.1.2 Sedimentation

Sedimentation occurs as particles suspended in the respiratory tract settle under the influence of gravity (Clark and Egan, 1994). According to the particle size range

between 1 and 40 µm diameter in a laminar airstream, the terminal velocity (V_t) at which this settling occurs is described by the Stokes' law (Stokes, 1908).

$$V_t = \frac{(\rho_p - \rho_a)d^2 g}{18\eta} \qquad \text{Equation 1.2}$$

where ρ_p is the particle density, ρ_a is the density of air, d is the particle diameter, g is acceleration due to gravity and η is the air viscosity. Particles <1 µm tend to settle with a faster terminal velocity than that predicted by Equation 1.2, whilst particles >40 µm diameter tend to settle at a slower terminal velocity (Nowak, Kakade et al., 2003).

Sedimentation is a time dependant process as particles must have a sufficient residence time in the airway to settle from their initial position to deposit on the respiratory surface (Taulbee and Yu, 1975). It is, therefore, the dominant mechanism of deposition in the bronchioles due to the small airway dimensions and low air flow velocities found in these regions (Heyder, Gebhart et al., 1986; Tsuda, Butler et al., 1994b; Lalor and Hickey, 1996).

1.2.1.3 Brownian Motion

As the diameter of a suspended particle drops below 1 µm, the influence of gravity on its motion decreases, whereas the influence of Brownian motion caused by the random bombardment of the particle by gas molecules becomes ever greater (Mcmurry and Rader, 1985). Brownian motion results in particles following a random and variable path. For particles which are less than 0.5 µm, Brownian motion will cause greater deposition than sedimentation and may be the primary mechanism of deposition in the peripheral regions of the lung (Mcmurry and Rader, 1985; Tsuda, Butler et al., 1994a). Nevertheless, due to the relative magnitudes of displacement caused by sedimentation and Brownian motion, particles >2 µm diameter are more likely to deposit in the airways than those <0.5 µm diameter (Tsuda, Butler et al., 1994b).

1.2.1.4 Interception

Interception occurs when a particle moving within the airstream makes contact with the respiratory surface (Taulbee and Yu, 1975). Elongated particles are most likely to

deposit in this manner. However, as the typical size of drug particles used in respiratory drug delivery is much smaller than that of the airways, this mechanism of deposition is relatively unimportant in most cases (Martonen and Katz, 1993).

1.2.1.5 Electrostatic Precipitation

During aerosolisation, drug particles may become electrostatically charged (Yeomans, Rogers et al., 1949). In theory, charged particles may influence the deposition mechanism either through the induction of an image charge on the respiratory surface and subsequent electrostatic attraction or via the repulsion between like charged aerosol particles directing them towards the airway walls (Balashazy and Hofmann, 1993).

1.2.2 The Effect of Particle Size on Deposition in the Respiratory Tract

From Equations 1.1 and 1.2, it is clear that particle size is one of the major variables controlling particle deposition in the lung (Taulbee and Yu, 1975; Park and Lee, 2000). Inhalation formulations need to produce an aerosol cloud of appropriately sized drug particles to circumvent deposition prior to reaching their target site (Timsina, Martin et al., 1994; Virchow, Crompton et al., 2008). Even before a particle enters the trachea, it must negotiate a 90° bend between the oral cavity and pharynx without impacting on the back of the throat (Taulbee and Yu, 1975). At each bifurcation, the cross-sectional area of an individual airway decreases, providing an ever more convoluted path for a particle to negotiate without succumbing to deposition (Balashazy and Hofmann, 1993). Drug particles with aerodynamic diameters larger than 10 µm will tend to impact on the throat and upper airways (Taulbee and Yu, 1975), whereas particles with an aerodynamic diameter less than 0.5 µm will tend to be exhaled (Hofmann, Sturm et al., 2003). The majority of particles with aerodynamic diameters between 2.5 µm and 6 µm will deposit in the conducting airways, whilst particles with an aerodynamic diameter less than 2.5 µm will tend to deposit in the alveoli (Tsuda, Butler et al., 1994a; Tsuda, Butler et al., 1994b). It is accepted that the target drug aerosol aerodynamic particle diameter for an inhalation formulation is between 1 and 5 µm, depending on the desired target site (Heyder, Gebhart et al., 1986).

1.2.3 Respiratory Drug Delivery Systems

In essence, there are three main drug delivery systems employed to deliver therapeutics to the lungs: pressurised metered dose inhalers (pMDIs), dry powder inhalers (DPIs) and nebulisers (Hickey and Dunbar, 1997). All three systems are used to treat local conditions within the lung, for example, in asthma and COPD (Lalor and Hickey, 1996).

1.2.3.1 Nebulisers

Nebulisers are devices used to convert aqueous solutions or aqueous suspensions of drug into an aerosol (Clarke, 1995). Nebulisers apply either compressed gas or ultrasonic energy for the aerosolisation of the aqueous based solution, which is then inhaled by the patient (Dalby and Suman, 2003). Unlike other devices, they do not require the use of a complicated breathing movement, and, by extending the time of operation, they can be used to deliver large doses (de Boer, Hagedoorn et al., 2003). However, due to the prolonged amount of time required to deliver an adequate dose (typically 10 to 15 minutes) and the high running cost, nebulisers are typically limited to hospital and non-ambulatory patients (Garcia-Contreras and Hickey, 2003). Recent developments in nebuliser technology are beginning to overcome some of these problems, allowing accurate metering of doses and increasing their portability (Dalby, Spallek et al., 2004).

1.2.3.2 Pressurised Metered Dose Inhalers (pMDIs)

Since 1956, pressurised metered dose inhalers (pMDIs) have been the drug delivery system of choice for respiratory diseases because of a result of their cheap, robust and convenient characteristics (Hickey and Dunbar, 1997). Traditionally, these devices consist of a solution or suspension of fine drug particles in a chlorofluorocarbon (CFC) propellant sealed in a canister at high pressure (Biddiscombe, Melchor et al., 1987). The formulation may also contain formulation additives including surfactants and co-solvents (McDonald and Martin, 2000). The propellant is the main component of pMDI formulations and performs the role of solvent and dispersion medium for drug substance and other excipients (Young, Price et al., 2003a). Actuation of the inhaler results in the release of a metered volume of this solution or suspension, which is driven by the high vapour pressure within the canister, which in turn emerges at a high

velocity through a narrow orifice (Smyth, Hickey et al., 2006). This process, combined with evaporation of the propellant, results in an aerosol of drug particles in the respirable size range that are able to enter and deposit in the respiratory tract (Berry, Kline et al., 2003). Despite pMDIs being the most frequently prescribed inhalation dosage form, the fact remains that most patients cannot use them correctly (Virchow, Crompton et al., 2008). This is because the high speed aerosol plume generated by a pMDI requires the patient to use accurate co-ordination of inspiration and inhaler activation to ensure correct inhalation and deposition of the drug in the lung (Virchow, Crompton et al., 2008). Even with the correct inhalation technique, pMDIs are inefficient, often delivering less than 1/3 of the emitted dose to the lungs (Virchow, Crompton et al., 2008). In addition to these problems, the introduction of the Montreal Protocol results in the phase out of chlorofluorocarbon (CFC) propellant gas in all aerosol-based products, including pMDIs. As a result, all pharmaceutical CFC-based pMDI products were re-formulated using hydrofluoroalkanes (HFAs) propellant and replaced (Richards, Hirst et al., 2001). The difficulties and expense, incurred in re-formulating pMDI products and long term issues regarding the future of HFA-based propellants, have prevented companies to launch new drugs as pMDI formulations (McDonald and Martin, 2000).

1.2.3.3 Dry Powder Inhalers (DPIs)

Dry powder inhalers (DPIs) permit a metered dose of drug to be delivered to the airways as a dry powder aerosol (Timsina, Martin et al., 1994). A patent from 1950, by Mack R. Fields, described the first metered dose DPI for the delivery of medicaments to lungs (Fields, 1950). Later, DPIs had their application in inhalation therapy as a CFC-free alternative for the older pMDIs (McDonald and Martin, 2000). Currently, the spectrum of application of DPIs has become much broader, due to the high lung deposition that can be attained and their suitability for pulmonary delivery of therapeutic peptides and proteins both for local and systemic conditions (Byron and Patton, 1994).

DPIs are breath-actuated drug delivery systems, which enable a respirable cloud to be produced in response to the patient's inspiratory effort (Timsina, Martin et al., 1994). DPIs may therefore have many advantages over pMDIs (Hannemann, 1999; Newman and Busse, 2002; Virchow, Crompton et al., 2008). Firstly, DPIs do not need a propellant, which has been the driving force behind the introduction of a large number of novel DPI devices in recent years (Timsina, Martin et al., 1994). The second benefit

is that DPIs eliminate the need for patient co-ordination of actuation and inhalation (Newman and Busse, 2002). Finally, in DPIs, the particles are travelling at a slower rate, therefore, an excessive drug loss due to impaction in the throat is avoided (Pauwels, Newman et al., 1997).

Successful deposition of drug particles into the lung requires the delivery of particles with a mass median aerodynamic diameter (MMAD) less than 5 µm (Heyder, Gebhart et al., 1986; Timsina, Martin et al., 1994; Prime, Atkins et al., 1997). A control of particle size of medicaments to be delivered by DPIs is typically achieved through high-energy micronisation techniques (Thibert and Tawashi, 1999), although numerous other technologies, for example, spray drying (Li, Seville et al., 2005) and supercritical fluid technologies (Shekunov, Feeley et al., 2003) have been evaluated. However, respirable sized particles exhibit high surface energies, which lead to particle aggregation, poor flow and entrainment properties, and thereby make re-dispersion of the drug a difficult process (Feeley, York et al., 1998).

The most common method employed to solve the problems associated with cohesive respirable powder materials is to formulate the drug with an excipient, traditionally lactose monohydrate (Bell, Hartley et al., 1971). The micronised drug is blended with carrier particles of a much larger size range (usually 20-100 µm), whereby the drug particles form an interactive mixture with the surfaces of the coarse lactose particles (Ganderton, 1992). The turbulent airflow generated within the device upon forced inspiration should be sufficient to fluidise the formulation from the device and to de-aggregate the drug particles from the carrier particles (Telko and Hickey, 2005; Shur, Harris et al., 2008). The drug particles are then entrained into the airstream, which enables the drug particle to enter the lungs (Shur, Harris et al., 2008). The carrier particles are subsequently deposited in the oropharynx of the patient. Although high levels of turbulence are required to be engineered into the device for efficient deaggregation (Louey, Van Oort et al., 2006), there is a need to balance the resistance of the inhaler to airflow and in inhaling through the device at a flow rate which produces optimum drug delivery (Crowder and Hickey, 2006). One way to provide high levels of turbulence without imposing large increase in airflow resistance is the use and placement of grids of varying mesh sizes (Helgesson, Jennings et al., 2005; Telko and Hickey, 2005).

There are currently three types of DPIs available on the market. These include a single-dose, multidose and reservoir-based device (Prime, Atkins et al., 1997; Malcolmson and Embleton, 1998; Smith and Parry-Billings, 2003). Early DPI devices were all unit-dose systems and were dependent on loading and triggering procedures. The Spinhaler® and Rotahaler® are two early examples of DPI technologies. Both utilise pre-metered doses packed into hard gelatin capsules although different mechanisms of powder delivery and power technology are employed (Vidgren, Karkkainen et al., 1987).

Multidose pre-metered DPIs include the successful Diskhaler® and Diskus® devices from GlaxoSmithkline. The Diskhaler® employs individual doses contained within blisters (4 or 8 blisters) on a disk. On actuation, a needle pierces the upper and lower surfaces of a blister. As the patient inhales, the contents of the blister are dispersed into the airstream. The drug particles are dissociated from the carrier and a fraction delivered to the lung. On re-priming the device, the disk rotates to expose the next blister to the piercing needle (Prime, Atkins et al., 1997). The Accuhaler® DPI device produced by GSK retains the blister pack and unit-dose approach of the Diskhaler®, but has the advantage of holding additional doses. The pack consists of a coiled, double-foil strip of 60 blisters, each containing one dose of drug powder formulated with a lactose carrier (Malcolmson and Embleton, 1998).

Reservoir DPIs contain all the doses in a bulk reservoir, and each dose is dispensed from this reservoir by manipulation of the device prior to inhalation (Smith and Parry-Billings, 2003). The first device employing a multi-dose reservoir was the Turbuhaler (Newman, Moren et al., 1991). The dose is metered into conical cavities by rotating the base of the inhaler. The inhaled airstream dislodges the drug from the cavities and dispersion continues in the inhalation channels, which are helical to induce turbulent flow (Helgesson, Jennings et al., 2005). A desiccant is employed to ensure that the powder reservoir remains dry during the shelf life of the inhaler. Other examples of reservoir DPI device are the Easyhaler® (Ranbaxy, UK Ltd), Clickhaler® (Vectura plc, Chippenham, UK) and Pulvinal® (Chiesi Farmaceutici SpA, Parma, Italy).

Every DPI device exhibits an internal resistance which determines the inhaled flow rate that a patient can achieve when using the device (Harris, 2007). As flow rate will inevitably be linked with inhaler performance, it is essential that such factors are considered in any *in vitro* comparative testing of DPIs (Harris, 2007). Successful

development of DPI systems requires development on two integrated fronts: device engineering and powder formulation engineering (Timsina, Martin et al., 1994).

1.3 Pharmaceutical Engineering of DPI Drug Delivery Systems

The engineering of DPI formulations has relied on 'top-down' manufacturing methods, where large crystalline drug particles are milled (micronised) to produce fine particles with a median geometric diameter 1–5 μm (Telko and Hickey, 2005). These particles are then blended with large lactose monohydrate carrier particles to improve powder fluidisation (Dunbar, Morgan et al., 2000). Owing to the strong interparticulate cohesive and adhesive forces noted with fine drug particles and the large carrier particles, lung delivery efficiencies of just 10–30% of the nominal dose are typically observed (Dunbar, Morgan et al., 2000). Hence, the process of entrainment and deposition of actives in the airways is largely dependent on the balance of interfacial forces between components of DPI formulation (Jones, Harris et al., 2008). The control and understanding of the interfacial properties of DPI formulations are critical to enable the formation of DPI drug product with defined quality and functionality (Edge, Muller et al., 2008).

Whilst it is known that the surface properties of the drug will dramatically affect DPI product performance, the primary design concept in drug particle manufacturing for DPIs remains particle size with limited understanding of the effects of processing on drug surface properties. Hence, to control the specific performance and stability properties of DPI dosage forms, the central design principle in DPI manufacturing must focus on tailoring the mesoscopic design of particle interfaces to enable careful control of particle-particle interactions and, therefore, product performance.

Current micronisation practises, adopted to generate respirable-sized drug particles, provide little hope in controlling particle size, morphology and surface properties (Hickey, Mansour et al., 2007). Therefore, there is a requirement of particle processing technologies that enable the control of these properties of particles to enable the formation of designer particles for inhalation.

1.3.1 Interparticulate Forces

Particle interactions that occur as consequence of long-range attractive forces, with intermolecular binding energies less than 40 $kJ.mol^{-1}$, are much weaker than short-range interactions, such as ionic or covalent bonding (Johnson, 1996). These long-range forces can be classified as either cohesive, between particles of similar size and the same chemical structure, or adhesive, between particles of different materials (Johnson, Kendall et al., 1971; Tabor, 1976). Hence, a powder is said to be cohesive when the component particles tend to stick to one another; the interaction forces between these particles are termed 'cohesive forces'. Similarly, a particle is adhesive when it readily adheres to the surface of an object of larger dimensions; the interaction forces are then termed 'adhesive forces'. When gravitational forces acting upon these particles become negligible then either the cohesive or adhesive forces become dominant (Tabor, 1976), which occurs when the dimensions of the particulate materials become smaller than 10 µm (Deryaguin, Krotova et al., 1978). Respirable powders employed typically in DPI formulations fall into this category, and much work has been done to fully understand the cohesive and adhesive forces that exist in such systems (Cline and Dalby, 2002; Begat, Morton et al., 2004).

The interactions between particles may be a result of a number of concurrently acting forces or mechanisms such as van der Waals, electrostatic, capillary forces and solid bridging (McFarlane and Tabor, 1950; Johnson, Kendall et al., 1971). Since pharmaceutical solids are often insulators, particles are likely to retain a charge during the powder handling process (Staniforth and Rees, 1982). Charged particles will exert electrostatic forces on adjacent particles. However, uncharged particles also interact with each other due to dispersion forces (van der Waals forces) (Castellanos, 2005).

When condensation occurs on solid-solid interfaces, particulate interactions due to capillary forces arise. These forces, resulting from the surface tension of the adsorbed liquid layer, may dominate over other forces if sufficient liquid is condensed on the solid-solid interface (McFarlane and Tabor, 1950; Price, Young et al., 2002).

1.3.1.1 van der Waals Forces

The omnipresent van der Waals forces are the major force of interaction between uncharged particles in a dry environment (Lifshitz, 1955). The van der Waals forces are

the summation of the attractive forces which arise due to the formation of temporary dipole moments between molecules as a result of random fluctuations in their surrounding electron cloud (Lifshitz, 1955).

The van der Waals forces (F_{VDW}) between two ideally smooth spheres in a vacuum can be described by Hamaker (Hamaker, 1937) :

$$F_{VDW} = \frac{H}{12s^2}\left(\frac{d_1 d_2}{d_1 + d_2}\right) \qquad \text{Equation 1.3}$$

where H is the Hamaker constant (Equation 1.4), s is the separation distance between the spheres and d_1 and d_2 are the diameters of the two spheres. The Hamaker constant is given by:

$$H = \pi^2 v_1 v_2 \lambda_{1,2}^d \qquad \text{Equation 1.4}$$

where v_1 and v_2 are the number of atoms per unit volumes of particle 1 and 2 and $\lambda_{1,2}^d$ is the constant of dispersion:

$$\lambda_{1,2}^d = -\frac{3}{4} hFa^2 \qquad \text{Equation 1.5}$$

where h is Planok's constant, F is the vibration frequency of the interacting electronic oscillators and a is the polarisability of the molecules.

The adhesive force between a sphere (diameter d_1) and a plane composed of the same material and separated by distance s is described by:

$$F_{VDW} = \frac{H_{11} d_1}{6s^2} \qquad \text{Equation 1.6}$$

whereas the adhesion between a sphere (diameter d_1) and a plane composed of different materials and separated by distance s is expressed by:

$$F_{VDW} = \frac{\sqrt{H_{11} H_{22}}}{6s^2} d_1 \qquad \text{Equation 1.7}$$

where H_{11} and H_{22} are the Hamaker constant for the particle and the plane surface, respectively.

Equations 1.3, 1.6 and 1.7 demonstrate the importance of the separation distance, s, in determining the van der Waals forces between two solid objects. It is clear that these will retard rapidly with increasing separation distance, so it is not surprising that van der Waals forces exert their influence only over a narrow range of approximately 10 nm (Hamaker, 1937).

1.3.1.2 Capillary Forces

At approximately 50-60% relative humidity, the partial water vapour pressure in the atmosphere may be sufficient for the water to condense onto particle surfaces and when two surfaces are brought into contact, this may produce a water bridge between contiguous surfaces (McFarlane and Tabor, 1950; Hiestand, 1966). The formation of a capillary bridge results in an increased force of adhesion between the particles, due to the surface tension force of the water and meniscus formed between contacting surfaces (McFarlane and Tabor, 1950). The magnitude of this capillary force (F_c) between two identical smooth spheres (radius r) can be calculated as:

$$F_c = 2\pi\gamma_w r\cos\alpha \qquad \text{Equation 1.8}$$

where γ_w is a surface tension of water and α is a contact angle between water and the spheres. In the case of a sphere (radius r) adhering to a surface, the capillary force resulting from the condensation of water in the interface can be calculated as:

$$F_c = 2\pi\gamma_w r(\cos\alpha + \cos\beta) \qquad \text{Equation 1.9}$$

where α and β are the contact angles of the water with the surface and particle, respectively.

Capillary forces become the dominant adhesion forces when the relative humidity is above 65-75% (Hiestand, 1966; Price, Young et al., 2002).

1.3.1.3 Electrostatic Forces

During powder handling, particles become charged by contact or friction with other particles or surfaces. This process is known as triboelectrification (Staniforth and Rees, 1982). If two charged particles are brought together, they will have an electrostatic force (either attractive or repulsive, depending whether the particles are like or oppositely charged) which can be described by Coulomb's law (Coulomb, 1785):

$$F_{EL} = \frac{q_1 q_2}{4\pi\varepsilon s^2} \qquad \text{Equation 1.10}$$

where F_{EL} is the electrostatic force, q_1 and q_2 are the electrical charges on the two particles, ε is the permitivity and s is the separation distance between the particles.

An uncharged particle may become charged if an image charge is induced upon it by the approach of a charged particle (Onsager and Samaras, 1934). The resultant electrostatic force may be shown by:

$$F_{EL} = \frac{q^2\left(1 - \frac{s}{\sqrt{r^2 + s^2}}\right)}{16\pi\varepsilon s^2} \qquad \text{Equation 1.11}$$

where s is the separation distance between charged and uncharged particles. This equation may be modified to describe the adhesion of a charged particle to a flat earthed conducting surface via the formation of an image charge by making the assumption that $r \rightarrow \infty$:

$$F_{EL} = \frac{q^2}{16\pi\varepsilon s^2} \qquad \text{Equation 1.12}$$

Contact between two uncharged particles with different work functions will appear in the flow of electrons from the particle with the lower work function to the particle with the higher work function until an equilibrium is established (Tabor, 1976). The resultant force of attraction (F_w) can be described as:

$$F_w = \pi\varepsilon r \frac{(\Delta U)^2}{s} \qquad \text{Equation 1.13}$$

where r is the radius of the particles and ΔU is the potential difference arising from the difference in work functions.

Equations 1.10 to 1.13 show that electrostatic forces are significantly dependent on the electrical properties of the particles involved and the separation distance between them. Under normal environmental conditions, electrostatic forces are at least ten times smaller than van der Waals forces (Tabor, 1976). This leads to increase van der Waals forces, which are thereafter largely responsible for the strength of the adhesion, especially if the electrostatic charge dissipates (Johnson, 1996).

1.3.1.4 Mechanical Interlocking

Generally, pharmaceutical particles exhibit irregular shapes and microscopically rough surface topography. Thus, the contact and resulting adhesion between two such particles can result in the interlocking of asperities, thereby leading to an increase in interparticulate interactions (Jayasing, Pilpel et al., 1970; Adolfsson, Olsson et al., 1997). In addition, if roughness causes particle-particle contact to only occur over a small surface area, the interparticulate forces acting on this small area will produce an extremely high pressure (Fuller and Tabor, 1975). This may exceed the yield value of the material, resulting in increased mechanical interlocking and van der Waals forces.

1.3.2 Factors Affecting Interparticulate Forces

Many factors can affect the magnitude of the adhesion between particles. These relate to characteristics of the particles themselves, their process history and the conditions under which they are stored. The following sections briefly review some of the more important of these factors.

1.3.2.1 Particle Size

According to the equations shown in Section 1.3.1**,** van der Waals (the major force responsible for adhesion) are directly proportional to the particle diameter (d), whilst gravitational forces are proportional to diameter cubed (d^3). Thus, as particle size is reduced, the adhesion forces experienced by a particle become more and more significant when compared to the gravitational forces to which they are exposed (Visser,

1995). For particle smaller than approximately 10 µm, adhesive forces dominate gravitational forces, which explain the cohesiveness and poor flowability of fine respirable powders.

1.3.2.2 Particle Shape

Van der Waals and electrostatic forces both decrease as a function of the square of the separation distance between particles (Equations 1.3, 1.6, 1.7 and 1.10 to 1.12). Hence, the increase of this distance would reduce particulate interaction. Additionally, the range over which the latter exerts the influence is only ~10 nm. Thus, any effect of particle shape on interparticulate distance may significantly influence particle interactive forces (Johnson, Kendall et al., 1971). For instance, small, non-interlocking surface asperities which increase the separation distance between particles will reduce the force of adhesion upon contact (Johnson, Kendall et al., 1971). When the asperities are of the order of 1 µm, the separation distance will be large, thereby limiting the van der Waals attractions to almost zero (Castellanos, 2005). Alternatively, flat elongated particles which pack as shown in Figure 1.2A will experience increased interparticulate adhesion due to their reduced separation distance and increased interparticulate contact area. The packing of such particles depends on their process history, however, in the absence of handling, they tend to be loosely packed together (Figure 1.2B), giving rise to higher separation distance and reduced area of contact leading to a reduction in their adhesive interactions (Valverde, Ramos et al., 1998).

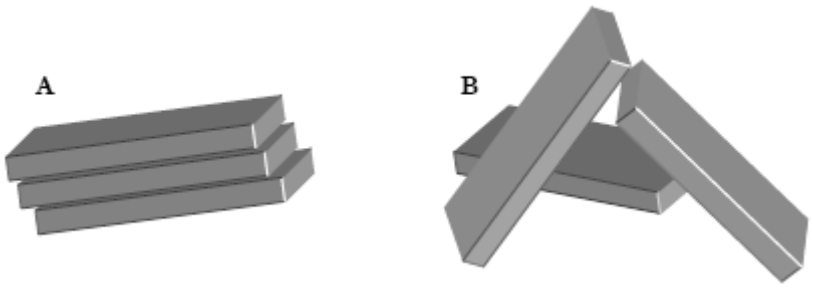

Figure 1.2: Packing arrangements for flat elongated particle (Zeng, Martin et al. 2001): (A) Closely packed orientation, typically found after powder handling. (B) Loosely packed orientation

1.3.2.3 Surface Roughness of Particles

The effect of roughness on adhesion is dependent on the relative size of the roughness and the contact geometry between adhering particles (Fuller and Tabor, 1975). As shown in Figure 1.3A, if the roughness of a substrate is of a smaller scale than the adhering particle, the contact area between the particle and the surface will be decreased and the separation distance increased when compared to adhesion to a flat surface (Figure 1.3B), resulting in decreased interparticulate forces (Johnson, Kendall et al., 1971; Fuller and Tabor, 1975; Johnson, 1996). When the roughness of substrate is on a larger scale than the adhering particle, the situation is reversed (Figure 1.3C). In addition, mechanical interlocking can occur, resulting in increased interparticulate forces.

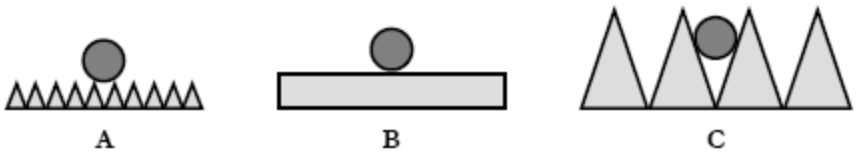

Figure 1.3: The effects of roughness on particle-surface adhesion. (A) Surface roughness on a smaller scale the particle size. (B) A smooth surface. (C) Surface roughness on a larger scale than particle size

For most pharmaceutical powders, adhesion occurs between two rough particles or a rough particle and a rough surface, so the examples shown in Figure 1.3 (where the particle is smooth) are a simplification of the situation (Zeng, Martin et al., 2001).

1.3.2.4 Particle Deformation

Attractive forces can generate deformation at the contact site of the adhering surface (Krishnan, Busnaina et al., 1994). The extent of any deformation is dependent on the elastic properties of the particles, the magnitude of the attractive forces and the magnitude and duration of any external forces applied to the particles (Johnson, 1996). For certain materials such as polymer-like materials, the duration of contact is also important as deformation will increase with time resulting in increased adhesion, a phenomenon known as aging (Krupp, 1967). However, in the context of DPI formulations, deformation does not lead to greater adhesion but may influence particle re-entrainment upon aerosolisation (Johnson, 1998).

1.3.2.5 Surface Free Energy

The surface free energy from a solid material is described as the energy required to produce a unit area of surface and is analogous to the surface tension of a liquid (Johnson, Kendall et al., 1971). Unlike liquids, the molecules of a solid are not free to move, therefore, surface free energy is not uniform over a surface and depends on the history of the material (Johnson, 1998). The quantity of work required to separate two surfaces of two materials is called the work of adhesion (W_a) and is related to the surface free energy of the surfaces by the following equation:

$$W_a = A_s(\gamma^C + \gamma^D - \gamma^{CD}) \qquad \text{Equation 1.14}$$

where A_s is the area of surface produced by the separation, γ^C and γ^D are the free energies per unit surface area of solids C and D in air, respectively; and γ^{CD} is the free energy of the C-D interface per unit area. Therefore, the work of cohesion (W_c) (i.e. the work requires to separate two surfaces of the same material) is shown by:

$$W_c = 2A_s\gamma^C \qquad \text{Equation 1.15}$$

The thermodynamic work of adhesion and cohesion is directly related to the force of adhesion and cohesion and is critically dependant on the surface free energies of the interacting particles (Johnson, Kendall et al., 1971).

1.3.2.6 Relative Humidity

Interparticulate forces are influenced by relative humidity via two opposing mechanisms. On the one hand, the relative humidity increases particulate interaction because of the capillary forces when a significant amount of water is condensed on the surface of the interacting system (McFarlane and Tabor, 1950; Price, Young et al., 2002). On the other hand, the conductivity of both interactive particles will be increased and will accelerate the dissipation of electrostatic charges on the particles (Byron, Peart et al., 1997). Hence, water at high relative humidity can condensate at the contact points between particles, resulting in the formation of liquid bridges and an increase in capillary forces (Price, Young et al., 2002; Young, Price et al., 2003b).

1.3.3 Particle Physical State

Many materials can form solids that are crystalline or amorphous, depending on the states of growth. Therefore, it is completely important to know the physical properties of solids.

1.3.3.1 The Crystalline State

Crystals are solids in which the atoms are arranged in a periodic repeating pattern that extends in three dimensions (Myerson, 2002). The simplest repeating unit in a crystal is described as a unit cell. Each unit cell is defined in terms of lattice points. It was observed in 1848 by Bravais that there are 14 possible point lattices which can be constructed (Myerson, 2002). Also, these point lattices can be divided into seven categories, which differ in the three unit-cell edge lengths and three internal angles, as shown in the Figure 1.4.

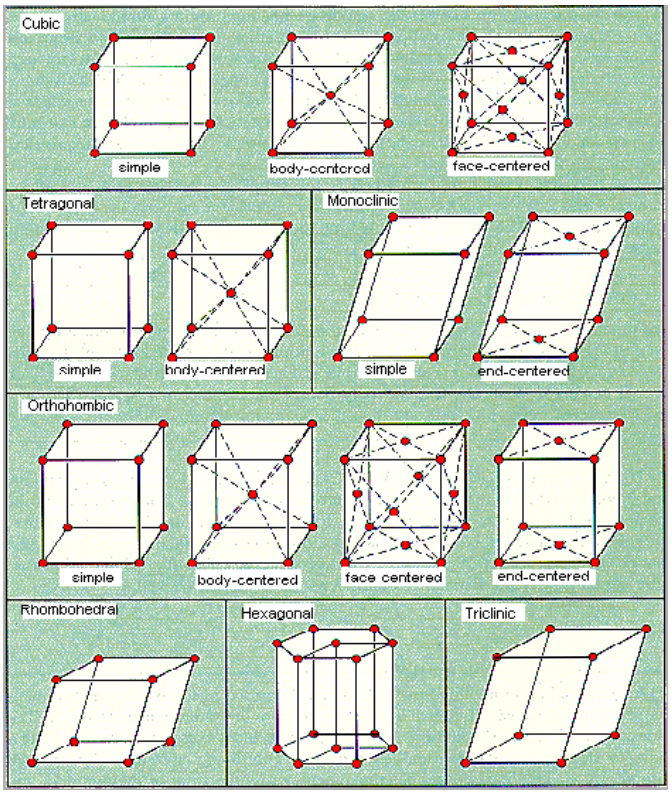

Figure 1.4: The Bravais lattices modified from http://chemed.chem.purdue.edu/genchem/topicreview/bp/ch13/unitcell.php

Crystals are nucleated and grown from supersaturated solutions. A saturated solution is a thermodynamic equilibrium between the solid phase and the liquid phase at a specified temperature (Mullins, 1992). This requirement for a supersaturated solution is critical for nucleation and crystal growth.

Nucleation happens spontaneously in a homogeneous solution or induced by a heterogeneous process. These processes are named primary homogeneous nucleation and heterogeneous nucleation, respectively. Young and Berkeley discovered that agitation, mechanical shock, friction extreme pressures and temperature cooling can increase the degree of nucleation (Young, 1911; Berkeley, 1912). A supersaturated solution may nucleate at a lower supersaturation when crystals of the solute are already present or added. These crystals, typically described as seeds, perform as nucleation centres for crystal growth. Such a process can be referred as secondary nucleation (Botsaris, 1976).

The external appearance of a crystal is referred to crystal habit (Mullins, 1992). Despite the fact that crystals can be classified to seven general systems, the relative sizes of the faces of a particular crystal can greatly vary. This variation is called a modification of habit. The crystals may grow more rapidly, or be stunted in one direction; an elongated growth of the habit gives a needle-shaped crystal and a stunted growth brings a flat plate-like crystal (Mullins, 1992). A description of the morphology of a crystal requires the characterisation of each crystal face present, their relative dominance, specific angles between the faces, relative areas and shape factors. These are used to describe the macroscopic geometry of a crystal. However, knowing the internal structure of a crystal unit cell is not adequate to represent the external habit of the resulting crystals formed. External habit is not only controlled by its internal structure, but also by the conditions in which the crystal has been grown. The rate of crystal growth, the solvent used, and the impurities present in the solution may have a substantially influence on the crystal habit (Strickland-Constable, 1968; Laudise, 1970).

1.3.3.2 Polymorphism

Polymorphism is the name used to describe the phenomenon of chemical species having more than one crystal structure (Brittain, Bogdanowich et al., 1991). When a material crystallises into different polymorphs, the chemical nature of the species remains identical. However, due to the alteration in the crystal unit cell, physical

properties including density, melting point, solubility and hygroscopicity may vary (Brittain, 1997). During crystallisation, inhibiting polymorphism may be particularly crucial. This can sometimes be achieved by optimising and controlling the crystallisation conditions (e.g. solution temperature, solvents) as well as storage condition (e.g. temperature and relative humidity), in preventing the formation of undesired polymorphs. For example, cimetidine, a specific competitive histamine H_2-receptor antagonist, has seven known polymorphs (Danesh and Chen, 2000). Two of them are of particular interest to the pharmaceutical industry, with one being used in tabletting (form A) and other in suspensions (form B). While form A can be re-crystallised from non-aqueous solvents at room temperature, form B requires slow cooling from a hot aqueous solution. Also, lactose is known to have two anomeric forms namely, α and β. Both are simultaneously present in aqueous solution with an α/β ration close to 40/60, but only the α-lactose monohydrate crystallises spontaneously below 93.5°C (Nickerson, 1974).

1.3.3.3 The Amorphous State

A solid in the amorphous state is also known as a supercooled liquid in which the molecules are arranged in a random behaviour as in the liquid state (Yu, 2001). Substances such as glass and many synthetic plastics are amorphous in nature. They are different from crystalline solids in that they have to flow when subjected to sufficient pressure over a period of time, and they do not exhibit melting points (Hancock and Zografi, 1994).

An amorphous state is identified by the absence of three-dimensional long range order which exists in a crystalline state (Hancock, Shamblin et al., 1995). Rapid cooling, fast evaporation or precipitation may happen in the formation of amorphous solids in a glassy or rubbery state (Hancock, Shamblin et al., 1995). Amorphous areas on solid particles may also be generated from mechanical treatments (Salekigerhardt, Ahlneck et al., 1994). The differences in physical properties between crystalline and amorphous material have been found to have a significant effect on the stability and performance of DPI formulations (Buckton, 1997). Molecules within an amorphous region are randomly arranged, and demonstrate a higher surface energy than the crystalline material (Ambarkhane, Pincott et al., 2005). Moreover, amorphous materials have different mechanical properties in comparison to crystalline materials, where amorphous materials are softer and subject to greater deformation under stress

(Andronis, Yoshioka et al., 1997). The degree of molecular mobility within a particular amorphous material will be related on a number of factors, including temperature and solvent vapour pressure (Hancock and Zografi, 1994). The sorption of a solvent into an amorphous region would increase molecular mobility and thus lower the glass transition temperature (T_g) (Buckton and Darcy, 1996). If the partial pressure of the solvent is high enough to lower the T_g below the experimental temperature, the region may recrystallise and remove the solvent (Hancock and Zografi, 1994). It is important to note that a system is a thermodynamic process and not a kinetic process. It will not reach a true equilibrium until the system re-crystallises, but the process may take time. In pharmaceutical applications, dosage forms must have a specific functionality that requires a high-energy processing such as milling or micronisation. This process leads to the formation of molecular defects, dislocation and the creation of amorphous areas within the crystalline material (Begat, Young et al., 2003). In general, amorphous materials are thermodynamically unstable and will experience re-crystallsation if the right conditions and the kinetics are favourable (Buckton and Darcey, 1999). The amorphous regions will directly affect the stability of a formulation as the surface energetics will become unpredictable, leading to batch-to-batch variations in the stability and aerosolisation properties of the powder blend (Feeley, York et al., 1998).

1.3.4 Particle Engineering

To generate respirable drug particles, different processes have been widely used, for example, micronisation, spray drying, spray freeze drying, supercritical fluid technology, and crystallisation.

1.3.4.1 Micronisation

Inhalation products such as DPIs, pMDIs and suspension nebulisers consist of micronised drug in either agglomerated or blended form. Such particles are generally produced by batch crystallisation, followed by filtering, drying and micronisation (Shekunov, Feeley et al., 2003). The particle size reduction can be achieved by pressure, attrition, impact, or shear. Vibration milling, ball milling and jet-milling are well-established techniques used to manufacture dry powders for inhalation. Although milling can be carried out on a dry or wet basis, dry grinding is more generally employed as it is less labor-intensive. In the jet-milling process, the starting material

has many impact events before a significant quantity of the required particle size fraction is achieved and separated from the larger particles by inertial impaction (Steckel, Rasenack et al., 2003). This classification ensures that the particle size distribution required for respiratory drug delivery can be obtained.

Particles produced by micronisation are adversely affected by such a high energy process and the resultant particles have been shown to increase surface rugosity, surface free energy, electric charge and most significantly with a degree of crystalline disorder (Ticehurst, Rowe et al., 1994; Feeley, York et al., 1998). These disordered regions are thought to be on the particle surfaces and are metastable (Begat, Young et al., 2003). Under certain conditions, for example, elevated temperature or humidity, these amorphous surface regions on particles may undergo a re-crystallisation process, inducing solid crystal bonding and particle agglomeration (Price and Young, 2005). The material is also subjected to chemical decomposition and water sorption. All physical and chemical changes are highly undesirable, and can affect the *in-vitro* and *in-vivo* performance of the respiratory formulation (Rasenack, Steckel et al., 2004).

1.3.4.2 Spray Drying

Spray drying has been employed as a routine technique for the production of pharmaceutical particles for decades (Broadhead, Rouan et al., 1992). A typical spray-drying process comprises four steps: (a) atomisation of feed solution into a spray; (b) spray-air contact involving flow and mixing; (c) drying of sprayed droplets at elevated temperatures; and (d) separation of dried product from the air (Masters, 1985). A feeding solution is atomised into droplets that dry rapidly in the spray drying process due to their high surface area and contact with the drying gas (Masters, 1985). The process conditions, for instance, flow rate, pump rate, aspiration rate and heat significantly influence the drying time of droplets (Chawla, Taylor et al., 1994; Li, Seville et al., 2005; Shur, Nevell et al., 2008). This drying time can start from a few seconds to less than 100 minutes (Masters, 1985). The temperature experienced by the droplets is lower than the temperature of the drying air due to evaporative cooling, which has enabled the processing of labile molecules such as proteins and genes (Seville, Kellaway et al., 2002; Li, Seville et al., 2005). The dried powder is protected from overheating by rapid removal of the drying zone. Finally, the final product can be removed from the air stream by the use of cyclones or filters (Masters, 1985).

The particles from the spray-drying process are commonly spherical and hollow as a result of the rapid evaporation of the solvent on the droplets surface and solidification of the surface (Broadhead, Rouan et al., 1992). The hollow structure of spray-dried particles can provide benefits in terms of the aerodynamic diameter, therefore, the overall density is low, allowing the formation of larger particles to reach the aerodynamic size range for inhalation (Edwards, Hanes et al., 1997; Bosquillon, Rouxhet et al., 2004). However, spray-dried products are typically amorphous, which, owing to their metastable state, precludes their use in conventional carrier-based DPI drug products.

1.3.4.3 Spray Freeze Drying

The technique of spray freeze drying involves the atomisation of an aqueous drug solution via a two-fluid or an ultrasonic nozzle into a chamber filled with a cryogenic liquids, for example, liquid nitrogen or halocarbon refrigerant (Maa, Nguyen et al., 1999). The spraying process can be run beneath or above the surface of the cryogenic liquid, depending on the position of nozzle (Leuenberger, Plitzko et al., 2006). Since the normal boiling point for such a liquid is very low, the droplets are quickly frozen. It has been established that these droplets may begin to freeze during the time of flight through the cold vapour phase and then entirely freeze upon contact with cryogenic liquid (Mumenthaler and Leuenberger, 1991; Maa, Nguyen et al., 1999). Once the spraying process is completed, the whole content can be lyophilized with conventional freeze drying (Rogers, Nelsen et al., 2003). After spray freezing, the frozen solvent is removed, as in the case of freezing with cryogenic liquids, by vacuum or atmospheric freeze drying. Limitations to this technique contain the fact that it is time consuming. Additionally, the nature of the process has safety issues involved with spraying into cryogenic fluids and it is expensive (Mumenthaler and Leuenberger, 1991). Furthermore, the metastable state of spray-freeze-dried particles may lead to drug product instability once such particles are incorporated into a given dosage form.

1.3.4.4 Supercritical Fluid (SCF) Technology

Supercritical fluids (SCFs) are gases and liquids at temperatures and pressures above their critical points which include critical temperature (T_c) and critical pressure (P_c) (Shekunov and York, 2000). In the area of the critical point, the SCFs occur as a single phase with several advantageous properties of both liquids and gases (Palakodaty,

York et al., 1998). The SCFs obtain density values which are able to reach salvation power, whilst the viscosity of solutes in SCFs is lower than in liquids (Kajimoto, 1999). The diffusivity of solutes in SCFs is completely higher than in liquids, hence, it is capable of facilitating mass transfer without difficulty (Eckert, Knutson et al., 1996). Most importantly, SCFs are highly compressible, particularly near the critical point, and their densities and thus salvation power can also be controlled by variation in temperature and pressure (Savage, Gopalan et al., 1995). According to the pharmaceutical applications, SCF is akin to supercritical CO_2 (SC CO_2) because of its low critical temperature (31.1˚C), moderate pressure (73.8 bar), non-toxic inert nature and low cost (Savage, Gopalan et al., 1995).

Particle engineering by SCFs can be separated into three different groups (York, 1999). The first method involves dissolving or solubilising the drug in a SCF followed by rapid expansion of the SCF solution through a heated orifice to minimise the density of the solution, thereby decreasing the salvation power of the SCF (York, 1999). The reduction of the salvation power leads to the precipitation of the drug (Pasquali, Bettini et al., 2006). This process is referred to as the “rapid expansion of supercritical solution” (RESS) (Pasquali, Bettini et al., 2006). The second method is similar to RESS because they both involve using SC CO_2 as a solvent rather than an anti-solvent. The process has been named as “precipitation from gas saturated solution” (PGSS). For this PGSS system, the SCF is firstly dissolved in molten solute, following with the step of transferring the supercritical solution from an orifice into a chamber to allow a rapid expansion under ambient conditions (Jung and Perrut, 2001). Particle formation from PGSS utilises the high solubility of CO_2 in certain materials such as polymers, which result in plasticisation, decreased viscosity, and depressed melting and glass-transition points. The essential benefit is to apply this procedure with blending, coating and encapsulation, which occur without the use of organic solvents (Jung and Perrut, 2001). The challenge of PGSS is the controlling of particle size because the high melt viscosity may stop the formation of fine particles. The third method is the most common method and different variants of technique have been developed. This typical technique employs a similar concept to the use of anti-solvent in solvent-based crystallisation processes (Palakodaty, York et al., 1998). The high solubility of SC CO_2 in organic solvents leads to volume expansion when the fluids make contact. This contributes to the reduction in solvent density and parallel fall in salvation capacity (York, 1999). Such reduction may cause increased level of supersaturation, solute nucleation and particle formation (York, 1999). The assorted names such as GAS

(gaseous anti-solvent), ASES (aerosol solvent extraction system), SEDS (solution enhanced dispersion by SCF), and PCA (precipitation by compressed anti-solvent) have been assigned to different applications via this technique (Jung and Perrut, 2001). For example, Steckel *et al.* used ASES process on particle properties of budesonide and found that the process condition in ASES may influence the aerodynamic properties, although other physico-chemical parameters appear to be similar (Steckel, Pichert et al., 2004). The principal disadvantage of this process is the lack of control for particle formation. In batch procedure conditions, it has been shown that the level of saturation is not maintained (Jung and Perrut, 2001).

1.3.4.5 Controlled Crystallisation

The separation of a solid substance from solution by changing the physical or chemical properties of the material concerned is termed crystallisation (Shekunov and York, 2000). A compound may crystallise from a solution when its solubility in a particular solvent is exceeded and the solution becomes supersaturated. Supersaturation can be accomplished in many ways, for instance, the evaporation of the solvent, cooling the solution or by producing additional solute as a result of chemical reaction or a change in the solvent system (Mullins, 1992). Controlled crystallisation has advantages over both micronisation and spray drying in that it may generate particles with high crystallinity and of predetermined size, size distribution and shape (Rasenack, Steckel et al., 2004; Westmeier and Steckel, 2008). For diagnosis of asthma and bronchial-related disorder, Abbas and Srour found that the generated NaCl particles with size ranging from approximately 1 μm to sub-micron range were achieved by sonocrystallisation with optimal conditions of temperature (<5˚C), ultrasonic power output (~35W) and salt concentration (~32g/100g water) (Abbas, Srour et al., 2007). Controlled crystallisation is an important technique, which may aid the generation of particles suitable for drug delivery to the lungs.

1.4 Solution Atomisation and Crystallisation by Sonication (SAX)

1.4.1 SAX Process

The solution atomisation and crystallisation by sonication (SAX) process consists of three interdependent processes: (a) the production of aerosol droplets of the solute

from a carrier solvent using a suitable aerosol generator; (b) the collection of the highly supersaturated droplets in a crystallisation vessel containing a non-solvent of the drug; (c) the application of ultrasonic waves to a crystallisation vessel to controllably induce homogeneous nucleation and crystal growth (Kaerger and Price, 2004). An atomiser in the SAX process produces highly supersaturated spherical constructs of the active ingredient within a well-defined particle size for controlled crystallisation. The atomised droplets are collected in a crystallisation vessel containing a non-solvent of the drug, which is preferably miscible with the solvent in which the drug is solubilised (Kaerger and Price, 2004). The surface tension of the collecting solution in the crystallisation vessel should be low or possibly minimised to prevent structural changes to the droplet shape on impingement. The generation of micrometer-sized droplets of drug solution leads to rapid vaporisation of the solvent and the production of highly supersaturated droplets of the solute molecules. However, rapid crystallisation within these droplets does not readily occur because of the dramatic increase in the viscosity, which limits the mass transport properties of the solute molecules to form a critical nucleus for nucleation and subsequent crystal growth (Kaerger and Price, 2004). To induce homogeneous nucleation, such highly supersaturated droplets require a sufficient degree of molecular motion within the droplets. This process is aided by the application of sonic energy, which increases the molecular motion within the droplets and induces nucleation and growth of crystals.

The relative viscosity of these droplets will be drug specific and highly dependent on the rate of vaporisation of the drug solvent. The vaporisation process is dependent on a number of parameters including vapor pressure of the solvent, dimensions of the initial atomised droplet, solute-to-solvent composition, temperature, and flow rate. In the SAX process, the degree of vaporisation of the solvent is controlled by the separation distance between the atomiser and the non-solvent solution. As a batch process, the crystallised particles are filtered from the resulting suspension and dried over silica-gel at room temperature (Kaerger and Price, 2004).

By combining these processes and controlling relevant parameters, high-purity micron-sized sphere-like crystalline particles can be readily produced in a single droplet-to-particle operation. The major advantage of this low-cost technique relates to the use of any suitable aerosol generator, and the whole process can be carried out under atmospheric pressure and ambient conditions. Furthermore, it has the potential for batch and continuous processing at an industrial scale.

1.4.2 Theory of Crystallisation

The crystalline state is different from the amorphous state by the manner in which constituent molecules, atoms or ions arrange into a thermodynamically stable crystalline lattice. A crystalline lattice presents long-range molecular order with the configuration of the molecules, atoms or ions into a fixed and periodic pattern (Mullins, 1992).

1.4.2.1 Nucleation

Crystals are typically nucleated and grown from a supersaturated solution or from a supercooled melt of the solid (Mullins, 1992). Supersaturation is defined as a state in which the concentration of substance in a solvent at a specific temperature and pressure is higher than the saturated solubility of the drug under such conditions (Shekunov and York, 2000). Supersaturation can be expressed as concentration driving force Δc :

$$\Delta c = c - c^* \qquad \text{Equation 1.16}$$

or as a supersaturation ratio S :

$$S = \frac{c}{c^*} \qquad \text{Equation 1.17}$$

or as a relative supersaturation σ :

$$\sigma = \frac{\Delta c}{c^*} \qquad \text{Equation 1.18}$$

where c is actual concentration and c^* is equilibrium saturated concentration at a well-defined temperature and pressure. In general, the solubility of a drug increases with increasing temperature (Shekunov and York, 2000).

The formation of a supersaturated or supercooled state alone is not a sufficient cause for a system to induce nucleation (Shekunov and York, 2000). Prior to crystal growth, there must exist a number of agglomerated molecules that act as growth centres (Botsaris, 1976). These critical nuclei may occur spontaneously at certain conditions of supersaturation. This problem can be avoided by secondary nucleation, where artificial seed crystals are introduced into the supersaturated solution. Seed crystals can either catalyse the formation of other nuclei or act as a growth centre for crystal growth (Botsaris, 1976).

According to primary nucleation, it can be divided into two categories. On the one hand, foreign particles such as impurities or the material of the vessel provide the breeding ground for nuclei formation (Mullins, 1992). This process is termed heterogeneous primary nucleation. On the other hand, a sufficient number of molecules can spontaneously agglomerate to form a nucleus, and such number of molecules can vary between ten to several thousands (Mullins, 1992). This process is referred to as the homogeneous primary nucleation.

The free energy changes associated with the process of homogeneous nucleation may be described as follows. In Figure 1.5, the diagram shows the free energy of nucleation explaining the existence of a critical nucleus. The overall Gibbs free energy (ΔG) results from the addition of the surface excess free energy ΔG_s, which is the difference between the energy on the surface and inside a sphere with radius *r*, and the volume excess free energy ΔG_v, which is the difference in energy between the bulk and particles in solution. The total Gibbs free energy ΔG can be expressed as:

$$\Delta G = \Delta G_s + \Delta G_v \qquad \text{Equation 1.19}$$

$$= 4\pi r^2 \gamma + \frac{4}{3}\pi r^3 \Delta G_v \qquad \text{Equation 1.20}$$

where ΔG_v is the free energy change of the transformation per unit volume and γ is the surface tension (Mullins, 1992).

The value of ΔG_s is dependent on the surface of the sphere, which increases as a function of r^2, whereas ΔG_v proportionally increases to r^3. Thus, for small r with a small number of molecules in the lattice, ΔG_s increases more dramatically than ΔG_v. However, upon reaching a critical radius (r_{crit}) shown in Equation 1.21, ΔG_v increases faster than ΔG_s and it becomes thermodynamically more attractive to increase the size of the nucleus instead of re-dissolving. At this critical point, nucleation ceases and crystal growth begins (Myerson, 2002).

$$r_{crit} = \frac{-2\gamma}{\Delta G_v} \qquad \text{Equation 1.21}$$

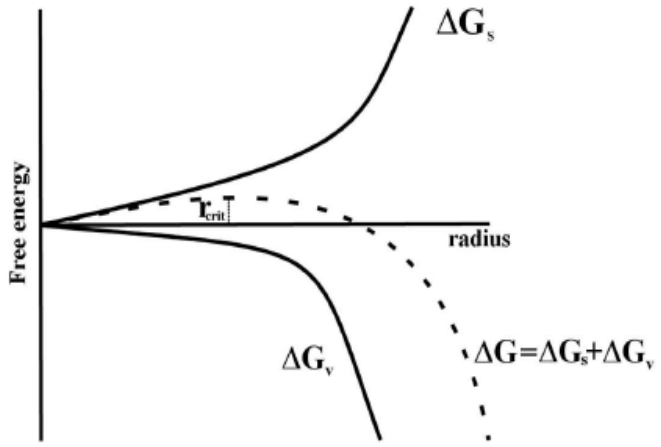

Figure 1.5: Free energy diagram of nucleation showing free energy versus cluster size

The number of nuclei formed per unit time, known as the rate of nucleation (J), can be expressed in the form of an Arrhenius equation, which is commonly used for determining the rate of thermodynamically activated processes:

$$J = Ae^{\frac{-\Delta G_{crit}}{kT}} \qquad \text{Equation 1.22}$$

where k is the Boltzmann constant. The Gibbs-Thomson relationship (Mullin 1992) which relates the solubility to the particle size may be written as:

$$\ln S = \frac{2\gamma V_m}{kTr} \qquad \text{Equation 1.23}$$

where V_m is the molecular volume. Combining equations 1.21, 1.22, 1.23, the result is thus:

$$J = A_{EXP}\left[\frac{-16\pi\gamma^3 {V_m}^2}{3k^3T^3(\ln S)^2}\right] \qquad \text{Equation 1.24}$$

The rate of nucleation, therefore, depends on temperature, supersaturation and surface free energy. Furthermore, it can be concluded that the majority of obtained nuclei will exhibit the lowest possible surface free energy of the material because an increase in surface tension would led to a decrease in the rate of nucleation.

Nucleation can often be induced by agitation, mechanical shock, friction and extreme pressure within the solutions or melts (Young, 1911). The effects of electric and magnetic fields, spark discharge and ultrasonic irradiation have previously been studied, and are slowly finding significant applications in industrial crystallisation (Mullins, 1992).

1.4.2.2 The Influence of Ultrasonication on Nucleation

Ultrasonication has been applied to initiate nucleation and crystallisation in supersaturated solutions on the laboratory scale (Kaerger and Price, 2004; Abbas, Srour et al., 2007). However, there still remains a degree of uncertainty on how the arrangement of molecules in a crystalline structure during nucleation and crystallisation is linked to ultrasonic waves.

Ultrasound is the name given to sound waves having frequencies higher than those to which the human ear can respond (f > 20 kHz) (Ruecroft, Hipkiss et al., 2005). Being a sound wave, it is transported by solids, liquids and gases with elastic behaviour. The movement of molecules in a vibrating body is a vibration around a mean rest-position, and energy is transported by transmission to adjoined particles (Ruecroft, Hipkiss et al., 2005). This movement produces compressed areas, followed by an area of enhanced mean molecular distance. In gases and liquids, particles oscillate in the direction of producing longitudinal waves (Lorimer and Mason, 1987). However, in solids, the shear elasticity can also support tangential stresses and allow perpendicular movement of the particles and transversal waves (Ruecroft, Hipkiss et al., 2005).

If an acoustic field is applied to a liquid, it creates an additional acoustic pressure (P_a) to the ambient hydrostatic pressure (P_h). If A^* is the amplitude of the wave, the acoustic pressure can be described as:

$$P_a = A^* \sin(2\pi f t) \qquad \text{Equation 1.25}$$

where t is the time and f the frequency of the wave (Lorimer and Mason, 1987).

The corresponding energy (I) transmitted to the liquid (per second per cm^2) can be determined by:

$$I = \frac{A^{*2}}{2\rho_f V_s} \qquad \text{Equation 1.26}$$

where ρ_f is the density of the fluid and V_s the velocity of sound in the liquid. Molecules vibrating under the action of a sound wave additionally experience a viscous interaction, which decreases the amplitude of the sound wave. The lost energy is represented in bulk heating and the energy loss can de described by:

$$I* = I_0 e^{-2a^* l} \qquad \text{Equation 1.27}$$

where $I*$ is the intensity of the wave at a pre-set distance l, I_0 the intensity at the source and a^* the absorption coefficient. The absorption coefficient a^* of a liquid is described by the Kirchoff equation, where:

$$a^* \propto f^2 \qquad \text{Equation 1.28}$$

From equation 1.28, increasing in frequency leads to a greater degree of absorption. Because this energy, which is lost within the system, is converted into heat, it has to be taken in account either by continuous cooling or by applying the energy in intervals when using a high frequency system.

A sound wave induces areas of high and low pressure. If the pressure in a specific area is sufficiently low, the critical distance between molecules will be exceeded. This leads to the formation of cavitations (Lorimer and Mason, 1987) . In general, there are two different kinds of cavitations – stable and transient cavitations (Lorimer and Mason, 1987). Stable cavities are bubbles, which form and oscillate around a mean radius in a sound field and exist for many acoustic cycles (Ruecroft, Hipkiss et al., 2005). Thus, the amount of expansion must be the same as the contraction. A transient cavity exists for only a few acoustic cycles. During its existence, it grows in the low pressure part of a frequency cycle. The constant growth of the bubble is caused by diffusion into the cavity. Upon reaching a critical bubble size, the hydrostatic pressure combined with the

acoustic pressure leads to implosion of the cavity, creating an area of high pressure and temperature (Lorimer and Mason, 1987).

The mechanical influence of ultrasonic treatment on the erosion of solid material, and the increase in the degree of nucleation and crystallisation, induced by the application of acoustic wave energy to supercooled melts have been well studied (Lorimer and Mason, 1987; Kaerger and Price, 2004; Ruecroft, 2007). There is a general agreement that nucleation triggered by sonication leads to the formation of smaller particles (Ruecroft, 2007). The increase of the amplitude of applied ultrasonic waves has also been found to decrease the particle size (Abbas, Srour et al., 2007). However, the scientific principle behind the influence of sonication on nucleation has still to be fully understood. Virtually, all theories agree that the effect of ultrasonic waves during nucleation is not due to the transmission of sound waves but due to effects caused by cavitation (Ruecroft, Hipkiss et al., 2005).

Two theoretical approaches have been established on the influence of cavitation on nucleation and crystal growth (Lorimer and Mason, 1987). In considering bulk nucleation behaviour within supercooled melts, Sobolev described that the pressure inside a cavity during an adiabatic expansion increased the degree of supercooling which led to homogenous nucleation (Sobolev, 1989). However, earlier work by Hem indicated that nucleation only occurred during the collapse of cavitations inside the areas of elevated temperature and pressure (Hem, 1967).

1.4.2.3 Crystal Growth

If a nucleus grows to a critical size, the supersaturated system is thermodynamically driven to increase the particle size via crystal growth. The various mechanisms of crystal growth have received several theoretical explanations (Mullins, 1992; Davey and Garside, 2000). The most plausible explanation is based on a thermodynamic viewpoint, where molecules attach to a growing crystal surface at the site of highest surface free energy (Burton and Cabrera, 1951). This will predominantly occur on a ledge, where there are two-unsaturated bonds, or at a kink site on a ledge, where there will be three-unsaturated bonds (Mullins, 1992). The areas between two ledges, known as a terrace, will have the lowest surface free energy with only a single unsaturated bond. As a result, growth proceeds in a layer-by-layer process, where the growth of a new layer only occurs upon growth of the previous layer (Mullins, 1992). The rate-

limiting step for crystal growth is the formation of a two-dimensional nucleus for growth of a new surface later. The process, which is more commonly described as a two-dimensional nucleation and growth, is dependent on the degree of supersaturation for the formation of a stable two-dimensional nucleus (Mullins, 1992). At low degrees of supersaturation, 2-D nucleation and crystal growth do not proceed.

However, the presence of defects and dislocations on the surface of a growing crystal, which may displace the molecular arrangement between two crystal planes, provides an area of increased surface free energy for crystal growth (Frank, 1949). The three-dimensional character and unmovable nature of the dislocation source provide an ever winding source of high surface free energy sites for growth around the centre of the dislocation. This growth process is more commonly known as a screw dislocation growth process (Frank, 1949), which dominates at low levels of supersaturation.

Since a nucleus exhibits the lowest possible surface free energy, it is expected that crystals preferably grow on faces where the overall surface free energy of the particle can be reduced. This is called the Wulff condition (Mullins, 1992). However, the observed habit of crystal growth from solution is often quite different from theoretical predictions. Hartman and Perdik related the crystal morphology to the internal crystal structure and concluded that the morphology of a crystal is governed by a chain of strong bonds (periodic bond chain – PBC) which run though the structure (Hartman and Perdok, 1955). As a result, crystals preferably grow in the direction of the bonds. Therefore, faces which have the PBCs as a vector will grow faster. This analysis has been shown to result in a typical crystal habit for each material and crystal structure.

1.5 Aims of the Study

Technologies for modifying particles in order to achieve a greater control of size and surface properties of particles for DPI formulations have been investigated for a number of years. However, these processes are inefficient and difficult to control to ascertain particles of defined physical properties. There continues to remain a need to develop novel particle processing technologies for the successful control of the surface characteristics and surface geometry of active drug materials.

The key aim of this study is to investigate whether the SAX technology enables the production of respirable particles for both binary and combined DPI dosage forms, with

defined physicochemical functionality. The outline of the thesis in relation to the key aim is shown in Figure 1.6.

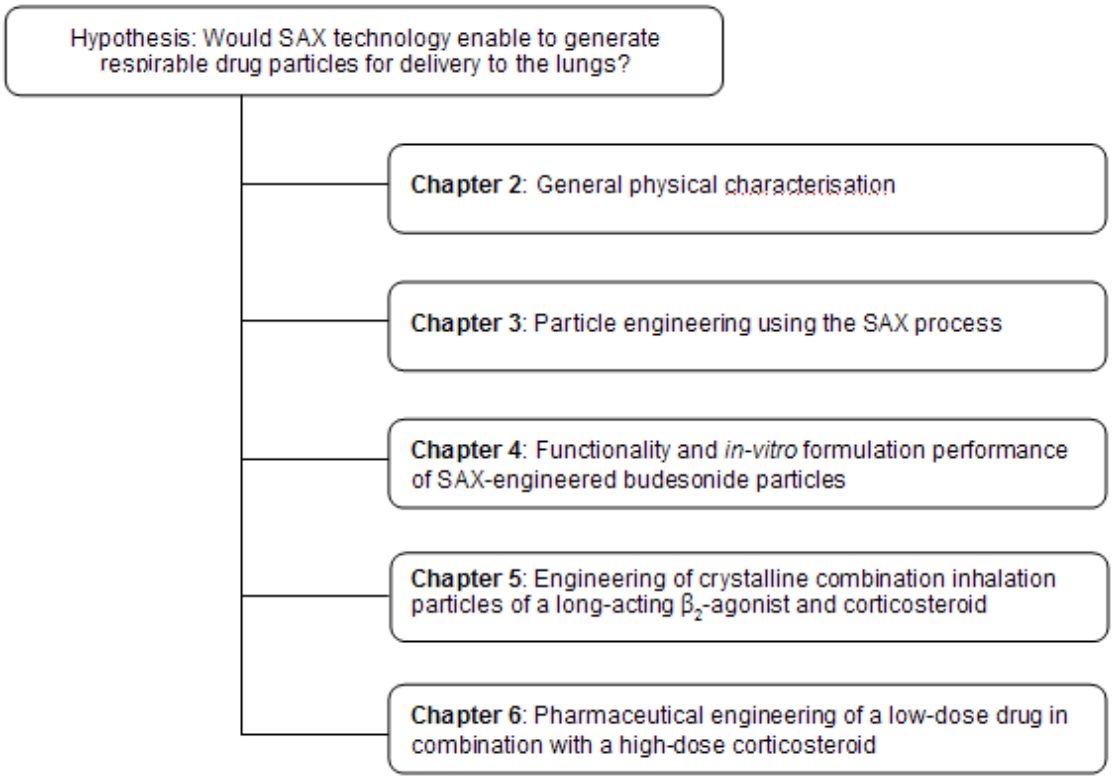

Figure 1.6: Flow diagram of the structure of the thesis in relation to the key aim of the project

In Chapter 2, the drugs and excipients will be generally characterised in the term of physical properties of particles. Chapter 3 of this study is related to the development of the lab-scale SAX system by using the principle from the first SAX generation (Kaerger and Price, 2004). For developing the SAX system, many important factors have been involved in the controlling conditions such as pressure, carrier solvents, non-solvents and temperatures. In Chapter 4, SAX process has been applied to generate the single crystalline drug particles. Furthermore, all produced materials have been characterised for the physical properties and formulated in DPI formulations to investigate to *in-vitro* performance.

The role of combined inhalation products containing β_2-agonist plus ICS can help improve the clinical effectiveness for asthma and COPD patients. The improved clinical outcome on application of combination products is thought to be related to synergistic

actions of the different agents at receptor, cellular and molecular levels. For this effect to occur, both drugs need to be present on the same cell in the airways. Current DPI formulation technologies are not efficient and effective to enable both actives to be delivered to the same site of action at the cellular level. One method of achieving this may be through engineering of single geometric particles that contain both actives in the appropriate concentrations. Therefore, in Chapter 5, the combined drug particles of fluticasone propionate and salmeterol xinafoate with the high-dose ratio have been produced via SAX process. Moreover, the physical characterisation of such combined drug particles and their formulation performance will also be examined. For Chapter 6, similar method for producing combined particles of budesonide and formoterol fumarate dihydrate will be used to evaluate the low-dose ratio of this combination product. The study gained from this research work will help elucidate how SAX may be used to generate respirable particles.

Chapter 2: General Physical Characterisation

In Chapter 1, the importance of the physicochemical properties of components of inhalation dosage forms was highlighted. Physicochemical properties such as particle size, shape and crystallinity can have a dramatic effect on interparticulate forces within inhalation dosage forms and drug product performance. This chapter, therefore, describes the comprehensive physicochemical characterisation of the materials used throughout this study.

2.1 Materials

Table 2.1 shows the details of materials applied for this study. All solvents were supplied by Fisher Scientific UK (Loughborough, UK) and were of at least analytical grade. Water for the overall study was prepared by reverse osmosis (MilliQ, Molsheim, France).

Table 2.1: Sources of materials used in this study

Materials	***Manufacturers***
Micronised budesonide	Scior, Milan, Italy
Micronised fluticasone propionate	Merck Generics, Potters Bar, UK
Micronised formoterol fumarate dihydrate	Scior, Milan, Italy
Micronised salmeterol xinafoate	Merck Generics, Potters Bar, UK
Lactose monohydrate - Lactohale	Friesland Foods DOMO – Borculo, The Netherlands

It should be noted that, unless otherwise specified, for the remainder of this thesis, budesonide, fluticasone propionate, formoterol fumarate dihydrate and salmeterol xinafoate will be abbreviated to Bud, FP, FFD and SX, respectively.

2.2 Temperature-Controlled Dissolution of Carrier Lactose

The carrier lactose used in this study was subjected to a temperature-controlled dissolution process known as etching in order to reduce the proportion of intrinsic fines. This technique is described in detail elsewhere (El-Sabawi, Price et al., 2006), but will be briefly described here.

The carrier lactose (Lactohale) used in this study was sieved to obtain the 63-90 µm size fraction using stainless steel sieves (Endecotts Limited, London, UK) and an Analysette 3 PRO vibratory sieve shaker (Fritsch GmbH, Idar-Oberstein, Germany) set to an amplitude of 1 mm.

Saturated aqueous lactose solution of 400 ml was prepared and continuously stirred at the constant temperature of 20°C in a water-jacketed vessel. Approximately, 100 g of 63-90 µm Lactohale was added to the saturated lactose solution and etched by increasing the temperature to 25°C. From knowledge of the solubility versus temperature profile of lactose, this combination of variables was calculated to dissolve 10% of the initial mass of lactose (El-Sabawi, Price et al., 2006). After 24 hours of stirring at 25°C, the etched lactose was removed by filtration and washed several times with lactose saturated ethanol. Finally, it was spread out and allowed to air dry under ambient laboratory conditions (20-25°C and 30-40% RH) for seven days before using.

2.3 Scanning Electron Microscopy

2.3.1 Introduction

Drug and carrier morphology plays an important role on drug delivery in dry powder formulations (Timsina, Martin et al., 1994). Scanning electron microscopy (SEM) is used to characterise particle morphology of materials because particle morphology can affect formulation performance (Adi, Traini et al., 2008). SEM produces magnified images by using electrons instead of light waves (Brittain, Bogdanowich et al., 1991). An electron gun emits a beam of high energy electrons and this beam travels downward through a series of magnetic lenses designed to focus the electrons to a very fine spot. At the bottom, a set of scanning coils moves the focused beam back and

forth across the specimen, row by row. As the electron beam hits each spot on the sample, secondary electrons are knocked out from its surface. A detector counts these electrons and sends the signals to an amplifier. The final image is built up from the number of electrons emitted from each spot on the sample. Given the large amount of electrical energy, analysis is carried out in a vacuum and samples must be conductive. Non-conductive samples are coated with a thin layer of gold, a conducting material.

2.3.2 Method

Samples were fixed to sticky carbon tabs mounted on aluminium stubs and excess powder removed with a puff of air. The resulting particles were then coated with gold using a splutter coater (model S150B, Edwards High Vacuum, Sussex, UK) and examined using a scanning electron microscope (model JSM6310 or JSM6480LV, Japanese Electron Optics Ltd., Tokyo, Japan) at 10 kV.

2.3.3 Results and Discussion

2.3.3.1 Micronised Drugs

It can be observed from Figure 2.1 that inspection of SEM images of the four micronised drugs shows the different shape of particles produced from the micronisation process. Bud particles (Figure 2.1A and B) were more round with varying size range of particles, whereas FFD (Figure 2.1C and D), FP (Figure 2.1E and F), and SX (Figure 2.1G and H) particles shared a similar plate-like shape. The plate-like shapes of FFD and FP were also wider, whereas particles from SX had the narrow plate-like shapes. Most particles of FFD FP and SX exhibited in the form of agglomerates, while Bud particles tended to be more dispersed, suggesting that FFD, FP and SX powders were more cohesive. This may be attributable to post-micronisation conditioning of these Bud particles, which they may have been exposed to organic and/or water vapours to induce recrystallisation of surface amorphous domains, thus reducing powder cohesiveness.

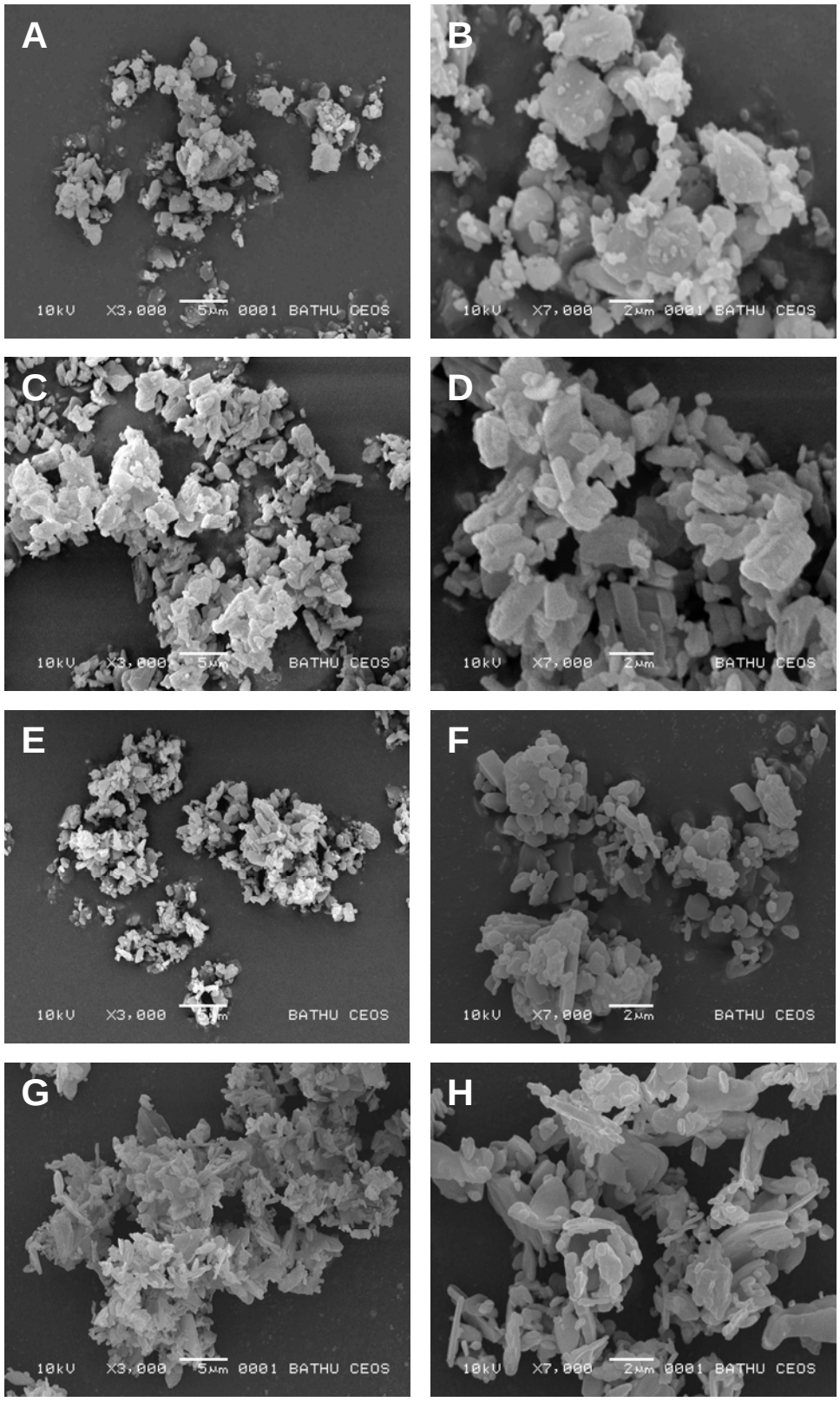

Figure 2.1: Representative SEMs of the four micronised drugs at x3000 and x7000 magnifications for A, B = Micronised Bud; C, D = micronised FFD; E,F = Micronised FP; G, H = Micronised SX

2.3.3.2 Lactose

Scanning electron micrographs of the lactose samples before and after etching are shown in Figure 2.2. For lactohale (Figure 2.2A and B), the coarse carrier particles exhibited the tomahawk shape typical of lactose monohydrate, whilst the intrinsic fines had a more round, irregular morphology. This suggests that intrinsic fines may be formed by the breakage from larger tomahawk-shaped crystals during powder processing, rather than during the crystallisation of the material. Further investigation reveals that the etched-lactohale sample (Figure 2.2C and D) contained fewer fine particles, both adhered and unadhered to the surface of the coarser particles. From these SEM results, it may be suggested that the method of temperature-controlled dissolution for carrier lactose can successfully apply to generate the smooth surface with less intrinsic fine particles.

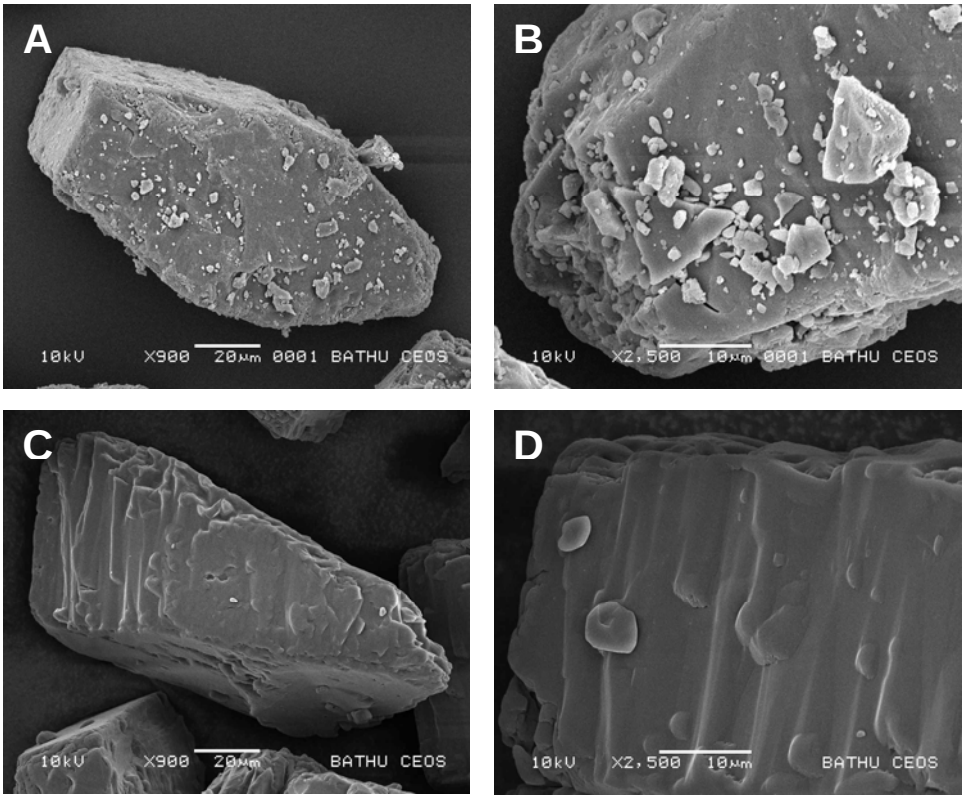

Figure 2.2: SEMs of the two lactose at x3000 and x7000 magnifications for: A, B = lactohale; C, D = etched lactohale

2.4 Particle Size Analysis

2.4.1 Introduction

It is well known that the particle size distribution of the drug and excipient in a carrier-based DPI formulation is crucial as they can affect both fluidisation properties of the formulations and the deposition profile in the lungs (Shur, Harris et al., 2008). Many different techniques for the measurement of a particle size distribution are available, for instance, sieving, microscopy, and impaction (Brittain, Bogdanowich et al., 1991). The technique chosen for use in this study is laser diffraction (low angle laser light scattering) as the ability of this method to rapidly and accurately measure the particle size of an ensemble of particles has led to a widespread use within the field of inhalation science (de Boer, Gjaltema et al., 2002; Guchardi, Frei et al., 2008).

Particle size analysis by laser diffraction is based on the principle that the light is scattered by particles in its path (Shekunov, Chattopadhyay et al., 2007). With smaller particles, the scattering light shows larger angles (Bosquillon, Lombry et al., 2001). A beam of coherent, monochromatic laser light, is directed at the particles to be sized and then, the pattern and intensity of the scattered light detected. When a sample with a polydisperse particle size distribution is analysed, the resultant scattering pattern is achieved by integration of the scattering patterns of the particles. This pattern can then be used to derive a volume-weighted distribution of volume equivalent diameters by applying one of several mathematical models which describes the scattering of light by particles and the comparison of experimental and theoretical diffractograms (Shekunov, Chattopadhyay et al., 2007).

These phenomena can be described by the Fraunhoffer diffraction or Mie theory. Mie theory requires knowledge of the refractive index of the particles and makes the assumption that they are smooth spheres (Mie, 1908). The Mie theory states that the induction of light scattering is triggered by the difference between the refractive indices of the particle and the surrounding medium (Mie, 1908). It can be difficult to apply Mie theory for the derivation of the particle size distribution of pharmaceutical materials, due to their variable shape, roughness and unknown refractive index. In these situations and when particle size is significantly greater than the wavelength of the light, it can be considered more appropriate to apply the Fraunhofer approximation to derive

the particle size distribution (Shekunov, Chattopadhyay et al., 2007). This technique only describes the diffraction of light at the contour of the particle and makes the assumptions that only forward light scattering occurs and the particle size is much larger than the wavelength of the light (Shekunov, Chattopadhyay et al., 2007). Therefore, the Fraunhofer approximation is applied to derive particle size distribution.

2.4.2 Method

Particle sizing was carried out in wet cell with a small quantity of the particles being re-dispersed in a 0.1% w/v of lecithin (BDH Ltd., Poole, UK) in cyclohexane by sonicating for 5 minutes. The resultant suspension was then diluted down to 50 ml in the cuvette and particle size measured using a HELOS laser diffraction sensor (Sympatec GmbH, Clausthal-Zellerfeld, Germany). The particle size analysis was performed using WINDOX 4.0 software (Sympatec GmbH, Clausthal-Zellerfeld, Germany). Size distribution and values presented are the average of three determinations.

2.4.3 Results and Discussion

2.4.3.1 Micronised Drugs

Inspection of the particle size distribution of the micronised drugs (Figure 2.3) shows the cumulative distribution of micronised Bud, micronised FFD, micronised FP and micronised SX. The cumulative distribution for such four micronised drugs all indicated narrow distribution. As seen from Figure 2.3, micronised FP had a slightly broader distribution than micronised Bud, FFD and SX. In addition, the data were summarised using the d_{10}, d_{50} and d_{90} values shown in Table 2.2. It is apparent that d_{50} values of micronised Bud, FFD, FP and SX are 2.21, 2.42, 3.28 and 2.13 µm, respectively. From the results of d_{50} values, these four micronised drug particles confirm the suitable size range for a DPI formulation.

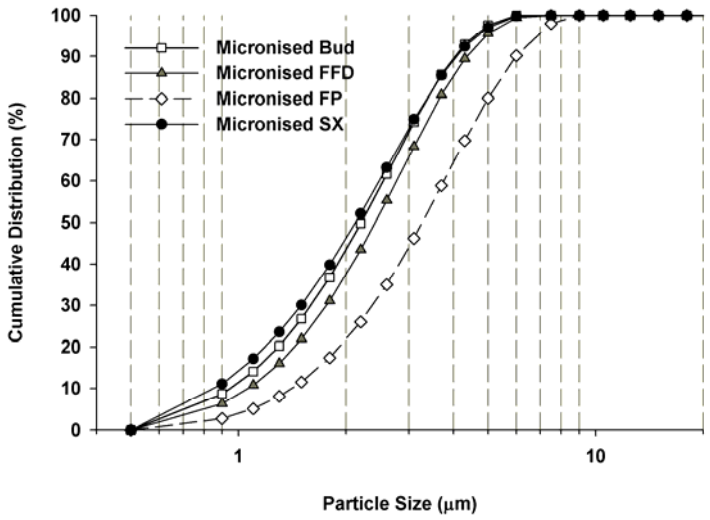

Figure 2.3: Particle size distribution of four micronised drugs

Table 2.2: Summary particle size statistics of the micronised drugs

	$d_{10\%}$ (µm) ± SD	$d_{50\%}$ (µm) ± SD	$d_{90\%}$ (µm) ± SD
Micronised Bud	0.95 ± 0.00	2.21 ± 0.01	4.06 ± 0.00
Micronised FFD	1.07 ± 0.00	2.42 ± 0.00	4.36 ± 0.01
Micronised FP	1.41 ± 0.00	3.28 ± 0.00	5.98 ± 0.00
Micronised SX	0.86 ± 0.00	2.13 ± 0.00	4.09 ± 0.01

2.4.3.2 Carrier Lactose

Inspection of the particle size distribution of the carrier lactose before and after etching (Figure 2.4) reveals that the cumulative distribution patterns of both were similar. The particle size statistics of 63-90 µm of lactohale before and after etching are also shown in the table 2.3 by using the d_{10}, d_{50} and d_{90} values. The d_{50} values of the lactose before and after etching appear in the size of 90.05 and 82.15 µm. It can be suggested that the etching process did not generate the dramatic change in the size of lactose particles. During etching process, the surface rearrangement of the lactose particles can happen and it is possible that this process may cause a slightly smaller particle

size and smoother surface on lactose particles with less level of fine lactose material via the d_{10}.

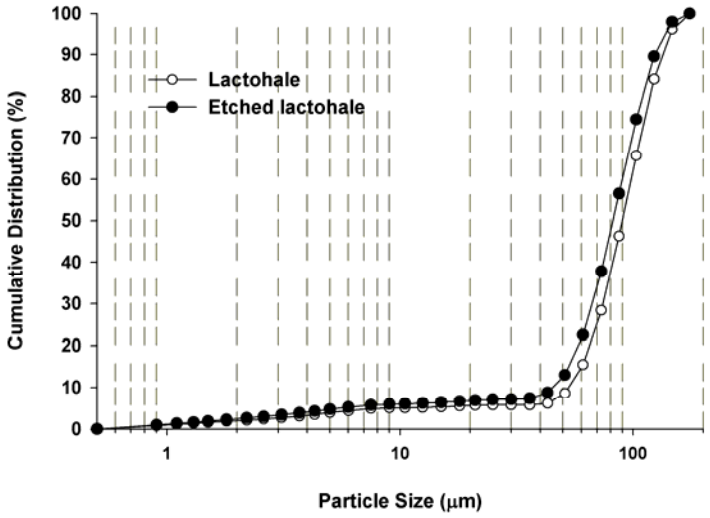

Figure 2.4: Particle size distribution of 63-90 μm of lactohale before and after etching

Table 2.3: Summary particle size statistics of 63-90 μm of lactohale before and after etching

	$d_{10\%}$ (μm) ± SD	$d_{50\%}$ (μm) ± SD	$d_{90\%}$ (μm) ± SD
Lactohale	53.07 ± 0.19	90.05 ± 0.14	134.99 ± 0.07
Etched lactohale	45.36 ± 0.17	82.15 ± 0.21	124.38 ± 0.44

2.5 Differential Scanning Calorimetry

2.5.1 Introduction

Differential scanning calorimetry (DSC) is used to investigate the identity and crystallinity of many pharmaceutical materials (Buckton, 1997). DSC measures energy differences associated with chemical and physical changes in the sample including crystallisation, melting, and decomposition in relation to changing temperature (Duncanhewitt and Grant, 1986). This is achieved by measuring the heat flow required

to maintain the sample and reference at the same temperature during heating and cooling (Buckton, 1997). There are two types of DSCs in common use. In a power compensated DSC, the temperatures of the sample and reference are controlled independently using separate furnaces (Wendlandt, 1986). Temperature differences of the sample and reference are made identical by varying the power input to the two furnaces; this energy difference is calculated as a function of sample temperature. In a heat flux DSC, which was used in this study, a single furnace is utilised so the sample and reference are heated by a single source. Enthalpy changes in the sample cause a difference in its temperature relative to the reference (Wendlandt, 1986).

2.5.2 Method

Study material thermal properties were investigated using a differential scanning calorimeter (DSC 2920, TA Instruments, Surrey, UK) calibrated with indium standards. For most materials, approximately 1-5 mg of the sample was accurately weighed into an aluminium pan and crimped with a lid to form a hermetic seal. The sample and reference (identical, but empty, hermetically sealed pan) were heated at the rate of $10^{\circ}C.min^{-1}$ from $30^{\circ}C$ to $350^{\circ}C$. The calorimeter head was flushed with dry nitrogen gas at $0.2\ L.min^{-1}$ during all measurements.

2.5.3 Results and Discussion

2.5.3.1 Micronised Drugs

The DSC thermogram of the micronised Bud sample (Figure 2.5A) shows an endothermic response at ~262°C, which is typical of the melt with decomposition seen for crystalline Bud (Velaga, Berger et al. 2002). The thermogram relating to micronised FFD (Figure 2.5B) was more complicated with three endothermic peaks at ~113°C, ~129°C and ~144°C. The literature does not contain a FFD thermogram for comparison. However, it is known that FFD may be thermally dehydrated. Formoterol anhydrous polymorph A melts at the range 125-129°C (Jarring, Larsson et al. 2006) and formoterol anhydrous polymorph B melts at the range 143-148°C (Jarring, Larsson et al. 2006). Therefore, the first endothermic peak represented dehydration and the second peak at ~129°C showed the melting of anhydrous polymorph A. The third peak was the melting of anhydrous of polymorph B.

The micronised FP thermogram in Figure 2.5C was similar to Bud with a single endothermic peak at ~290°C. For SX thermogram (Figure 2.5D), the peak was also complex. Endothermic peaks were detected at ~126°C and ~141°C and an exothermic peak at ~132°C appeared in the DSC thermogram. The first endothermic event at ~126°C represents the melting of SX form I, which recrystallises to SX form II at ~132°C before melting again at ~141°C. Micronisation of SX form I is thought to induce the formation of trace seeds of SX form II, which enables this recrystallisation to occur (Beach, Latham et al., 1999; Tong, Shekunov et al., 2003).

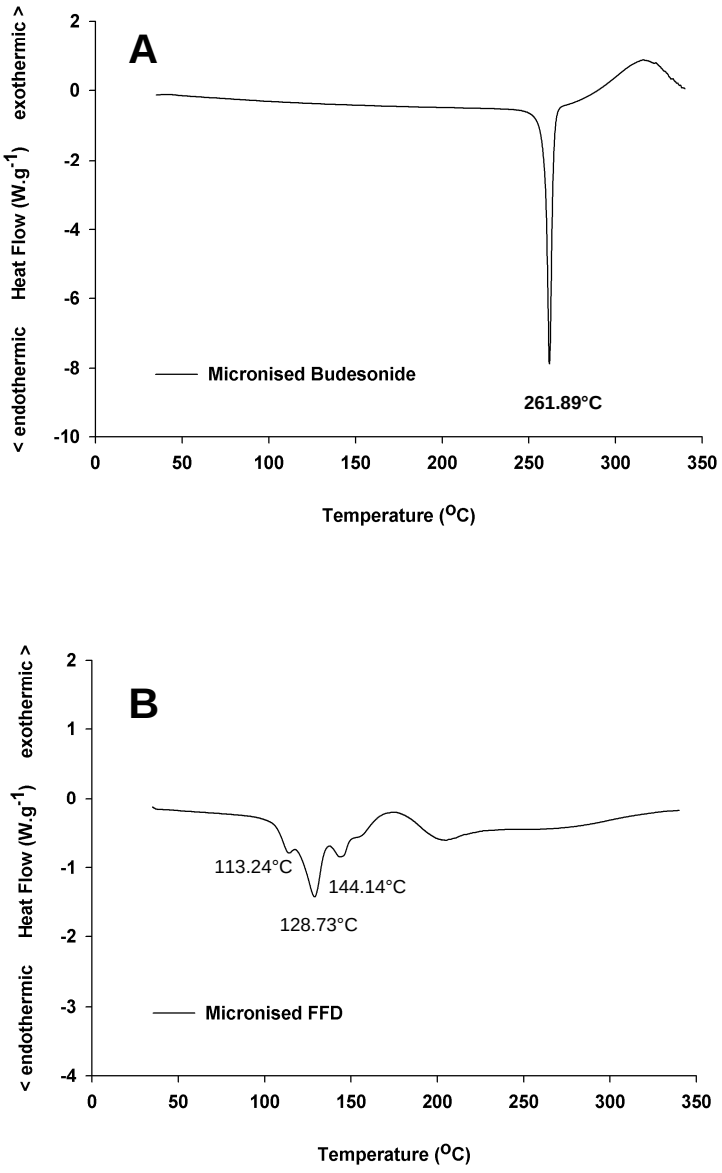

Figure 2.5 (continued on next page): DSC thermograms of the four micronised drugs

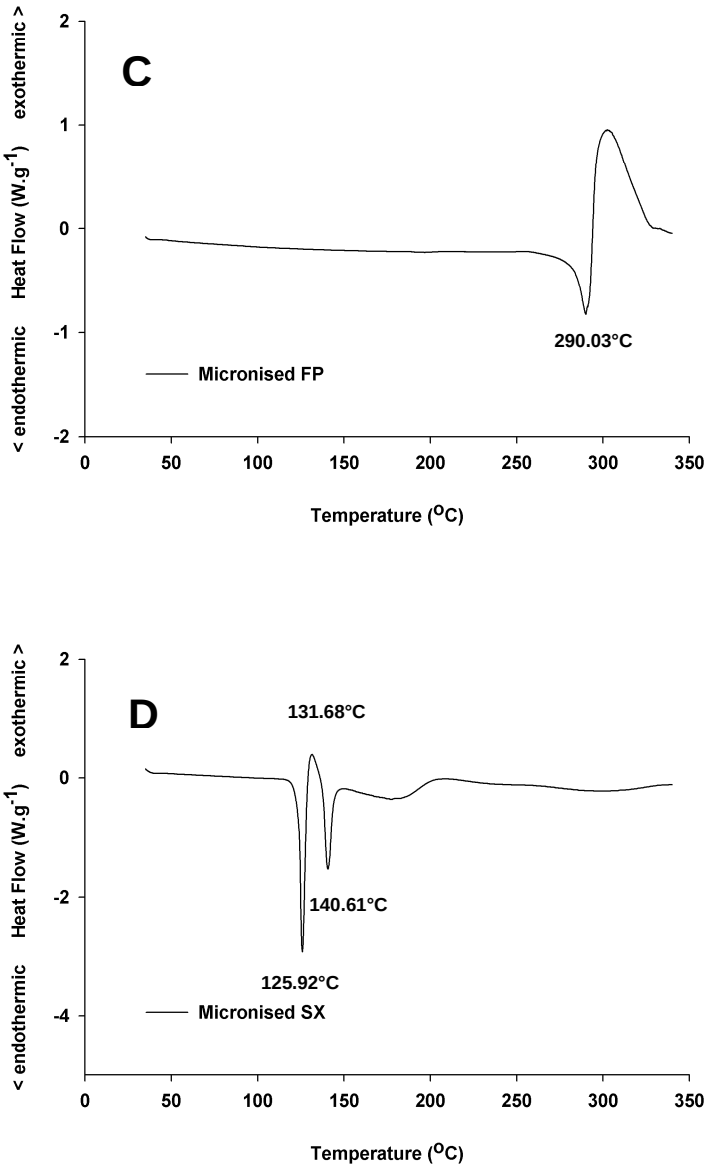

Figure 2.5 (continued from previous page): DSC thermograms of the four micronised drugs

2.5.3.2 Carrier Lactose

The thermograms of the lactohale carrier before and after the dissolution process are very similar (Figure 2.6), confirming that this process did not bring about any changes in the lactose crystal structure. In comparison with literature, thermograms also confirmed that the materials were α–lactose monohydrate (Angberg 1995). The endothermic peaks at ~140°C exhibited dehydration and the endotherms between 210 and 215°C showed the melting of α–lactose (Angberg 1995).

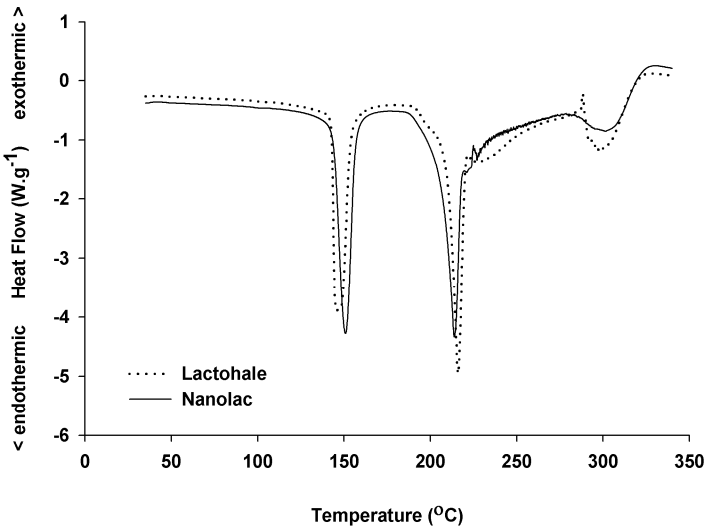

Figure 2.6: DSC thermograms of the lactohale before and after etching

2.6 X-Ray Powder Diffraction

2.6.1 Introduction

X-ray powder diffraction (XRPD) is used to confirm the identity and crystallinity of the study materials (Buckton, 1997). Every crystalline form of a compound has a unique X-ray powder pattern. XRPD was, therefore, utilised to identify the respective polymorphic forms of the compounds (Suryabarayanan, 1995). More importantly, this is necessary as amorphous materials are thermodynamically unstable and have a propensity to recrystallise during storage (Buckton, 1997).

A parallel and monochromatic X-ray beam incident on a crystalline solid is scattered in all directions. At certain angles, the scattered radiation is in phase with itself and so is reinforced (Suryabarayanan, 1995). This phenomenon occurs whenever Bragg's law is satisfied:

$$n\lambda = 2d_p \sin\theta \qquad \text{Equation 2.1}$$

where n is an integer (the order of reflection), λ is the wavelength of the X-rays, d_p is the distance between the planes of the crystal and θ is the angle between the incident X-rays and the crystal surface (Suryabarayanan, 1995).

Every crystalline solid leads to the diffraction of X-rays at a unique combination of angles, enabling identification of the material and its polymorph. In addition, amorphous materials do not create scattering at well defined angles, allowing them to be distinguished from crystalline samples. XRPD can be able to detect amorphous content at the lower limit of approximately 10% w/w (Buckton, 1997).

2.6.2 Method

XRPD spectra were obtained using a Phillips analytical X-ray powder diffractometer (Cambridge, UK) with a CuK$_\alpha$ source ($\lambda = 1.5418\,\mathring{A}$) operated at 40 kV and 25 mA. A single sweep between diffraction angles (2θ) 5˚ and 50˚ with a step size of 0.02˚ and step time of 13 seconds was employed for each measurement.

2.6.3 Results and Discussion

2.6.3.1 Micronised Drugs

The presence of distinct peaks in the XRPD spectra of the four micronised drugs (Figure 2.7) suggests that they had a predominately crystalline structure. Additionally, the spectra are comparable with previously published data for these materials, confirming their identity as Bud (Steckel, Pichert et al. 2004), FFD (Apperley, Harris et al. 2003; Jarring, Larsson et al. 2006), FP form I (Louey, Van Oort et al. 2004), and SX

form I (Beach, Latham et al. 1999; Tong, Yu Shekunov et al. 2001; Shekunov, Feeley et al. 2002; Murnane, Marriott et al. 2008).

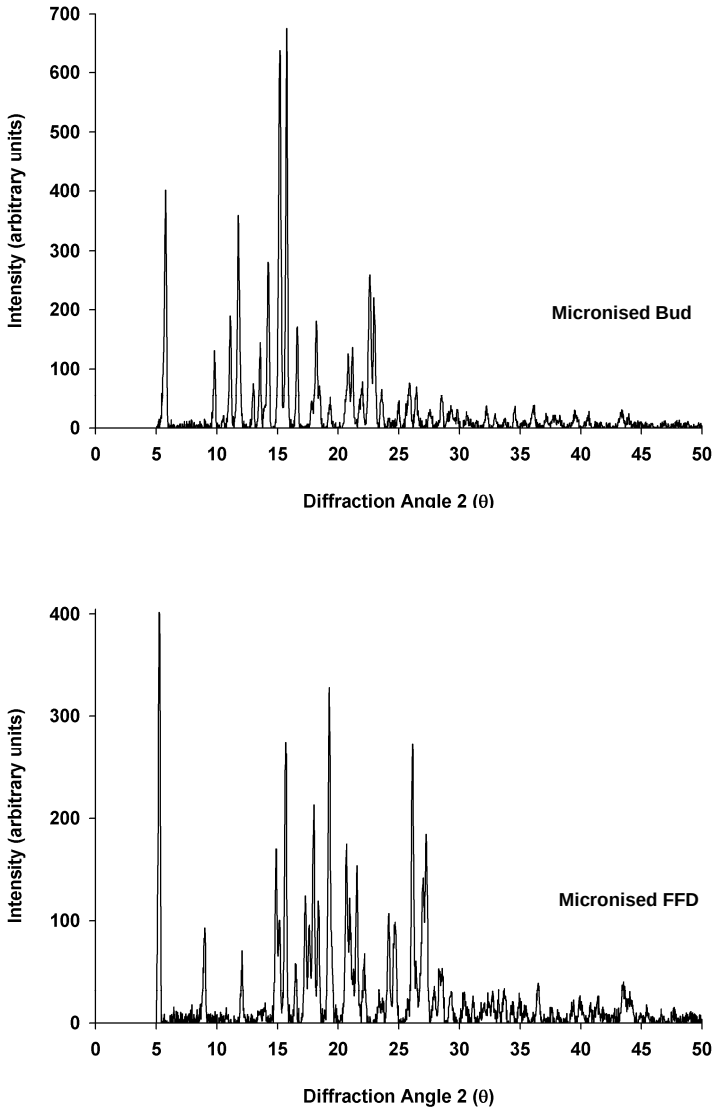

Figure 2.7 (continued on next page): XRPD spectra of the four micronised drugs used in this study

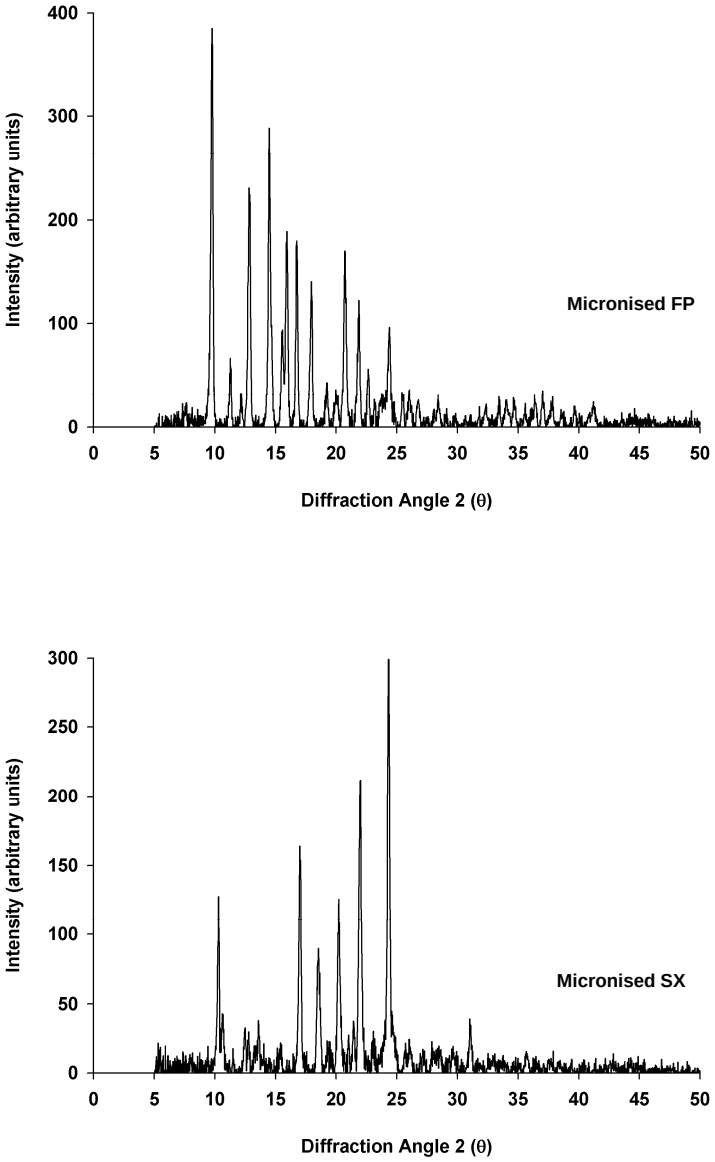

Figure 2.7 (continued from previous page): XRPD spectra of the four micronised drugs used in this study

2.6.3.2 Carrier Lactose

As shown in Figure 2.8, the XRPD spectrum of the lactohale carrier was unchanged by the etching process, confirming that this procedure did not bring about any change to the lactose crystal structure. Once again, the presence of distinct peaks confirmed that both materials were largely crystalline and, in comparison with the previously published data, spectra also confirmed the identity as lactose monohydrate (El-Sabawi, Price et al., 2006).

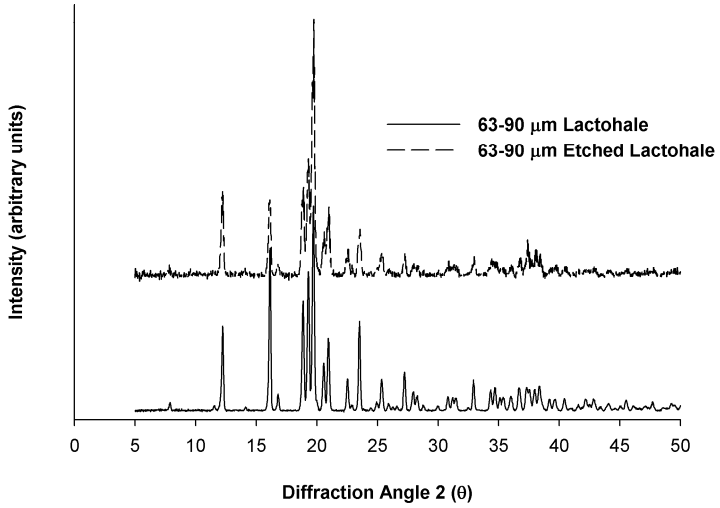

Figure 2.8: XRPD spectra of lactohale carrier before and after dissolution process

2.7 Dynamic Vapour Sorption

2.7.1 Introduction

Dynamic vapour sorption (DVS) is generally used to investigate the effect of humidity on the water sorption and desorption of materials (Buckton, 1997). The hydrophilic/hydrophobic nature of materials may affect interparticulate forces, therefore, DVS is widely applied to investigate the stability and crystallinity of a material at elevation conditions of relative humidity (% RH) (Young, Edge et al., 2005).

A DVS instrument employs a Cahn microbalance housed within a temperature-controlled incubator. The twin pans of the microbalance (one for the sample, one as a reference) are contained within glass cells perfused with nitrogen, the relative humidity

of which is controlled by a mass flow controller that mixes dry and water saturated gas (Buckton and Darcey, 1999).

The instrument can be used to measure changes in sample mass upon exposure to varying humidity. Amorphous materials are thermodynamically unstable, which enables their detection by DVS as they absorb water molecules from the atmosphere during the experiment (Pfeiffer-Brodka, Langguth et al., 2003). This relates to the plasticisation of the amorphous phase, progressively lowering its glass transition temperature until it falls below the experimental temperature. At this point, molecules in the amorphous phase have sufficient mobility to align and so recrystallise, resulting in the expulsion of the absorbed vapour, which can be seen as a rapid loss of mass on the DVS trace (Buckton, 1997). The presence of amorphous materials can be deduced from DVS traces showing >1% mass increase or rapid mass loss with increasing humidity (Buckton, 1997).

2.7.2 Method

DVS experiments were performed with a DVS-1 instrument (Surface Measurement Systems Ltd., London, UK). An appropriate amount of sample (see Table 2.4) was weighed into the sample pan and its mass continually recorded during exposure to two humidity cycles of 0-90% RH in 10% RH steps at 25°C. Equilibrium mass, as defined by a specific change in mass to time ratio (dm/dt, see Table 2.4), was achieved for ten minutes before progression to the next step of the cycle.

Table 2.4: DVS sample masses and equilibrium conditions for various materials

Material	*Approximate Sample Mass (mg)*	*Equilibrium dm/dt (%)*
Micronised drugs	50	0.0002
Lactohale	100	0.0005
Etched Lactohale	100	0.0002

2.7.3 Results and Discussion

2.7.3.1 Micronised Drugs

None of the DVS moisture sorption isotherms of the micronised drugs (Figure 2.9) showed >1% w/w mass increase or a mass loss during the first sorption cycle, indicating very low levels of amorphicity. Bud, FP and SX each had a mass increase of ~0.1% w/w at 90% RH.

FFD showed a rapid increase in mass by ~0.13% w/w at 10% RH followed by only ~0.15% w/w mass increase between 10% and 90% RH. This suggests that reversible partial dehydration of the formoterol fumarate dihydrate may occur at very low humidities, but once rehydrated, the material shows similar adsorption properties to the other drugs, although it is thought that FFD is stable at low humidities and ambient temperatures (Jarring, Larsson et al. 2006). However, at 50% RH of the first cycle sorption, the sorption isotherm tended to drop down from 0.2% to 0.15% mass decrease and then the mass change came up to 0.25% at 90% RH. This event suggests that the process of recrystallisation may happen after FFD is rehydrated.

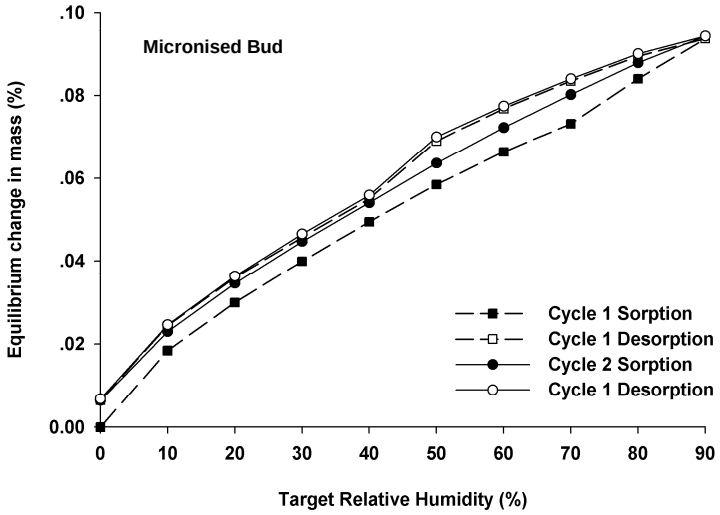

Figure 2.9 (continued on the next two pages): DVS moisture sorption isotherms at 25°C for the four micronised drugs

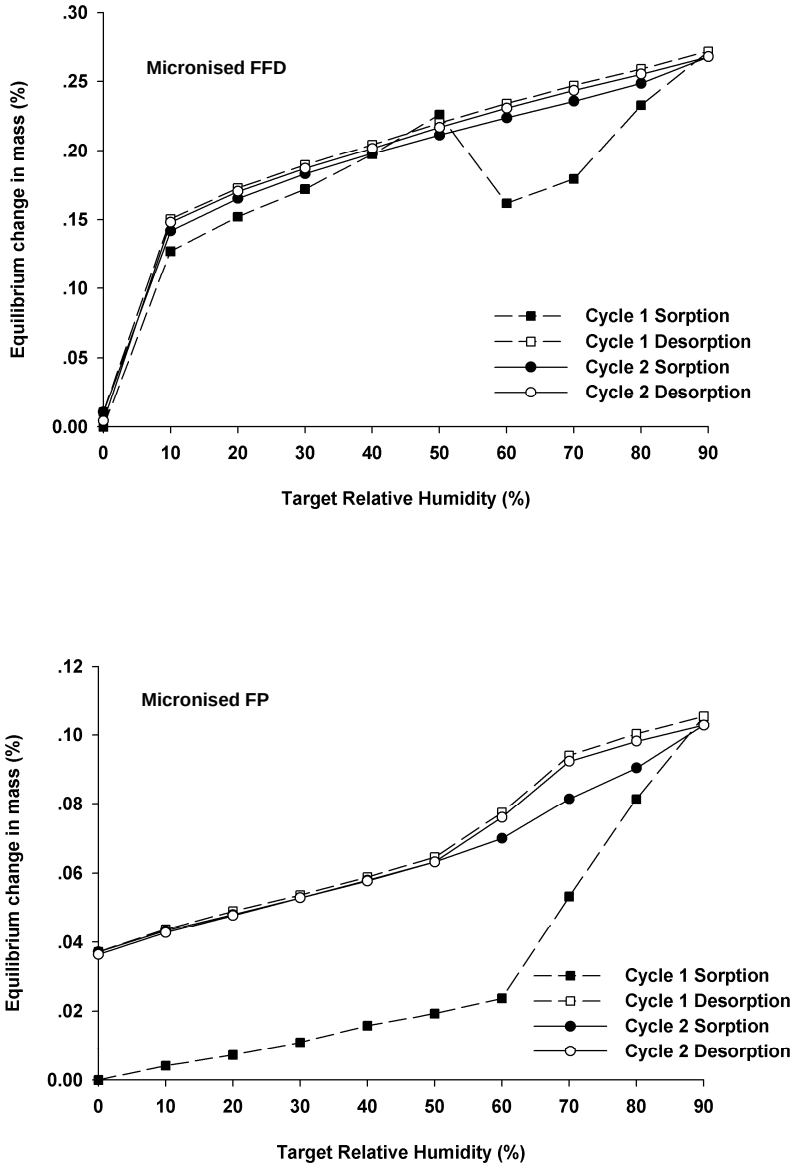

Figure 2.9 (continued from previous page): DVS moisture sorption isotherms at 25°C for the four micronised drugs

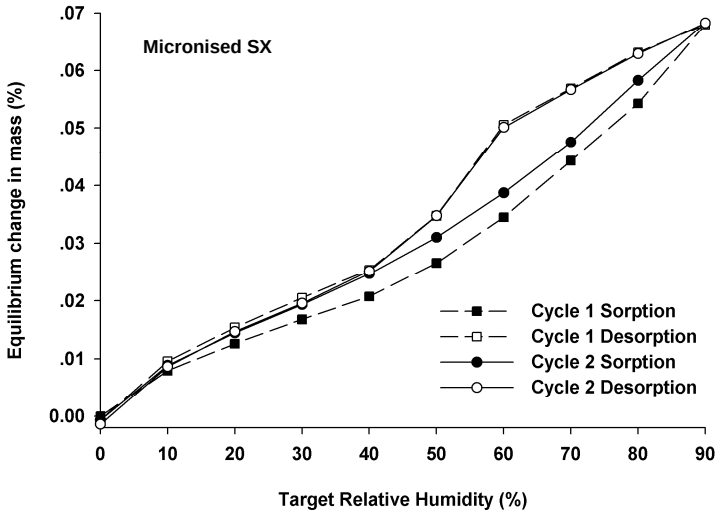

Figure 2.9 (continued from previous page): DVS moisture sorption isotherms at 25°C for the four micronised drugs

2.7.3.2 Carrier Lactose

The DVS moisture sorption isotherms for the lactose carrier (Figure 2.10), both before and after etching, did not show >1% w/w mass increase or a mass loss during the first sorption cycle, so no amorphous material was detected. Lower levels for the etched lactose may be related to the decrease in surface area due to the removal of fines and the reduction in surface roughness of the coarse carrier.

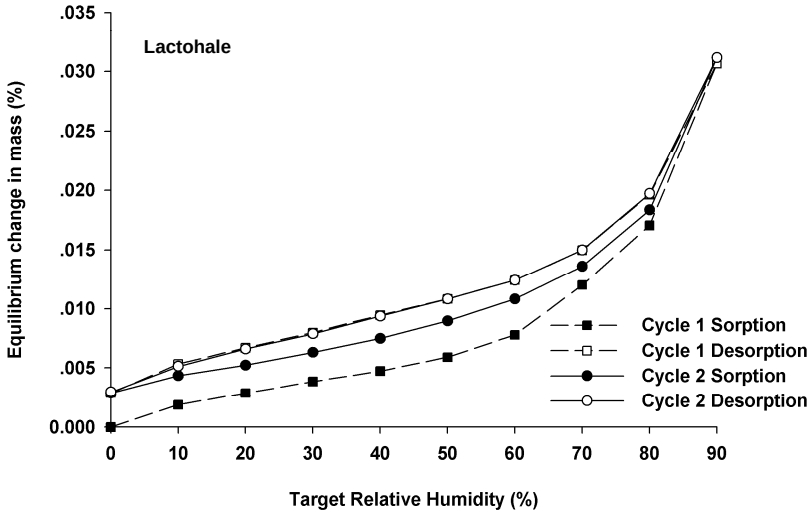

Figure 2.10 (continued on next page): DVS moisture sorption isotherms at 25°C for the carrier lactose before and after etching

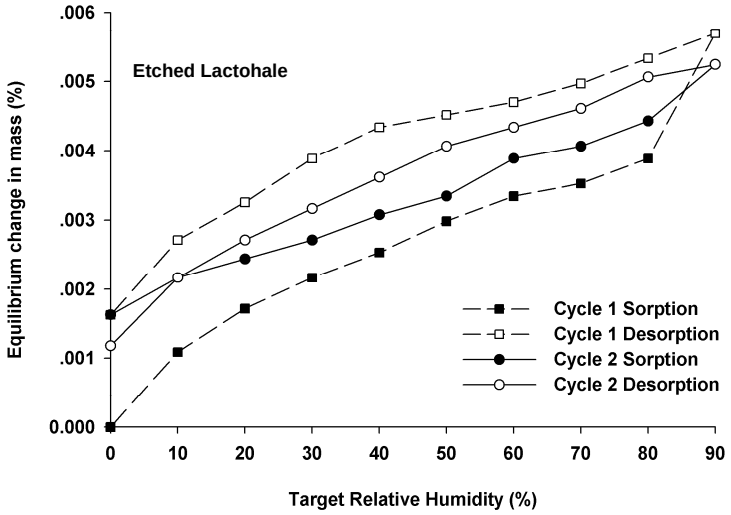

Figure 2.10 (continued from previous page): DVS moisture sorption isotherms at 25°C for the carrier lactose before and after etching

2.8 Conclusions

The physicochemical characterisation of the materials was investigated using an array of analytical methods. Moreover, similarities and differences in the physical properties of such materials were also investigated. The supplied micronised drugs were similar to each other in terms of particle size and shape. The differences between materials characterised using DVS, DSC and XRPD were observed. Similar techniques were also used to investigate the physicochemical properties of the carrier lactose. The process of etching lactose did not affect the anomeric form of the material, however, the fines content of the etched lactose was lower than that of the as-supplied material. Importantly, the physicochemical characterisation of the pharmaceutical materials shown in this chapter will be compared to those of SAX-engineered particles in the following chapters.

Chapter 3: Particle Engineering using the SAX Process

3.1 Introduction

Particle processing technologies are vital for the generation of fine particles in the 1–5 µm particle size range for delivery to the lungs. This can be implemented by a number of constructive and destructive methods although pharmaceutical scientists tend to employ the latter (Feeley, York et al., 1998). The most common destructive method used is air jet milling, which shatters large crystalline particles to reduce their size (Malcolmson and Embleton, 1998). Such pharmaceutical processing is inefficient and it remains difficult to control key physicochemical properties of the resultant particles, which may lead to downstream problems with drug product performance and stability (Vogel and Peukert, 2004). As a result, particle engineering processes have been widely explored to generate particles for inhaled drug delivery systems with defined functionality (Broadhead, Rouan et al., 1992; York, 1999; Li, Seville et al., 2005). Most techniques such as spray drying (Broadhead, Rouan et al., 1992; Li, Neill et al., 2003), spray freeze drying (Maa, Nguyen et al., 1999) and supercritical fluid technology (Jung and Perrut, 2001) have been applied.

Recently, Kaerger and Price showed that the novel development of a solution atomisation and crystallisation by sonication (SAX) technology enabled significant control in the engineering of respirable sized particles (Kaerger and Price, 2004). The SAX process, as described by Kaerger and Price (Kaerger and Price, 2004), consists of three key stages that included: solution atomisation to produce aerosol droplets of the solute from a carrier solvent using a suitable aerosol generator; generation of highly supersaturated droplets by evaporation of carrier solvent from aerosol droplet; and collection of droplets in a crystallisation vessel containing an appropriate non-solvent with the application of ultrasonic waves to the crystallisation vessel. The choice of non-solvent is dependent on the material that is to be processed and should preferably be miscible with the carrier solvent in which the drug is solubilised. Furthermore, the surface tension of the non-solvent should be low or minimised to prevent structural change of the droplets upon collection in the crystallisation vessel.

The formation of crystalline particles on collection of highly supersaturated droplets may be kinetically restricted due to the level of viscosity within the droplets. To enhance the molecular mobility to induce crystallisation, the SAX process utilises ultrasonic energy, which is understood to reduce the metastable zone width for nucleation (Lorimer and Mason, 1987; Ruecroft, 2007). Ultrasonic energy provides sufficient kinetic energy for the formation of a stable cluster of molecules for crystal growth, which is achieved through the formation of cavitations on application of ultrasonic energy (Ruecroft, 2007). The implosion of cavitations generates areas of extremely high pressure and temperature over a short time interval, which induces an increase in the diffusion of the drug molecules within the viscous droplets and a concomitant decrease in the activation energy barrier for the formation of a stable nucleus or nuclei for crystal growth (Lorimer and Mason, 1987). Crystallised particles are subsequently collected from the non-solvent by filtration of the resulting suspension. Product isolation from the non-solvent by means of filtration is inefficient and may have detrimental effects on the morphology and flowability of SAX-processed particles. This remains a key difficulty of the first generation SAX process. Hence, more robust and efficient means of powder isolation are required.

The early studies by Kaerger and Price showed that the SAX technology had 'dial-a-particle' potential, where key process parameters could be modified and controlled to generate particles of desired functionality (Kaerger and Price, 2004). However, despite being able to produce micron-sized crystalline particles, the first generation SAX process was not robust and efficient. Furthermore, the system was difficult to manipulate to generate different types of particles in sufficient quantities.

This chapter explores the further development of the SAX process as a technology that possesses 'dial-a-particle' properties. Key factors that affect the size, shape and morphology of the resultant particles are also investigated. The SAX-produced particles are characterised using scanning electron microscopy (SEM), particle size analysis, differential scanning calorimetry (DSC) and X-ray powder diffraction (XRPD) to ensure the suitable physical properties of the particles, which are related to appropriate conditions that result in the generation of particles with defined properties.

3.2 Materials

Micronised budesonide was obtained from the suppliers listed in Chapter 2. All organic solvents were of at least analytical grade and were supplied by Fisher Chemicals (Loughborough, UK). Water was prepared by MilliQ from reverse osmosis (Molsheim, France). Nylon filter membranes from Whatman International Ltd. (Maidstone, UK) with pore size 0.45 µm were used in the study.

3.3 Methods

3.3.1 The SAX Apparatus Set-Up

The SAX process consists of three interdependent steps (Kaerger and Price 2004). These three main steps include atomisation, generation of highly supersaturated droplets and collection of droplets in a non-solvent. In the process of atomisation, small aerosol droplets of the drug solution are generated using an appropriate atomiser. This step is followed by the collection of the highly supersaturated droplets in a crystallisation vessel containing a non-solvent of the drug. The final step is the crystallisation; the application of ultrasonic energy in a crystallisation vessel is used for inducing homogeneous nucleation and crystal growth.

3.3.1.1 Laboratory-Scale SAX System

The laboratory-scale SAX (lab-scale SAX) process was predominately fabricated from glass as shown in Figure 3.1 and 3.2. The key strategy for particle production using the SAX process involved the controlled production of supersaturated droplets. Such droplets were then collected and exposed to ultrasonic energy to help induce nucleation and crystal growth of crystalline particles with defined morphology and size. The lab-scale SAX process used a pneumatic atomiser (Büchi Mini Spray Dryer B-191, Flawil, Switzerland), operated with compressed air consumption at 600 $L.h^{-1}$, to produce micron-sized droplets from the drug solution; the system operated under at positive N_2 air pressure with vertical laminar flow. This increased the evaporation rate of the solvent inside droplets, which aided the formation of supersaturated droplets for

producing crystalline drug particles. In addition, the air flowed through a ‘bubbler’ tube containing small holes, which enabled the deposition of the droplets in the non-solvent.

The separation distance between the atomiser and non-solvent was set in order to have the sufficient evaporation of the droplets for generating of highly supersaturated droplets. The appropriate separation distance at 60 cm between the atomiser and the surface of the non-solvent was, therefore, selected in this process. Under these conditions, the highly supersaturated droplets were removed from the airflow and into the non-solvent using a ‘bubbler’ immersed in the non-solvent. The temperature of the non-solvent in which the droplets were collected was controlled using a temperature-controlled vessel (Haake K20 from Thermo Haake, Karlsruhe, Germany). Finally, the ultrasonic energy was supplied using an ultrasonic probe immersed in the non-solvent set at 20 kHz (Sonic processor P100, Sonic system, Somerset, UK). The probe induced nucleation through the mechanism of cavitation and created crystalline particles in the collecting vessel.

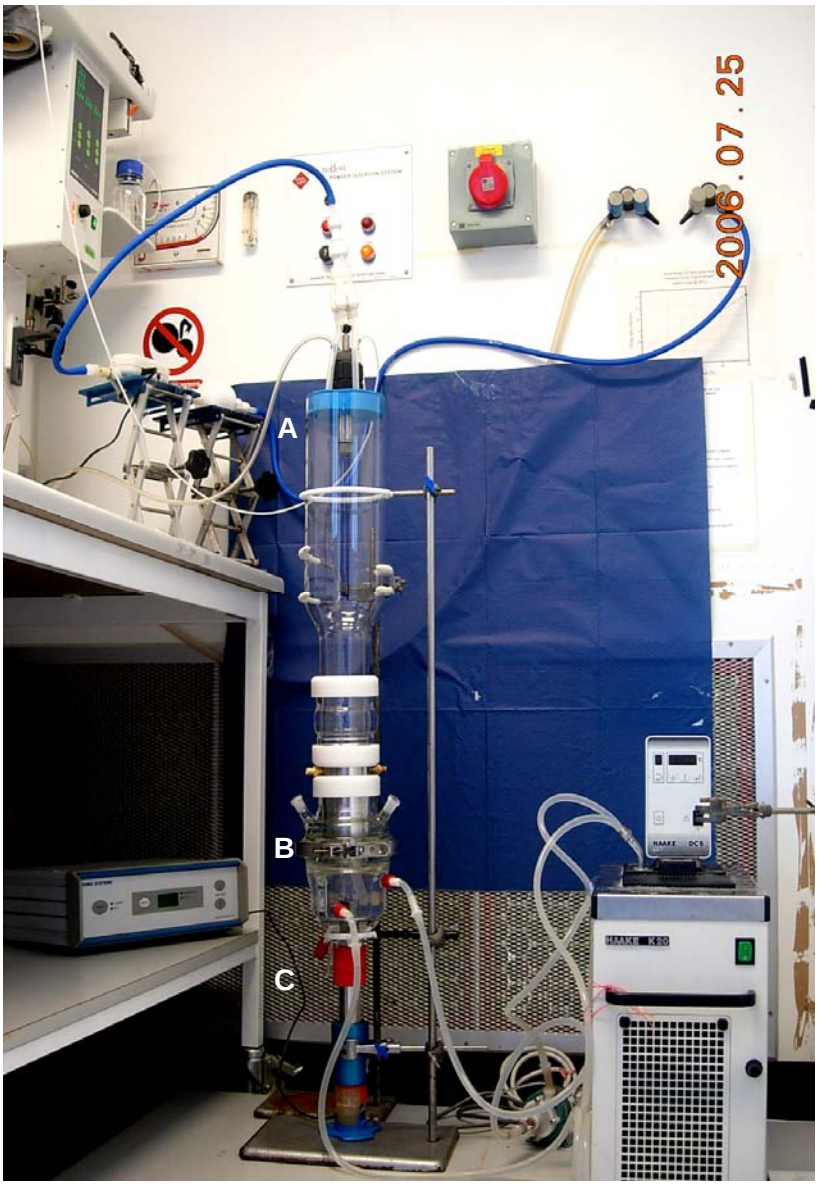

Figure 3.1: The image of the lab-scale SAX experimental set-up

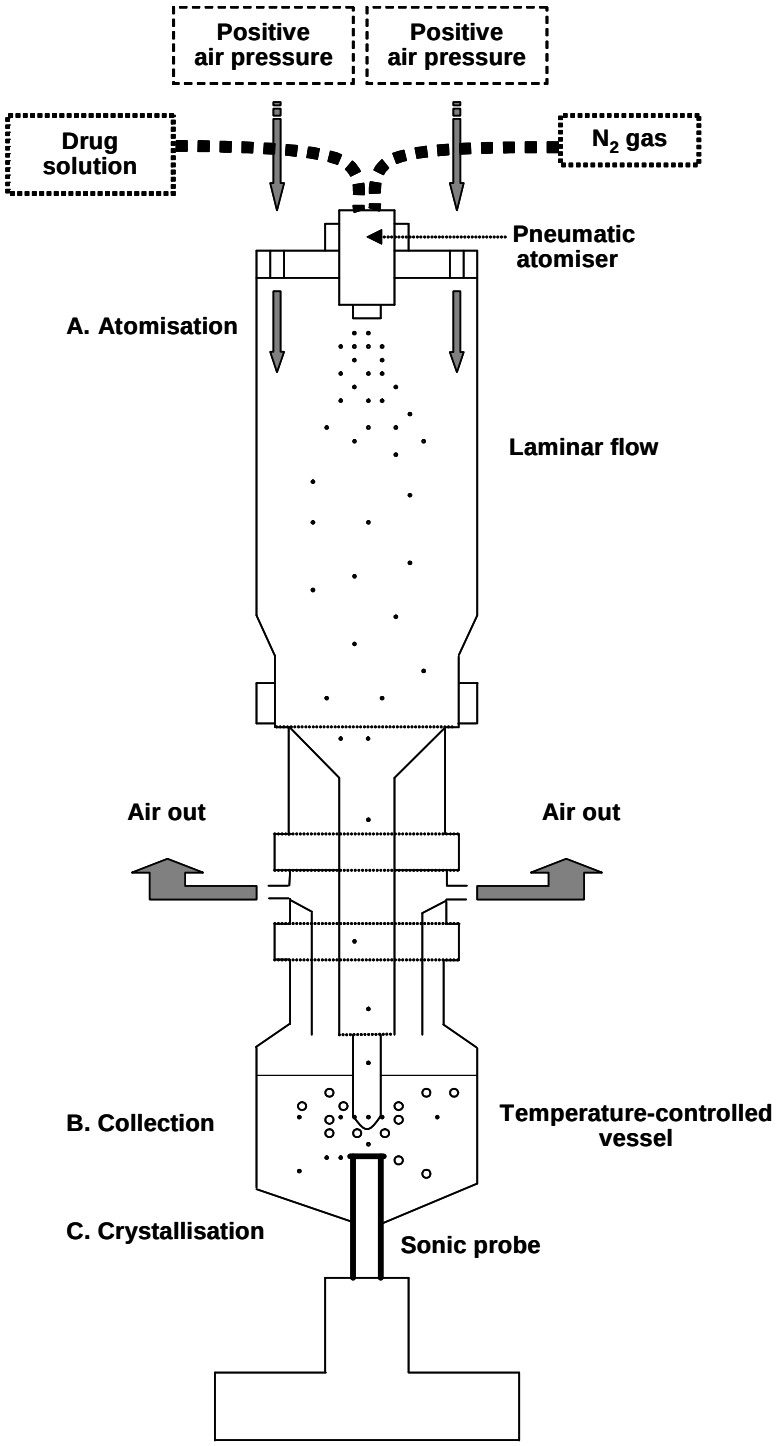

Figure 3.2: Schematic diagram of the lab-scale version of the SAX experimental set-up

3.3.1.2 Isolation of SAX-Processed Particles from the Non-solvent using Supercritical Fluid-Carbon dioxide (SCO_2) Solvent Extraction

A supercritical fluid can be defined as a substance existing as a single fluid phase above its critical temperature (T_c) and pressure (P_c) (Kajimoto, 1999). Supercritical fluids exhibit interesting physicochemical properties that can vary between liquid-like and gas-like characteristics. These features enable supercritical fluids to possess higher diffusivity, and lower surface tensions and viscosities than liquid solvents (York, 1999). Furthermore, the densities of supercritical fluids can be varied between gas-like and liquid-like values in a controlled manner by changing the temperature and pressure conditions, which enhance their salvation power and mass transfer rates compared with those of liquids (Eckert, Knutson et al., 1996). Carbon dioxide (CO_2) is the most widely used supercritical fluid solvent because it has easily accessible critical parameters (T_c = 31.1˚C; P_c = 73.8 bar) and is generally regarded as having safe (GRAS) status (Jung and Perrut, 2001). Moreover, it is also relatively inexpensive and non-toxic.

Supercritical fluids have been widely employed for the extraction of compounds such as hydrocarbons, oils, nutraceuticals and pharmaceuticals (Eckert, Knutson et al., 1996; York, 1999; Sievers, Milewski et al., 2000; Jung and Perrut, 2001). The objective of supercritical fluid extraction (SFE) is to isolate specific compounds by removal of the solvent (Sievers, Milewski et al., 2000). For this to be achieved, the compound to be extracted should be insoluble in the supercritical fluid. In some cases, the material to be isolated is a solid that is suspended in a liquid. In this situation, the liquid solvent must be completely soluble in SCO_2 to enable the removal of the liquid, whereas the solids must have completely insolubility in the supercritical fluid to aid isolation of the solid material. It must be noted that this process is not a particle formation or crystallisation step, and is purely related to the extraction of the solid component suspended in the liquid non-solvent.

A schematic representation of the SFE rig applied in this study is shown in Figure 3.3. The extraction of the non-solvent hexane and isolation of SAX particle were carried out using a 150 ml volume extraction vessel. The supercritical fluid delivery system consisted of a liquid CO_2 pump (P-500, Thar Technologies, Inc., Pittsburgh, PA, USA) and a heat exchanger, which provided SCO_2 to the bottom of the extraction column through a 0.2 µm porous membrane at a flow rate of 10 $g.min^{-1}$. This porous membrane

maximised the mass-transfer efficiency during extraction. The suspension of SAX particles in the non-solvent was charged into a 150 ml extraction vessel, to which SCO_2 was delivered via the liquid CO_2 pump into the bottom of the extraction vessel at a constant flow rate of 10 $g.min^{-1}$. The extraction temperature maintained constant at 40°C within an air-heated oven (Thar, Inc.), whilst the automated backpressure regulator BP-1580-81 (Thar, Inc.) maintained a constant working pressure of 100 bar during the run. The effluent SCO_2 was vented from the top of the column. The extraction process was run for a total of 3 h, and then the vessel de-pressurised slowly at a rate of 2 $bar.min^{-1}$. Following completion of the extraction process, dried particulates were removed from the vessel and stored over silica gel.

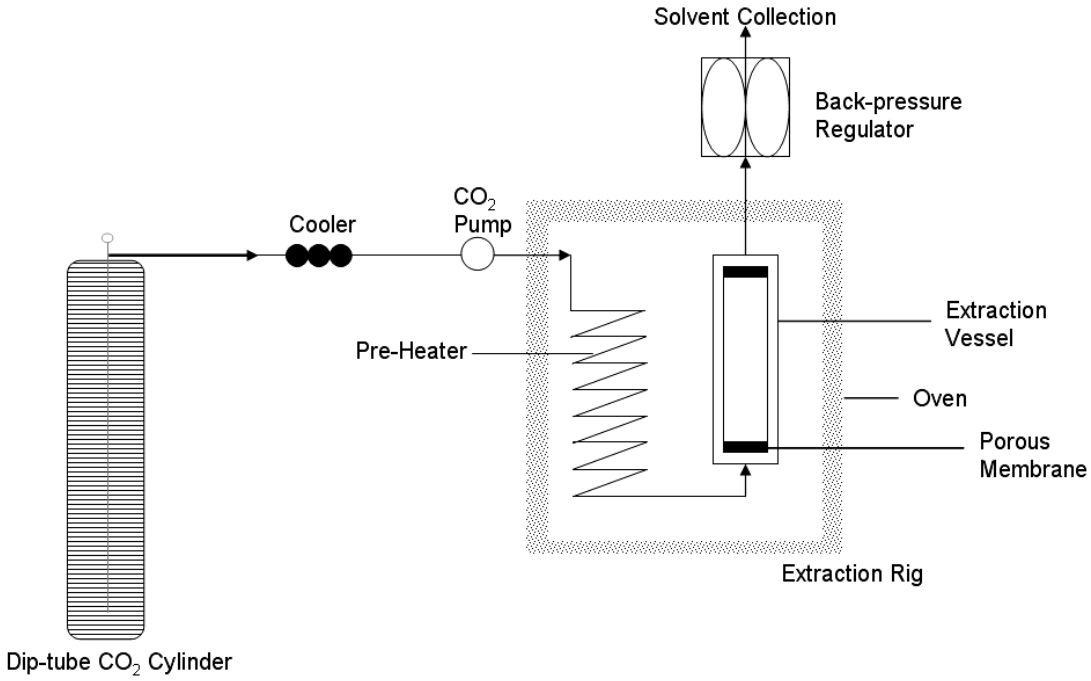

Figure 3.3: Schematic of SFE system

3.3.2 Characterisation

All SAX-produced particles were characterised using scanning electron microscopy (SEM), particle size analysis, differential scanning calorimetry (DSC), and X-ray powder diffraction (XRPD). The details of the characterisation are described in Chapter 2.

3.4 Results and Discussion

3.4.1 The Lab Scale Development of the SAX Process

Based on the original SAX system developed by Kaerger and Price, a laboratory scale system has been developed. This section highlights studies carried out to investigate the influence of process parameters such as atomisation pressures, carrier solvents, non-solvents and crystallisation temperatures on the physicochemical properties of resultant particles.

3.4.1.1 The Effect of Operating the SAX System under Negative or Positive Pressure

Budesonide particles produced from the lab-scale SAX process by spraying a 3% w/v budesonide in acetone through a pneumatic atomiser at a sprayed rate of 0.8 ml.min^{-1} over a separation distance of 60 cm are shown in Figure 3.4. These particles were collected in hexane set at 5˚C, using either negative or positive air pressure set at 30 L.min^{-1}. Under both operation conditions, the crystallisation vessel was exposed to sonic energy to induce nucleation and crystal growth.

Budesonide particles collected from the system with the negative air pressure of 30 L.min^{-1} (Figure 3.4A) possessed an orthorhombic crystalline habit with smooth surfaces. Budesonide particles generated under the positive air pressure as shown in Figure 3.4B were similar to those particles produced under the negative pressure, but were smaller. This is supported by particle size distribution analysis shown in Figure 3.5. By applying the negative air pressure within the system, the data exhibited a broad size distribution. On the contrary, the cumulative particle size distribution for the particles produced from the positive air pressure system indicated that the size of the materials was significantly smaller than those produced under the negative pressure. The under size particle size data of such materials are also confirmed by Table 3.1. The $d_{10\%}$, $d_{50\%}$ and $d_{90\%}$ of the material produced under the negative pressure were 1.61 ± 0.05, 14.43 ± 0.3, and 22.77 ± 0.54 µm, respectively. However, the $d_{10\%}$, $d_{50\%}$ and $d_{90\%}$ of the material produced under the positive air pressure were at 0.99 ± 0.02, 5.79 ± 0.08 and 10.36 ± 0.43 µm, respectively. The significant difference of the results from the shape

and size of SAX-budesonide particles can be related to the evaporation rate of the carrier solvent in the droplets, which may be affected by the different air-flow systems within the SAX process. The positive air pressure may have aided greater evaporation of the carrier solvent, which may have resulted in the formation of small supersaturated droplets. Upon exposure of these droplets to sonic energy, the formation of small crystalline budesonide particles would be generated in this system.

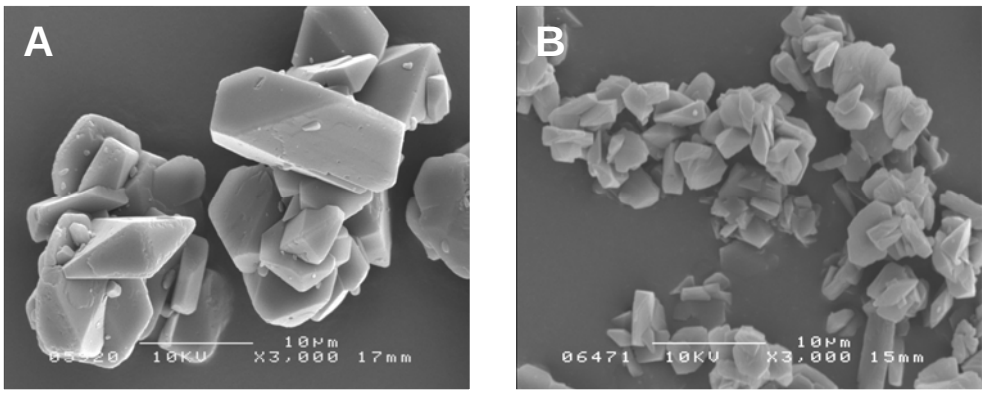

Figure 3.4: Scanning electron micrographs of budesonide particles generated using: (A) negative air pressure; (B) positive air pressure in the lab-scale SAX process

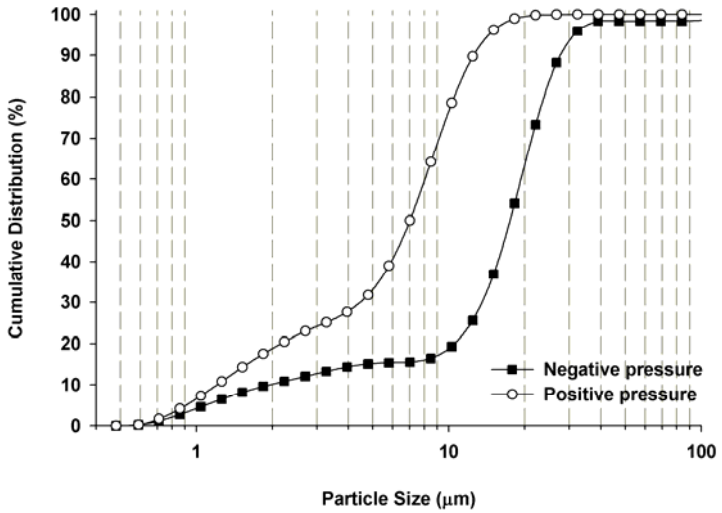

Figure 3.5: Particle size distribution of budesonide particles produced from different types of air pressures in the lab-scale SAX process

Table 3.1: Summary particle size statistics of budesonide particles generated using negative and positive air pressures in the lab-scale SAX process

	$d_{10\%}$ (µm) ± SD	$d_{50\%}$ (µm) ± SD	$d_{90\%}$ (µm) ± SD
Negative pressure	1.61 ± 0.05	14.43 ± 0.30	22.77 ± 0.54
Positive pressure	0.99 ± 0.02	5.79 ± 0.08	10.36 ± 0.43

The DSC thermographs shown in Figure 3.6 both present a single endothermic peak, which suggests that SAX-produced budesonide particles from both negative and positive air flow pressures were of the same crystalline polymorph. The endothermic transition of SAX-budesonide particles from the negative air pressure clearly exhibited the melting temperature at 259.9˚C, which is typical of the endothermic melting transition for crystalline budesonide (Jones, Young et al., 2008). In addition, the endothermic peak of such particles produced with the positive air flow in the system also indicated the clear peak at 257.9˚C. In order to confirm the crystallinity of particles, XRPD was employed. The XRPD patterns in Figure 3.7 show sharp diffraction peaks associated with crystalline materials in both SAX-budesonide particles from the negative and positive pressures. The XRPD spectra are comparable with previously published data, confirming the identity as budesonide (Jones, Young et al., 2008). The results from DSC and XRPD reveal that the lab-scale SAX process could generate budesonide crystalline particles by applying either negative or positive air flow pressure in the SAX process. However, the positive air flow provided much smaller particles.

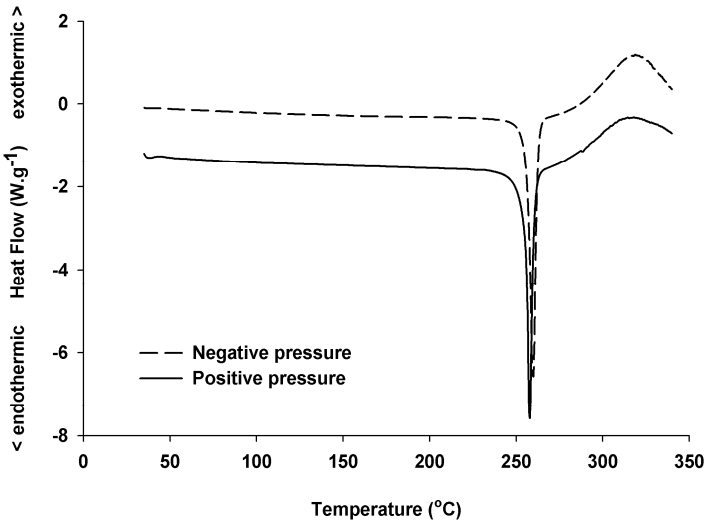

Figure 3.6: DSC thermograms of budesonide particles generated using different types of air pressures in the lab-scale SAX process

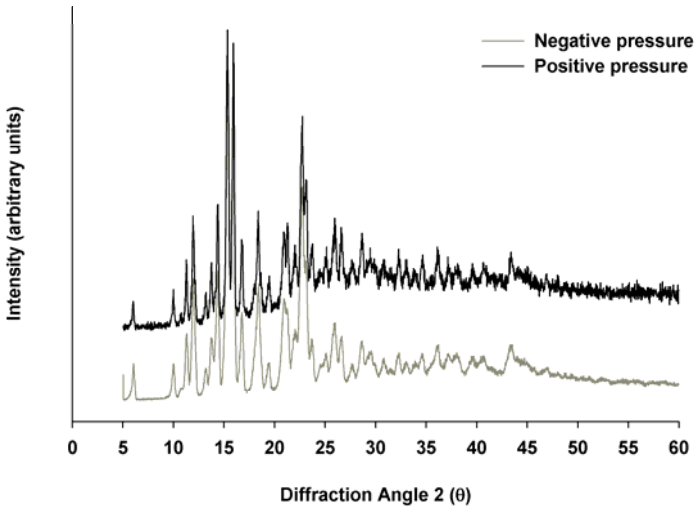

Figure 3.7: X-ray powder diffraction patterns of budesonide particles produced using different types of air pressures in the lab-scale SAX process

3.4.1.2 The Influence of Different Carrier Solvents on the Physicochemical Properties of SAX-Engineered Particles

The electron micrographs in Figure 3.8 reveal budesonide particles prepared by spraying drug solution of (A) a 2.5% w/v budesonide in ethanol and (B) a 3% w/v budesonide in dichloromethane. Solutions of budesonide in ethanol and budesonide in dichloromethane were prepared in different concentrations in order to be close to their solubility limits. Then such solution was sprayed through a pneumatic atomiser at a sprayed rate of 0.8 $ml.min^{-1}$ to generate supersaturated droplets with having the positive air pressure of 30 $L.min^{-1}$ in this SAX system. These highly viscous droplets were collected in hexane set at 5˚C with sonication. Particles produced from ethanol exhibited planar crystalline particles with smooth and flat surface (Figure 3.8A), whereas SAX-budesonide particles produced from dichloromethane possessed a more spherical morphology. Moreover, particles produced from dichloromethane appeared to be encrusted with nano-sized budesonide particles (Figure 3.8B). The striking differences in morphology of SAX-budesonide particles prepared from different carrier solvents may be attributed to the different vapour pressures of the carrier solvent. For example, ethanol, with a vapour pressure of 44.6 mm.Hg at 25˚C, resulted in more planar particles, whilst the more volatile dichloromethane, with a vapour pressure of 353.21 mm.Hg at 25˚C, led to the formation of more spherical shaped particles. Solvents such as dichloromethane may experience rapid evaporation from the droplets containing the drug solute, resulting in highly viscous droplets, which were able to retain their spherical morphology upon collection. The highly corrugated nature of budesonide particles produced using dichloromethane may be a result of the volatility of the dichloromethane during evaporation of the solvent from the droplets, which may be the reason for the processing of shell like particles. Low vapour pressure solvents such as ethanol may not have sufficient time to form the level of viscosity to prevent the deformation of the droplet upon collection. These data suggest that by using different solvents, particularly with varying vapour pressures, it may be possible to introduce a control on particle morphology and surface geometry, which may further enhance control of surface interfacial properties of resultant particles (Adi, Traini et al., 2008).

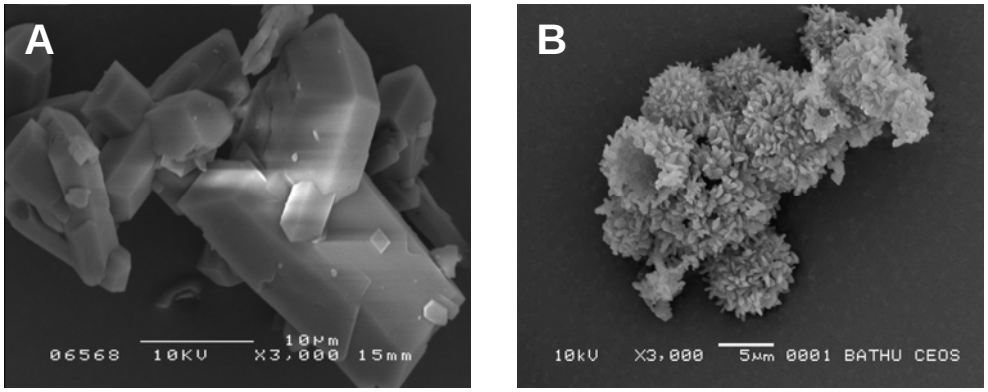

Figure 3.8: SEMs of budesonide particles prepared from: (A) a 2.5% w/v budesonide in ethanol; (B) a 3% w/v budesonide in dichloromethane from the lab-scale SAX process

In addition, Figure 3.9 shows that SAX-produced particles from different types of solvents had a slight variation in the size of the resultant particles. As described in Table 3.2, the particle size data for the ethanol-processed particles, expressed by $d_{10\%}$, $d_{50\%}$ and $d_{90\%}$, were 1.39 ± 0.03, 12.8 ± 0.26 and 20.91 ± 0.39 µm, respectively, whereas the results of $d_{10\%}$, $d_{50\%}$ and $d_{90\%}$ from dichloromethane were 1.11 ± 0.03, 10.56 ± 0.03 and 22.81 ± 1.30 µm, respectively. Hence, there was no significant effect of carrier solvents on particle size of SAX-processed materials for the same atomisation conditions.

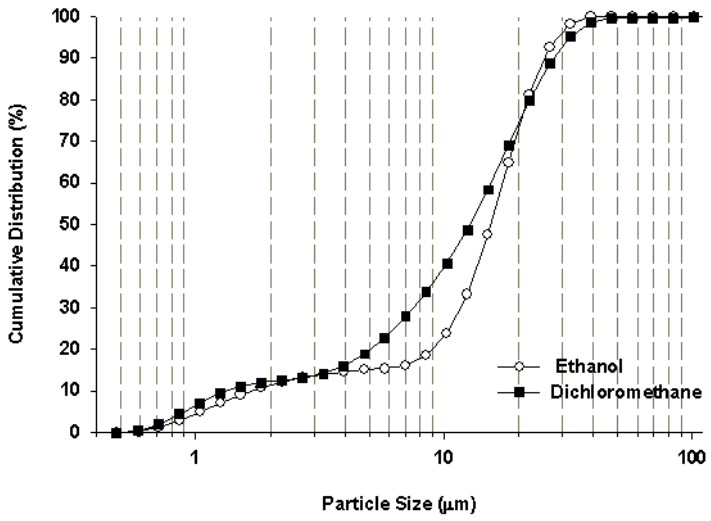

Figure 3.9: Particle size distribution of budesonide particles prepared from different solvents in the lab-scale SAX process

Table 3.2: Summary particle size statistics of budesonide particles prepared from different solvents

	$d_{10\%}$ (µm) ± SD	$d_{50\%}$ (µm) ± SD	$d_{90\%}$ (µm) ± SD
2.5% w/v budesonide in ethanol	1.39 ± 0.03	12.8 ± 0.26	20.91 ± 0.39
3% w/v budesonide in dichloromethane	1.11 ± 0.03	10.56 ± 0.30	22.81 ± 1.30

DSC thermograms of the particles generated from different solvents are shown in Figure 3.10. Budesonide particles produced from ethanol as a carrier solvent exhibited an endothermic peak at 259.9˚C and the endothermic peak of particles from dichloromethane appeared at 258.0˚C. These endothermic peaks corresponded to the melting endotherm of crystalline solid of budesonide. In addition, XRPD diffractograms of SAX-budesonide particles produced from the different carrier solvents are also shown in Figure 3.11. Both samples prepared from ethanol and dichloromethane illustrated characteristic sharp diffraction peaks associated with highly crystalline materials, and the results confirmed that the same polymorphic form was formed regardless of carrier solvents used. These data suggest that the lab-scale SAX process is able to generate budesonide crystalline particles with defined size, shape and morphology through the use of different carrier solvents.

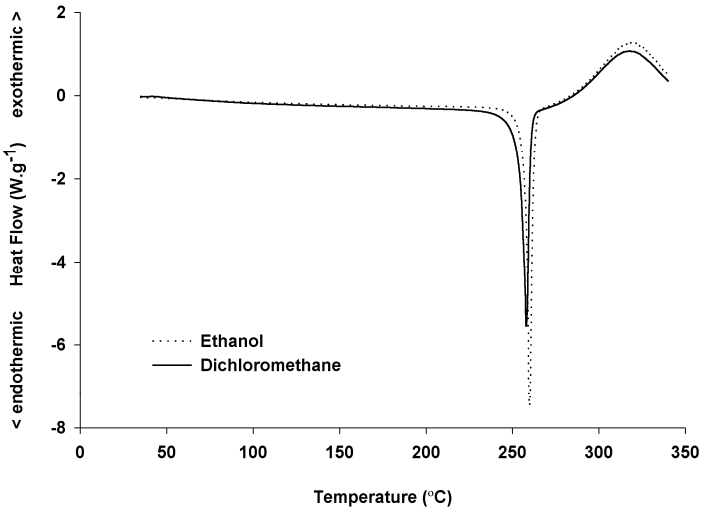

Figure 3.10: DSC thermographs of budesonide particles prepared from different solvents in the lab-scale SAX process

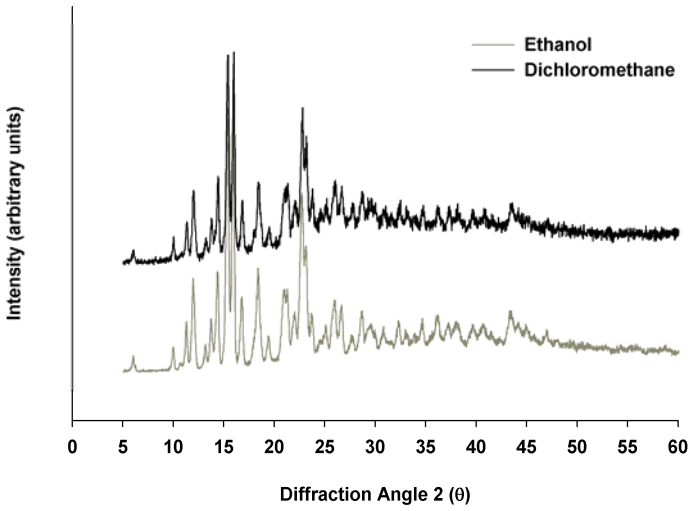

Figure 3.11: X-ray powder diffraction patterns of budesonide particles prepared from different solvents in the lab-scale SAX process

3.4.1.3 The Influence of Different Non-Solvents on the Physicochemical Properties of SAX-Engineered Particles

The effect of spraying a 3% w/v of budesonide in dichloromethane through a pneumatic atomiser (a spray rate of 0.8 ml.min^{-1}) into a non-solvent of either water or hexane at 5˚C was investigated. Under both conditions, each non-solvent was exposed to the same sonication frequency.

The shape and morphology of budesonide particles produced upon collection in water and hexane at 5˚C are shown in Figure 3.12A and B. Particles crystallised in water indicated an irregular shape of planar particles fused together, and the surface of particles appeared rough (Figure 3.12A). By changing the non-solvent from water to hexane, particles shown in Figure 3.12B exhibited a marked difference in shape. SAX-budesonide particles crystallised in hexane possessed a more spherical morphology and appeared to be encrusted with nano-sized budesonide particles on the surface. These differences in shape of SAX-budesonide particles may be related to the different physico-chemical properties of the non-solvent, for example, the surface tension of the liquids, solubility of the drug in the non-solvent and the miscibility of the carrier solvent with the non-solvent, which may have led to a change in overall shape or deformation of the droplet.

The greater surface tension of water (72.8 mN/m) in comparison to hexane (18.4 mN/m) may have influenced the morphology of the resultant SAX-budesonide particles. The droplets of budesonide generated by atomisation may have impacted at the air-liquid interface of the water non-solvent, which may have resulted in the loss of the droplets spherical shape, thereby resulting in the crystallisation of planar crystals. Such impaction of droplets may have been limited when droplets were collected in a non-solvent of hexane, which possesses a lower surface tension than water. As a result, the spherical nature of the droplets would have been maintained, which would result in the crystallisation of spherical particles.

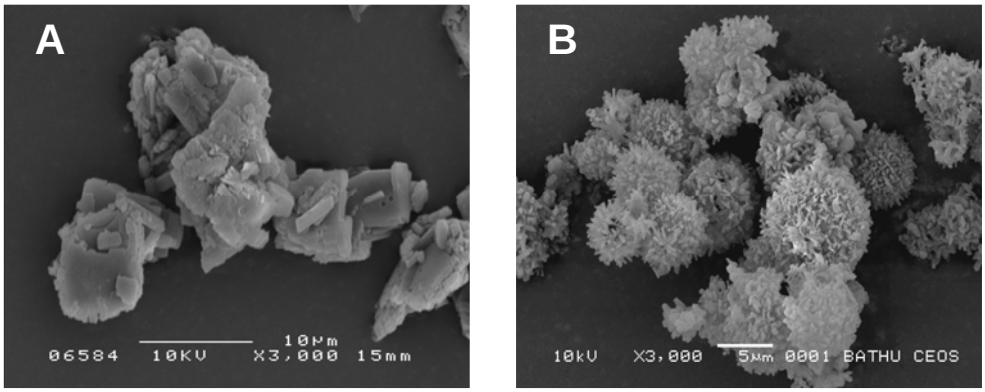

Figure 3.12: Scanning electron micrographs of budesonide particles collected in (A) water and (B) hexane from the lab-scale SAX process

The particle size distribution of SAX-budesonide particles produced using different non-solvents is shown in Figure 3.13. The cumulative particle size distribution of SAX-budesonide particles collected from hexane was slightly broader, with $d_{10\%}$, $d_{50\%}$ and $d_{90\%}$ values of 1.11 $\pm$ 0.03, 10.56 $\pm$ 0.30 and 22.81 $\pm$ 1.30 µm, respectively (see Table 3.3). The $d_{10\%}$, $d_{50\%}$ and $d_{90\%}$ values of SAX-budesonide particles obtained from water were 1.25 $\pm$ 0.05, 8.44 $\pm$ 0.03 and 14.92 $\pm$ 0.21 µm, respectively. Hence, there was no significant difference on the size of SAX-processed particles when either hexane or water was used as non-solvents. However, these data suggest that careful consideration of the non-solvent is required to generate particles with different shapes and surface morphologies.

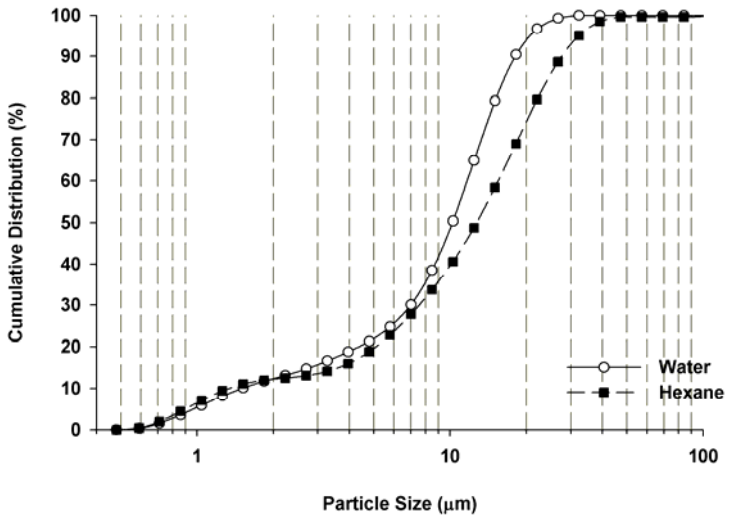

Figure 3.13: Particle size distribution of budesonide particles obtained from different non-solvents from the lab-scale SAX process

Table 3.3: Summary particle size statistics of budesonide particles collected from different non-solvents from the lab-scale SAX process

	$d_{10\%}$ (μm) ± SD	$d_{50\%}$ (μm) ± SD	$d_{90\%}$ (μm) ± SD
Water	1.25 ± 0.05	8.44 ± 0.03	14.92 ± 0.21
Hexane	1.11 ± 0.03	10.56 ± 0.30	22.81 ± 1.30

The DSC thermograms of budesonide particles collected from two non-solvents are presented in Figure 3.14. SAX-produced budesonide particles obtained from water showed the sharp endothermic peak at 253.84˚C and hexane appeared at 257.97˚C, which corresponded to the melting endotherm of budesonide. The slightly lower onset of the melt of such material produced using water as a non-solvent may be associated with residual solvent content, which may have shifted the melt of the material.

The XRPD diffractograms of SAX-budesonide particles generated from the different non-solvents are shown in Figure 3.15. Both samples, prepared from two different types of non-solvents, presented the same pattern of sharp diffraction peaks associated with highly crystalline materials. Furthermore, these data suggest that both

sets of materials are of the same polymorphic form, which is not affected by the non-solvents used.

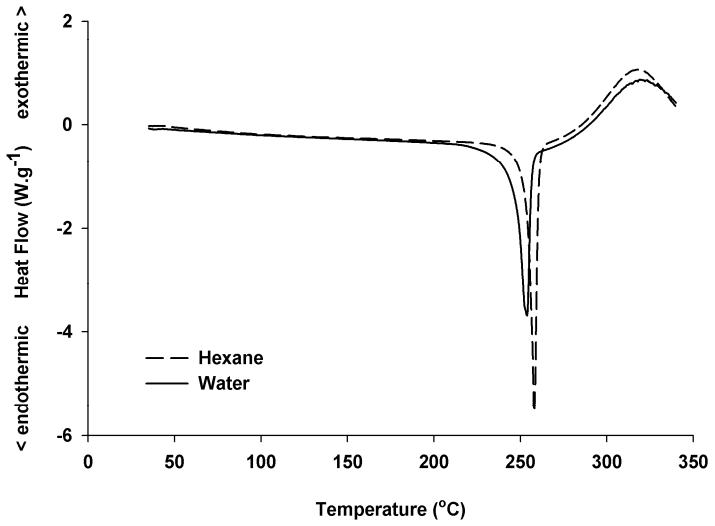

Figure 3.14: DSC thermograms of budesonide particles obtained from different non-solvents from the lab-scale SAX process

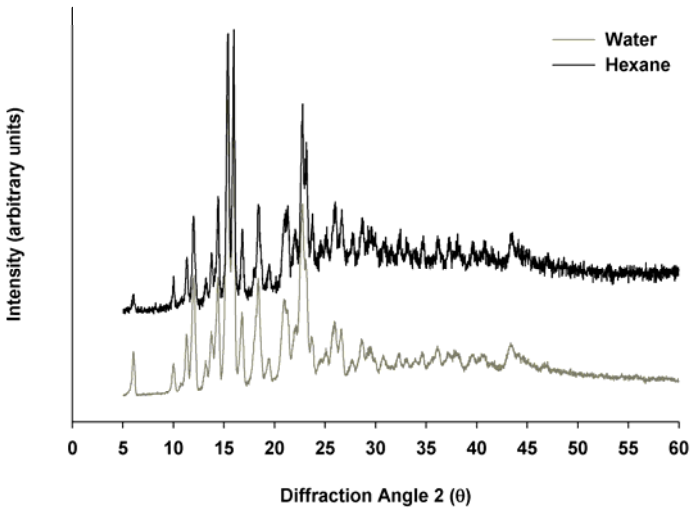

Figure 3.15: X-ray powder diffraction patterns of budesonide particles collected from different non-solvents from the lab-scale SAX process

3.4.1.4 The Effect of Crystallisation Temperatures on the Physicochemical Properties of SAX-Processed Materials

A 3% w/v solution of budesonide in dichloromethane was sprayed through a pneumatic atomiser (a spray rate of 0.8 $ml.min^{-1}$), which was crystallised in hexane using sonication at 20˚C and 5˚C. Figure 3.16A exhibits SAX-budesonide particles crystallised at 20˚C and these particles appear less spherical and more corrugated, whereas particles crystallised at 5˚C possess a spherical morphology with defined surface geometry (Figure 3.16B). Furthermore, the particle size distribution of SAX particles collected from hexane at 20˚C and 5˚C is shown in Figure 3.17. The size distribution of SAX-budesonide particles collected at 20˚C from hexane was slightly broader than those particles obtained at 5˚C. As can be seen in Table 3.4, the particle size data of material crystallised in hexane at 20˚C expressed by $d_{10\%}$, $d_{50\%}$ and $d_{90\%}$ were 1.19 ± 0.04, 13.8 ± 0.88 and 24.49 ± 0.59 µm, respectively. The $d_{10\%}$, $d_{50\%}$ and $d_{90\%}$ values of SAX-budesonide particles crystallised in hexane at 5˚C were 1.11 ± 0.03, 10.56 ± 0.30 and 22.81 ± 1.30 µm, respectively. Hence, crystallisation temperatures did not have a significant effect on the size of resultant particles.

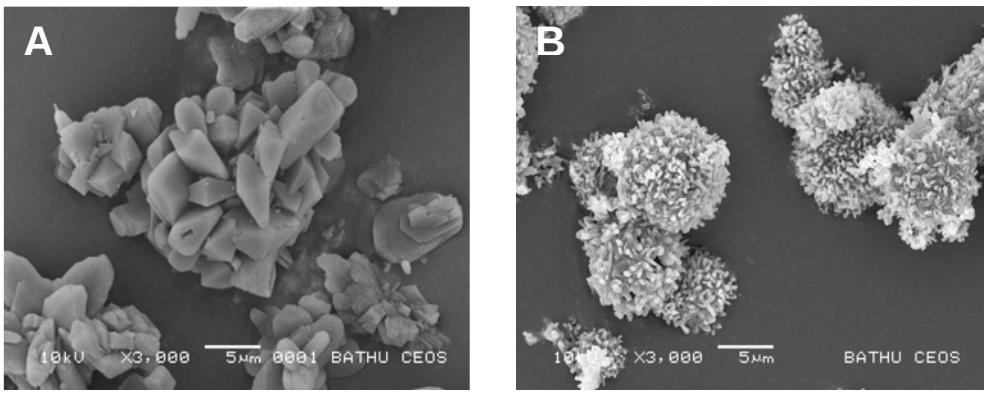

Figure 3.16: Scanning electron micrographs of budesonide particle collected from temperature-controlled vessels at (A) 20˚C and (B) 5˚C in the lab-scale SAX process

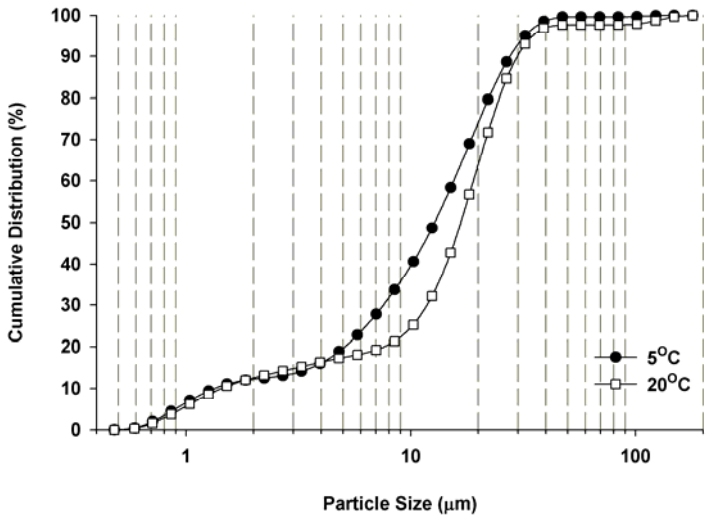

Figure 3.17: Particle size distribution of budesonide particles collected from temperature-controlled vessels at 20˚C and 5˚C in the lab-scale SAX process

Table 3.4: Summary particle size statistics of budesonide particles obtained from temperature-controlled vessels at 20˚C and 5˚C in the lab-scale SAX process

	$d_{10\%}$ (μm) ± SD	$d_{50\%}$ (μm) ± SD	$d_{90\%}$ (μm) ± SD
Temperature at 20˚C	1.19 ± 0.04	13.80 ± 0.88	24.49 ± 0.59
Temperature at 5˚C	1.11 ± 0.03	10.56 ± 0.30	22.81 ± 1.30

The effect of crystallisation temperatures on particle morphology is interesting and may be related to kinetics of crystallisation as a function of temperature. The crystallisation kinetic at 20˚C would be significantly more rapid than at 5˚C. Hence, the slower crystallisation at 5˚C would provide sufficient time for the droplet to crystallise as a spherical particle and enable the outer topography of the particle to form. However, the rate of crystal growth did not seem to affect the size of the resultant particle. These data suggest that the control of crystallisation temperature may enable intricate control of particle surface geometry. Furthermore, these data suggest that the morphological features of SAX particles occur within the solution and not prior to collection.

The DSC thermograms in Figure 3.18 show the particles collected in hexane at different temperatures. These SAX-budesonide particles controlled in the vessel at 20˚C revealed the endothermic peak at 259.59˚C; at 5˚C, such particles indicated the endothermic peak at 257.97˚C, which corresponded to the melting of the crystalline solid of budesonide. The XRPD diffractograms for SAX-budesonide particles produced from two different temperatures are shown in Figure 3.19. The resulting particles demonstrated the similar X-ray patterns associated with highly crystalline materials. It can be confirmed that the same polymorphic form was produced regardless of the temperatures used. These data suggest that the lab-scale SAX process can generate budesonide crystalline particles. Additionally, by controlling the temperatures in the controlled vessels, the morphology of particles can be manipulated.

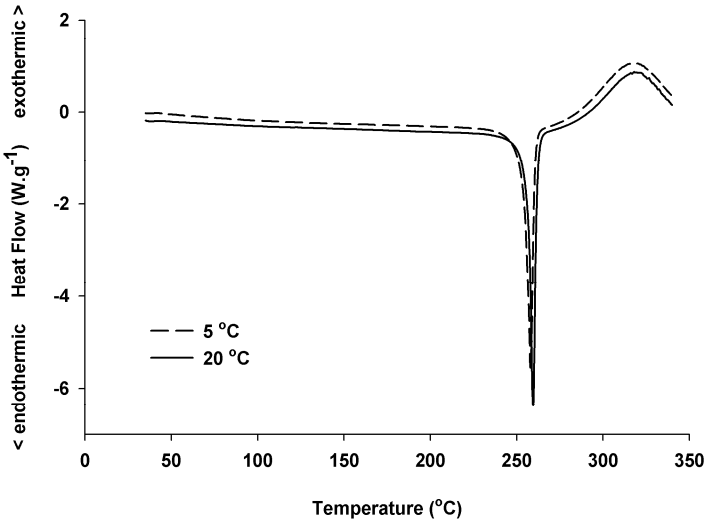

Figure 3.18: DSC thermograms of budesonide particles collected from temperature-controlled vessels at 20˚C and 5˚C in the lab-scale SAX process

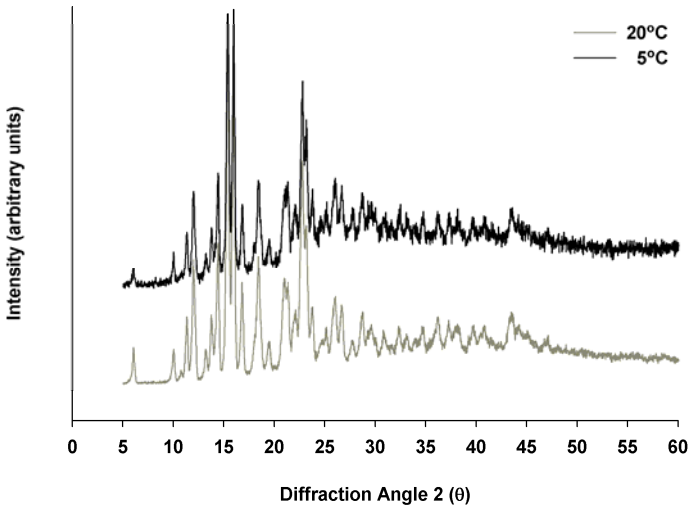

Figure 3.19: XRPD patterns of budesonide particles collected from temperature-controlled vessels at 20˚C and 5˚C in the lab-scale SAX process

3.4.2 The Influence of Material Isolation by SCO_2 Extraction on Physicochemical Properties of SAX Particles

One of the key concerns with the SAX process has been the isolation of processed material from the non-solvent. This was traditionally achieved using vacuum filtration, which is an inefficient process when dealing with large quantities of material. As a result, the use of SCO_2 solvent extraction was evaluated.

The SAX set-up was purged with a constant air-flow of dry nitrogen at 30 $L.min^{-1}$ to enable evaporation of the solvent from the atomised droplets. Following this, a solution of budesonide (3% w/v) prepared in dichloromethane was atomised using a pneumatic atomiser (Buchi, Fawali, Switzerland) at a constant air-flow rate of 800 $L.h^{-1}$. The generated aerosol droplets were then allowed to pass through a column to aid solvent evaporation from the aerosol droplets, thereby forming highly supersaturated droplets. These droplets were then collected in a crystallisation vessel containing the non-solvent (n-hexane), which was exposed to ultrasonic energy using an ultrasonic probe resonating at 20 kHz, to induce nucleation and crystal growth. In this way, one batch of SAX processed-budesonide particles was isolated using either membrane filtration or SCO_2 solvent extraction.

Optical images of SAX particles were isolated using vacuum filtration (Figure 3.20A) and SCO_2 extraction (Figure 3.20B). As can be seen from the images, particles obtained by using vacuum filtration in the collecting method seemed to be more agglomerated and tended to have difficulty in preparing DPI formulations. However, the particles gained from SCO_2 extraction presented a highly flowable powder which was easy to handle in terms of formulation preparation. The reason for the difference in physical property may be related to the isolation method. During vacuum filtration, negative air flow provides the driving force for the filtration process. Therefore, filtrated particles may have compacted together and caked. In contrast, the SCO_2 extraction process utilises CO_2 in the supercritical phase to remove the solvent and enables dry powder isolation. The greater diffusivity and lower surface tension of supercritical fluids enable efficient drying of powders. Furthermore, the SCO_2 is percolated into the extraction vessel, which prevents the material from caking. For this reason, SAX particles isolated using SCO_2 extraction exhibit excellent flow properties and are suitable for preparation of DPI formulations.

Figure 3.20: Optical images of SAX particles isolated using (A) vacuum filtration and (B) SCO_2 extraction

The particle morphology and shape of SAX-processed materials isolated using either membrane filtration or SCO_2 solvent extraction are shown in Figure 3.21A and B. Furthermore, the particle size distribution of both materials is shown in Figure 3.22. It is evident from Figure 3.21 that isolation by SCO_2 solvent extraction did not affect the morphology or size of the resultant particles. Furthermore, Figure 3.22 shows that the particle size distribution of the materials was similar. Hence, the SCO_2 solvent extraction process did not induce further crystal growth or damage.

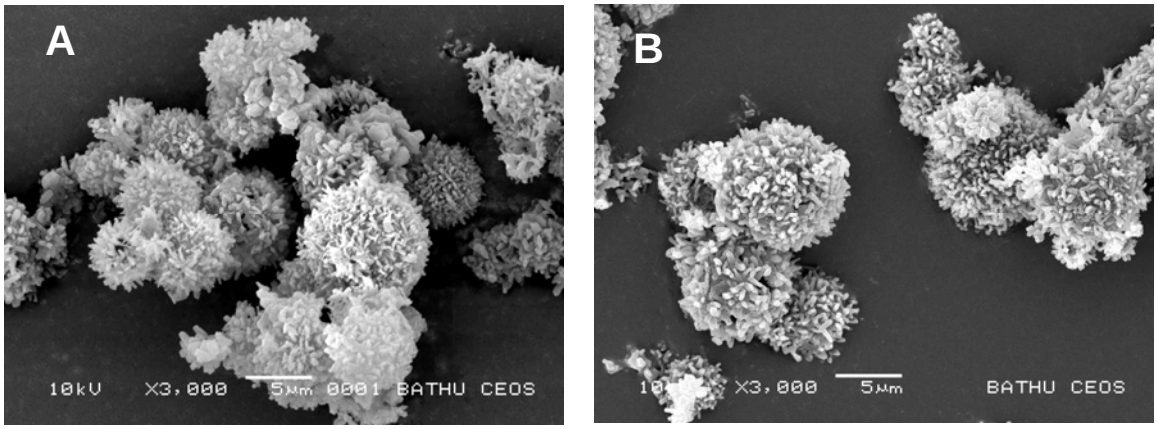

Figure 3.21: Scanning electron micrographs of budesonide particles isolated using (A) membrane filtration and (B) SCO_2 solvent extraction

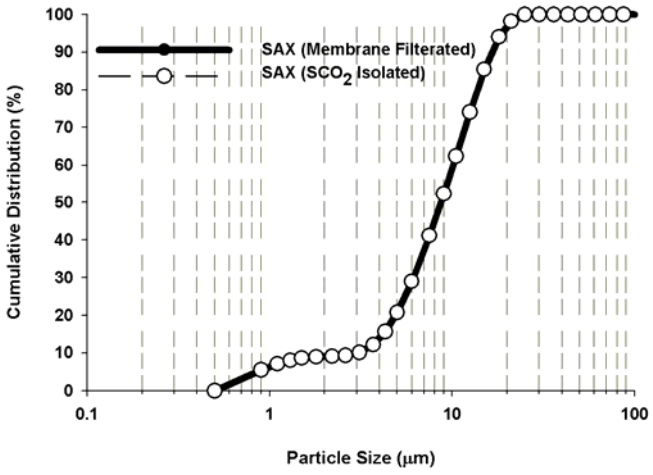

Figure 3.22: Particle size distribution of materials isolated using different isolation methods

DSC thermograms of particles, collected using membrane filtration and SCO_2 solvent extraction, are shown in Figure 3.23. The thermograms of both materials were similar to both crystalline and micronised budesonide, which suggests that the SCO_2 isolation process did not influence the crystallinity or polymorphic form of the drug.

The ability to isolate using SCO_2 solvent extraction enables improved efficiency in product isolation and allows material to be directly employed in formulations without secondary processes such as sifting.

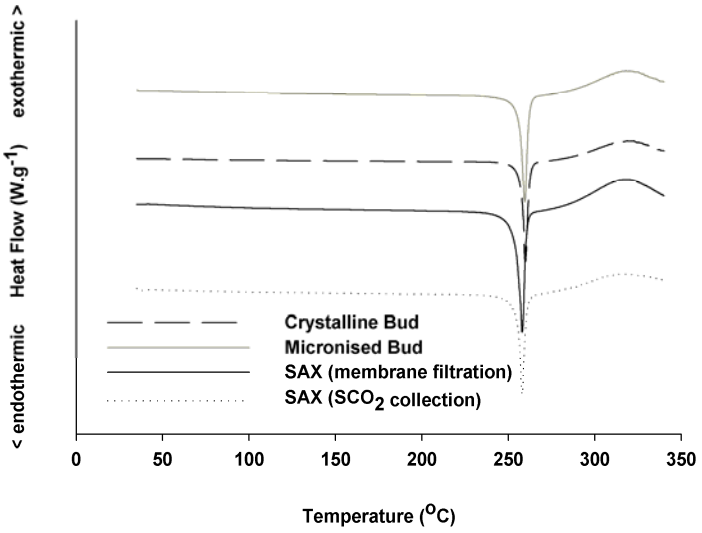

Figure 3.23: DSC thermograms of materials isolated using different isolation methods

3.5 Conclusions

A variety of factors has been shown to influence the SAX process in manipulating the physical properties of active pharmaceutical particles. In development of the lab-scale SAX system, all factors, including air flow pressures, carrier solvents, non-solvents, and temperatures were shown to have a significant effect on the particle engineering process. All factors had a significant influence on the evaporation rate of the small supersaturated droplets, which is critical to generating crystalline particles with defined shape, size and morphology.

The control of the lab-scale SAX process by adjusting these factors is critical to any further development of the SAX apparatus. In the following chapters, these critical parameters are controlled and manipulated in the processing of SAX particles of both single actives and combination drug particles.

Chapter 4: Functionality and *In-vitro* Formulation Performance of SAX-Engineered Budesonide Particles

4.1 Introduction

The objective of pharmaceutical manufacturing is the generation of dosage forms that enable the delivery of medicines to the human body *via* many different routes. Whilst current pharmaceutical manufacturing practices remain empirical in nature, the future of pharmaceutical manufacturing is the generation of products with well-defined properties and functionality. This is the primary goal of pharmaceutical product engineering, which is achieved through control of the product 'property function' (Price and Edge, 2007).

The 'property function' was initially defined by Rumpf (Rumpf, 1967) and later Peukert (Peukert, 2005) as the relationship between the physicochemical properties of particulate systems (*i.e.* particle size, morphology, surface properties) and product properties. A further consideration in producing products with well-defined properties is the 'process function', which relates specific process parameters (*e.g.* unit operations such as mills, centrifuges etc.) to the physicochemical properties of the product (Krekel and Polke, 1992). Hence, both the process and property functions must be known, understood and controlled in order to achieve products with defined functionality and properties that have been built into the product by design (Peukert, 2005).

In designing pharmaceutical products with well-defined properties, it is important to determine the key functionalities that affect product performance and stability. In the case of dry powder inhaler (DPI) dosage forms, surface interfacial interactions play a dominant role in product performance. As a result, the drug-drug and drug-excipient surface interfacial interactions within DPI formulations are critical in determining the dose that reaches the patients' lung (Kawashima, Serigano et al., 1998; Begat, Morton et al., 2004). Whilst it is known that the surface properties of the active pharmaceutical ingredient (API) will dramatically affect DPI product performance, the primary design concept in API manufacturing for DPIs remains particle size, with limited understanding of the effects of processing on API surface properties. Hence, to control the specific

performance and stability properties of DPI dosage forms, the central product design principle in DPI manufacturing must focus on tailoring the mesoscopic design of particle interfaces to enable careful control of particle-particle interactions, and therefore, product performance.

Current pharmaceutical manufacturing strategies for DPI dosage forms generally involve the engineering of the API into specific crystalline forms. The API crystals are then processed into particles in the required particle size range using destructive 'top-down' strategies (*e.g.* micronisation) and formulated into dosage forms. Although, it is possible to control particle size of materials using such processes, the control of particle surface properties and morphology is extremely difficult. The inability to control surface properties of micronised materials is directly related to variability in batch-to-batch performance of products, as small differences in batch preparations can result in extreme variations in surface properties of processed products. Hence, equivalent batches may possess varying property function (Feeley, York et al., 1998). Furthermore, the use of high-energy comminution is also known to result in undesirable product properties such as disorder of the crystalline lattice of the material, which can adversely impact the overall performance and stability of the product (Krycer and Hersey, 1981; Buckton, 1997; Begat, Young et al., 2003).

Whilst current research and development exercises are being directed to define and understand process functions employed in pharmaceutical product design, there is a growing requirement to investigate new technologies to tailor specific functionalities and properties into products. Development in the engineering of pharmaceutical particulates has primarily focussed on controlled crystallisation strategies such as supercritical fluid crystallisation, which have made significant strides in controlling particle size, crystallinity and habit of particulates (Shekunov, Feeley et al., 2003). However, the inability to specifically control particle morphology and process scale-up issues has hampered the introduction of such process technologies into full-scale pharmaceutical manufacturing (Price and Edge, 2007). Recent developments in a range of 'bottom-up' strategies have shown potential in the production of pharmaceutical particles of defined property function. These include process technologies such as spray drying (Li, Neill et al., 2003), spray freeze drying (Maa, Nguyen et al., 1999) and high gravity precipitation (Chiou, Li et al., 2007).

The novel processing technology referred to as the solution atomisation and crystallisation by sonication (SAX) process shows great promise in enabling greater control on particle size, shape, morphology and surface properties, without compromising material stability (Kaerger and Price, 2004). The SAX process consists of defined stages, which begin with the generation of aerosol droplets of material, with defined droplet size distribution using an appropriate atomiser. Following atomisation, the carrier solvent evaporates resulting in the formation of highly supersaturated droplets, which are then collected in a crystallisation vessel containing a non-solvent of the processed material.

The aim of this investigation was to utilise the SAX particle engineering process to produce particles of budesonide with defined property function for delivery to the airways.

4.2 Materials

Micronised budesonide was obtained from suppliers listed in Chapter 2. All organic solvents were of at least analytical grade and were purchased from Fisher Chemicals (Loughborough, UK). Water was produced by MilliQ from reverse osmosis (Molsheim, France). Etched lactohale was prepared from coarse carrier lactose monohydrate (Friesland Foods Domo – Pharma, Zwolle, The Netherlands).

4.3 Methods

4.3.1 The Production of SAX-Produced Budesonide Particles

As described in the previous chapter, a range of critical parameters can be manipulated and controlled in the SAX-particle engineering process to produce particles of defined functionality. In terms of producing particles for lung delivery, it is essential to control particle size, morphology and crystallinity. Based on the understanding gained during studies described in Chapter 3, it was discovered that the choice of carrier solvents and atomisation method was critical to achieving particles

suitable for delivery to the lungs. The following describes different configurations of the SAX process that are utilised to produce budesonide particles suitable for pulmonary drug delivery.

4.3.1.1 SAX-Produced Budesonide B (SAX B) Particles

SAX B particles were prepared from a 1.5% w/v solution of budesonide in dichloromethane, which was atomised using a co-axial two-fluid atomiser with an internal mixing principle (SU11, Spraying Systems Co., Illinois, USA). The atomiser was operated with a solution feed rate of 2 $ml.min^{-1}$, air pressure at 2 bar, a separation distance of 60 cm and a positive carrier gas of 30 $L.min^{-1}$. The resulting particles were then collected in hexane at 5˚C. The particles were isolated from the hexane using SCO_2 solvent extraction as described in Chapter 3.

4.3.1.2 SAX-Produced Budesonide C (SAX C) Particles

SAX C particles were generated upon atomisation of a 3% w/v solution of budesonide in dichloromethane using a pneumatic atomiser with an orifice of 0.7 mm (Büchi, Flawil, Switzerland). The atomiser was operated at a spray rate of 0.8 $ml.min^{-1}$ with the compressed air consumption of the atomiser at 10 $L.min^{-1}$, a separation distance of 60 cm and a positive carrier gas of 30 $L.min^{-1}$. The resulting particles were then collected in hexane at 5˚C and, finally, isolated from the non-solvent using SCO_2 solvent extraction. In addition, a small aliquot of the suspension was isolated using vacuum filtration to assess if the SCO_2 extraction process affected the physicochemical properties of the SAX particles.

All particles were characterised using scanning electron microscopy, particle size analysis, differential scanning calorimetry, X-Ray powder diffraction, and dynamic vapour sorption. The experimental methodologies for these techniques are described in Chapter 2.

4.3.2 Formulation Blending

A formulation containing a 0.4% w/w drug (SAX B) was prepared in 4 g batch by geometrically mixing the drug and surface-etched carrier lactose in a 15 ml glass container for 60 seconds on a Whirlimixer (Fisons Scientific Equipment, Loughborough, UK). The resultant blend was further mixed using a Turbula shaker-mixer (Willy A Bachofen AG, Basel, Switzerland) at 46 rpm for 45 minutes. Similarly, a formulation containing a 0.4% w/w micronised budesonide was also prepared by mixing with the same batch of surface-etched lactose. Both formulations were stored at 25˚C and 44% RH prior to testing. These materials were investigated as part of study I.

The *in-vitro* aerosolisation performance of SAX C particles was investigated as part of study II. A formulation containing a 0.8% w/w of SAX C was formulated in 4 g batch with surface-etched lactose using the same formulation preparation method as study I. In order to compare the aerosolisation properties of SAX C particles and conventional micronised budesonide, a further formulation containing a 0.8% w/w micronised budesonide was prepared with the same batch of surface-etched lactose.

4.3.3 Content Uniformity Determination

Upon blending, the content uniformity of formulations in both studies (I and II) was assessed. Each blend was spread over a clean surface and ten samples of 25 $\pm$ 1 mg taken from random positions. Each sample was dissolved with 15 minutes sonication in 45% methanol, 35% acetonitrile and 20% water to 100 ml final volume and drug concentration assessed by high performance liquid chromatography (HPLC). The proportion of drug in each sample was calculated and the content uniformity expressed as the coefficient of variation (CV):

$$CV = \frac{SD \times 100}{\bar{x}} \qquad \text{Equation 4.1}$$

where $\bar{x}$ is the mean drug proportion and SD is the standard deviation.

4.3.4 Capsule Filling

The formulations for both studies I and II were manually loaded into size 3 hydroxypropyl methylcellulose (HPMC) capsules (Qualicaps, Madrid, Spain). Fill weight was 25 ± 1 mg, giving a nominal dose of 100 ± 10 µg drug per capsule for formulations used in study I. For study II, the fill weight was 25 ± 1 mg, giving a nominal dose of 200 ± 15 µg drug per capsule. Following filling, capsules were stored in a sealed container containing a saturated solution of potassium carbonate (giving a relative humidity of 44%) for at least 24 hours prior to analysis.

4.3.5 *In-Vitro* Performance Analysis

4.3.5.1 Next Generation Impactor (NGI) and Multi-Stage Liquid Impinger (MSLI)

Inertial impaction has been the pharmacopoeial and industry standard technique for the determination of drug aerosol particle size distribution (Marple, Roberts et al., 2003). This is because this method allows the aerodynamic size distribution of the entire inhaled dose to be characterised in a way that is specific to the drug (Marple, Roberts et al., 2003). An impactor is a device into which the aerosolised formulation is drawn, under an airstream at a defined flow rate. It passes through a series of stages which consists of a plate containing a number of nozzles or jets with a defined diameter located above a flat collection surface. As the aerosol passes from stage-to-stage, the jet sizes become progressively smaller. As the airstream passes through each stage, it changes direction. Any airborne particles will be subject to two forces: their momentum, which acts to keep them travelling in their current direction; and the hydrodynamic forces exerted by the air travelling in the new direction (Marple, Roberts et al., 2003). Particles with a larger momentum, which is a function of their mass and thus diameter, will be less likely to relax into a change in direction of the air flow, and may impact on the collection surface, removing them from the airstream (see Figure 4.1).

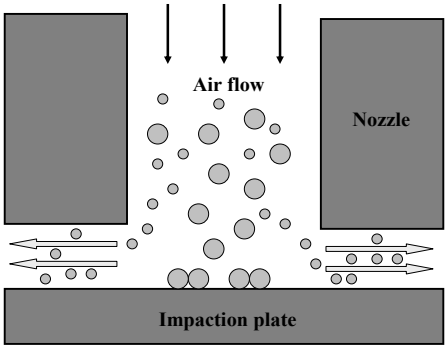

Figure 4.1: The impactor consisting of a nozzle and an impaction plate

For a given nozzle diameter, particles above a certain size (the cut-off diameter) will impact on the collection surface. In practice, the efficiency with which particles of varying sizes impact in a given stage follows a sigmoidal function. Therefore, the cut-off diameter for a given stage is characterised by the aerodynamic diameter at which 50% of particles impact (C_{50}) (Marple, Roberts et al., 2003). The cut-off diameter of a stage can be described using Stokes' law (Marple, Roberts et al., 2003):

$$C_{50} = \sqrt{\frac{9\pi\eta n_n W_n}{4\rho_p C_{ae} Q}} \times \sqrt{St_{50}} \qquad \text{Equation 4.2}$$

where η is the viscosity of air, n_n is the number of circular nozzles in the stage, W_n is the nozzle diameter, ρ_p is the particle density, C_{ae} is the Cunningham slip correction factor, Q is the volumetric air flow rate and $\sqrt{St_{50}}$ is the square root of the Stokes' number that gives a 50% chance of particle deposition, which is ~0.49 for a well-designed impactor.

By passing the aerosolised formulation through an impactor and then recovering and quantifying the amount of drug deposited on each stage, the aerodynamic particle size distribution can be determined. In order to mimic the anatomy of the respiratory tract, impactors also feature an induction port that is placed between the inhaler and the stages. This contains a 90˚ bend and acts as a very simple model of the mouth and throat, enabling deposition in this area to be approximated.

In-vitro formulation performance is assessed using a NGI (Figure 4.2), which is an instrument recently designed specifically for pharmaceutical inhaler testing (Marple, Roberts et al., 2003). When used for testing DPIs, the NGI employs a metal throat, pre-separator and eight stages and the last stage is a micro orifice collector (MOC), which performs the role of a filter. When operated at a flow rate of 60 $L.min^{-1}$, the cut-off diameters of each NGI stage exhibit as follows:

- Throat and pre-separator: >12.8 µm
- Stage 1: 8.06 – 12.8 µm
- Stage 2: 4.46 – 8.06 µm
- Stage 3: 2.82 – 4.46 µm
- Stage 4: 1.66 – 2.82 µm
- Stage 5: 0.94 – 1.66 µm
- Stage 6: 0.55 – 0.94 µm
- Stage 7: 0.34 – 0.55 µm
- MOC 0.14 – 0.34 µm

The fine particle dose (FPD) can, therefore, be defined as the mass of drug deposited on stage 3 and below (<4.46 µm).

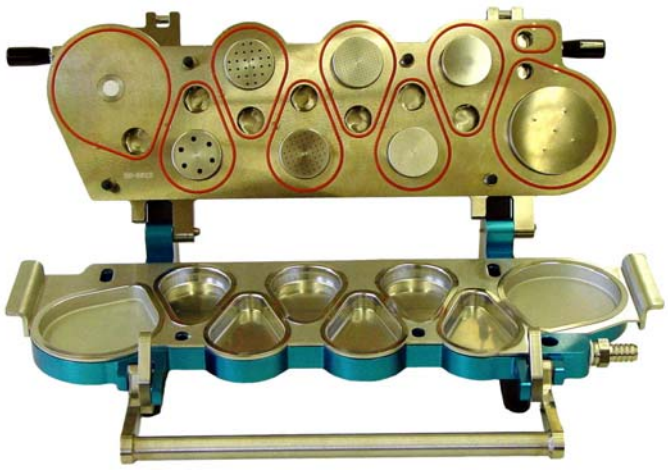

Figure 4.2: Next generation impactor (NGI) adapted from http://www.mspcorp.com

Where the NGI relies on particle impaction, Figure 4.3 shows the multi-stage liquid impinger (MSLI) that collects particles impinging onto liquid interfaces. The MSLI has five liquid impinging stages and the cut-off diameters at a flow rate of 60 $L.min^{-1}$ of stages 1, 2, 3 and 4 are 13, 6.8, 3.1 and 1.7 µm, respectively. Additionally, stage 5 comprises an integral paper filter to capture the remaining fraction of particle less than 1.7 µm.

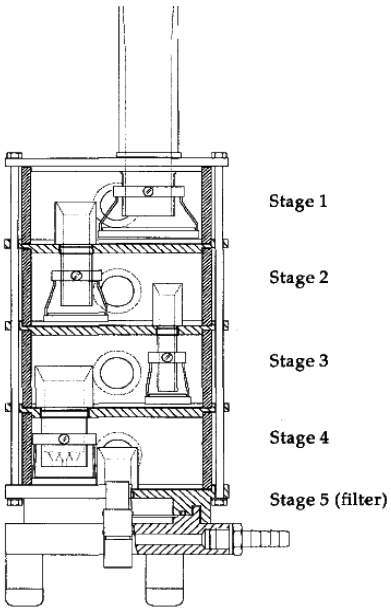

Figure 4.3: Multi-stage liquid impinger (MSLI) reproduced from Microbiol. Mol. Biol. Rev. (May 1966)

4.3.5.2 Study I – In-vitro Inhalation Performance of SAX B

The NGI was used to investigate the performance of micronised budesonide and SAX B formulations. The NGI collection cups were immersed in a 1% v/v solution of silicone oil (Acros Organics, Geel, Belgium) in hexane and allowed to air dry. The NGI (Copley Scientific Ltd, Nottingham, UK) in Figure 4.2 was then assembled with pre-separator (containing 15 ml of wash solvent) and connected to a vacuum pump (Gaast, Benton Harbour, MI, USA) *via* a solenoid valve. The flow rate at the inlet to the throat was set to 60 $L.min^{-1}$ using a digital flow meter with model DFM 2000 (Copley Scientific Ltd., Nottingham, UK). A Cyclohaler™ was attached to the throat of the NGI using a rubber mouthpiece. A capsule was inserted in the Cyclohaler and pierced by two sharp pins within this Cyclohaler to generate two small holes at the respective ends of the capsule.

The contents of the capsule were then aerosolised into the NGI by drawing air through the apparatus at 60 $L.min^{-1}$ for 4 seconds (controlled by the solenoid valve). Once the contents of ten capsules were aerosolised in this way, the device was disconnected, and capsules and each stage washed down into separate known volumes of 45% methanol, 35% acetonitrile and 20% water, which were sonicated to aid dissolution. The concentration of drug in each solution was investigated by HPLC, from which the mass of drug deposited on each stage of the NGI could be determined at stages 1 to 7 and the MOC. Between experiments, the NGI was washed in water and methanol, dried in an oven, and allowed to cool to room temperature before re-use.

Each formulation was tested in triplicate. The emitted dose (ED) was defined as the mass of drug recovered from all parts of the NGI. The fine particle dose (FPD) was the mass of drug recovered from stage 3 and below of the NGI and the fine particle fraction (FPF_{ED}) was the FPD expressed as a percentage of the ED.

4.3.5.3 Study II – In-vitro Inhalation Performance of SAX C

A MSLI (Copley Scientific Ltd, Nottingham, UK), shown in Figure 4.3, was used in this study. Each stage (1-4) contained 20 ml of wash solvent and MSLI connected to a vacuum pump (Gaast, Benton Harbour, MI, USA) *via* a solenoid valve. The flow rate at the inlet to the throat was set to 60 $L.min^{-1}$ using a digital flow meter with model DFM 2000 (Copley Scientific Ltd., Nottingham, UK). A Cyclohaler was attached to the throat of the MSLI using a rubber mouthpiece, in fact, a capsule was inserted in the Cyclohaler and pinned by the two sharp pins within this Cyclohaler to generate two small punctures. The contents of the capsule were then aerosolised into the MSLI by drawing air through the apparatus at 60 $L.min^{-1}$ for 4 seconds (controlled by the solenoid valve). Once the contents of ten capsules were aerosolised in this way, the device was disconnected and capsules and each stage washed down into separate known volumes of 45% methanol, 35% acetonitrile and 20% water, which were sonicated to add dissolution and allowed to cool. The concentration of drug in each solution was investigated by HPLC, from which the mass of drug deposited on each stage of the MSLI could be determined. The MSLI was washed in water and methanol, dried in a low temperature oven, and allowed to cool to room temperature.

Each formulation was tested three times in this way. The emitted dose (ED) was defined as the mass of drug recovered from all parts of the MSLI. The fine particle dose (FPD) was the mass of drug recovered from stage 3 and below of the NGI and the fine particle fraction (FPF_{ED}) was the FPD expressed as a percentage of the ED.

4.3.6 High Performance Liquid Chromatography

Drug concentrations were determined by HPLC. The HPLC system consisted of a PU-980 intelligent HPLC pump, an AS950 intelligent autosampler, a CO-866 column oven (all from Jasco, Japan) and a 1050 variable wavelength UV detector (Agilent Technologies, Wokingham, UK). Data were collected and analysed using Azur v4.0 software (Datalys, Saint Martin D'Heres, France). Unknown sample concentration was determined from duplicate injections by comparison of peak area with reference peaks from external standard solutions of known concentration.

Both two studies were analysed using the same HPLC method. This employed a 4.6 mm x 250 mm C18 5 µm Hypersil column (Thermo Electron Corporation, Waltham, MA, USA) and a mobile phase consisting of 45% v/v methanol, 35% v/v acetonitrile and 20% v/v water. The flow rate was 1.5 $ml.min^{-1}$; column temperature was 40˚C with the injection volume of 200 µl. Drug retention time was 3.2 minutes, so a run time of 5 minutes was employed. UV detection wavelength of budesonide was 244 nm.

The relationship between drug concentration (0.1, 0.25, 0.5, 2, 10 and 50 $\mu g.ml^{-1}$) and peak area for each drug was found to be linear, with linear regression analysis yielding a coefficient of determination (R^2) of 1.0 in study I and II (Figure 4.4).

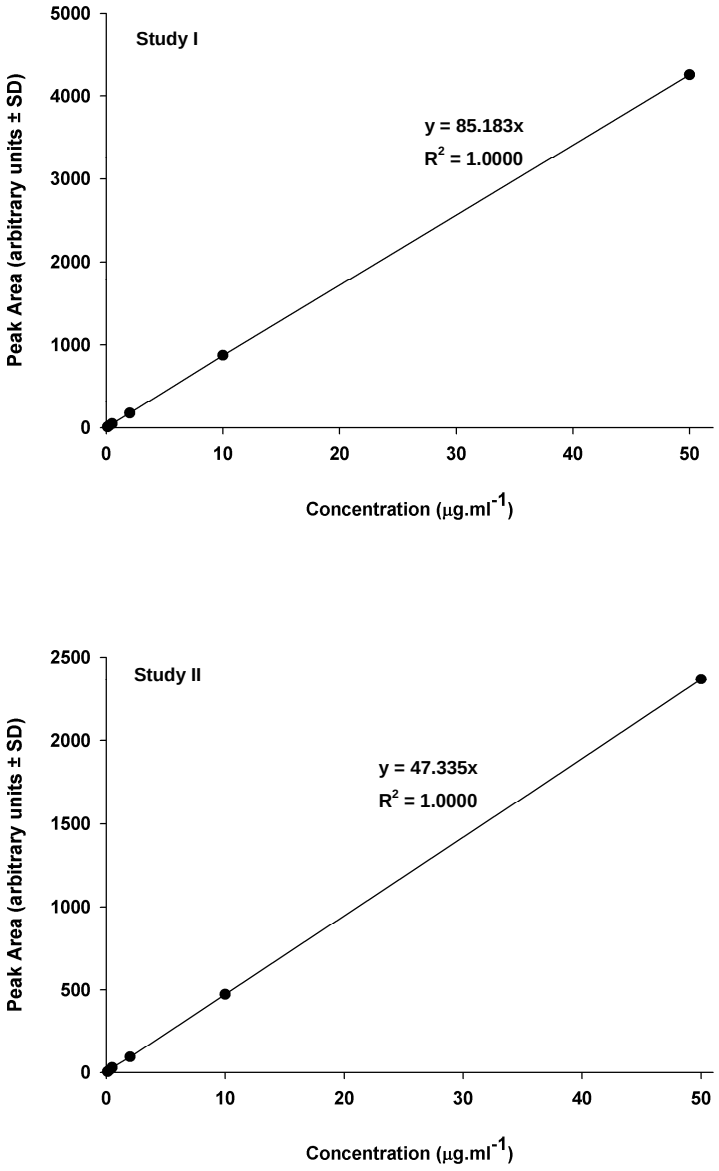

Figure 4.4: HPLC calibration curves for budesonide in study I and II

4.4 Results and Discussion

4.4.1 Characterisation of SAX-Engineered Budesonide Particles

4.4.1.1 Scanning Electron Microscopy

Electron micrographs of budesonide particles obtained from micronised budesonide, SAX B and SAX C are shown in Figure 4.5. The SAX-produced budesonide particles possessed more defined and uniform morphology than micronised budesonide. Micronised budesonide particles were irregular and appeared agglomerated with varying size, whereas SAX B and SAX C particles, which were produced from the lab-scale of SAX process, exhibited uniform shape. SAX B was prepared from a 1.5% w/v of budesonide in dichloromethane and the drug solution sprayed by SU11 atomiser. These SAX-produced B particles appeared to have a granular shape possessed a greater degree of sphericity with more uniform size. SAX C particles were produced from a 3% budesonide in dichloromethane through a pneumatic atomiser. These particles were spherical and encrusted with nanometre-sized particles.

The different morphologies of micronised and SAX-engineered budesonide were related to the different engineering process of the particles. The irregular morphology of the micronised budesonide particles is attributed to the highly energetic and destructive micronisation process, which relies on fragmentation of crystals to produce small particles. Such approach provides a little control of particle morphology, which is a significant drawback of the micronisation process. However, it seems possible to manipulate particle morphology using the SAX process, whilst maintaining particle size control *via* a single droplet to particle operation. The highly corrugated nature of SAX B and C produced using dichloromethane may be a result of rapid evaporation of the solvent from the droplet, owing to its highly volatile nature. The differences in morphology between particles of SAX B and SAX C may be associated to the differences in solution concentrations used to fabricate the respective particles using the SAX process. The more concentrated solution of budesonide employed in the fabrication of SAX C particles may be responsible for the encrustation of smaller particles on the surface of the larger spherical budesonide particles. This may be related to the rapid solvent removal from droplets or ‘blow-out’, which may have led to

implantation of further seeds for crystallisation on the surface of the droplet resulting in the formation of nano-sized budesonide crystallites on the surface of the carrier budesonide particle. Furthermore, the high volatility of dichloromethane may in itself operate as a pore-forming agent, which may lead to particles of SAX C exhibiting low porosity. Such a phenomena has been previously described in the formation of particles using the Pulmosphere technology, where fluorocarbons serve a similar purpose and aid the formation of hollow/porous particles (Duddu, Sisk et al., 2002). These data suggest that by controlling critical parameters such as carrier solvents and solution concentrations of the SAX process, the engineering of particles with defined property function is possible.

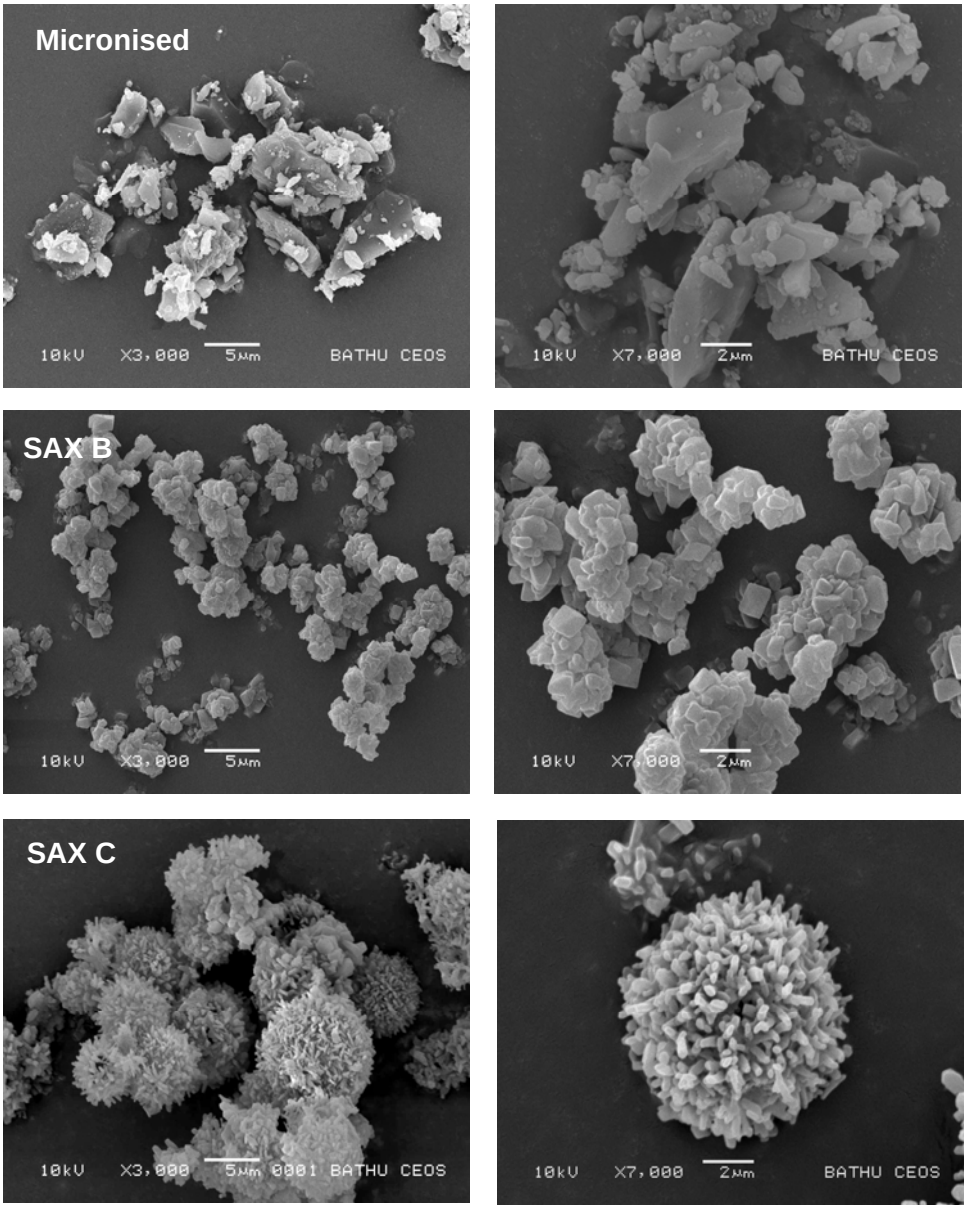

Figure 4.5: Representative SEMs of micronised budesonide, SAX B and SAX C particles at magnifications of x3000 and x7000

4.4.1.2 Particle Size Analysis

Inspection of the particle size distribution in Figure 4.6 shows the cumulative distribution of micronised budesonide, SAX B and SAX C particles. The cumulative particle size distribution of the three budesonide particles was different. The particle size distribution of SAX C was broader than both micronised budesonide and SAX B particles. As supported by the summary data in Table 4.1, it was apparent that the volume median diameters (d_{50}) of micronised budesonide, SAX B and SAX C were at 3.27, 3.07 and 8.68 µm, respectively. In addition, the span of the size distribution which was calculated from $(d_{90} – d_{10})/d_{50}$ was shown in Table 4.1, and such data indicated that the span of SAX B and C was narrower than micronised budesonide. These data can be explained by the fact that the SAX process could generate the aerosol droplets with a narrower span of size distribution in comparison with particles gained from micronisation process. The particle size of SAX C suggests that the material was not suitable for pulmonary drug delivery. However, due to the porous nature and likely low density of these particles, they were formulated for aerodynamic particle size classification.

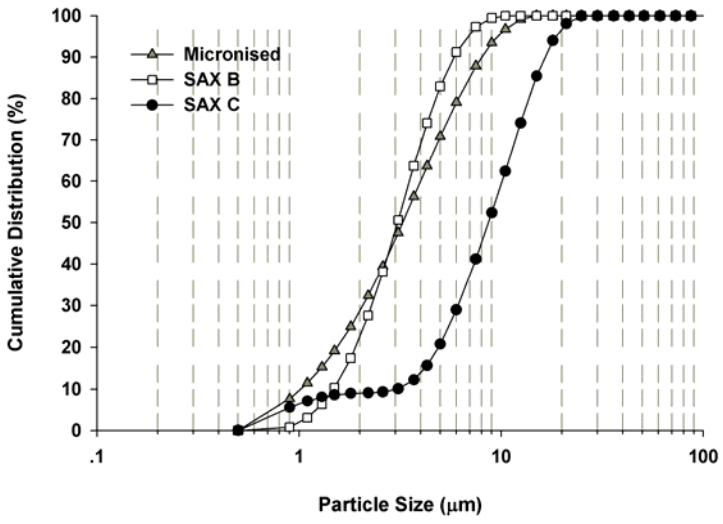

Figure 4.6: Particle size distribution of micronised budesonide, SAX B and SAX C particles

Table 4.1: Summary of particle size data of micronised budesonide, SAX B and SAX C particles

	$d_{10\%}$ (µm) ± SD	$d_{50\%}$ (µm) ± SD	$d_{90\%}$ (µm) ± SD	Span
Micronised Bud	1.02 ± 0.01	3.27 ± 0.02	8.08 ± 0.04	2.16
SAX B	1.48 ± 0.01	3.07 ± 0.01	5.86 ± 0.02	1.43
SAX C	3.04 ± 0.05	8.68 ± 0.12	16.61 ± 0.12	1.56

4.4.1.3 Differential Scanning Calorimetry

The DSC thermograms of micronised budesonide, SAX B and SAX C are shown in Figure 4.7. Three samples all exhibited a single endothermic peak, which corresponded to the melting point of budesonide. Micronised budesonide showed the sharp endothermic peak at 261.84˚C and SAX B appeared at 260.86˚C. Additionally, SAX C had the endothermic peak at 257.97˚C. These data suggest that processing of budesonide by SAX did not change the polymorphic form of the material.

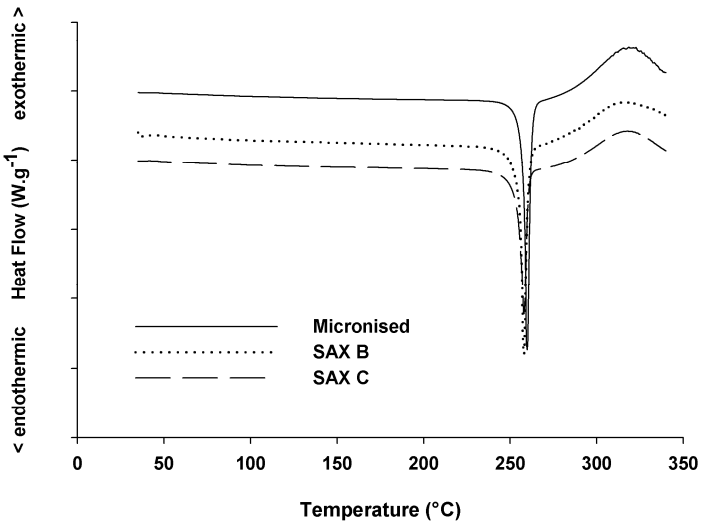

Figure 4.7: DSC thermograms of micronised budesonide, SAX B and SAX C particles recorded at a heating rate of 10˚C.min^{-1}

4.4.1.4 X-ray Powder Diffraction

XRPD diffractograms of budesonide particles from micronised budesonide, SAX B and SAX C are shown in Figure 4.8. All particles presented similar diffraction peaks associated with crystalline budesonide. It can be confirmed that the materials were of the same polymorphic form of budesonide. These results supported that the lab-scale SAX process generated crystalline budesonide particles.

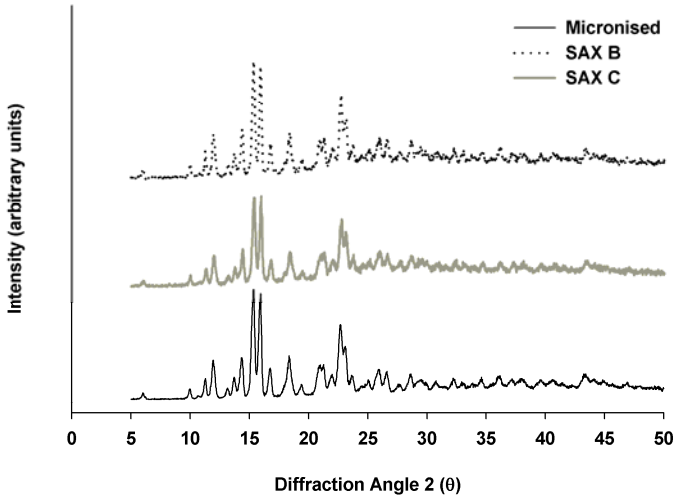

Figure 4.8: XRPD spectra of micronised budesonide, SAX B and SAX C particles

4.4.1.5 Dynamic Vapour Sorption

DVS isotherms of micronised budesonide, SAX B and SAX C particles are provided in Figure 4.9. The DVS moisture sorption isotherms of all budesonide samples showed <1% w/w mass increase or a mass loss during the first sorption cycle, indicating no detectable level of amorphous material. According to micronised budesonide, the following desorption and the subsequent second sorption cycle suggests that approximately 0.007% of water has been retained. Additionally, micronised budesonide and SAX C had a mass increase of ~0.1% w/w at 90% RH, and SAX B had a mass increase of ~0.2% w/w at 90% RH. All data suggest that no amorphous content was detected in all samples. Therefore, crystalline budesonide particles were successfully produced *via* the lab-scale of SAX process.

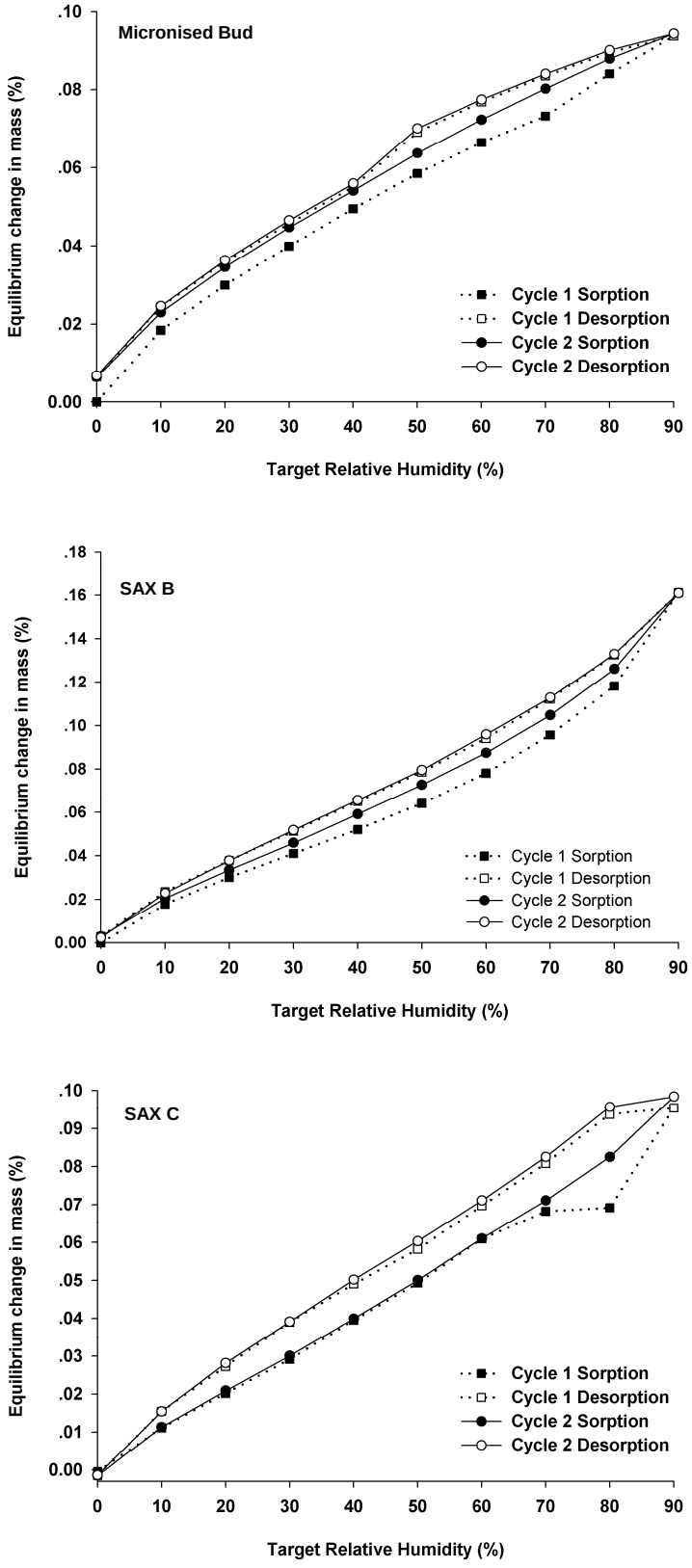

Figure 4.9: DVS isotherms of micronised budesonide, SAX B and SAX C particles

4.4.2 Study I: *In-Vitro* Performance of SAX B

4.4.2.1 SEMs of the Formulations

Figure 4.10 shows representative SEMs of: (A) etched lactohale; (B) the formulation of micronised budesonide, formulated by mixing microinised budesonide with etched lactohale; and (C) the formulation of SAX B, prepared by mixing SAX B with etched lactohale. The formulations of micronised budesonide and SAX B in Figure 4.10B and 4.10C demonstrated that the etched lactohale, which had the smooth surface, was covered with the small drug particles. Etched lactohale (see Figure 4.10A), prepared from the method of temperature-controlled dissolution for carrier lactose and sieved the size to 63-90 µm, possessed a smooth surface and exhibited the tomahawk shape. In addition, such etched lactohale appeared to have less intrinsic fine lactose particles. The formulations of micronised budesonide and SAX B were prepared by blending such drug particles to the etched lactohale. As a result, the SEMs micrograph B and C both exhibited the similar pattern of the small drug particles embedded on the surface of the etched lactohale.

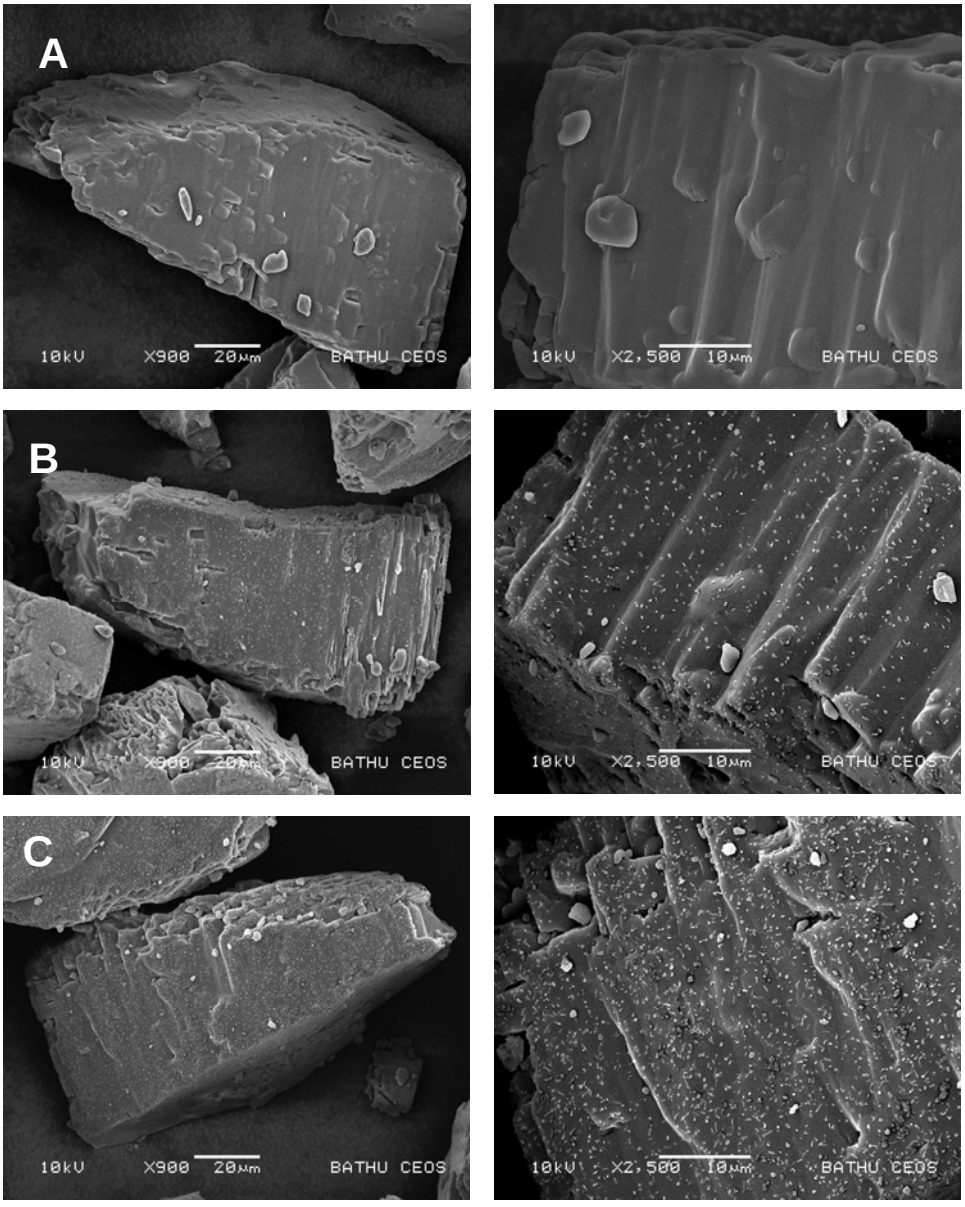

Figure 4.10: Representative SEMs of: (A) etched lactohale; (B) the formulation of micronised budesonide; (C) the formulation of SAX B at magnifications of x900 and x2500

4.4.2.2 Content Uniformity

The coefficient of variation (CV) of the drug content of the two formulations for micronised budesonide and SAX B was <6%, which is the upper limit of what is commonly acceptable as uniformity for a carrier-based DPI formulation. The micronised budesonide blended with etched lactohale showed the CV at 3.47%, whereas the CV of the SAX B formulation was at 2.65%. These results demonstrated that both formulations were uniformly blended.

4.4.2.3 Drug Impactor Deposition Measurements

The mean mass data of drug deposited per capsule on each stage of the NGI for micronised budesonide and SAX B formulations are shown in Table 4.2 and Figure 4.11. Table 4.2 also summarises the emitted dose (ED), fine particle dose (FPD), fine particle fraction of emitted dose (FPF_{ED}) and mass median aerodynamic diameter (MMAD).

Table 4.2: NGI deposition per capsule of drug aerosolised from micronised Bud and SAX-produced Bud B formulations

Bud = budesonide; D & C = device and capsules; MP & T = mouthpiece and throat; PS = pre-separator; S = stage

Formulations	***Mean Drug Deposition on Impactor Stages (µg ± SD)***											***Mean ED (µg ± SD)***	***Mean FPD (µg ± SD)***	***Mean FPF_{ED} (% ± SD)***	***MMAD (µm ± GSD)***
	D & C	**MP &T**	**PS**	**S1**	**S2**	**S3**	**S4**	**S5**	**S6**	**S7**	**MOC**				
Micronised Bud	19.67 ± 3.41	11.58 ± 0.52	38.89 ± 3.25	2.52 ± 0.71	3.39 ± 0.82	2.06 ± 0.45	1.32 ± 0.18	0.48 ± 0.08	0.12 ± 0.01	0.00 ± 0.00	0.00 ± 0.00	60.37 ± 3.57	3.99 ± 0.70	6.6 ± 1.0	4.48 ± 1.48
SAX-produced Bud B	22.70 ± 2.04	5.55 ± 0.56	57.93 ± 2.61	0.86 ± 0.14	1.93 ± 0.20	3.06 ± 0.67	3.70 ± 0.73	1.45 ± 0.28	0.21 ± 0.04	0.00 ± 0.00	0.00 ± 0.00	74.69 ± 4.30	8.42 ± 1.70	11.23 ± 1.88	3.41 ± 1.41

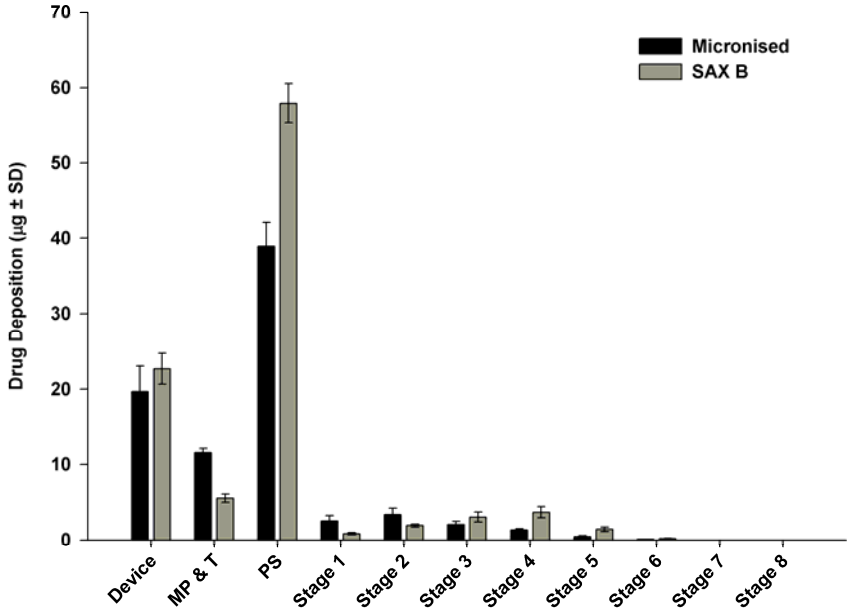

Figure 4.11: NGI deposition per capsule of budesonide aerosolised from the formulations of micronised budesonide and SAX-produced budesonide B

The ED and FPD of micronised budesonide and SAX B formulations are shown in Figure 4.12. As can be seen in Figure 4.12, both ED and FPD aerosolised per capsule for SAX B formulation were different from the micronised formulation. The ED of the micronised budesonide formulation was 60.37 ± 3.57 µg, whereas the SAX B formulation was significantly higher 74.69 ± 4.30 µg ($P<0.05$). The FPD of the SAX B formulation (8.42 ± 1.70 µg) was significantly higher than the micronised formulation (3.99 ± 0.70 µg) ($P<0.05$). Figure 4.13 shows the comparison of FPF_{ED} of micronised budesonide and SAX B formulations. As shown in Figure 4.13, FPF_{ED} aerosolised per capsule for SAX B formulation was significantly higher than the micronised formulation ($P<0.05$), with the FPF_{ED} increasing from 6.60% for the micronised formulation to 11.23% for the SAX B formulation. These data suggest that the greater delivery of budesonide from the SAX B formulation may be attributed to the corrugated morphology of the particles, which may have lowered the contact area between the particle and lactose carrier, thereby increasing the liberation of SAX B particles on aerosolisation. Such behaviour of corrugated particles as also been shown by Chew and Chan (Chew and Chan, 2001).

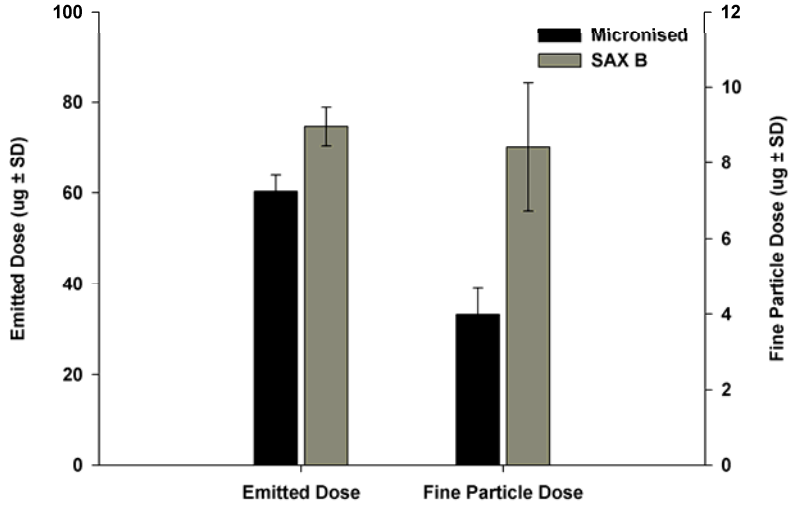

Figure 4.12: The emitted dose and fine particle dose per capsule of budesonide aerosolised from the formulations of micronised budesonide and SAX-produced budesonide B

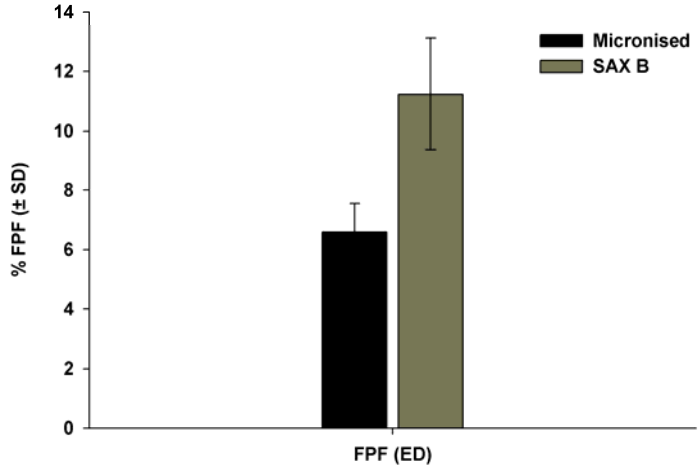

Figure 4.13: The percent fine particle fraction of emitted dose of budesonide aerosolised from the formulations of micronised budesonide and SAX-produced budesonide B

4.4.3 Study II: *In-Vitro* Performance of SAX C

4.4.3.1 SEMs of the Formulations

Representative SEMs of: (A) etched lactohale; (B) the formulation of micronised budesonide, formulated by blending micronised budesonide with etched lactohale; and (C) the formulation of SAX C, formulated by mixing SAX-produced Bud C with etched lactohale are all shown in Figure 4.14. The formulations of micronised budesonide and SAX C in Figure 4.14B and 4.14C exhibited that the etched lactohale, which had the smooth surface, was covered with the small drug particles. The formulations of micronised budesonide and SAX C were prepared by blending such drug particles to the etched lactohale. Therefore, the SEM micrographs of both B and C exhibited the same patterns of small drug particles embedded on the surface of the etched lactose crystals.

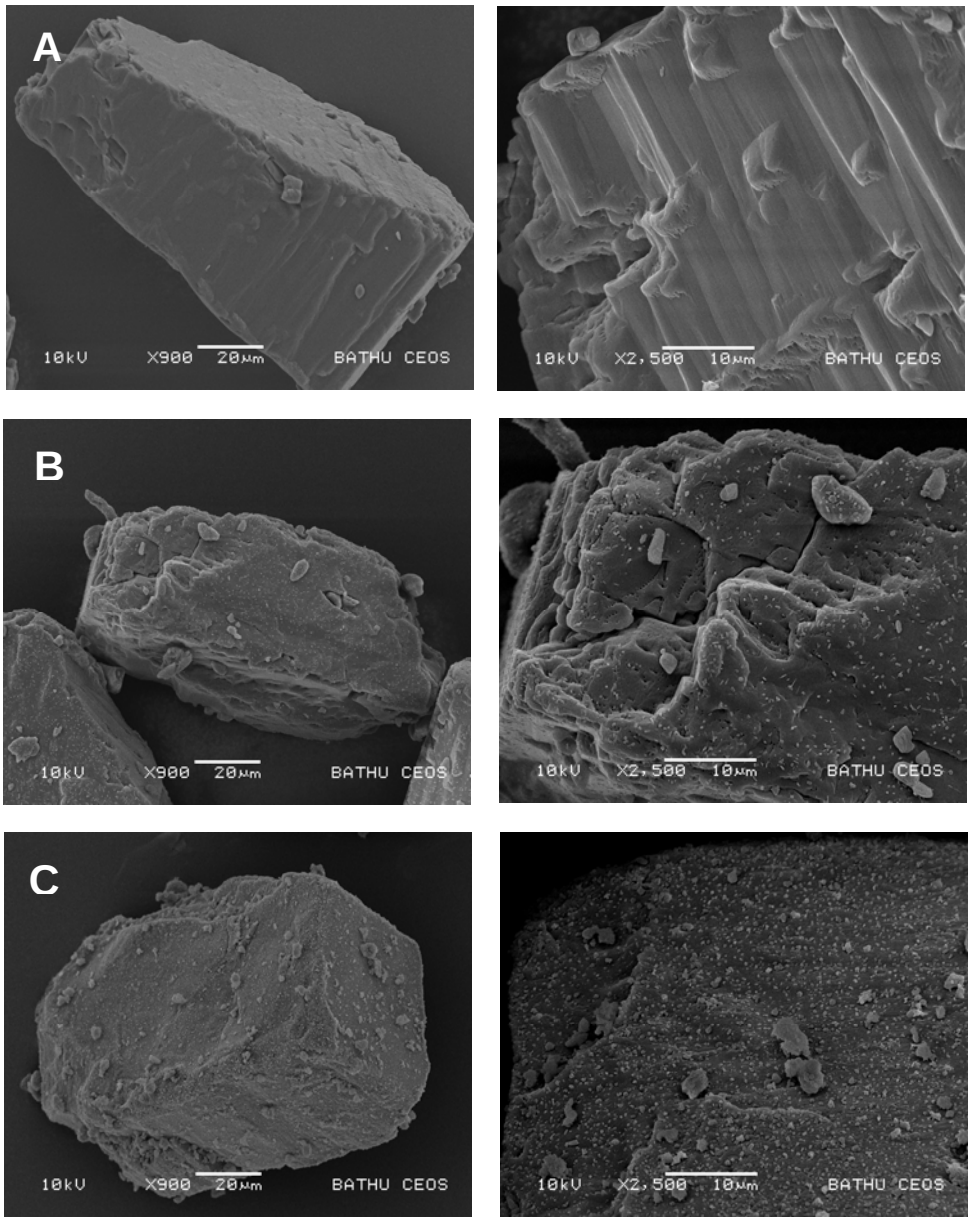

Figure 4.14: Representative SEMs of: (A) etched lactohale; (B) the formulation of micronised budesonide; (C) the formulation of SAX C at magnifications of x900 and x2500

4.4.3.2 Content Uniformity

The coefficient of variation (CV) of the drug content of the two formulations for micronised budesonide and SAX C was <6%, which is the upper limit of what is generally acceptable as uniformity for a carrier-based DPI formulation. The micronised budesonide blended with etched lactohale showed the CV at 0.90 %, whereas the CV of the SAX C formulation was at 2.23 %. These results revealed that both formulations were uniformly mixed.

4.4.3.3 Drug Impactor Deposition

The mean mass data of drug deposited per capsule on each stage of the MSLI for micronised budesonide and SAX C formulations are shown in Table 4.3 and Figure 4.15. Table 4.3 also demonstrates the ED, FPD, FPF_{ED} and MMAD.

Table 4.3: MSLI deposition per capsule of drug aerosolised from micronised Bud and SAX-produced Bud C formulations

Bud = budesonide; D & C = device and capsules; MP & T = mouthpiece and throat; PS = pre-separator; S = stage

Formulations	***Mean Drug Deposition on Impactor Stages (µg ± SD)***							***Mean ED (µg ± SD)***	***Mean FPD (µg ± SD)***	***Mean FPF_{ED} (% ± SD)***	***MMAD (µm ± GSD)***
	D & C	***Throat***	***S1***	***S2***	***S3***	***S4***	***Filter***				
Micronised Bud	40.63 ± 6.14	5.57 ± 0.42	90.55 ± 15.70	7.00 ± 0.79	7.57 ± 1.91	8.25 ± 0.78	2.89 ± 0.86	121.84 ± 8.75	18.71 ± 3.23	15.38 ± 1.58	3.75 ± 1.88
SAX-produced Bud C	40.22 ± 8.13	15.42 ± 2.39	89.60 ± 1.20	7.10 ± 1.82	7.74 ± 1.06	7.52 ± 1.54	2.52 ± 0.31	129.90 ± 3.54	17.78 ± 1.99	13.68 ± 1.38	3.88 ± 1.86

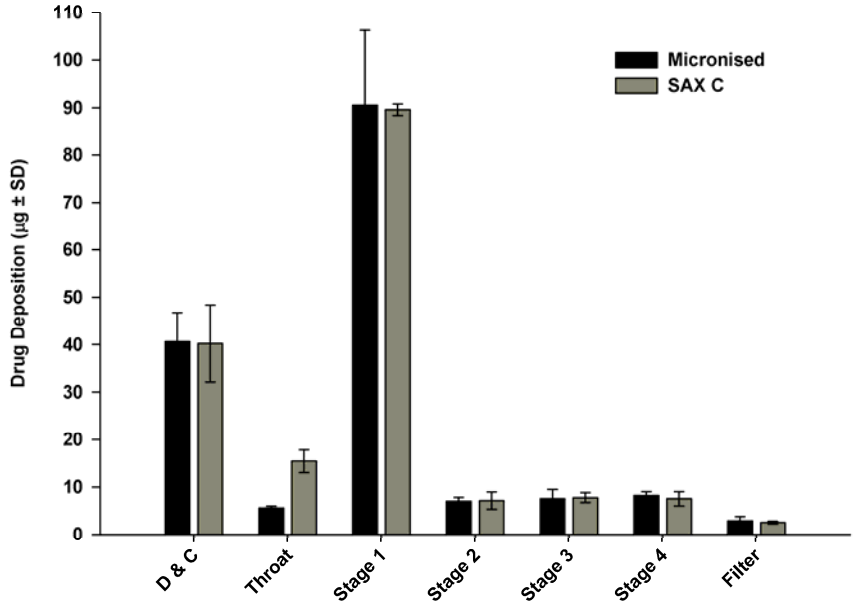

Figure 4.15: MSLI deposition per capsule of budesonide aerosolised from the formulations of micronised budesonide and SAX-produced Bud C

As shown in Figure 4.16, both ED and FPD aerosolised per capsule of the micronised formulation were not significantly different from the SAX C formulation. The ED of the micronised budesonide and the SAX C formulations were 121.84 ± 8.75 µg and 129.90 ± 3.54 µg, respectively. The FPD of the micronised budesonide and SAX C formulations were 18.71 ± 3.23 µg and 17.78 ± 1.99 µg, respectively. The similarities in delivery may be related to their mass median aerodynamic diameter (MMAD) measurements. The MMAD of SAX C was 3.88 ± 1.86 µm ($d_{50\%}$ = 8.68 µm), which was similar to the MMAD of 3.75 ± 1.88 µm for the micronised budesonide. The significant increase in the fine particle delivery of SAX C particles may be related to a reduction in surface contact geometry owing to the morphology of the particles, which would result in greater aerosolisation efficiency. However, it is suggested that the density and the size of the nanometer-sized crystals exhibited by SAX C particles may also increase the effective contact area due to their number and size. This mechanism of increasing adhesion is similar to the manner in which the setae of geckos are able to support the weight of the lizard by van der Waals forces. The high surface density of the gecko setae is thought to correspond to greater contact area and, therefore, greater adhesion (Autumn, Sitti et al., 2002). Similarly, the high surface density of budesonide particles at the surface may also correspond to greater adhesion to the lactose.

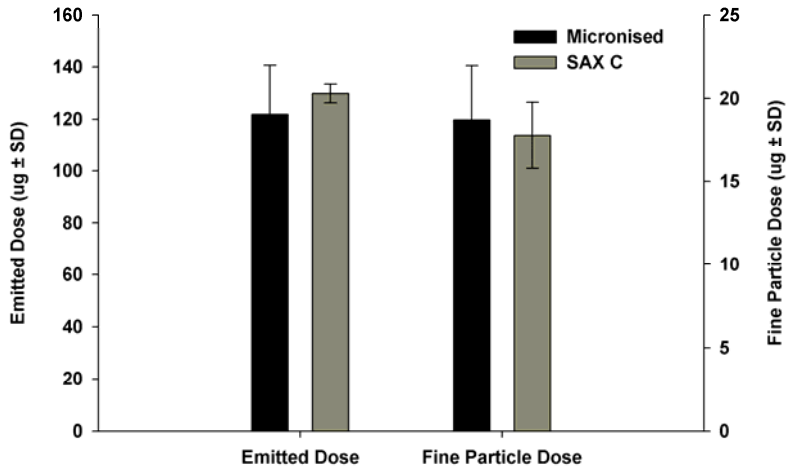

Figure 4.16: The emitted dose and fine particle dose per capsule of budesonide aerosolised from the formulations of micronised budesonide and SAX-produced budesonide C

The FPF_{ED} of micronised budesonide and SAX C formulations are shown in Figure 4.17. Micronised budesonide formulation presented a FPF_{ED} of 15.38%, and the FPF_{ED} of SAX C formulation was 13.68%. It is apparent that there was no significant difference between the FPF_{ED} of micronised budesonide and SAX C formulations (p=0.233). These data suggest that owing to the hollow/porous nature of the SAX C particles, the aerodynamic diameters of both SAX C and micronised budesonide were similar as their aerosolisation properties. These data confirm that the SAX process may be utilised to produce hollow particles, which possess smaller aerodynamic diameters that enable penetration of particles into the lower airways. There are many particle engineering processes that may be applied to fabricate porous particulates. However, this is usually achieved by compromising on physical stability of materials, as many of these processes result in the generation of amorphous metastable solids. The advantage of the SAX process is that particles such as SAX C are predominately crystalline and, therefore, likely to remain stable over product shelf-life.

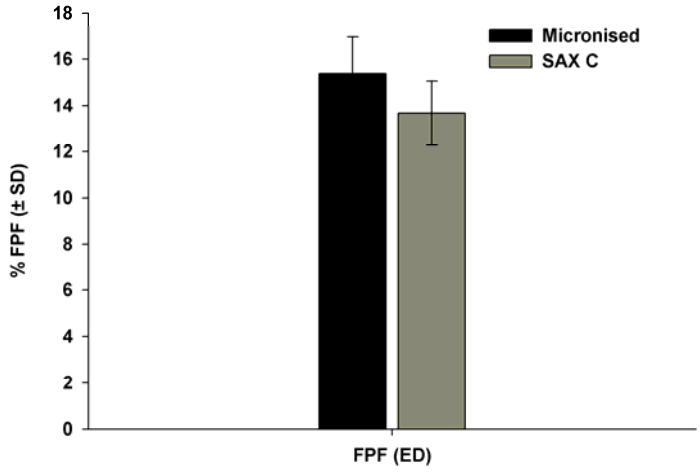

Figure 4.17: The % FPF_{ED} of budesonide aerosolised from the formulations of micronised budesonide and SAX-produced Bud C

4.5 Conclusions

In conclusion, the SAX process has been successfully employed in engineering particles of budesonide with the desired property function for delivery to the lungs. The SAX-produced budesonide particles were crystalline and these particles displayed no polymorphic variations upon processing. The SAX B particles possessed the desired physical properties with appropriate particle size for lung delivery. Moreover, *in-vitro* performance analysis suggested that the morphological characteristics of SAX B particles may have resulted in the significantly greater delivery than the micronised formulation. The SAX C particles were unique as, although the particle size of the material was not optimal for delivery to the lungs, the materials' hollow/porous nature resulted in the particles displaying a smaller aerodynamic diameter. As a result, the larger SAX C particles showed almost equivalent aerosolisation deposition patterns as the smaller micronised particles.

These data show that the SAX process can be used almost as a 'dial-a-particle' process, where particles with the desired property function can be produced for inhaled dosage forms.

Chapter 5: Engineering of Crystalline Combination Inhalation Particles of a Long-acting β_2-agonist and Corticosteroid

5.1 Introduction

Chronic respiratory diseases such as asthma and chronic obstructive pulmonary disease (COPD) have become major global epidemics with increasing mortality rates (World Health Organisation, 2007). According to the latest World Health Organisation (WHO) estimates, approximately 300 million people suffer from asthma (Masoli, Fabian et al., 2004) and almost 210 million have COPD (Halbert, Natoli et al., 2006). WHO estimates for 2030 suggest that COPD will become the third commonest cause of death (Lopez and Mathers, 2006). With limited treatment options to slow the relentless progression of these diseases, chronic respiratory diseases constitute a serious public health problem in all countries throughout the world (Bousquet, Dahk et al., 2007).

The preferred route of administration of medicaments to treat chronic airway diseases is by inhalation *via* a pressurised metered dose inhaler (pMDI) or dry powder inhaler (DPI) (Virchow, Crompton et al., 2008). The delivery of therapeutic agents to the lungs affords many advantages, for example, rapid onset of action, enables smaller doses to be used and provides a greater efficacy to safety ratio in comparison to systemic therapy (Virchow, Crompton et al., 2008). While traditionally a single active pharmaceutical ingredient (API) was traditionally administered to the respiratory tract, the delivery of multiple drug agents *via* combined inhalation drug delivery systems has gained widespread acceptance by physicians and patients in the management of both asthma (Barnes, 2002; Ankerst, 2005; Nelson, 2005) and COPD (Dransfield and Bailey, 2004).

Medication non-compliance is a significant problem in the treatment of both asthma (Bateman, Britton et al., 1998) and COPD (Keating and McCormack, 2007), and has been a significant driver for the development of combined inhalation dosage forms (Barnes, 2002). These patients have a multitude of drugs to administer on a daily basis, which may often lead to the confusion in their treatment regimen (Stempel, Stoloff et al., 2005). Furthermore, patients tend to forget to take their anti-inflammatory medication

because, unlike a bronchodilator, it does not provide immediate relief from acute symptoms (Wallin, Sue-Chu et al., 2003). Since the regular use of anti-inflammatory drugs is central to treating the underlying disease of asthma and COPD, the combination of an anti-inflammatory drug with a long-acting bronchodilator has been shown to vastly improve disease management for both patients and physicians (Miller-Larsson and Selroos, 2006). Although the interest in combined inhalation therapy has been primarily driven from a patient compliance stand-point, recent clinical studies support the deployment of multiple actives in a single inhalation dosage form to improve treatment efficacy and clinical outcome (Nelson, Chapman et al., 2003).

Asthma and COPD are complex disease conditions of the airways that share some similarities; both are characterised by air flow limitation and airway inflammation (Barnes, Shapiro et al., 2003; Barnes, 2008). However, they are disparate conditions since the airflow limitations experienced by people with asthma are fully reversible with bronchodilators, whereas in COPD they are not (Dransfield and Bailey, 2004; Cazzola, Ando et al., 2007). Furthermore, airway inflammation in COPD is characterised by the presence of neutrophils and macrophages (Barnes, Shapiro et al., 2003; Barnes, 2004), while the predominant inflammatory cells observed in asthma are eosinophils and mast cells (Barnes, Chung et al., 1998). These histological differences in the cellular infiltration between asthma and COPD suggest major differences in the chronic inflammatory processes involved in each disease condition, which is confirmed by the presence of different inflammatory chemokines and cytokines in each condition. However, one pro-inflammatory chemokine that plays a key role in the inflammatory processes of severe asthma and COPD is IL-8. This chemokine is a potent neutrophil chemo-attractant up-regulated in response to inflammatory stimuli such as cigarette smoke or bacterial products (Kunkel, Standiford et al., 1991). The recruitment of large numbers of inflammatory cells to the lungs in response to increase IL-8 secretion leads to the tissue damage that typifies pathophysiologies in cystic fibrosis (Dean, Dai et al., 1993), asthma (Shute, Vrugt et al., 1997) and eosinophilic pneumonia (Barnes, Chung et al., 1998). Such complexities associated with the chronic inflammatory processes in each disease condition pose significant challenges in determining a treatment strategy.

In order to manage respiratory disease conditions such as asthma and COPD, therapies are required to control symptoms, reduce exacerbations and improve health status in patients. The first-line treatments in treating both conditions are long-acting β_2-

agonists (LABA) and inhaled corticosteroids (ICS), which are employed to aid bronchodilation and reduce inflammation, respectively (Greening, Ind et al., 1994; Matz, Emmett et al., 2001). Inhalation dosage forms combining a LABA and ICS are available in both pMDI and DPI platforms (Keating and McCormack, 2007). For the combined inhalation products available, the salmeterol xinafoate (SX, LABA) and fluticasone propionate (FP, ICS) combination inhalation product (Seretide®/Advair® Inhaler, GlaxoSmithKline, UK) has shown a greater efficacy compared with monotherapy with the individual components (Nelson, 2005). The product is highly successful and this product is currently listed amongst the top ten best-selling pharmaceutical products with annual sales of approximately $4.3 billion (Davis, 2008).

Clinical studies have indicated that combination inhaled therapy of LABAs and ICSs improves health outcomes in asthma and COPD in comparison to mono-therapy with LABA and ICS (Calverley, Pauwels et al., 2003; Bergmann, Lindemann et al., 2004; Calverley, Anderson et al., 2007; Cazzola, Ando et al., 2007). Furthermore, observational studies suggest that combination inhalation therapy may actually reduce mortality in COPD (Sin and Man, 2007). In addition, recent studies have also shown that the superior efficacy of combined inhalation therapy with LABAs and ICSs could be due to complementary and synergistic interactions (Nelson, Chapman et al., 2003).

The two classes of compounds have very different modes of action and thereby target different elements of the disease process. For example, SX, a selective long-acting β_2-adrenoceptor agonist, has almost fifty times the selectivity for the β_2-adrenoceptor than salbutamol (Cazzola, Testi et al., 2002). The mechanism of action corresponds to the binding to the β_2-adrenoceptor, thereby activating intracellular adenylyl cyclase, which catalyses the conversion of adenosine triphosphate (ATP) to cyclic adenosine monophosphate (cAMP). The increased levels of cAMP lead to bronchial smooth muscle relaxation (Cazzola, Testi et al., 2002; Keating and McCormack, 2007). In contrast, the FP (ICS) is a potent glucocorticosteroid with anti-inflammatory properties that are predominately mediated by the glucocorticoid receptor (Dransfield and Bailey, 2004). Hence, the enhanced clinical benefit of combining both classes of compounds in a single inhaler may be related to such additive effects of administering both agents simultaneously to the lung because they have complementary modes of action and different target aspects of the underlying disease pathophysiology (Barnes, 2002; Nelson, 2005). However, the increased clinical efficacy of inhaled therapies combining

FP and SX has been reported to be more than just additive effects of co-administering both agents, but may be due to synergistic interactions of the two classes of compounds at the receptor, molecular and cellular level (Nelson, Chapman et al., 2003). Several molecular mechanisms have been postulated to explain the synergistic action of FP and SX. It is thought that the corticosteroid may provide protection against down regulation of the β_2-adrenoceptor through up-regulation of β_2-receptor gene expression, thereby increasing synthesis of respiratory mucosal β_2-adrenoceptor (Baraniuk, Ali et al., 1997). The LABAs, for example SX, have been shown to prime the inactive glucocorticoid receptor through a phosphorylation mechanism that renders the receptor more sensitive to steroid-dependent activation (Johnson, 2002). Furthermore, there has been the evidence of enhanced glucocorticoid receptor translocation into the nucleus when FP and SX are co-administered, suggesting that SX may amplify the anti-inflammatory effects of FP (Usmani, Ito et al., 2005). This synergistic action is thought to occur when both drugs reach the same cell together in adequate concentrations (Nelson, Chapman et al., 2003). The administration of both drugs from a single inhalation dosage form is likely to enhance the probability co-deposition in comparison to monotherapy of the individual drug agents. This is primarily related to the lower variability in patient inspiratory action when a single inhalation device is employed to deliver both actives to the lungs, which prevents different lung deposition patterns of both drugs. The delivery of both drugs in a single inhalation is also likely to expose regions of the lung to a single aerosol cloud containing both actives, which may also enhance the likelihood for co-deposition. Moreover, recent studies have shown that the opportunity for synergistic action is further enhanced in the Seretide formulation by co-deposition of FP and SX particles in the airways as a result of particle co-association within the delivery device (Michael, Snowden et al., 2001; Nelson, Chapman et al., 2003; Theophilus, Moore et al., 2006).

Current DPI-combined inhalation dosage forms are physical mixtures of comminuted fine drug particles of both actives and coarse carrier particles of lactose monohydrate, which are employed within DPI formulations to improve flow properties and metering of the highly cohesive drug particles (Hersey, 1975; Malcolmson and Embleton, 1998; Edge, Kibbe et al., 2005). During inhalation, the patient's inspiratory force is employed to detach the fine drug particles from the carrier in order to deposit in the deep lung (Telko and Hickey, 2005). Hence, the process of entrainment and deposition of both actives in the airways is largely dependent on the balance of interfacial forces between

components of the formulation (Jones, Harris et al., 2007). As a result, the prospect of co-depositing of both actives to the same site of action in the correct dose ratio is rather limited and cannot be controlled (Taki, Zeng et al., 2006). Hence, these dosage forms are subject to greater variability in fine particle delivery of each active. Furthermore, as the actives deployed in DPI dosage forms are micronised using high-energy mechanical processing, the presence of process-induced structural disorder at the surfaces of these particles may perpetuate the variability in dose delivery of both actives as a function of product storage conditions. These factors may ultimately limit the enhanced clinical efficacy of combination inhalation therapy achieved through synergistic action between actives delivered together at the same site of action. Thus, there is a requirement of processes that may enable the preparation of combination DPI products which will allow both drugs to be delivered more efficiently and independently of dose variations.

One approach to circumvent problems associated with the development of combination DPI products is to locate separate formulations of both actives in different compartments of a single device (Braithwaite and Williams, 2005). Upon inhalation, both formulations can be aerosolised in one inhaled air-stream, thereby enabling delivery of both actives in one aerosol cloud to the site of action. Another approach would be to combine multiple actives into a single particle, an approach previously suggested by Westmeier and Steckel (Westmeier and Steckel, 2008). They employed a precipitation process to produce combined particles consisting of FP and SX in the presence of crystal growth inhibitors. The authors were able to generate combined co-precipitated particles of FP and SX in the respirable range using a mixture of polysorbate and HPMC. However, the product was found to be partly crystalline following spray drying and, therefore, this approach would require optimisation (Westmeier and Steckel, 2008). The use of the solution atomisation and crystallisation by sonication (SAX) process may provide an alternative route of producing crystalline combined inhalation particles of FP and SX.

The SAX process consists of three interdependent processes: (a) the production of aerosol droplets of the solute from a carrier solvent using a suitable aerosol generator; (b) the collection of the highly supersaturated droplets in a crystallisation vessel containing a non-solvent of the drug; (c) the application of ultrasonic waves to a crystallisation vessel to controllably induce homogeneous nucleation and crystal growth

(Kaerger and Price, 2004). An atomiser in the SAX process produces highly supersaturated spherical constructs of the active ingredient within a well-defined particle size for controlled crystallisation. By combining these processes and controlling relevant parameters, high-purity micron-sized sphere-like crystalline particles can be readily produced in a single-step (droplet-to-particle) operation. The major advantage of this low-cost technique relates to the use of any suitable aerosol generator and the whole process can be carried out under atmospheric pressure and ambient conditions. Furthermore, it has the potential for batch and continuous processing at an industrial scale.

The potential application of the SAX process has been investigated in this study in order to produce single crystalline particles containing both FP and SX *via* a single droplet to particle operation.

5.2 Materials

Micronised FP and SX were obtained from sources stated in Chapter 2. All organic solvents were of at least analytical grade and were supplied by Fisher Chemicals (Loughborough, UK). Water was prepared by MilliQ from reverse osmosis (Molsheim, France). Etched lactose was produced from coarse carrier lactose monohydrate as indicated in Chapter 2.

5.3 Methods

5.3.1 The Production of SAX-produced FP/SX Particles

Combined SAX FP/SX particles were prepared by atomisation of a 2% w/v solution containing FP:SX in the ratio 10:1 in acetone. Atomisation was conducted using a SU11 co-axial two-fluid atomiser with an internal mix (Spraying Systems Co., Illinois, USA). The atomiser was used at a sprayed rate of 4 $ml.min^{-1}$ with air pressure at 2.5 bar in the lab scale of the SAX process over 60 cm of separation distance including positive pressure 30 $L.min^{-1}$ in the system with an ultrasonic probe. The particles were collected in perfluorodecalin at 5˚C, and the resulting combined SAX particles of FP/SX

were isolated using supercritical CO_2 extraction of perfluorodecalin. The process conditions for the extraction of perfluorodecalin using supercritical CO_2 extraction was the same as the extraction of hexane as described in Chapter 3.

5.3.2 Formulation Blending

A formulation, containing 1.6% w/w combined SAX FP/SX particles, was prepared by geometric blending with 63 - 90 µm sieve fraction of surface-etched lactose produced as described in Chapter 2. The combined SAX particles and coarse ethed-lactose were mixed in a 15 ml glass tube for 60 seconds in a Whirlimixer (Fisons Scientific Equipment, Loughborough, UK). The resultant blend was further processed using a Turbula shaker-mixer (Willy A Bachofen AG, Basel, Switzerland) at 46 rpm for 45 minutes.

In order to compare the *in-vitro* inhalation performance of SAX FP/SX and micronised FP/SX, a combination formulation containing 1.45% w/w micronised FP and 0.15% w/w micronised SX, (ratio 10 to 1), was prepared by geometric blending with 63 - 90 µm sieve fraction of surface-etched lactose. The drug and ethched-lactose were mixed in a 15 ml glass tube for 60 seconds in a Whirlimixer (Fisons Scientific Equipment, Loughborough, UK). The resultant blend was then mixed using a Turbula shaker-mixer (Willy A Bachofen AG, Basel, Switzerland) at 46 rpm for 45 minutes. Both the formulations containing either combined SAX particles of FP:SX or micronised FP and SX were stored at 44 % RH and 25 °C for 24 h before formulation testing.

5.3.3 Content Uniformity Determination

The content uniformity of the respective formulations was determined by obtaining ten random samples of 25 $\pm$ 1 mg from various positions of the powder bed. Each sample was dissolved in a solution of 45% methanol, 35% acetonitrile and 20% water, which was sonicated for 15 minutes and made up to a 100 ml final volume. Following this, the drug concentration was assessed by HPLC. The proportion of drug in each sample was calculated and the content uniformity expressed as the coefficient of variation (Equation 4.1)

5.3.4 Capsule Filling

Each formulation was manually loaded into size 3 HPMC capsules (Qualicaps, Madrid, Spain). Fill weight was 25 ± 1 mg, giving a nominal dose of 364 ± 20 µg for FP and 36 ± 2 µg for SX per capsule. In order to investigate the influence of the storage on the performance of micronised and SAX FP/SX preparation, formulations were stored at different environmental conditions. In Study I, filled capsules of both micronised and SAX FP/SX formulations were stored in a sealed chamber containing a saturated solution of potassium carbonate (giving a relative humidity of 44%) at 25˚C and re-tested four weeks later. For Study II, the filled capsules were stored in a sealed chamber containing a saturated solution of sodium chloride (giving a relative humidity of 75%) at 25˚C, and re-tested at two weeks and four weeks. In Study III, the filled capsules were also stored in a sealed chamber containing a saturated solution of sodium chloride (giving a relative humidity of 75%) at 40˚C and re-investigated at two weeks and four weeks.

5.3.5 *In-vitro* Performance Analysis

In-vitro formulation performance was assessed using a NGI (Copley Scientific Ltd, Nottingham, UK). All NGI collection cups were immersed in a 1% v/v solution of silicone oil (Acros Organics, Geel, Belgium) in hexane and allowed to air dry. The NGI was then assembled with a pre-separator (containing 15 ml of wash solvent) and connected to a vacuum pump (Gast, Benton Harbour, MI, USA) *via* a solenoid valve. The flow rate at the inlet to the throat was set to 60 $L.min^{-1}$ using a digital flow meter with model DFM 2000 (Copley Scientific Ltd., Nottingham, UK). A capsule was inserted in the Cyclohaler and punctured by two sharp pins to generate two small holes. Then, a Cyclohaler was attached to the throat of the NGI using a rubber mouthpiece. The contents of the capsule were then aerosolised into the NGI by drawing air through the apparatus at 60 $L.min^{-1}$ for 4 seconds (controlled by a solenoid valve). Once the contents of ten capsules were aerosolised in this way, the device was disconnected. The device and capsules, inlet port, pre-separator and each stage of the NGI were washed down into separate known volumes of 45% methanol, 35% acetonitrile and 20% water, which were sonicated to aid dissolution and allowed to cool. The concentration of drug in each solution was investigated by HPLC, from which the mass

of drug deposited on each stage of the NGI was determined from stages 1 to 7 and on the micro-orifice collector (MOC). Between experiments, the NGI was washed in water and methanol, dried in an oven, and allowed to cool to room temperature.

5.3.6 High Performance Liquid Chromatography (HPLC)

Drug concentrations were determined by HPLC. The HPLC system consisted of the pump, autosampler, column oven, UV detector and analyser as indicated in Chapter 4. Unknown sample concentration was determined from duplicate injections by comparison of the peak area with reference peaks from external standard solutions of known concentration.

The HPLC employed a 4.6 mm x 250 mm C18 5 µm Hypersil column (Thermo Electron Corporation, Waltham, MA, USA) and a mobile phase consisting of 45% v/v methanol, 35% v/v acetonitrile and 20% v/v water. The flow rate was 1.5 $ml.min^{-1}$; column temperature was 40˚C and injection volume was 200 µl. Drug retention times were 3.75 minutes for FP and 1.30 minutes for SX, so a run time of 5 minutes was employed. UV detection wavelengths were 235 nm for FP and 252 nm for SX.

The relationship between drug concentrations of FP and the peak area for each drug was found to be linear, with linear regression analysis yielding a coefficient of determination (R^2) of 0.9999. Similarly, the relationship between the drug concentrations of SX and integrated peak area for each drug was found to be linear, with linear regression analysis yielding a coefficient of determination (R^2) of 0.9992 (see Figure 5.1).

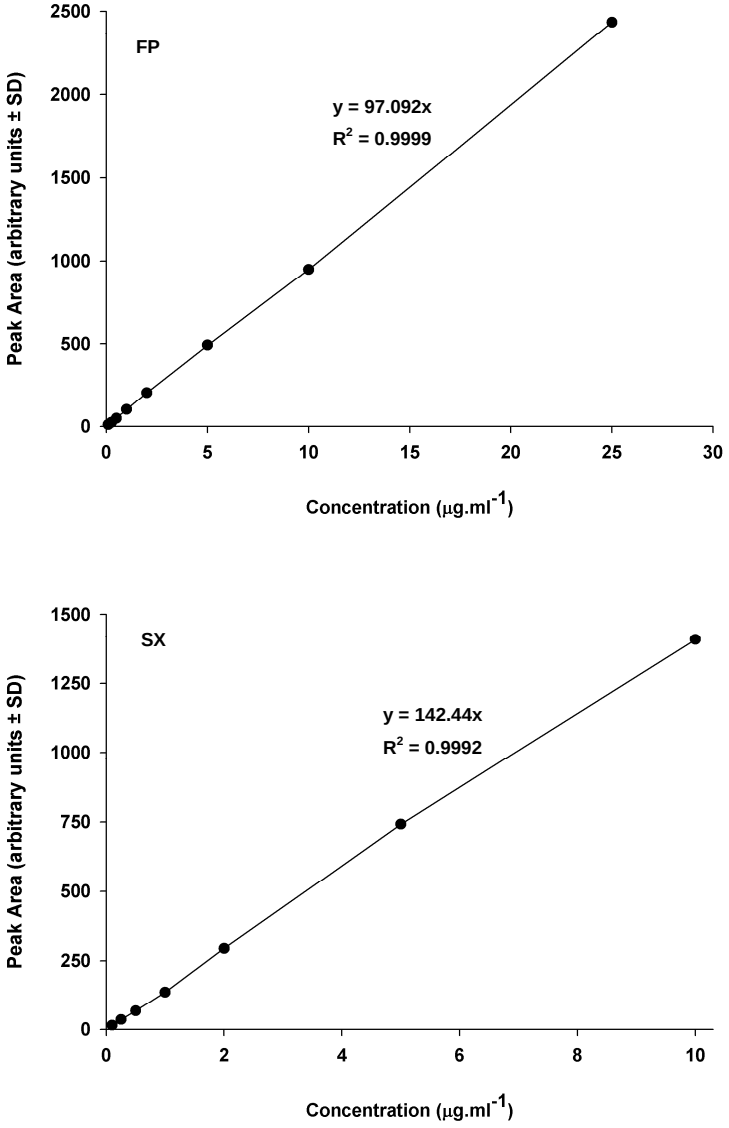

Figure 5.1: HPLC calibration curve for FP and SX

5.4 Characterisation of SAX-produced FP/SX Particles

5.4.1 Results and Discussion

5.4.1.1 Scanning Electron Microscopy

Representative scanning electron micrographs of micronised FP, micronised SX and SAX-produced FP/SX particles are shown in Figure 5.2. The morphology of the SAX-produced FP/SX particles appeared different from micronised FP and micronised SX. Micronised FP and SX particles shared a similar plate-like shape. The plate-like shapes of micronised FP were also slightly wider, whereas micronised particles of SX appeared to possess a narrow plate-like shape. The combined SAX-produced FP/SX particles were spherical in nature and these particles also possessed a defined corrugated morphology. Most particles of micronised FP and SX appeared in the form of agglomerated particles, whilst the SAX-produced FP/SX particles tended to be more dispersed, suggesting that the micronised FP and SX powders were more cohesive. This may be attributable to the corrugated morphology of the combined SAX particles, which may reduce contact between particles and, therefore, the level of agglomeration.

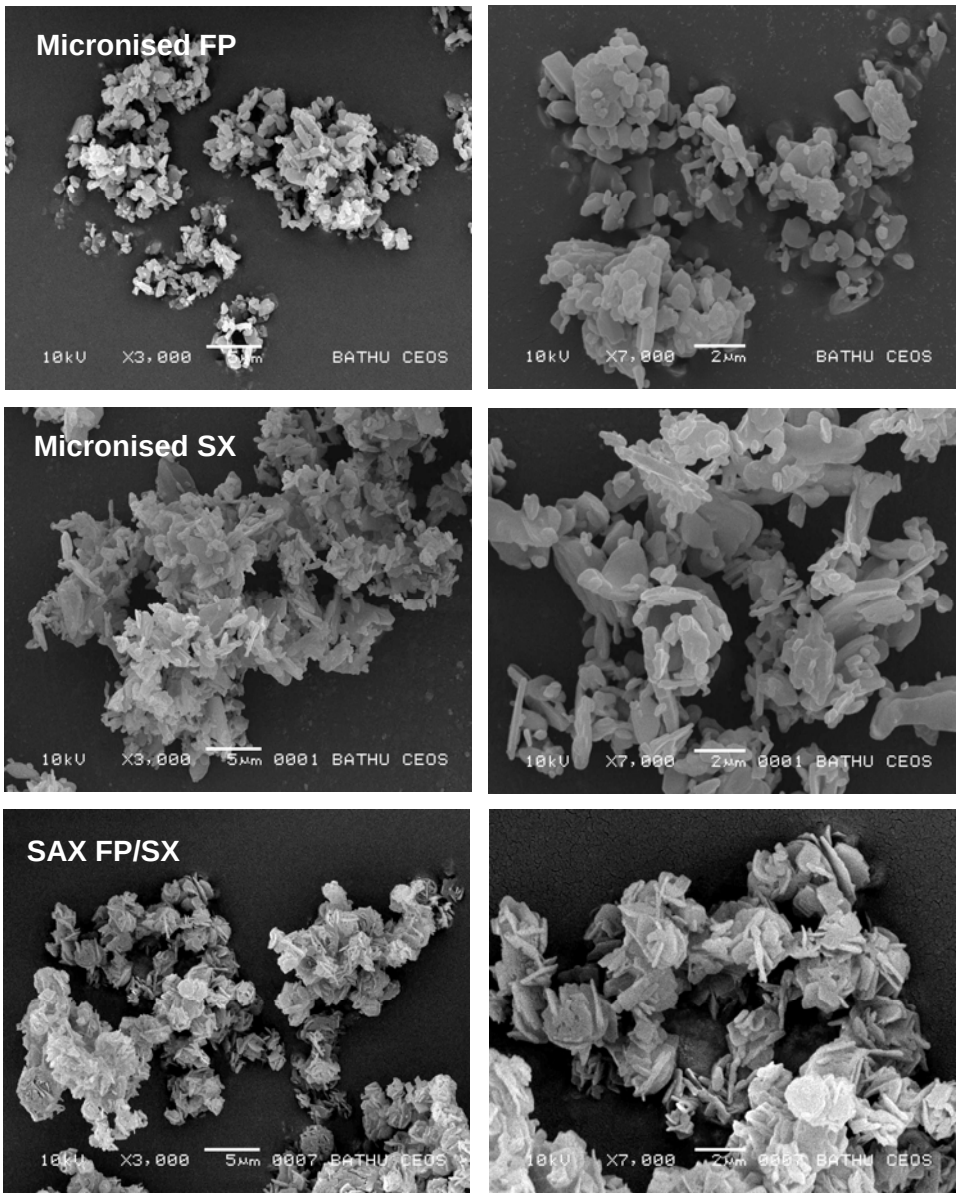

Figure 5.2: Representative SEMs of micronised FP, micronised SX and SAX-produced FP/SX particles at magnifications of x3000 and x7000

5.4.1.2 Particle Size Analysis

The particle size distribution of micronised FP, micronised SX and SAX-produced FP/SX is shown in Figure 5.3. The cumulative distribution of particles from micronised FP and SX was slightly narrower than SAX-produced FP/SX. In addition, the size distribution of micronised FP was marginally broader than micronised SX, but slightly narrower than SAX-produced FP/SX. These data are summarised in Table 5.1 using the d_{10}, d_{50} and d_{90} percentiles. It is apparent that the d_{50} values of micronised FP, SX and SAX-produced FP/SX are 3.28, 2.13 and 4.68 µm, respectively. These data suggest that the micronised drug particles and SAX-produced FP/SX confirmed the suitable size range for the preparation of DPI formulations (Zeng, Martin et al., 2001). Furthermore, the particle size distribution of the SAX-produced combined FP/SX particles was mono-modal, which suggests that both FP and SX may have been successfully processed into one particle.

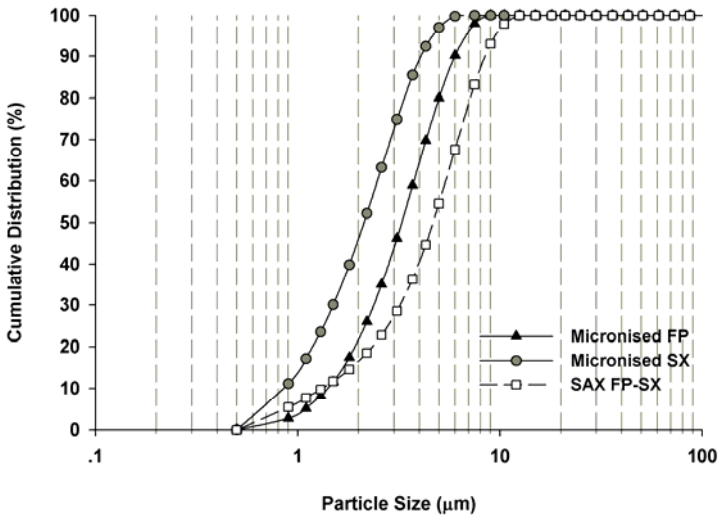

Figure 5.3: Particle size distribution of micronised FP, micronised SX and SAX-produced FP/SX particles

Table 5.1: Summary of particle size data of micronised FP, micronised SX and SAX-produced FP/SX particles

	$d_{10\%}$ (µm) ± SD	$d_{50\%}$ (µm) ± SD	$d_{90\%}$ (µm) ± SD
Micronised FP	1.41 ± 0.01	3.28 ± 0.01	5.98 ± 0.01
Micronised SX	0.86 ± 0.01	2.13 ± 0.01	4.09 ± 0.01
SAX FP/SX	1.33 ± 0.01	4.68 ± 0.01	8.53 ± 0.01

5.4.1.3 Differential Scanning Calorimetry

The DSC thermograms of micronised FP and SX are shown in Figure 5.4. The thermogram of micronised FP showed an endothermic peak at ~292°C, related to the melting temperature of FP. The thermogram of SX exhibited two endothermic peaks at ~124°C and ~139°C and exothermic peak at ~130°C. The first large endothermic at ~124°C represented the melting of SX form I, which re-crystallised to SX form II at ~130°C before melting again at ~139°C. Micronisation of SX form I has been reported to induce the formation of trace seeds of SX form II, which enabled this re-crystallisation to occur (Beach, Latham et al., 1999; Tong, Yu Shekunov et al., 2001). The DSC thermogram of SAX-produced FP/SX revealed three endothermic peaks as suggested in Figure 5.5. The two endothermic peaks exhibited at ~122°C and ~138°C, which were relevant to the SX peaks. The first endothermic at ~122°C represented the melting of SX form I, which re-crystallised to SX form II before melting again at ~138°C. Also, the last large endothermic peak appeared at ~294°C, related to the melting point of FP. These data suggest that both FP and SX were present in the combined FP/SX particles, and the SAX process did not change the polymorphic form of two active ingredients.

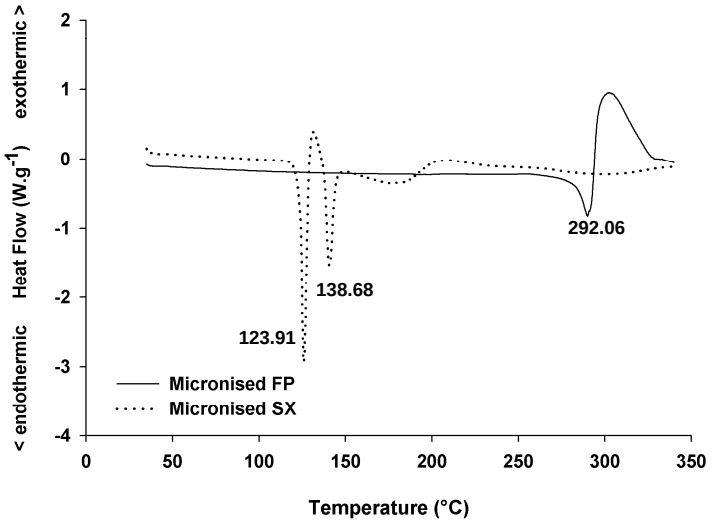

Figure 5.4: DSC thermograms of micronised FP, micronised SX particles

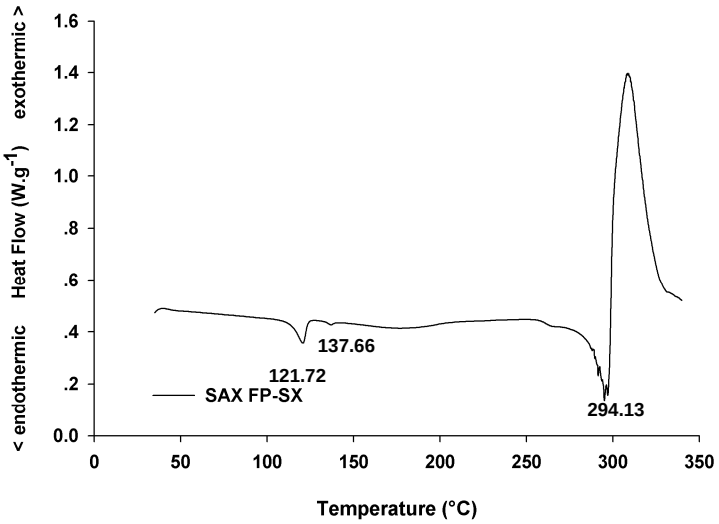

Figure 5.5: DSC thermogram of SAX-produced FP/SX particles

5.4.1.4 X-ray Powder Diffraction

In order to confirm the crystallinity of particles, XRPD was applied in this investigation. The XRPD patterns in Figure 5.6 show sharp diffraction peaks associated with crystalline materials of micronised FP, micronised SX and SAX-produced FP/SX. The XRPD diffractograms shown in this figure, show that the SAX-produced FP/SX had

similar X-ray patterns as micronised FP. This was expected as the combined particles produced by SAX contained predominately more FP. Moreover, these data confirm that the SAX particles were predominately crystalline.

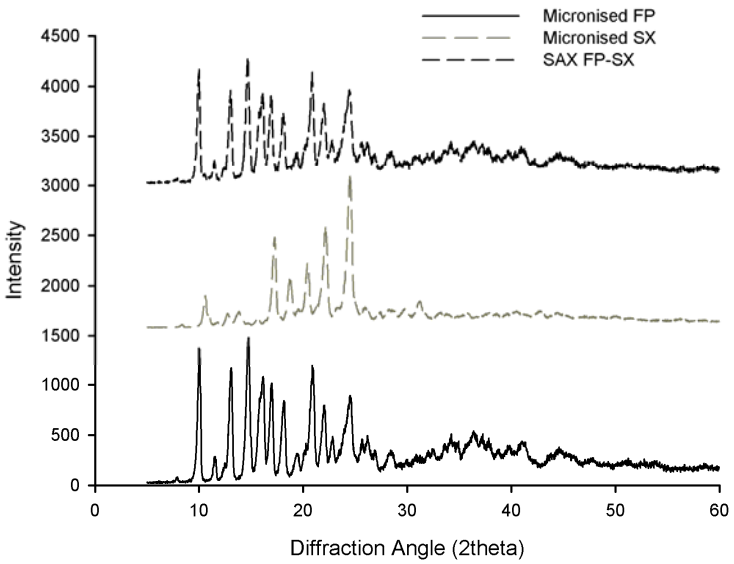

Figure 5.6: XRPD spectra of micronised FP, micronised SX and SAX FP/SX particles

5.4.1.5 Dynamic Vapour Sorption

The moisture sorption properties of micronised FP, micronised SX and SAX-produced FP/SX particles are demonstrated by the DVS isotherms shown in Figure 5.7. The DVS moisture sorption isotherms of the all materials showed <1% w/w mass increase or mass loss during the first sorption cycle. With respect to micronised FP, there is a significant increase in moisture sorption above 60% RH for the first sorption cycle. The following desorption and the subsequent second sorption cycle suggests that approximately 0.04% of water has been retained. Although the SAX FP/SX sample does not undergo such as step change at 60% RH, it also retains a similar amount of water. The significant increase in water sorption for SAX FP/SX may be due to the larger surface area of the material with respect to the corrugated morphology of the particles. These data suggest no indication of material re-crystallisation because the sorption profiles of second cycle are similar, which is indicative of a stable crystalline material.

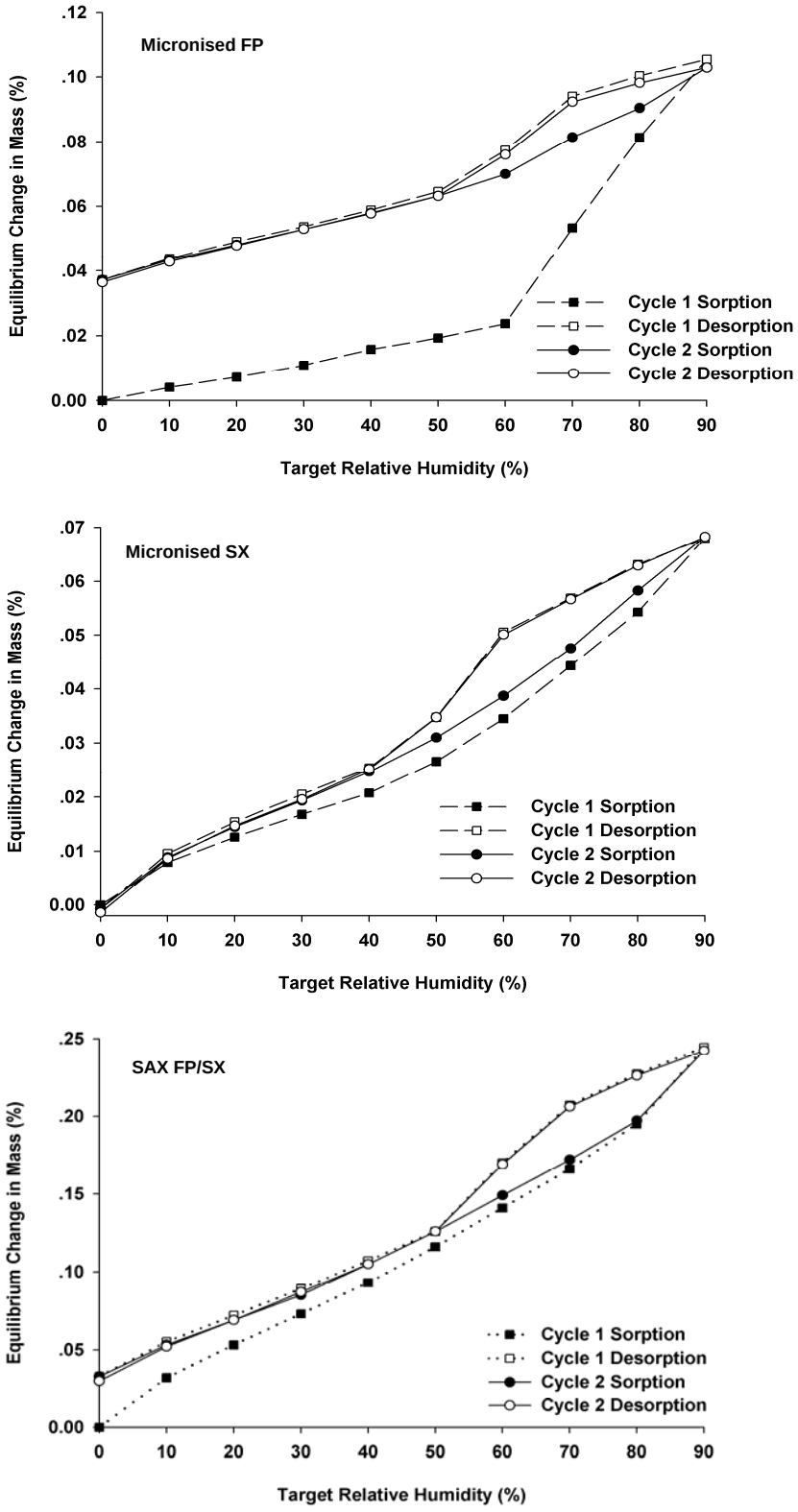

Figure 5.7: DVS isotherms of micronised FP, micronised SX and SAX-produced FP/SX particles

5.5 *In-vitro* Performance of FP/SX Formulations

5.5.1 Results

5.5.1.1 SEMs of the FP/SX Formulations

Representative SEMs of (A) etched lactohale, (B) the formulation containing both micronised FP and SX, and (C) the formulation containing combined SAX FP/SX are shown in Figure 5.8. The etched lactose exhibited the typical tomahawk shape of lactose monohydrate and displayed a smooth surface with limited amount of intrinsic fine lactose particles. The formulations containing micronised FP and SX and combined SAX FP/SX particles presented particulates deposited on the surface of the etched lactose upon blending.

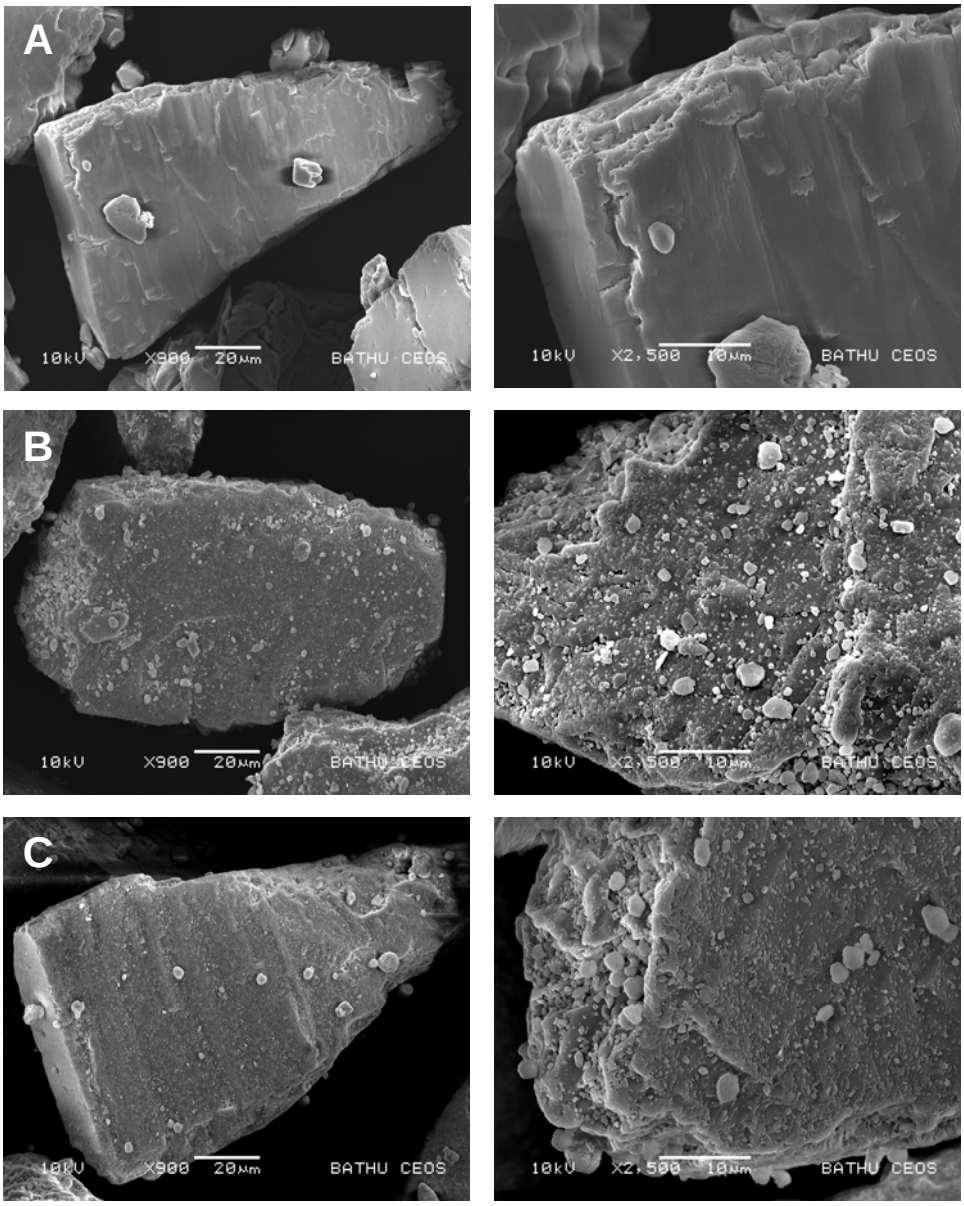

Figure 5.8: Representative SEMs of (A) etched lactohale, (B) the formulation of micronised physical mixture of FP/SX, and (C) the formulation of SAX-produced FP/SX at magnifications of x900 and x2500

5.5.1.2 Content Uniformity of FP/SX Formulations

The coefficient of variation (CV) of the drug content of the two formulations containing either micronised FP and SX or combined SAX particles of FP/SX was <6%, which is the upper limit of what is commonly acceptable as uniformity for a carrier based DPI formulation. These results demonstrated that both formulations were uniformly blended.

5.5.1.3 Study I: In-vitro Performance of FP/SX at 25˚C/44% RH

The *in-vitro* aerosolisation properties of combination DPI formulations composed of either micronised FP/SX or combined SAX FP/SX particles were evaluated using inertial impaction testing. The mean mass data of drug deposited per capsule on each stage of the NGI for both micronised FP/SX and SAX FP/SX formulations are shown in Table 5.2. These two formulations were investigated again after storing at 25˚C/44% RH for four weeks. Table 5.2 also shows the mean ED, FPD, FPF_{ED} and MMAD upon storage. The mean drug deposition data per capsule of both combined formulations at the initial time-point and the following storage at 44% RH at 25°C for four weeks are shown in Figure 5.9 and 5.10. It is evident from these data that aerosolisation of the SAX FP/SX formulation corresponded to higher drug deposition than the micronised FP/SX formulation.

Table 5.2: NGI deposition per capsule of drug aerosolised from the formulations of micronised FP:SX and SAX-produced FP:SX with ratio 10:1 stored at 25˚C/44% RH from different periods of time (week 0 and 4) FP = fluticasone propionate; SX = salmeterol xinafoate

No.	Formulations	Mean Drug Deposition on Impactor Stages (µg ± SD)											Mean ED (µg ± SD)	Mean FPD (µg ± SD)	Mean FPF_{ED} (% ± SD)	MMAD (µm ± GSD)
		D & C	MP &T	PS	S1	S2	S3	S4	S5	S6	S7	MOC				
1	Micronised FP at time 0	24.97 ± 2.58	9.39 ± 1.24	273.29 ± 3.49	2.90 ± 0.60	4.58 ± 0.26	6.64 ± 1.57	9.52 ± 0.63	5.35 ± 0.22	2.01 ± 0.16	0.87 ± 0.06	0.45 ± 0.06	315.00 ± 5.13	24.83 ± 1.76	7.88 ± 0.46	2.50 ± 2.40
	Micronised SX at time 0	3.56 ± 0.54	1.11 ± 0.03	32.56 ± 0.07	0.41 ± 0.09	0.43 ± 0.05	0.58 ± 0.10	0.81 ± 0.02	0.48 ± 0.08	0.26 ± 0.05	0.19 ± 0.03	0.17 ± 0.03	36.99 ± 0.25	2.48 ± 0.21	6.70 ± 0.53	2.30 ± 3.00
2	SAX-produced FP at time 0	32.88 ± 4.11	19.02 ± 2.98	166.37 ± 1.47	6.99 ± 1.29	10.20 ± 0.82	9.05 ± 0.30	7.71 ± 0.45	4.04 ± 0.02	1.83 ± 0.47	0.96 ± 0.17	0.62 ± 0.06	226.78 ± 3.09	24.21 ± 0.53	10.68 ± 0.32	3.60 ± 2.80
	SAX-produced SX at time 0	3.35 ± 0.37	2.36 ± 0.42	18.25 ± 2.19	0.83 ± 0.09	1.17 ± 0.19	1.06 ± 0.10	0.93 ± 0.11	0.49 ± 0.04	0.25 ± 0.05	0.16 ± 0.04	0.16 ± 0.04	25.66 ± 2.44	3.05 ± 0.14	11.96 ± 1.09	3.30 ± 3.10
3	Micronised FP at week 4	29.95 ± 1.23	8.95 ± 0.98	273.20 ± 6.77	2.09 ± 0.16	4.23 ± 0.20	7.12 ± 0.23	8.59 ± 0.17	2.49 ± 0.08	0.26 ± 0.00	0.02 ± 0.00	0.01 ± 0.00	306.96 ± 6.37	18.49 ± 0.44	6.03 ± 0.15	3.30 ± 1.90
	Micronised SX at week 4	3.60 ± 0.80	1.22 ± 0.04	35.40 ± 0.67	0.27 ± 0.04	0.35 ± 0.02	0.55 ± 0.02	0.76 ± 0.03	0.26 ± 0.01	0.08 ± 0.02	0.07 ± 0.01	0.08 ± 0.01	39.03 ± 0.71	1.79 ± 0.08	4.60 ± 0.18	2.70 ± 2.70
4	SAX-produced FP at week 4	60.26 ± 3.34	17.48 ± 0.71	202.60 ± 6.75	6.13 ± 0.93	14.41 ± 3.11	14.67 ± 3.26	12.29 ± 2.00	3.49 ± 0.90	0.40 ± 0.08	0.04 ± 0.02	0.01 ± 0.01	271.53 ± 16.80	30.90 ± 6.24	11.31 ± 1.66	3.90 ± 1.90
	SAX-produced SX at week 4	7.42 ± 0.39	2.13 ± 0.06	20.87 ± 0.45	0.67 ± 0.09	1.48 ± 0.32	1.51 ± 0.31	1.35 ± 0.25	0.47 ± 0.04	0.10 ± 0.01	0.09 ± 0.01	0.09 ± 0.01	28.76 ± 0.74	3.61 ± 0.57	12.52 ± 1.72	3.50 ± 2.60

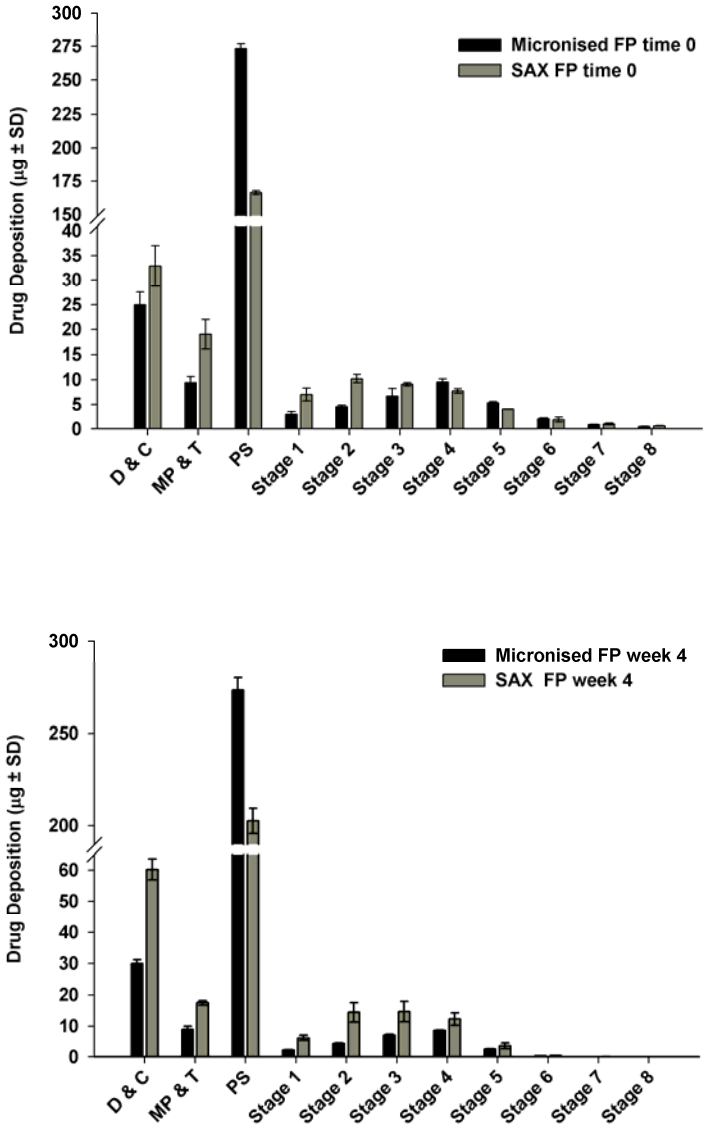

Figure 5.9: NGI deposition per capsule of FP aerosolised from the combination formulations of micronised FP:SX (10:1) compared with SAX-produced FP:SX (10:1) at 25˚C/44% RH from different periods of time (week 0 and 4)

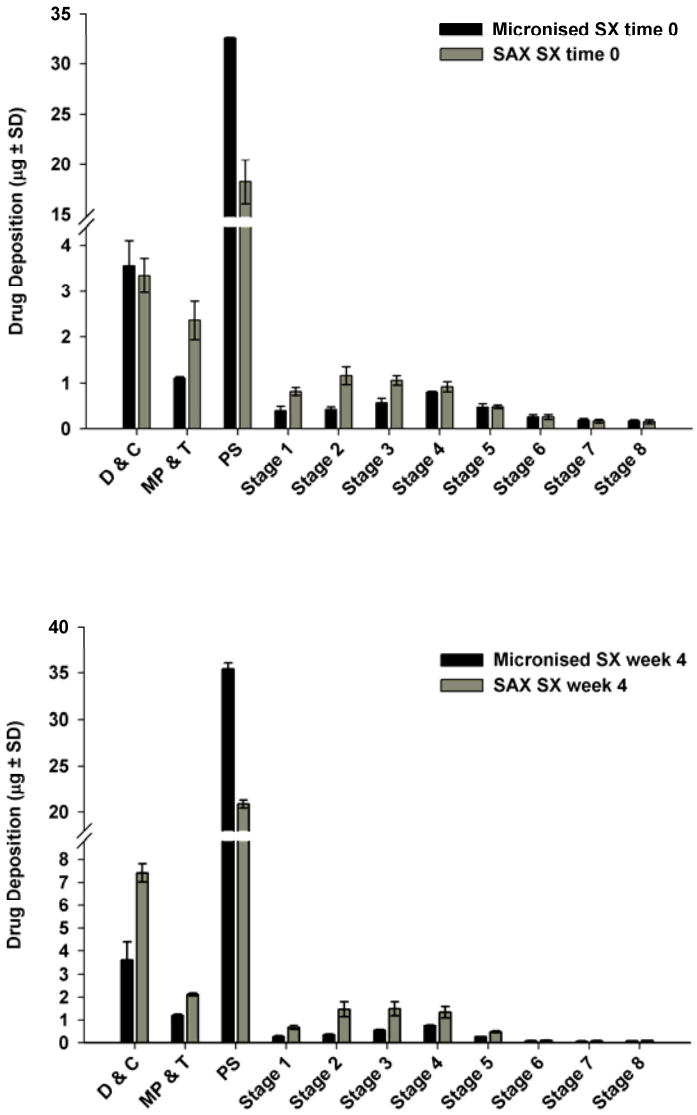

Figure 5.10: NGI deposition per capsule of SX aerosolised from the combination formulations of micronised FP:SX (10:1) compared with SAX-produced FP:SX (10:1) at 25˚C/44% RH from different periods of time (week 0 and 4)

At the initial time-point, the emitted dose (ED) of the micronised FP/SX formulation was 315.00 ± 5.13 µg for FP and 36.99 ± 0.25 µg for SX (Figure 5.11). In comparison, Figure 5.11 shows that the formulation of SAX processed FP/SX particles showed significantly ($p<0.05$) lower ED of FP (226.78 ± 3.09 µg) and SX (25.66 ± 2.44 µg).

Upon storage at 44% RH for four weeks, the micronised FP/SX formulation did not affect the ED of FP, however, a small but significant ($p<0.05$) increase of the emitted dose of SX was observed (Figure 5.11). In contrast, such figure also shows that on storage of the SAX FP/SX formulation under the same conditions, the results exhibited a significant ($p<0.05$) increase of the ED of FP, whilst the ED of SX remained unchanged.

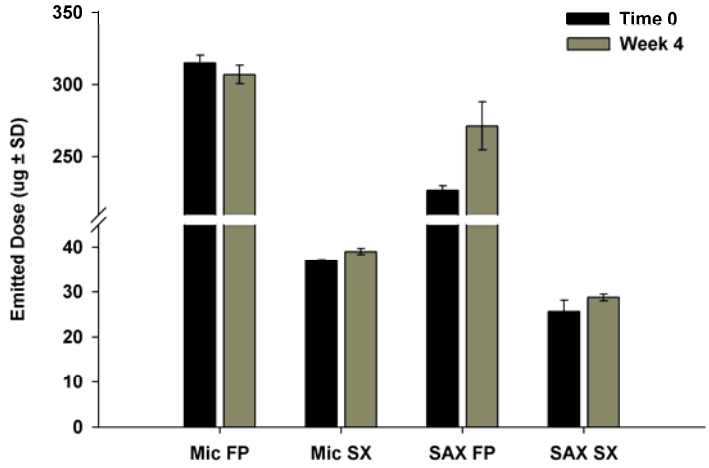

Figure 5.11: The emitted dose per capsule of micronised and SAX combined formulations stored at 25˚C/44% RH from different periods of time (week 0 and 4)

According to Figure 5.12, the FPD of FP and SX upon aerosolisation of the micronised FP/SX formulation at the initial time-point were 24.83 ± 1.76 and 2.48 ± 0.21 µg, respectively. In comparison, Figure 5.12 demonstrates no significant difference between the FPD of FP on aerosolisation of either the micronised FP/SX or the SAX FP/SX formulation. However, this figure reveals that the FPD of SX from the SAX FP/SX formulation was significantly ($p<0.05$) greater than that of micronised SX.

Upon storage of both formulations at 44% RH for four weeks, the FPD of both micronised FP and SX significantly ($p<0.05$) decreased, whilst no significant changes in the FPD of the SAX material were observed (Figure 5.12).

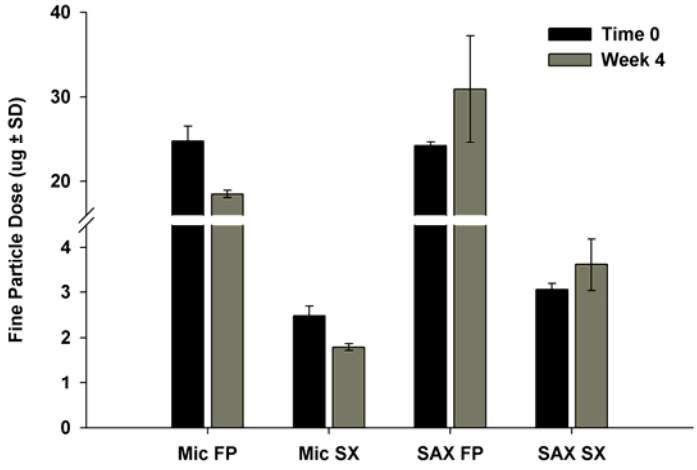

Figure 5.12: The fine particle dose per capsule of micronised and SAX combined formulations stored at 25˚C/44% RH from different periods of time (week 0 and 4)

At the initial time-point, the FPF_{ED} of the micronised FP/SX formulation was 7.88 ± 0.46% for FP and 6.70 ± 0.53% for SX (see Figure 5.13). In comparison, such figure exhibits that the formulation of SAX-produced FP/SX particles showed significantly ($p<0.05$) higher FPF_{ED} of FP (10.68 ± 0.32%) and SX (11.96 ± 1.09%).

After storage at 44% RH for four weeks, the micronised FP/SX formulation had a significant ($p<0.05$) change in the FPF_{ED} of both FP and SX. In contrast, Figure 5.13 demonstrates that the SAX FP/SX formulation remained unchanged with $p<0.05$ in both FP and SX upon storage under the same condition.

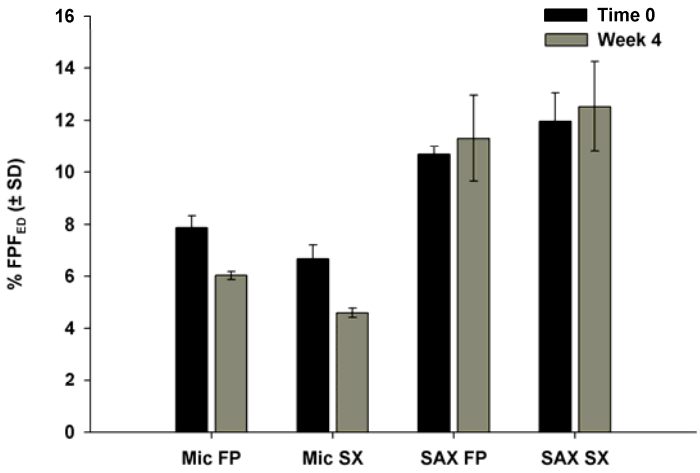

Figure 5.13: The fine particle fraction of emitted dose (FPF_{ED}) per capsule of micronised and SAX combined formulations stored at 25˚C/44% RH from different periods of time (week 0 and 4)

The mean normalised mass ratios of FP:SX as a function of recovered dose deposited on stages 2 to 5 of the NGI following aerosolisation of both formulations at the initial time-point and after storage at 25˚C/ 44% RH for four weeks are shown in Figure 5.14. As shown in this figure, the ratio of FP:SX from mean normalised data from stages 2 to 5 at the initial time-point following aerosolisation of the formulation containing micronised FP and SX was greater than one. These data suggest that deposition of both drugs was inconsistent and that materials were not deposited in their 10:1 (FP:SX)

ratio. As proposed earlier, such an occurrence *in-vivo* may reduce the potential for synergistic action between the actives, as the probability of delivery of both actives to the same site of action in the required concentrations will be limited. In contrast, the mean normalised ratio of FP:SX following aerosolisation of the SAX formulation on stages 2 to 5 was close to unity across stages 2 to 5. These data suggest that combined SAX particles of FP/SX may be effectively delivered through the lower respiratory system with the constant ratio of both combined drugs, which will increase the probability of synergistic effect of the class molecules at the receptor and cellular level. As can also be seen in Figure 5.14, at week 4, the ratio of FP:SX at 25˚C/44% RH tended to maintain the same pattern as the initial time-point. This suggested that FP and SX from SAX formulation were stable and maintained a constant ratio upon storage at 25˚C/44% RH for four weeks. In contrast, following aerosolisation of the micronised FP and SX formulation upon storage, the deposition of FP and SX varied significantly, which may correspond to increase chances of under or over-dosing of the class molecules.

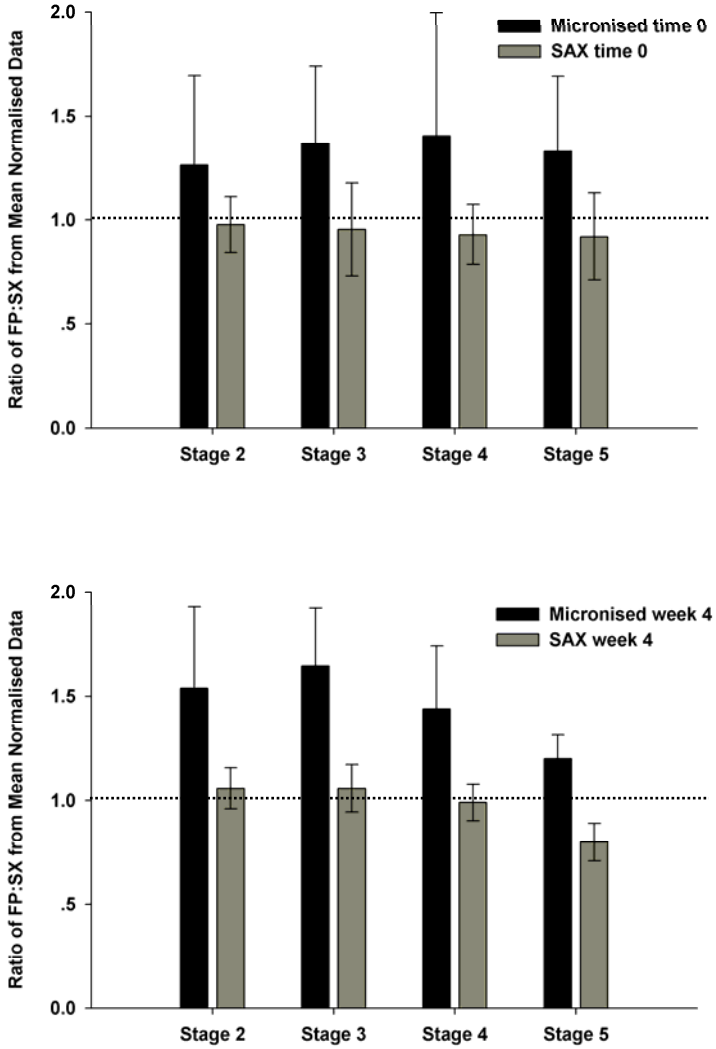

Figure 5.14: Ratio of FP:SX from mean normalised data of stages 2 to 5 of micronised FP:SX (10:1) compared with SAX-produced FP:SX (10:1) stored at 25˚C/44% RH from different periods of time (week 0 and 4)

5.5.1.4 Study II: In-vitro Performance of FP/SX at 25˚C/75% RH

The mean mass data of drug deposited per capsule on each stage of the NGI for both micronised FP/SX and SAX FP/SX formulations upon storage at 25˚C/75% RH for two and four weeks are shown in Table 5.3. Table 5.3 also shows the ED, FPD, FPF_{ED} and MMAD. As can be seen in Figure 5.15 and Figure 5.16, the mean drug deposition per capsule of both combined formulations individually compared at week 0, week 2 and week 4. These data suggest that aerosolisation of the SAX FP/SX formulation resulted in greater drug deposition than the micronised FP/SX formulation.

Table 5.3 (continued on next page): NGI deposition per capsule of drug aerosolised from the formulations of micronised FP:SX and SAX-produced FP:SX with ratio 10:1 stored at 25˚C/75% RH from different periods of time (week 0, 2 and 4)

FP = fluticasone propionate; SX = salmeterol xinafoate

No.	Formulations	Mean Drug Deposition on Impactor Stages (µg ± SD)											Mean ED (µg ± SD)	Mean FPD (µg ± SD)	Mean FPF_{ED} (% ± SD)	MMAD (µm ± GSD)
		D & C	MP &T	PS	S1	S2	S3	S4	S5	S6	S7	MOC				
1	Micronised FP at time 0	24.97 ± 2.58	9.39 ± 1.24	273.29 ± 3.49	2.90 ± 0.60	4.58 ± 0.26	6.64 ± 1.57	9.52 ± 0.63	5.35 ± 0.22	2.01 ± 0.16	0.87 ± 0.06	0.45 ± 0.06	315.00 ± 5.13	24.83 ± 1.76	7.88 ± 0.46	2.50 ± 2.40
	Micronised SX at time 0	3.56 ± 0.54	1.11 ± 0.03	32.56 ± 0.07	0.41 ± 0.09	0.43 ± 0.05	0.58 ± 0.10	0.81 ± 0.02	0.48 ± 0.08	0.26 ± 0.05	0.19 ± 0.03	0.17 ± 0.03	36.99 ± 0.25	2.48 ± 0.21	6.70 ± 0.53	2.30 ± 3.00
2	SAX-produced FP at time 0	32.88 ± 4.11	19.02 ± 2.98	166.37 ± 1.47	6.99 ± 1.29	10.20 ± 0.82	9.05 ± 0.30	7.71 ± 0.45	4.04 ± 0.02	1.83 ± 0.47	0.96 ± 0.17	0.62 ± 0.06	226.78 ± 3.09	24.21 ± 0.53	10.68 ± 0.32	3.60 ± 2.80
	SAX-produced SX at time 0	3.35 ± 0.37	2.36 ± 0.42	18.25 ± 2.19	0.83 ± 0.09	1.17 ± 0.19	1.06 ± 0.10	0.93 ± 0.11	0.49 ± 0.04	0.25 ± 0.05	0.16 ± 0.04	0.16 ± 0.04	25.66 ± 2.44	3.05 ± 0.14	11.96 ± 1.09	3.30 ± 3.10
3	Micronised FP at week 2	19.92 ± 6.01	6.40 ± 1.10	188.46 ± 35.90	2.31 ± 0.17	3.88 ± 0.91	5.51 ± 0.86	5.72 ± 1.05	2.17 ± 0.48	0.98 ± 0.09	0.48 ± 0.10	0.18 ± 0.07	216.08 ± 39.48	15.03 ± 2.52	6.98 ± 0.36	3.00 ± 2.40
	Micronised SX at week 2	1.59 ± 0.22	0.93 ± 0.36	28.19 ± 5.30	0.36 ± 0.08	0.34 ± 0.05	0.52 ± 0.02	0.70 ± 0.11	0.35 ± 0.04	0.25 ± 0.05	0.17 ± 0.02	0.14 ± 0.01	31.96 ± 5.21	2.14 ± 0.09	6.83 ± 1.29	2.30 ± 3.10
4	SAX-produced FP at week 2	45.35 ± 2.14	19.90 ± 1.69	195.92 ± 7.02	7.18 ± 0.58	15.83 ± 1.69	15.90 ± 1.50	11.62 ± 1.11	4.17 ± 0.55	0.98 ± 0.19	0.22 ± 0.05	0.07 ± 0.01	271.79 ± 13.85	32.95 ± 3.09	12.11 ± 0.54	3.90 ± 2.10
	SAX-produced SX at week 2	4.44 ± 0.30	1.89 ± 0.09	18.95 ± 0.98	0.73 ± 0.06	1.47 ± 0.09	1.40 ± 0.08	1.16 ± 0.07	0.49 ± 0.04	0.19 ± 0.02	0.15 ± 0.03	0.11 ± 0.01	26.54 ± 1.32	3.50 ± 0.15	13.19 ± 0.12	3.40 ± 2.70

Table 5.3 (continued from previous page): NGI deposition per capsule of drug aerosolised from the formulations of micronised FP:SX and SAX-produced FP:SX with ratio 10:1 stored at 25˚C/75% RH from different periods of time (week 0, 2 and 4)

FP = fluticasone propionate; SX = salmeterol xinafoate

No.	Formulations	Mean Drug Deposition on Impactor Stages (µg ± SD)											Mean ED (µg ± SD)	Mean FPD (µg ± SD)	Mean FPF_{ED} (% ± SD)	MMAD (µm ± GSD)
		D & C	MP &T	PS	S1	S2	S3	S4	S5	S6	S7	MOC				
5	Micronised FP at week 4	27.94 ± 4.59	11.42 ± 0.17	303.89 ± 6.29	2.96 ± 0.97	5.27 ± 1.93	6.97 ± 0.88	6.60 ± 0.32	3.19 ± 0.65	1.30 ± 0.35	0.49 ± 0.12	0.28 ± 0.16	342.39 ± 8.88	18.84 ± 2.36	5.50 ± 0.61	3.00 ± 2.40
	Micronised SX at week 4	2.36 ± 0.36	1.41 ± 0.11	34.27 ± 1.02	0.30 ± 0.04	0.37 ± 0.11	0.52 ± 0.11	0.58 ± 0.02	0.30 ± 0.06	0.14 ± 0.03	0.10 ± 0.01	0.10 ± 0.05	38.09 ± 0.81	1.74 ± 0.28	4.57 ± 0.79	2.60 ± 3.00
6	SAX-produced FP at week 4	69.84 ± 1.83	20.19 ± 0.64	198.23 ± 1.81	7.09 ± 0.36	15.17 ± 0.96	15.44 ± 1.21	11.24 ± 0.65	2.25 ± 0.10	0.23 ± 0.03	0.02 ± 0.01	0.00 ± 0.00	269.87 ± 4.23	29.19 ± 1.85	10.81 ± 0.56	4.20 ± 1.90
	SAX-produced SX at week 4	8.30 ± 0.31	2.44 ± 0.08	21.35 ± 0.60	0.79 ± 0.06	1.60 ± 0.13	1.59 ± 0.08	1.24 ± 0.08	0.32 ± 0.04	0.20 ± 0.18	0.10 ± 0.01	0.12 ± 0.07	29.76 ± 0.75	3.57 ± 0.31	12.01 ± 0.98	3.60 ± 2.80

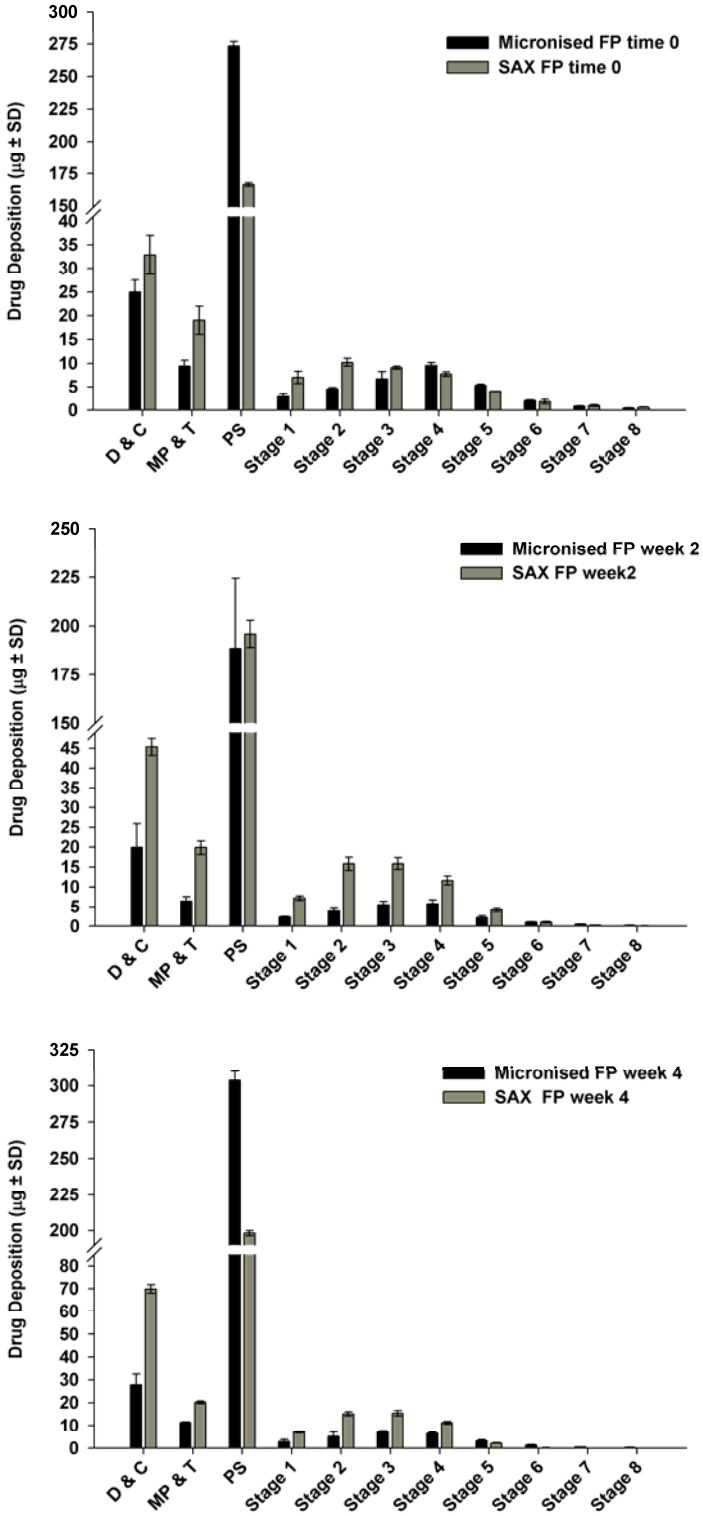

Figure 5.15: NGI deposition per capsule of FP aerosolised from the combination formulations of micronised FP:SX (10:1) compared with SAX-produced FP:SX (10:1) at 25˚C/75% RH from different periods of time (week 0, 2 and 4)

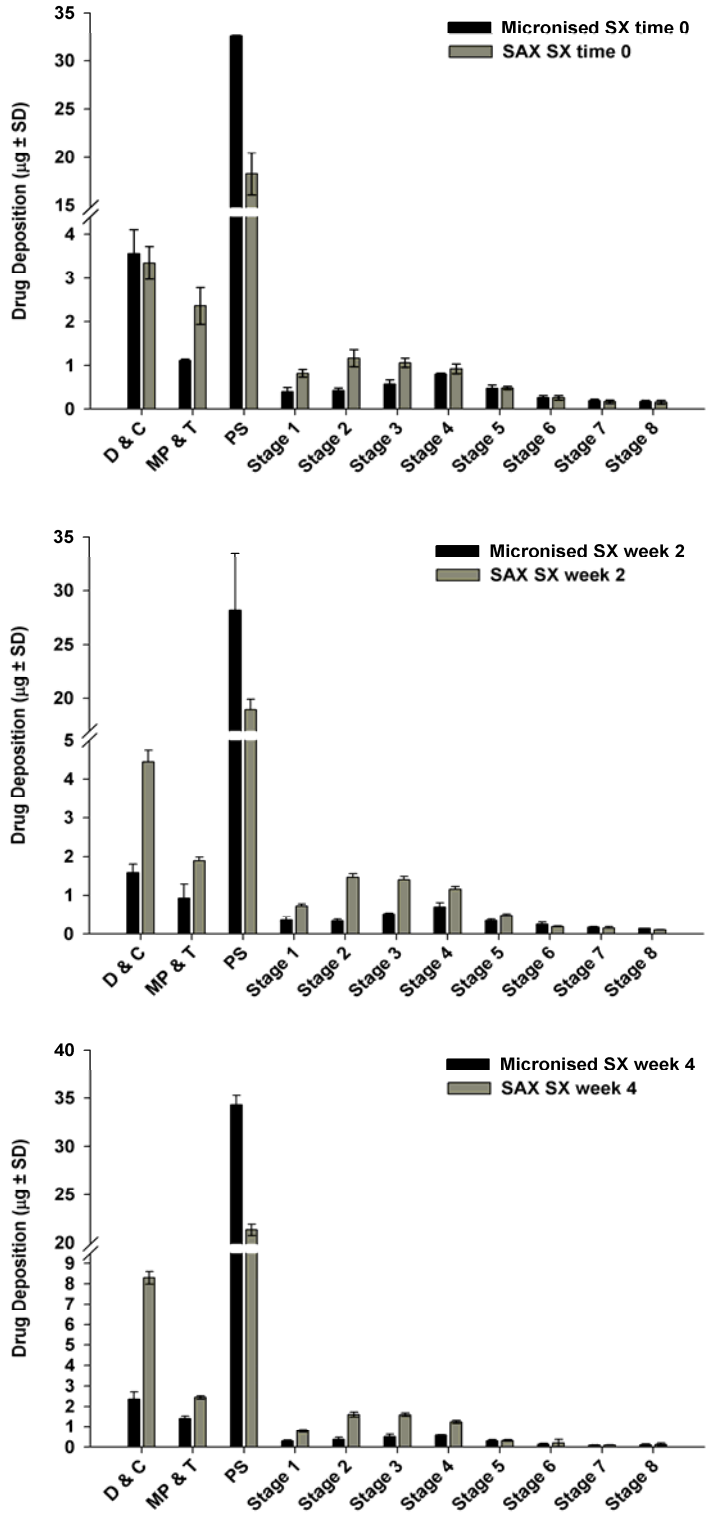

Figure 5.16: NGI deposition per capsule of SX aerosolised from the combination formulations of micronised FP:SX (10:1)compared with SAX-produced FP:SX (10:1) at 25˚C/75% RH from different periods of time (week 0, 2 and 4)

Upon storage of the micronised FP/SX formulation at 25˚C and 75% RH for two weeks, the ED of FP decreased significantly ($p<0.05$) in comparison to the initial time point as shown by Figure 5.17. Following storage of the formulation for four weeks under the same conditions, the ED of FP increased significantly ($p<0.05$) in comparison to the initial time-point and two week storage at 25˚C and 75% RH. It is evident from Figure 5.17 that storage of the formulation at two and four weeks at 25˚C and 75% RH did not significantly impact the ED of SX.

In contrast, storage of the SAX FP/SX formulation at 25˚C and 75% RH for two weeks resulted in a significant ($p<0.05$) increase in the ED of FP, which did not change significantly following storage for four weeks under the same conditions. As observed with the micronised FP/SX formulation, the ED of SX was not affected by the storage conditions.

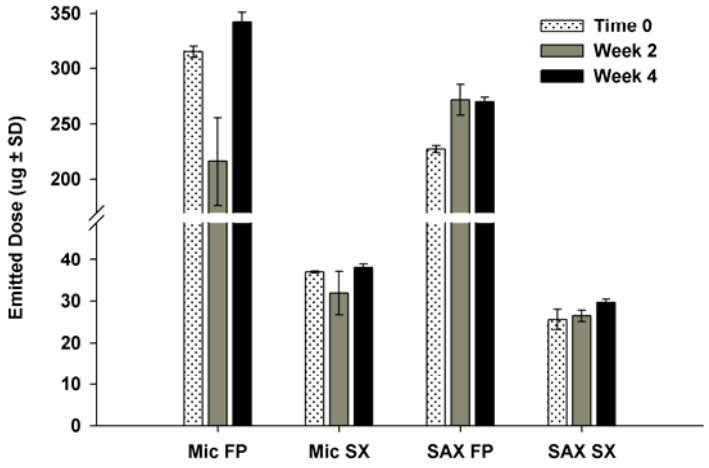

Figure 5.17: The emitted dosed per capsule of micronised and SAX combination formulations stored at 25˚C 75% RH from different periods of time (week 0, 2 and 4)

Upon storage at 25˚C and 75% RH for two weeks, the FPD of FP and SX upon aerosolisation of the SAX FP/SX formulation were 32.95 ± 3.09 µg for FP and 3.50 ± 0.15 µg for SX, which were significantly ($p<0.05$) greater than the FPD of FP (15.03 ± 2.52 µg) and SX (2.14 ± 0.09 µg) following aerosolisation of the micronised FP/SX formulation (Figure 5.18). Following storage at 25˚C and 75% RH for four weeks, the FPD of FP and SX following aerosolisation of the SAX FP/SX formulation were 29.19 ± 1.85 µg for FP and 3.57 ± 0.31 µg for SX, which were significantly greater ($p<0.05$)

than the FPD of FP (18.84 ± 2.36 µg) and SX (1.74 ± 0.28 µg) following aerosolisation of the micronised FP/SX formulation as shown by Figure 5.18.

Storage of the micronised FP/SX formulation for two weeks at 25˚C and 75% RH resulted in a significant ($p<0.05$) decrease in the FPD of FP in comparison to the initial time-point. Following storage of the formulation under the same conditions for four weeks resulted in a significant ($p<0.05$) decrease in the FPD of FP in comparison to the initial time-point, however, there were no significant differences in the FPD of FP following two and four week storage. These data suggest that the performance of FP following aerosolisation of the micronised FP/SX stored at 25˚C and 75% RH stabilised after two weeks. Figure 5.18 also shows that storage of the formulation at 25˚C and 75% RH for two and four weeks resulted in a significant ($p<0.05$) decrease in the FPD of SX in comparison to the initial time-point.

In contrast, storage of the SAX FP/SX formulation for two weeks at 25˚C and 75% RH resulted in a significant ($p<0.05$) increase in the FPD of FP in comparison to the initial time-point. No further change in the FPD of FP was observed after storage for four weeks at the same conditions as shown in Figure 5.18. Similarly, the FPD of SX increased significantly ($p<0.05$) after storage at 25˚C and 75% RH for two weeks, but did not change significantly after four week storage in comparison to the FPD of SX after two week storage.

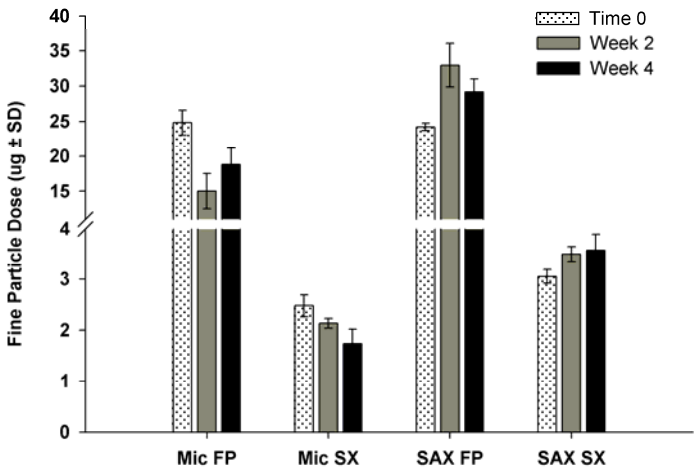

Figure 5.18: The fine particle dose per capsule of micronised and SAX combination formulations stored at 25˚C/75% RH from different periods of time (week 0, 2 and 4)

The %FPF_{ED} of FP and SX following aerosolisation of the micronised and SAX FP/SX formulation at the initial time-point and storage at 25˚C and 75% RH for two and four weeks are shown in Figure 5.19.

Upon storage of the micronised FP/SX formulation at 25˚C and 75% RH for two weeks, the %FPF_{ED} of FP decreased significantly ($p<0.05$) in comparison to the initial time-point. It is evident from Figure 5.19 that the %FPF_{ED} of FP also decreased significantly ($p<0.05$) following storage for four weeks in comparison to the initial time-point and two week storage under the same conditions. In contrast, the %FPF_{ED} of SX did not change significantly after two week storage at 25˚C and 75% RH, however, Figure 5.19 shows that the %FPF_{ED} of SX did decrease significantly ($p<0.05$) after four week storage at 25˚C and 75% RH in comparison to the initial time-point.

Storage of the SAX FP/SX formulation at 25˚C and 75% RH for two weeks resulted in a significant ($p<0.05$) increase in the %FPF_{ED} of FP in comparison to the initial time-point, however, this was not observed upon storage for four weeks under the same conditions. In addition, Figure 5.19 shows no significant change in the % FPF_{ED} of SX in comparison to the initial time-point following storage of the SAX FP/SX formulation for two and four weeks at 25˚C and 75% RH.

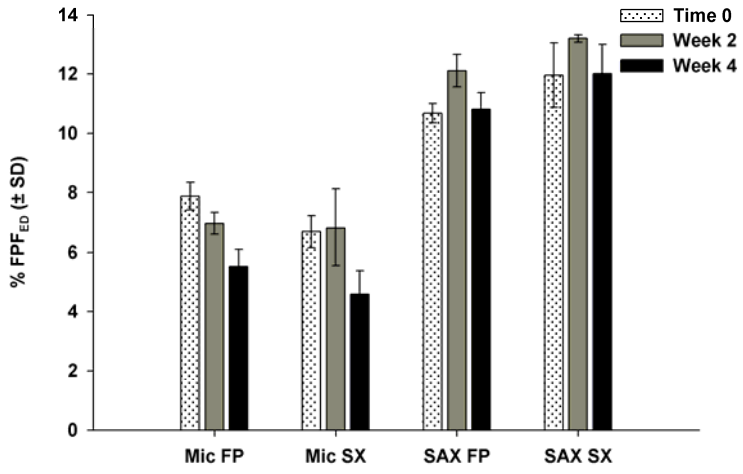

Figure 5.19: The fine particle fraction of emitted dose (FPF_{ED}) per capsule of micronised and SAX combination formulations stored at 25˚C/75% RH from different periods of time (week 0, 2 and 4)

The mean normalised mass ratios of FP:SX deposited on stages 2 and 5 of the NGI following aerosolisation of the micronised and SAX formulations at initial time-point and following storage at 25˚C/75% RH for two and four weeks are shown in Figure 5.20. The mean normalised mass ratio of FP:SX deposited on stages 2 to 5 following aerosolisation of the micronised FP/SX formulation at the initial time-point was greater than one across all stages. These data suggest that the deposition of FP and SX was variable and delivered inconsistently across stages 2 to 5. However, the mean normalised mass ratio of FP:SX deposited on stages 2 and 5 following aerosolisation of the SAX formulation was consistently around one. This implies that FP and SX can be affectively delivered through the lower stages of NGI at constant ratio when delivered using combined SAX FP/SX particles. Furthermore, the crystallinity of the SAX FP/SX material suggests that both performance and delivery are not affected by extreme storage conditions. As can be seen in Figure 5.20, the ratio of FP:SX from SAX FP/SX formulation at 25˚C/75% RH at week two and four maintained the same pattern with the initial time-point, whereas the micronised formulation showed deviations in the mass ratio of FP/SX on stages 2 to 5.

These data suggest that upon storage of micronised formulation, the delivery of FP and SX is highly variable which can lead to extreme under and overdosing of either active. The implications of this would mean the reduced efficacy of the drug product. In contrast, the SAX FP/SX preparation delivered both agents together to the lower stages of the NGI. Furthermore, the delivery of both actives as combined SAX particles was not influenced by storage conditions.

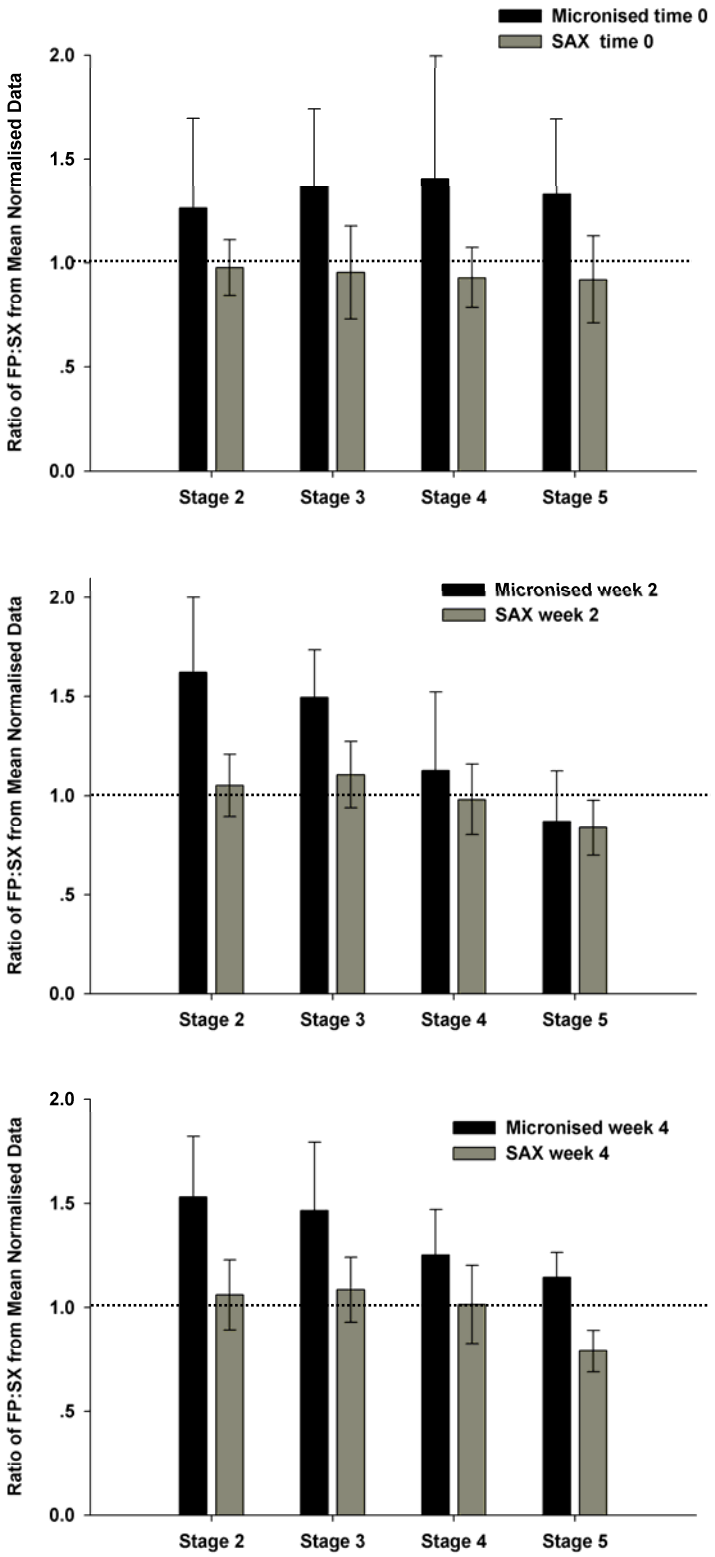

Figure 5.20: Ratios of FP:SX from mean normalised data of stages 2 to 5 of micronised FP:SX (10:1) compared with SAX-produced FP:SX (10:1) stored at 25˚C/75% RH from different periods of time (week 0, 2 and 4)

5.5.1.5 Study III: In-vitro Performance of FP/SX at 40˚C/75% RH

The mean mass data of drug deposited per capsule on each stage of the NGI for both micronised FP/SX and SAX FP/SX formulations are shown in Table 5.4. These two formulations were investigated again after storage at 40˚C/75% RH for two and four weeks in order to follow the stability profile of the materials. Table 5.4 also shows the ED, FPD, FPF_{ED} and MMAD. As can be seen in Figure 5.21 and Figure 5.22, the mean drug deposition per capsule of both combined formulations individually compared in bar charts of the week 0, week 2 and week 4. The SAX FP/SX formulation had higher drug deposition than the micronised FP/SX formulation.

Table 5.4 (continued on next page): NGI deposition per capsule of drug aerosolised from the formulations of micronised FP:SX and SAX-produced FP:SX with ratio 10:1 stored at 40˚C/75% RH from different periods of time (week 0, 2 and 4)

FP = fluticasone propionate; SX = salmeterol xinafoate

No.	Formulations	Mean Drug Deposition on Impactor Stages (µg ± SD)											Mean ED (µg ± SD)	Mean FPD (µg ± SD)	Mean FPF_{ED} (% ± SD)	MMAD (µm ± GSD)
		D & C	MP &T	PS	S1	S2	S3	S4	S5	S6	S7	MOC				
1	Micronised FP at time 0	24.97 ± 2.58	9.39 ± 1.24	273.29 ± 3.49	2.90 ± 0.60	4.58 ± 0.26	6.64 ± 1.57	9.52 ± 0.63	5.35 ± 0.22	2.01 ± 0.16	0.87 ± 0.06	0.45 ± 0.06	315.00 ± 5.13	24.83 ± 1.76	7.88 ± 0.46	2.50 ± 2.40
	Micronised SX at time 0	3.56 ± 0.54	1.11 ± 0.03	32.56 ± 0.07	0.41 ± 0.09	0.43 ± 0.05	0.58 ± 0.10	0.81 ± 0.02	0.48 ± 0.08	0.26 ± 0.05	0.19 ± 0.03	0.17 ± 0.03	36.99 ± 0.25	2.48 ± 0.21	6.70 ± 0.53	2.30 ± 3.00
2	SAX-produced FP at time 0	32.88 ± 4.11	19.02 ± 2.98	166.37 ± 1.47	6.99 ± 1.29	10.20 ± 0.82	9.05 ± 0.30	7.71 ± 0.45	4.04 ± 0.02	1.83 ± 0.47	0.96 ± 0.17	0.62 ± 0.06	226.78 ± 3.09	24.21 ± 0.53	10.68 ± 0.32	3.60 ± 2.80
	SAX-produced SX at time 0	3.35 ± 0.37	2.36 ± 0.42	18.25 ± 2.19	0.83 ± 0.09	1.17 ± 0.19	1.06 ± 0.10	0.93 ± 0.11	0.49 ± 0.04	0.25 ± 0.05	0.16 ± 0.04	0.16 ± 0.04	25.66 ± 2.44	3.05 ± 0.14	11.96 ± 1.09	3.30 ± 3.10
3	Micronised FP at week 2	21.80 ± 1.07	10.67 ± 0.54	315.80 ± 16.91	3.94 ± 0.80	5.10 ± 0.50	6.57 ± 0.59	6.57 ± 0.94	3.19 ± 0.46	1.41 ± 0.06	0.58 ± 0.14	0.25 ± 0.13	354.06 ± 18.15	18.56 ± 1.18	5.25 ± 0.32	3.20 ± 2.50
	Micronised SX at week 2	3.23 ± 1.11	1.20 ± 0.04	32.87 ± 1.95	0.42 ± 0.12	0.44 ± 0.04	0.61 ± 0.08	0.68 ± 0.05	0.35 ± 0.05	0.23 ± 0.05	0.12 ± 0.03	0.12 ± 0.04	37.05 ± 2.03	2.11 ± 0.19	5.70 ± 0.64	2.70 ± 3.00
4	SAX-produced FP at week 2	35.63 ± 3.83	19.55 ± 1.08	202.60 ± 4.48	7.50 ± 0.44	15.27 ± 1.12	13.54 ± 0.94	9.96 ± 0.81	3.13 ± 0.20	0.61 ± 0.08	0.13 ± 0.03	0.03 ± 0.01	272.34 ± 7.30	27.41 ± 1.68	10.06 ± 0.42	4.20 ± 2.10
	SAX-produced SX at week 2	4.45 ± 0.48	2.45 ± 0.04	22.19 ± 1.24	0.92 ± 0.07	1.74 ± 0.12	1.55 ± 0.09	1.20 ± 0.07	0.49 ± 0.07	0.21 ± 0.03	0.17 ± 0.02	0.12 ± 0.03	31.03 ± 1.44	3.73 ± 0.17	12.04 ± 0.48	3.60 ± 2.80

Table 5.4 (continued from previous page): NGI deposition per capsule of drug aerosolised from the formulations of micronised FP:SX and SAX-produced FP:SX with ratio 10:1 stored at 40˚C/75% RH from different periods of time (week 0, 2 and 4)

FP = fluticasone propionate; SX = salmeterol xinafoate

No.	Formulations	Mean Drug Deposition on Impactor Stages (µg ± SD)											Mean ED (µg ± SD)	Mean FPD (µg ± SD)	Mean FPF_{ED} (% ± SD)	MMAD (µm ± GSD)
		D & C	MP &T	PS	S1	S2	S3	S4	S5	S6	S7	MOC				
5	Micronised FP at week 4	28.13 ± 4.21	12.29 ± 1.28	330.84 ± 8.12	3.21 ± 0.16	4.90 ± 0.27	6.47 ± 0.20	6.32 ± 1.05	3.11 ± 0.14	1.18 ± 0.10	0.44 ± 0.07	0.14 ± 0.00	368.90 ± 9.11	17.66 ± 0.83	4.79 ± 0.17	3.10 ± 2.30
	Micronised SX at week 4	2.53 ± 0.74	1.17 ± 0.11	33.51 ± 0.44	0.32 ± 0.02	0.35 ± 0.02	0.55 ± 0.03	0.60 ± 0.04	0.32 ± 0.02	0.16 ± 0.03	0.13 ± 0.05	0.11 ± 0.02	37.20 ± 0.24	1.85 ± 0.14	4.98 ± 0.40	2.50 ± 3.00
6	SAX-produced FP at week 4	56.22 ± 1.52	20.82 ± 1.43	209.02 ± 4.04	7.51 ± 0.22	15.44 ± 0.68	14.37 ± 0.92	9.45 ± 0.50	1.67 ± 0.09	0.15 ± 0.01	0.02 ± 0.01	0.00 ± 0.00	278.46 ± 6.66	25.67 ± 1.46	9.22 ± 0.43	4.50 ± 1.90
	SAX-produced SX at week 4	7.77 ± 1.10	2.57 ± 0.10	24.46 ± 0.39	0.85 ± 0.02	1.71 ± 0.08	1.63 ± 0.09	1.15 ± 0.06	0.23 ± 0.02	0.03 ± 0.01	0.04 ± 0.02	0.06 ± 0.01	32.72 ± 0.62	3.12 ± 0.19	9.54 ± 0.39	4.40 ± 2.50

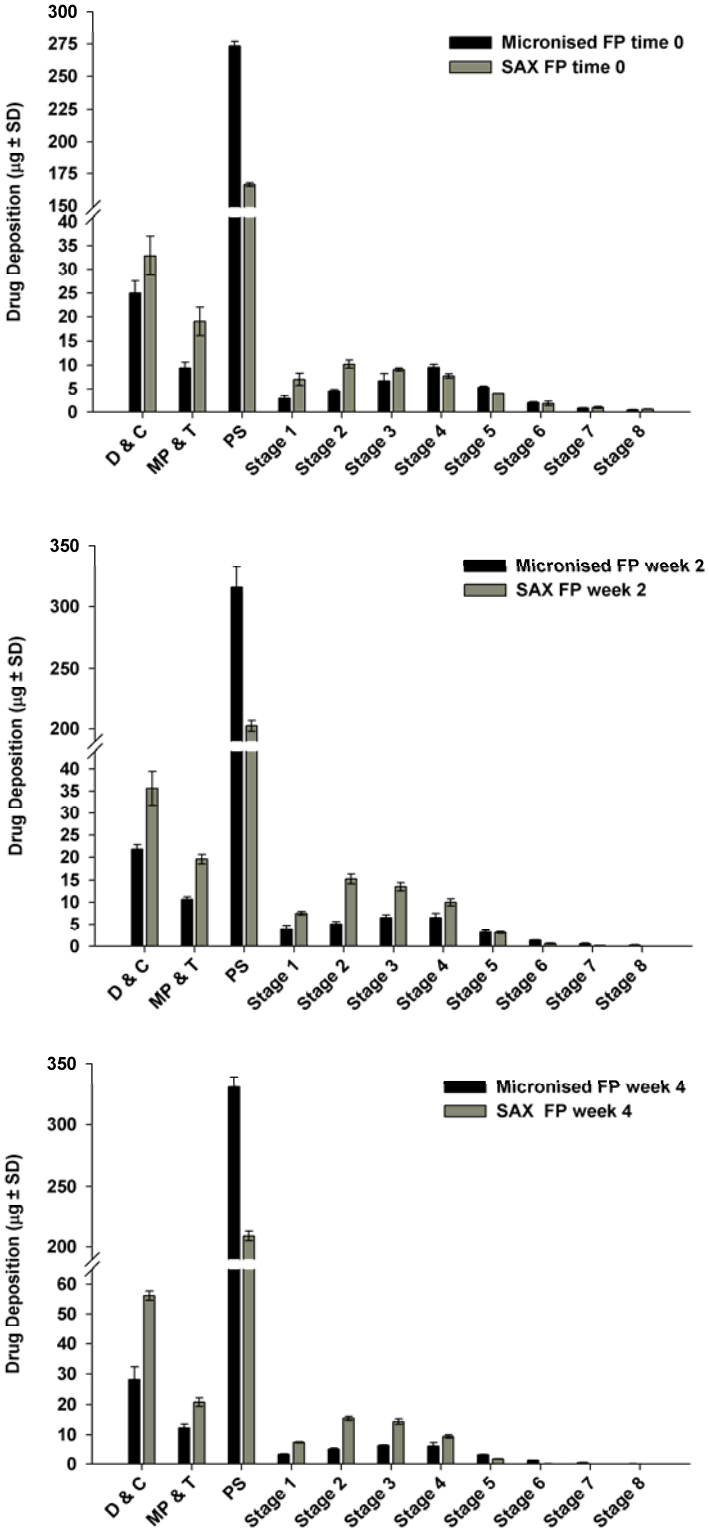

Figure 5.21: NGI deposition per capsule of FP aerosolised from the combination formulations of micronised FP:SX (10:1) compared with SAX-produced FP:SX (10:1) at 40˚C/75% RH from different periods of time (week 0, 2 and 4)

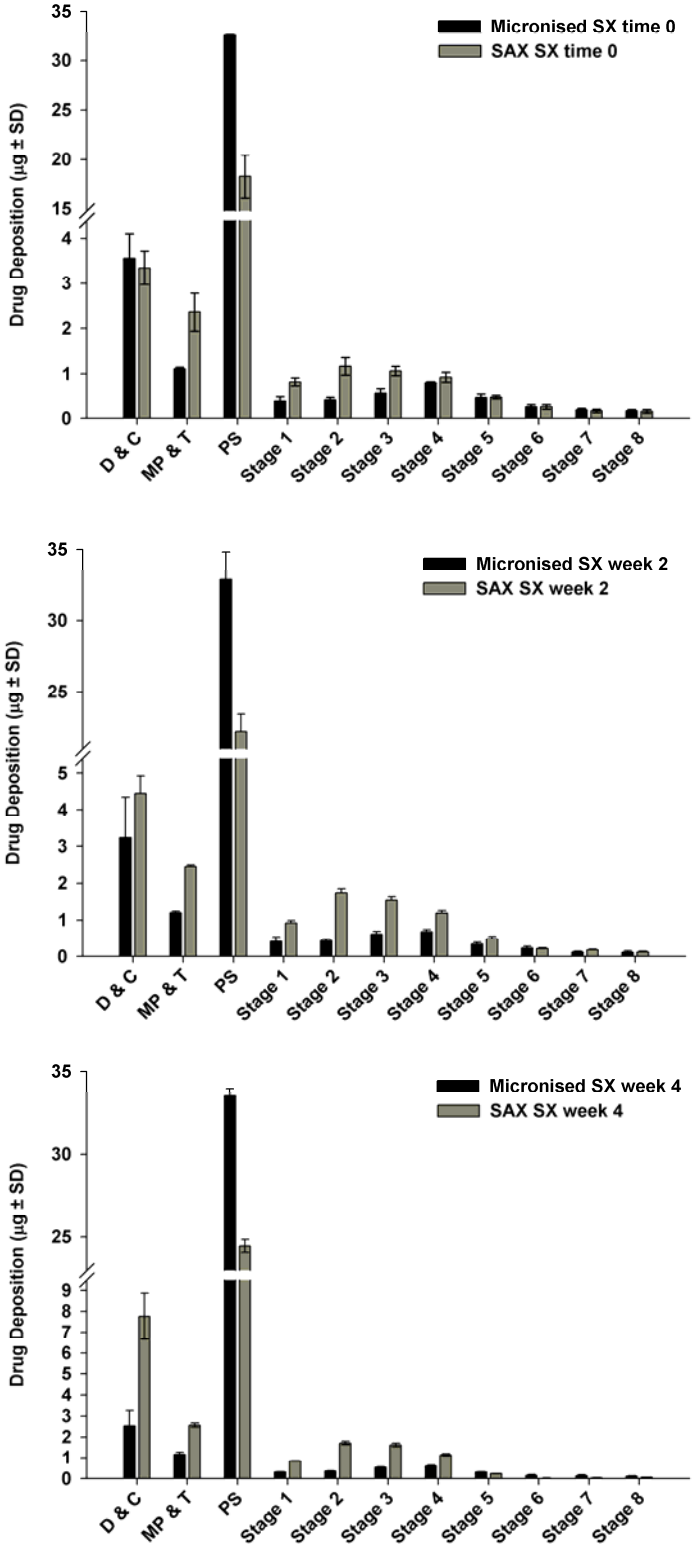

Figure 5.22: NGI deposition per capsule of SX aerosolised from the combination formulations of micronised FP:SX (10:1) compared with SAX-produced FP:SX (10:1) at 40˚C/75% RH from different periods of time (week 0, 2 and 4)

Storage of the micronised FP/SX formulation at 40˚C and 75% RH for two and four weeks demonstrated in a significant ($p<0.05$) increase in the ED of FP in comparison to the initial time-point as shown in Figure 5.23. In contrast, this figure revealed no significant difference in the ED of SX upon storage of the micronised FP/SX formulation at 40˚C and 75% RH for two and four weeks. Storage of the SAX FP/SX formulation at 40˚C and 75% RH for two and four weeks resulted in a significant ($p<0.05$) increase in the ED of FP and SX in comparison to the initial time-point (see Figure 5.23).

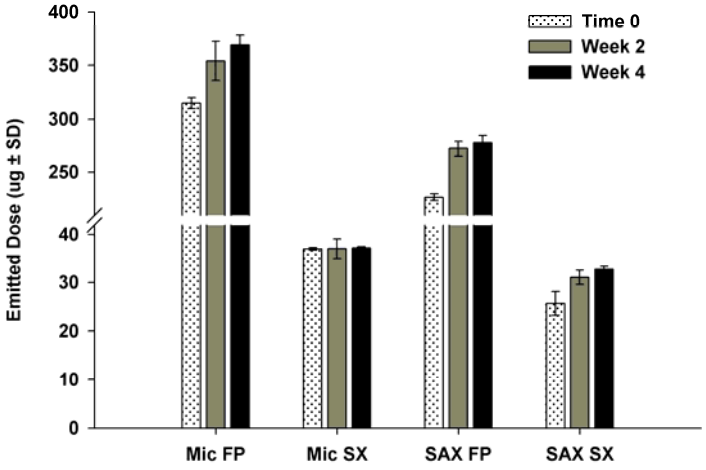

Figure 5.23: The emitted dosed per capsule of micronised and SAX combination formulations stored at 40˚C/75% RH from different periods of time (week 0, 2 and 4)

The fine particle dose (FPD) of FP and SX after storage of the micronised and SAX FP/SX formulations at 40˚C and 75% RH for two and four weeks are shown in Figure 5.24. Storage of the micronised FP/SX formulation for two and four weeks at 40˚C and 75% RH resulted in a significant ($p<0.05$) decrease in FPD of FP and SX in comparison to the initial time-point. However, Figure 5.24 suggests that this decrease was not observed between two and four week storage. In contrast, storage of the SAX FP/SX resulted in a significant ($p<0.05$) increase in the FPD of FP and SX after two week storage at 40˚C and 75% RH in comparison to the initial time-point. However, no significant differences in FPD of FP and SX were observed upon four week storage in comparison to the initial time-point.

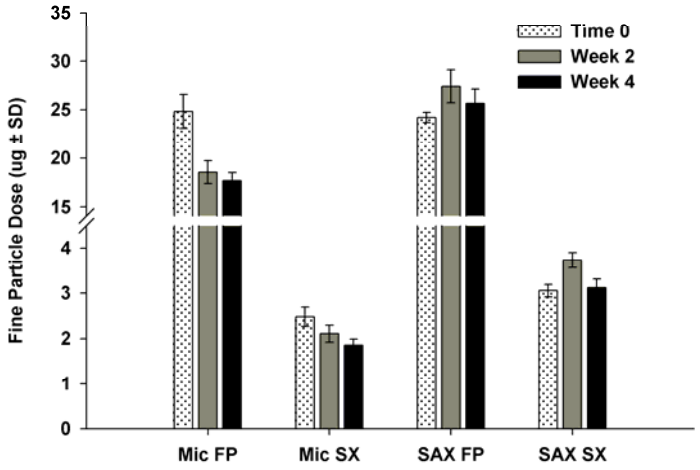

Figure 5.24: The fine particle dose per capsule of micronised and SAX combination formulations stored at 40˚C/75% RH from different periods of time (week 0, 2 and 4)

The $\%FPF_{ED}$ of FP and SX following aerosolisation of the micronised and SAX FP/SX formulations at the initial time-point and storage at 40˚C and 75% RH for two and four weeks are shown in Figure 5.25.

Storage of the micronised FP/SX formulation at 40˚C and 75% RH for two and four weeks resulted in a significant ($p<0.05$) decrease in the $\%FPF_{ED}$ of FP in comparison to the initial time-point. In contrast, there was no significant difference in the $\%FPF_{ED}$ of SX following two week storage, however, upon four week storage the $\%FPF_{ED}$ decreased significantly ($p<0.05$) in comparison to the initial time-point.

Upon storage of the SAX FP/SX formulation at 40˚C and 75% RH for two weeks the $\%FPF_{ED}$ of FP and SX did not change significantly in comparison to the initial time-point. However, four week storage of the formulation resulted in a significant decrease in the $\%FPF_{ED}$ of FP and SX in comparison to the initial time-point.

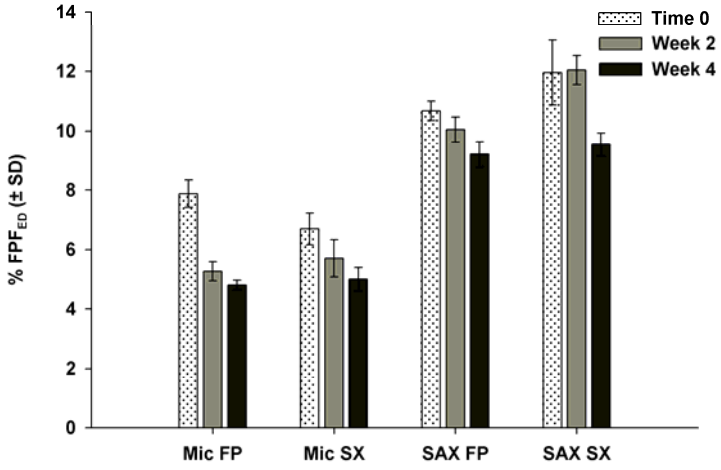

Figure 5.25: The fine particle fraction of emitted dose (FPF_{ED}) per capsule of micronised and SAX combination formulations stored at 40˚C/75% RH from different periods of time (week 0, 2 and 4)

The mean normalised mass ratios of FP:SX deposited on stages 2 and 5 of the NGI following aerosolisation of the micronised and SAX formulations at initial time-point and following storage at 40˚C/75% RH for two and four weeks are shown in Figure 5.26. The ratio of FP:SX upon aerosolisation of the SAX FP/SX formulation at 40˚C/75% RH at week two tended to consistently remain close to unity, which represents that both FP and SX were delivered to stages 2–5 in the ration of 10:1. Furthermore, these trends in the deposition of both actives on aerosolisation of the SAX FP/SX did not change as a function of formulation storage in comparison to the initial time-point. The deposition of both actives did change upon storage of the micronised FP/SX formulation. As shown in Figure 5.26, at the initial time-point the FP:SX ratio of the micronised formulation remained above unity. However, storage for two and four weeks at 40˚C/75% RH resulted in the FP:SX ratio decreasing towards unity. Such trends were not observed for the SAX FP/SX formulation. The deposition trends of FP and SX following aerosolisation of the micronised FP/SX formulation after storage suggest that product storage conditions may alter the delivery of the actives resulting in significant over and under dosing of the LABA or ICS.

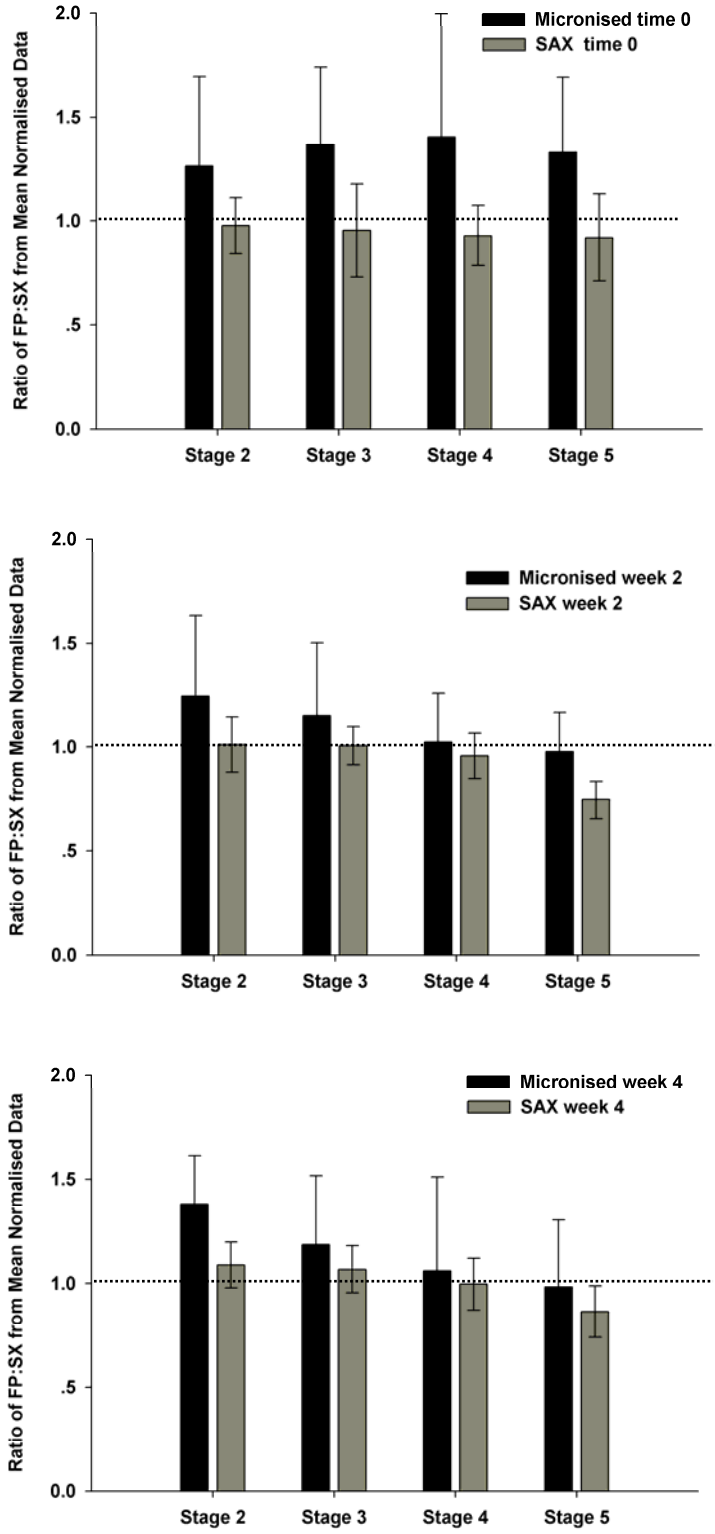

Figure 5.26: Ratios of FP:SX from mean normalised data of stages 2 to 5 of micronised FP:SX (10:1)compared with SAX-produced FP:SX (10:1) stored at 40˚C/75% RH from different periods of time (week 0, 2 and 4)

5.5.2 Discussion

Many studies have reported that co-administration of an ICS and LABA can interact synergistically to improve clinical outcomes in asthma and COPD control (Barnes, 2002; Nelson, Chapman et al., 2003; Theophilus, Moore et al., 2006). Current, combined inhalation dosage forms are unable to consistently deliver both actives in the required concentrations at the receptor, molecular and cellular level to enhance this synergistic action. Furthermore, these inconsistencies are likely to perpetuate as function of storage. These variations are likely to be associated with the use of mechanical blending processes to make current combined products. The SAX process may provide a means of engineering particles where both actives are incorporated into individual crystalline particles, which may then enhance co-deposition in the airways.

In this way, combined FP/SX particles were fabricated using the SAX process. The combined SAX particles exhibited a defined corrugated morphology. This may have resulted in the significantly ($p<0.05$) higher FPF_{ED} of FP and SX than the micronised FP/SX formulation owing to smaller contact area of the material, which would minimise particle adhesion to lactose. Both DSC and XRPD also showed that the SAX FP/SX particles were crystalline. The crystalline nature of these particles may also explain the better stability profile of the material as measured by *in-vitro* inhalation performance testing as function of storage. These data suggest that the aerosolisation efficiency of the SAX FP/SX particles is not compromised upon storage, whereas the micronised FP/SX formulation resulted in significant decrease in the delivery of both actives. This may be related to the presence of micronisation-induced surface structural disorder of the micronised particles, which relax over-time. The consequence of this relaxation is that the surface interfacial properties of the materials will change within the formulation, which will result in unstable product performance.

The surface interfacial properties of micronised FP and SX will be different with respect to each other and lactose, therefore, the delivery of both actives will be highly variable and independent of each other as shown in this study. The deposition of FP and SX on stages 2–5 following aerosolisation of the micronised FP/SX resulted in inconsistent delivery of the actives, which may impact clinical efficacy of the drug product. Furthermore, the probability of co-delivery of both actives in the required concentrations at the molecular, cellular and receptor level will be limited, which may

compromise any potential synergistic action of the molecules. In contrast, upon co-processing of both actives into one geometric particle, the delivery of both actives was consistent and in the desired concentrations. The deposition profile of both actives on stages 2 – 5 of the NGI was not affected upon storage, however, there were significant under and over dosing of either active following storage of the micronised FP/SX formulation. These data suggest that the engineering of combined particles of FP and SX using SAX may enable the co-delivery of both molecules at the receptor, molecular and cellular level, which may enhance clinical efficacy as a result of enhanced synergistic action of the materials.

5.6 Conclusions

These data suggest that combination SAX particles of FP:SX engineered by SAX can be produced and successfully delivered through the lower stages of NGI. Under the different storage conditions, FPF_{ED} data of FP and SX upon aerosolisation of all SAX FP/SX formulations were significantly higher than FPF_{ED} of FP and SX from the micronised FP/SX formulations. The increased performance of the SAX material in comparison to the micronised material may be attributed to the corrugated morphology of the SAX particles, which may have resulted in reduced drug particle-carrier adhesion, thereby increasing drug liberation. Furthermore, SAX FP/SX formulations maintained a constant ratio of FP and SX delivery, which was maintained following storage. In contrast, aerosolisation of the micronised FP/SX formulations did not show the consistency in the delivery of both actives to stages 2 to 5. The decreased performance of the micronised material may be attributed to relaxation of process-induced surface disorder present on particles, which may have affected their surface interfacial interactions and therefore product performance. As the SAX particles may be devoid of such process-induced surface disorder, the performance of the material is not affected in the same way as micronised material upon storage. This approach presents itself as a novel means to produce inhaled combination dosage forms which may lead to offer the potential for enhanced clinical efficacy for synergistic interaction.

Chapter 6: Pharmaceutical Engineering of a Low-Dose drug in Combination with a High-Dose Corticosteroid

6.1 Introduction

Delivery of multiple actives in combined inhaled drug delivery systems has been successful in the management of asthma (Barnes, 2002). The recommended strategy for the control of asthma is combined inhalation therapy with inhaled corticosteroids (ICS) and long-acting β_2-agonists (LABA). It has been demonstrated that addition of a long-acting β_2-agonist (LABA) to an inhaled corticosteroid (ICS) is superior to ICS alone in achieving asthma control (Matz, Emmett et al., 2001).

The benefit of paediatric asthma control from treatment with fixed-dose combination inhalation therapy with ICS and LABA are limited (Bisgaard, Le Roux et al., 2006). This may partly be because paediatric asthma is often an episodic disease with a particular strong seasonality, which is associated with few symptoms and near-normal lung function for long periods, with intermittent increase in symptoms and exacerbations (Pauwels, Sears et al., 2003). Traditional fixed-dosing strategies decided on the basis of patient history inevitably lag behind disease activity, and carry a risk of over-treatment or under-treatment (Bisgaard, Le Roux et al., 2006). Recently, the global initiative for asthma have endorsed the use of Symbicort™ for both maintenance and relief therapy (SMART®) in asthma (Masoli, Fabian et al., 2004). The SMART approach to asthma management challenges the traditional fixed-dosing of ICS/LABA for moderate-to-severe persistent asthma in paediatrics, instead emphasising intermittent use in addition to the regular low-dose use titrating the steroid dose dynamically to the disease activity (Bisgaard, Le Roux et al., 2006). Furthermore, the SMART approach requires the patient to only use one inhaler to control and treat their asthma symptoms without requirement for a separate short-acting rescue inhaler (Bisgaard, Le Roux et al., 2006). In a study examining over 2,700 asthma patients, the SMART approach was found to substantially reduce the incidence of exacerbations and repeat exacerbations, improve lung function, and reduce symptoms to a greater extent than a four-fold higher dose of ICS alone (O'Byrne, Bisgaard et al., 2005).

Symbicort contains budesonide (ICS) and formoterol (LABA), and is usually available in two strengths for maintenance and reliever therapy (100µg/6µg and 200µg/6µg), which are typically delivered using a dry powder inhaler (DPI). The preparation of combination DPI formulations containing low concentrations of actives can pose significant challenges during product development. Current combination therapies are commonly prepared by blending both the micronised LABA and ICS together with coarse lactose. These preparations are then loaded into a DPI device and actuated by the patient to receive both medicaments. However, there is very little control to ensure that both drugs are delivered together and in adequate concentrations. Furthermore, there is a greater likelihood of variations in dose delivery of the actives as a function of product storage conditions. Hence, there is a requirement of processes that may enable production of low-dose combination inhaled products that will allow both drugs to be delivered more effectively and independently of dose variations.

In the previous chapter, combined FP/SX particles were successfully fabricated using the SAX process. The aim of the present study was to employ the solution atomisation and crystallisation with sonication (SAX) process to generate individual particles that consisted of both the ICS (budesonide) and LABA (formoterol). The aerosolisation efficiency of these novel particles was also assessed.

6.2 Materials

Micronised Budesonide (Bud) and formoterol fumarate dihydrate (FFD) were obtained from sources stated in Chapter 2. All other materials used in this chapter are listed Chapters 2 and 5.

6.3 Methods

6.3.1 The Production of SAX-produced Bud-FFD Particles

SAX-produced Bud-FFD particles were prepared upon atomisation of a 1.5% w/v of solution of Bud:FFD in the ratio 36:1 prepared in a co-solvent mixture of methanol and dichloromethane (1:12). The solution was sprayed through a SU11 atomiser at a

sprayed rate of 4 ml.min^{-1} with air pressure at 2.5 bar of the atomiser in the lab scale of SAX process over 60 cm of separation distance including positive pressure 30 Lmin^{-1} in the system with an ultrasonic probe. The resulting particles were then collected in hexane at 5˚C, which were then isolated using supercritical CO_2 extraction as described in Chapter 3.

6.3.2 Formulation Blending

A formulation, containing 1.6% w/w combined SAX Bud/FFD particles, was prepared by geometric blending with 63-90 µm sieve fractions of surface-etched lactose. In order to compare the *in-vitro* inhalation performance of SAX Bud/FFD and micronised Bud/FFD, a further carrier-based combination formulation containing 1.56% w/w micronised Bud and 0.04% w/w micronised FFD was prepared by geometric blending with 63-90 µm sieve fractions of surface-etched lactose. The resultant blend was further mixed using a Turbula shaker-mixer (Willy A Bachofen AG, Basel, Switzerland) at 46 rpm for 45 minutes.

6.3.3 Content Uniformity Determination

The content uniformity of the formulations was assessed following blending. The blend was spread over a clean surface and ten samples of 25 ± 1 mg were taken from random positions. The mobile phase in this study was prepared from 60% acetonitrile, 40% of 5 mM Sodium dihydrogen orthophosphate (set to pH 3) and filtered under vacuum through a 0.45 µm membrane. The mobile phase was then sonicated in ultrasonic bath for 15 minutes. Each sample was dissolved with 15 minutes sonication in mobile phase to 100 ml final volume and drug concentration assessed by high performance liquid chromatography (HPLC). The proportion of drug in each sample was calculated and the content uniformity expressed as the coefficient of variation (Equation 4.1)

6.3.4 Capsule Filling

Each formulation was manually loaded into size 3 HPMC capsules (Qualicaps, Madrid, Spain). Fill weight was 25 ± 1 mg, giving a nominal dose of 389 ± 20 µg for Bud and 11 ± 1 µg for FFD per capsule. In order to investigate the influence of storage on the performance of micronised and SAX Bud/FFD preparation, formulations were stored at different conditions. In study I, filled capsules of both micronised and SAX Bud/FFD formulations were stored in sealed chambers containing a saturated solution of sodium chloride (giving a relative humidity of 75%) at 25˚C, and re-tested at two weeks and four weeks later. In study II, the filled capsules were also stored in a sealed chamber containing a saturated solution of sodium chloride (also giving a relative humidity of 75%) at 40˚C and re-tested at 2 weeks and four weeks later. In order to investigate the performance of micronised and SAX Bud/FFD preparation, all formulations were tested by using NGI.

In-vitro formulation performance of the micronised and SAX Bud/FFD preparations were assessed using a Next Generation Impactor (NGI) using the method described in Chapter 5. The device/capsules, mouthpiece/throat, pre-separator and each stage of the NGI were washed down into separate known volumes of 60% acetonitrile, 40% water, which were sonicated to aid dissolution and allowed to cool. The concentration of drug in each solution was investigated by HPLC, from which the mass of drug deposited on each stage of the NGI could be determined from stages 1 to 7 and on the micro-orifice collector (MOC).

6.3.5 High Performance Liquid Chromatography (HPLC)

Drug concentrations were determined by HPLC. The mobile phase consisted of 60% acetonitrile, 40% of 5 mM Sodium dihydrogen orthophosphate (set to pH 3). The flow rate was 1.5 $ml.min^{-1}$, column temperature was 30˚C and injection volume 200 µl. Drug retention times were 3.2 minutes for Bud and 9.8 minutes for FFD, therefore, the total analysis run time was 12 minutes. The UV detection wavelength used to detect both Bud and FFD was 214 nm. The drug concentrations of Bud and FFD and peak area for each drug were found to be linear, with linear regression analysis yielding a coefficient of determination (R^2) of 1 and 0.9999, respectively (see Figure 6.1).

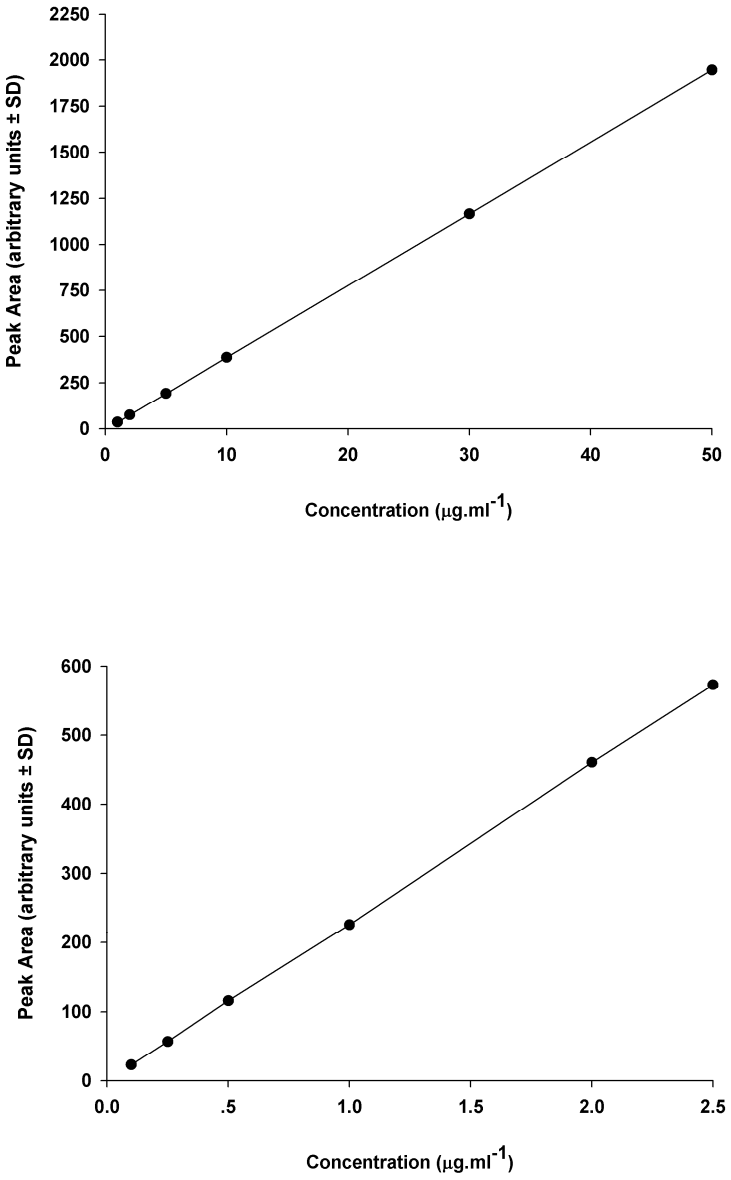

Figure 6.1: HPLC calibration curve for Bud and FFD

6.4 Characterisation of SAX-produced Bud-FFD Particles

6.4.1 Results and Discussion

6.4.1.1 Scanning Electron Microscopy

Representative scanning electron micrographs of micronised Bud, micronised FFD and SAX-produced Bud/FFD particles are shown in Figure 6.2. Both micronised Bud and FFD particles were irregular in shape and exhibited particles of different shapes and sizes, which were extensively agglomerated. These features are a result of the destructive micronisation process, which does not allow adequate control of particle shape and morphology. In contrast, the combined SAX Bud/FFD particles appeared more uniform in shape and morphology. Furthermore, these micrographs suggest that both Bud and FFD may have been successfully processed into individual particles. This is to be expected as the SAX operation utilises a droplet-to-particle approach to fabricate crystalline particles.

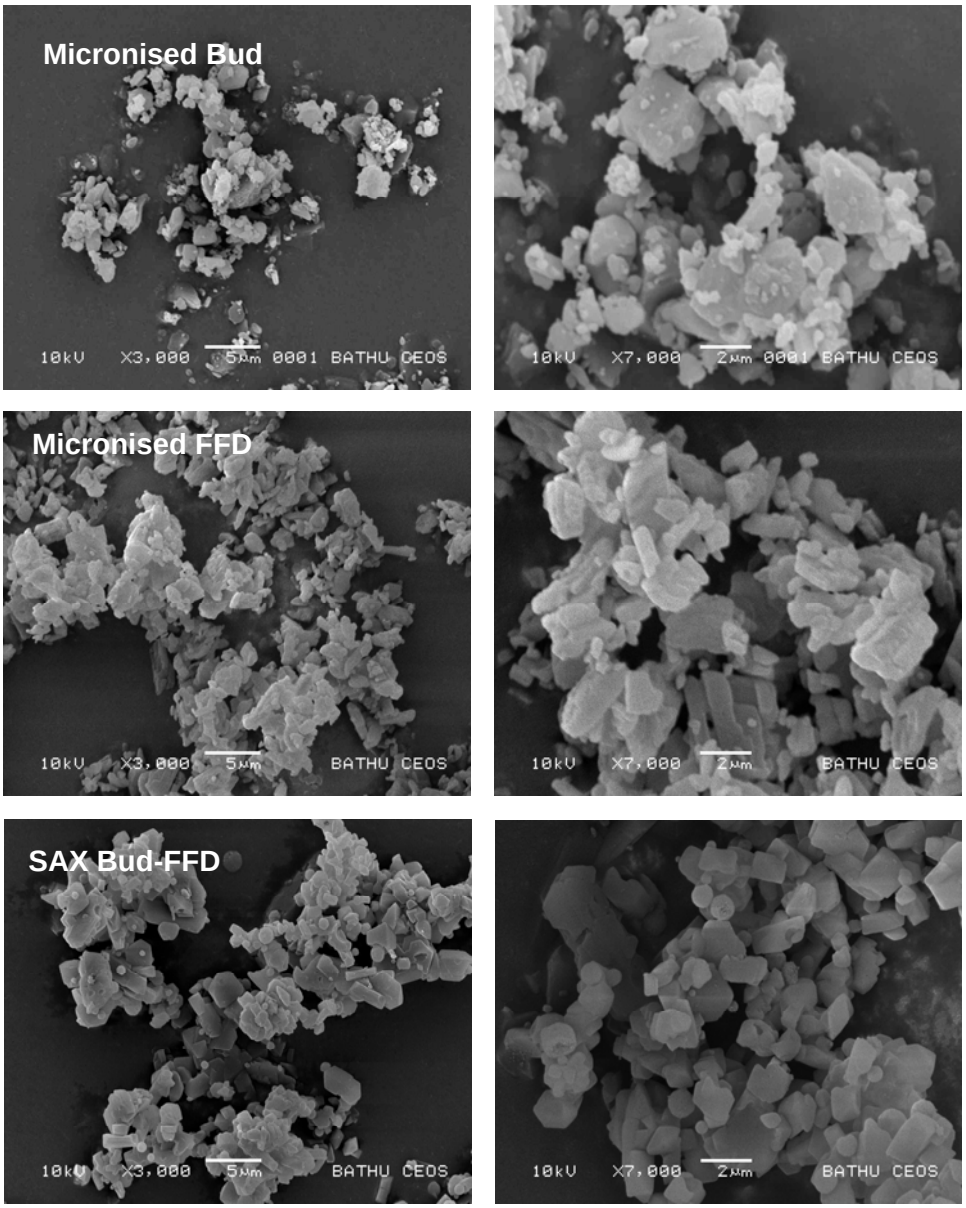

Figure 6.2: Representative SEMs of micronised Bud, micronised FFD and SAX-produced Bud-FFD particles at magnifications of x3000 and x7000

6.4.1.2 Particle Size Analysis

The cumulative particle size distribution of micronised Bud, micronised FFD and SAX-produced Bud/FFD is shown in Figure 6.3. The particle size distribution of SAX-produced Bud/FFD suggests that particles of the material were larger than micronised Bud and FFD. Table 6.1 shows that d_{50} values of micronised Bud, FFD and SAX-produced Bud/FFD are 2.21, 2.42 and 4.17 µm, respectively. It can be suggested from the results of d_{50} values that the micronised drug particles and SAX-produced Bud/FFD particles were suitable for pulmonary drug delivery.

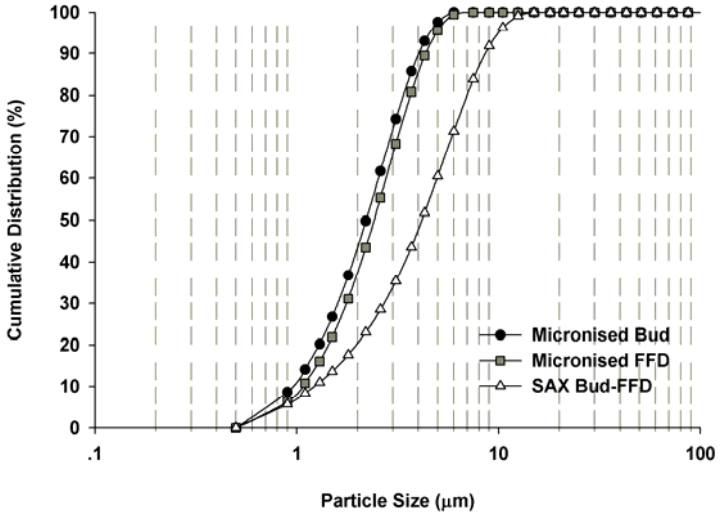

Figure 6.3: Particle size distribution of micronised Bud, micronised FFD and SAX-produced Bud-FFD particles

Table 6.1: Summary of particle size data of micronised Bud, micronised FFD and SAX-produced Bud-FFD particles

	$d_{10\%}$ (µm) ± SD	$d_{50\%}$ (µm) ± SD	$d_{90\%}$ (µm) ± SD
Micronised Bud	0.95 ± 0.00	2.21 ± 0.01	4.06 ± 0.00
Micronised FFD	1.07 ± 0.00	2.42 ± 0.00	4.36 ± 0.01
SAX-produced Bud-FFD	1.23 ± 0.01	4.17 ± 0.04	8.66 ± 0.05

6.4.1.3 Differential Scanning Calorimetry

The DSC thermograms of micronised Bud and FFD are shown in Figure 6.4. The DSC thermogram of micronised Bud exhibited an endothermic response at ~261°C, which is typical of the melt with decomposition seen for crystalline budesonide (Jones, Young et al., 2008). The thermogram relating to micronised FFD is more complicated, with three endothermic peaks at ~113°C, ~129°C and ~144°C. It is understood that FFD may be thermally dehydrated. Formoterol anhydrous polymorph A melts at the range 125-129°C (Jarring, Larsson et al. 2006) and formoterol anhydrous polymorph B melts at the range 143-148°C. Therefore, the first endothermic peak represents dehydration and the second peak at ~129°C shows the melting of anhydrous polymorph A. The third peak is the melting of anhydrous of polymorph B.

The DSC thermogram of SAX-produced Bud/FFD exhibited a single endothermic at ~261°C, as shown in Figure 6.5. This peak only confers to the presence of budesonide and not formoterol. However, owing to the significantly lower concentration of formoterol in the SAX combined particles, the presence of the material may not be detectable by DSC.

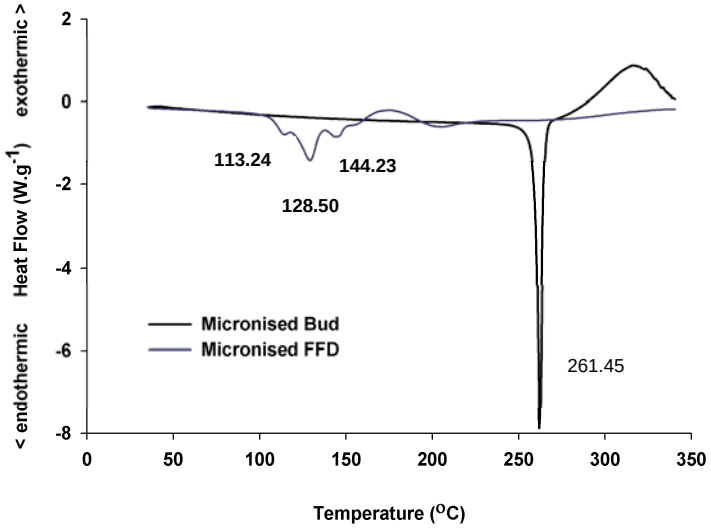

Figure 6.4: DSC thermograms of micronised Bud, micronised FFD particles

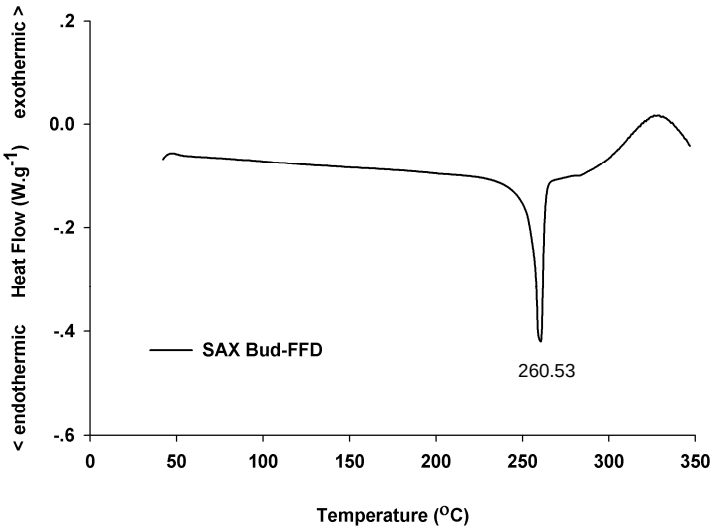

Figure 6.5: DSC thermograms of SAX-produced Bud-FFD particles

6.4.1.4 X-ray Powder Diffraction

To confirm the crystallinity of particles, XRPD analysis of micronised Bud, micronised FFD and SAX-Bud/FFD was conducted. The XRPD patterns in Figure 6.6 show sharp diffraction peaks associated with crystalline materials of micronised Bud, micronised FFD and SAX-produced Bud/FFD. The diffractograms suggest that the XRPD of SAX-produced Bud/FFD had similar peak and patterns to micronised Bud. Again, owing to the lower concentration of FFD in the combined SAX particles, it was not possible to detect the presence of FFD.

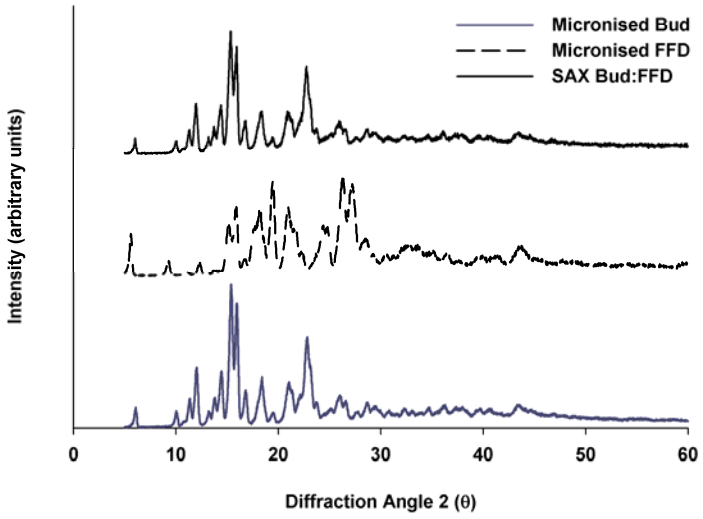

Figure 6.6: XRPD spectra of micronised Bud, micronised FFD and SAX-produced Bud-FFD particles

6.4.1.5 Dynamic Vapour Sorption

The DVS isotherms of micronised Bud, micronised FFD and SAX-produced Bud/FFD particles are shown in Figure 6.7. As shown in this figure, the DVS moisture sorption isotherms of micronised FFD showed a sharp loss in mass during the first sorption cycle upon exposure to 60% RH, which suggested that the materials contained undetectable amorphous material form. The small hysteresis in the 2 cycles for micronised Bud and SAX produced Bud/FFD suggests that these materials are crystalline in nature. As shown in the DVS trace for SAX FP/SX in Chapter 5, Figure 5.7, the increase in %mass uptake for the SAX materials appears to be related to an increase in surface area for moisture adsorption.

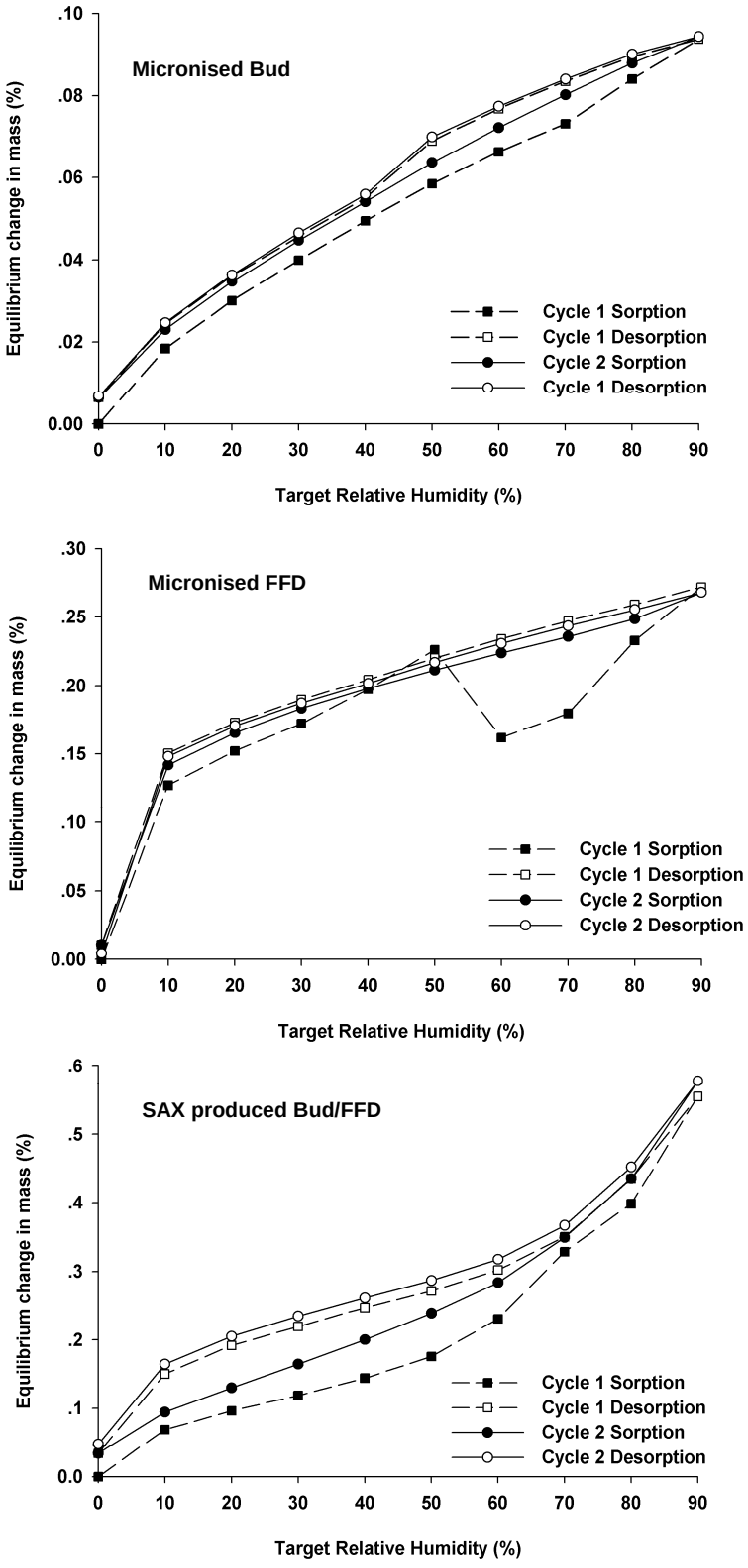

Figure 6.7: DVS isotherms of micronised Bud, micronised FFD and SAX-produced Bud-FFD

6.5 Formulation Performance of Micronised and SAX Bud/FFD Combination DPI Formulations

6.5.1 Results

6.5.1.1 SEMs of the Bud-FFD Formulations

Representative SEMs of (A) etched lactohale, (B) the formulation of micronised physical mixture of Bud/FFD, and (C) the formulation of SAX-produced Bud/FFD with etched lactohale are shown in Figure 6.8. The etched lactose, from the method of temperature-controlled dissolution as described in Chapter 2, exhibited less intrinsic fine particles of lactose. However, after preparing the formulations, the formulations from micronised physical mixture of Bud/FFD and, also, SAX-produced Bud/FFD presented the small drug particles deposited on the surface of the etched lactohale.

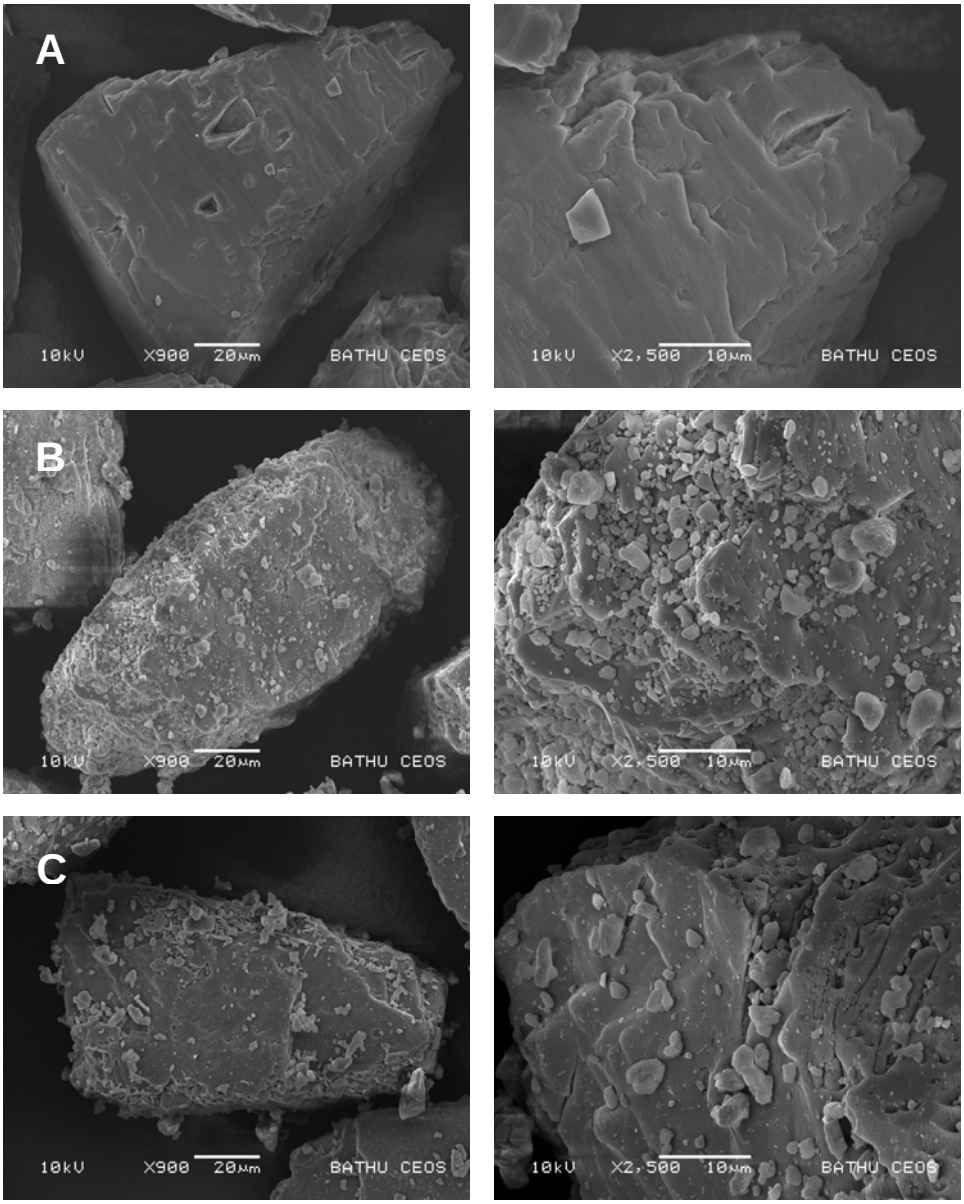

Figure 6.8: Representative SEMs of (A) etched lactohale, (B) the formulation of micronised physical mixture of Bud-FFD, and (C) the formulation of SAX-produced Bud-FFD at magnifications of x900 and x2500

6.5.1.2 Content Uniformity of Bud-FFD Formulations

The coefficient of variation (CV) of the drug content of the two formulations containing either micronised budesonide and formoterol or combined SAX particles of Bud/FFD was <6%, which is the upper limit of what is commonly acceptable as uniformity for a carrier-based DPI formulation. These results demonstrated that both formulations were uniformly blended.

6.5.1.3 Study I: In-vitro Formulation Performance of Combination Formulations of Bud/FFD following Storage at 25˚C/75% RH

The *in-vitro* inhalation performance of combination based DPI formulations comprising of micronised Bud and FFD and combined SAX particles of Bud/FFD was investigated using a Cyclohaler with a next generation impactor (NGI). In addition, the performance of both formulations was assessed following storage of the materials for 2 and 4 weeks at 25˚C/75% RH. The mean mass data of drug deposited per capsule on each stage of the NGI for both micronised Bud/FFD and SAX Bud/FFD formulations are shown in Table 6.2 along with the ED, FPD, FPF_{ED} and MMAD. Stage-by-stage deposition of both formulations before and after 2 and 4 week storage is shown in Figure 6.9 and 6.10, respectively. These data suggest that, upon aerosolisation for the SAX Bud/FFD formulation, more budesonide and formoterol were delivered to the lower stages of the impactor than the formulation containing micronised budesonide and formoterol.

Table 6.2 (continued on next page): NGI deposition per capsule of drug aerosolised from the formulations of micronised Bud:FFD and SAX-produced Bud:FFD with ratio 36:1 stored at 25˚C/75% RH in different periods of time (week 0, 2 and 4)

Bud = budesonide; FFD = formoterol fumarate dihydrate

Formulations	***Mean Drug Deposition on Impactor Stages (µg ± SD)***											***Mean ED (µg ± SD)***	***Mean FPD (µg ± SD)***	***Mean FPF_{ED} (% ± SD)***	***MMAD (µm ± GSD)***
	D & C	**MP &T**	**PS**	**S1**	**S2**	**S3**	**S4**	**S5**	**S6**	**S7**	**MOC**				
Micronised Bud at week 0	49.39 ± 10.84	12.38 ± 2.01	245.91 ± 6.31	4.79 ± 0.59	11.98 ± 0.55	16.09 ± 0.62	16.10 ± 2.71	8.34 ± 0.41	3.40 ± 0.28	2.31 ± 0.42	1.37 ± 0.23	322.69 ± 9.34	47.62 ± 2.75	14.75 ± 0.63	2.60 ± 2.50
Micronised FFD at week 0	0.65 ± 0.28	0.16 ± 0.02	6.93 ± 0.40	0.07 ± 0.02	0.13 ± 0.03	0.19 ± 0.06	0.18 ± 0.06	0.07 ± 0.02	0.02 ± 0.01	0.01 ± 0.01	0.00 ± 0.00	7.77 ± 0.25	0.48 ± 0.14	6.19 ± 1.87	3.20 ± 2.00
SAX-produced Bud at week 0	66.92 ± 13.04	23.29 ± 0.68	154.86 ± 14.75	8.94 ± 0.74	18.73 ± 4.67	21.59 ± 0.87	19.88 ± 0.70	8.84 ± 0.48	2.86 ± 0.91	2.49 ± 0.14	1.44 ± 0.17	262.89 ± 20.23	57.08 ± 0.91	21.78 ± 1.40	3.00 ± 2.60
SAX-produced FFD at week 0	1.11 ± 0.39	0.37 ± 0.04	5.15 ± 0.59	0.12 ± 0.03	0.26 ± 0.10	0.34 ± 0.03	0.36 ± 0.03	0.17 ± 0.01	0.06 ± 0.01	0.03 ± 0.01	0.01 ± 0.01	6.88 ± 0.81	0.97 ± 0.06	14.19 ± 0.92	2.90 ± 2.40
Micronised Bud at week 2	42.14 ± 2.09	13.30 ± 2.74	258.78 ± 3.26	4.58 ± 0.25	10.02 ± 0.47	12.25 ± 0.52	11.21 ± 1.51	4.94 ± 0.13	2.36 ± 0.26	1.01 ± 0.25	0.81 ± 0.16	319.26 ± 5.74	32.58 ± 0.69	10.21 ± 0.24	2.90 ± 2.50
Micronised FFD at week 2	0.73 ± 0.08	0.18 ± 0.03	6.91 ± 0.22	0.06 ± 0.01	0.11 ± 0.02	0.18 ± 0.01	0.18 ± 0.03	0.06 ± 0.01	0.01 ± 0.01	0.00 ± 0.00	0.00 ± 0.00	7.69 ± 0.16	0.43 ± 0.04	5.56 ± 0.60	3.40 ± 1.80
SAX-produced Bud at week 2	60.71 ± 7.10	25.52 ± 3.60	196.97 ± 7.46	10.35 ± 0.31	21.71 ± 0.85	17.76 ± 1.28	16.51 ± 1.51	6.92 ± 1.42	3.21 ± 0.17	1.82 ± 0.58	1.10 ± 0.05	301.87 ± 10.37	47.32 ± 2.24	15.69 ± 0.85	3.40 ± 2.70
SAX-produced FFD at week 2	0.97 ± 0.06	0.40 ± 0.05	5.88 ± 0.12	0.15 ± 0.01	0.30 ± 0.03	0.28 ± 0.02	0.27 ± 0.02	0.12 ± 0.03	0.05 ± 0.01	0.03 ± 0.01	0.00 ± 0.00	7.47 ± 0.20	0.74 ± 0.05	9.87 ± 0.64	3.40 ± 2.00

Table 6.2 (continued from previous page): NGI deposition per capsule of drug aerosolised from the formulations of micronised Bud:FFD and SAX-produced Bud:FFD with ratio 36:1stored at 25˚C/75% RH in different periods of time (week 0, 2 and 4)

Bud = budesonide; FFD = formoterol fumarate dihydrate

Formulations	***Mean Drug Deposition on Impactor Stages (µg ± SD)***											***Mean ED (µg ± SD)***	***Mean FPD (µg ± SD)***	***Mean FPF_{ED} (% ± SD)***	***MMAD (µm ± GSD)***
	D & C	**MP &T**	**PS**	**S1**	**S2**	**S3**	**S4**	**S5**	**S6**	**S7**	**MOC**				
Micronised Bud at week 4	35.83 ± 4.49	13.99 ± 1.83	239.51 ± 29.93	5.24 ± 0.19	11.43 ± 0.38	13.98 ± 1.15	13.73 ± 0.43	6.31 ± 0.10	2.92 ± 0.13	1.25 ± 0.21	0.79 ± 0.13	309.16 ± 31.01	38.99 ± 0.79	12.72 ± 1.60	2.90 ± 2.50
Micronised FFD at week 4	0.60 ± 0.07	0.22 ± 0.03	6.78 ± 0.96	0.06 ± 0.01	0.13 ± 0.02	0.21 ± 0.01	0.23 ± 0.02	0.09 ± 0.01	0.03 ± 0.01	0.00 ± 0.00	0.00 ± 0.00	7.74 ± 1.02	0.55 ± 0.03	7.24 ± 0.91	3.10 ± 1.80
SAX-produced Bud at week 4	52.05 ± 3.09	27.88 ± 1.15	197.35 ± 2.07	10.14 ± 0.31	19.08 ± 0.29	15.37 ± 1.03	13.01 ± 0.98	5.64 ± 0.89	2.32 ± 0.41	1.15 ± 0.15	0.55 ± 0.09	292.49 ± 4.03	38.04 ± 1.09	13.01 ± 0.24	3.70 ± 2.60
SAX-produced FFD at week 4	0.49 ± 0.04	0.44 ± 0.01	7.35 ± 0.63	0.25 ± 0.03	0.42 ± 0.17	0.35 ± 0.07	0.28 ± 0.09	0.14 ± 0.07	0.04 ± 0.07	0.02 ± 0.03	0.00 ± 0.00	9.30 ± 1.00	0.83 ± 0.23	8.85 ± 1.96	3.90 ± 2.10

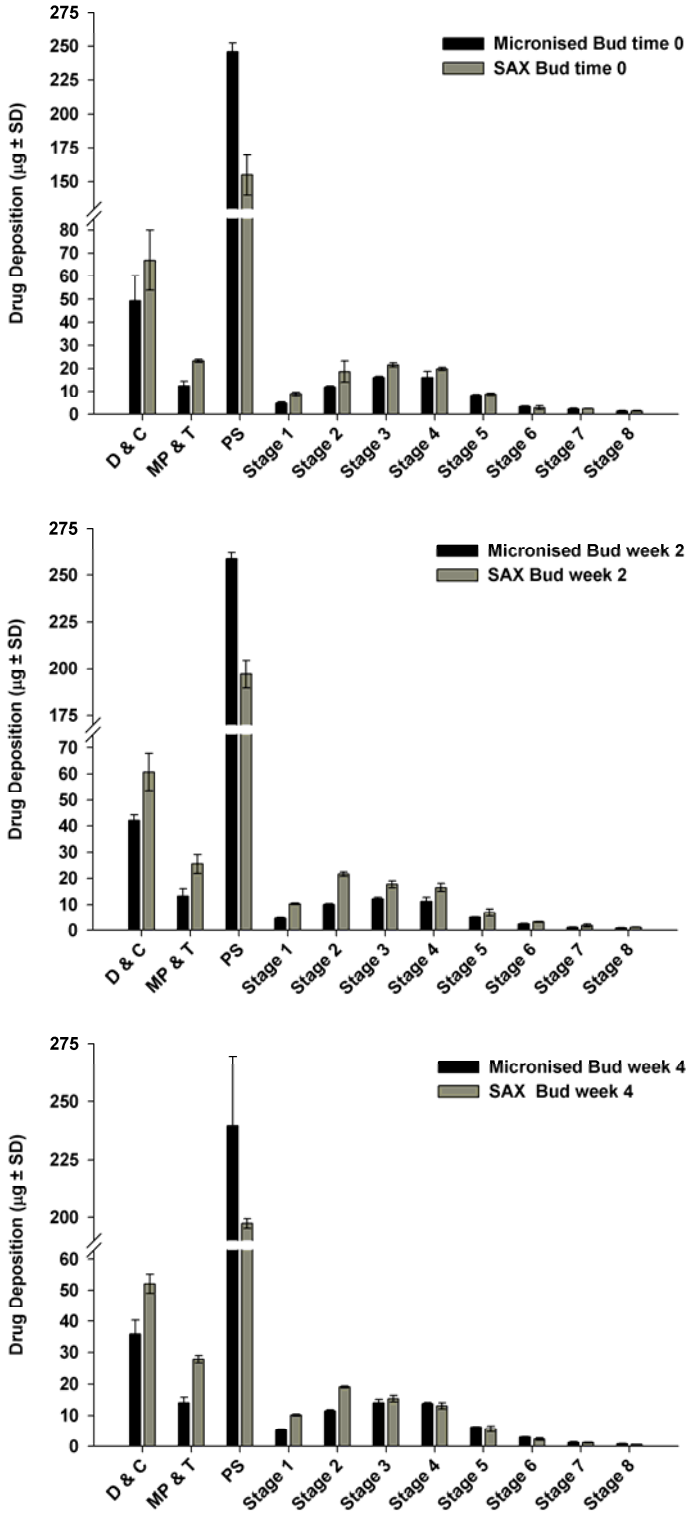

Figure 6.9: NGI deposition per capsule of Bud aerosolised from the combination formulations of micronised Bud:FFD (36:1) compared with SAX-produced Bud:FFD (36:1) at 25˚C/75% RH in different periods of time (week 0, 2 and 4)

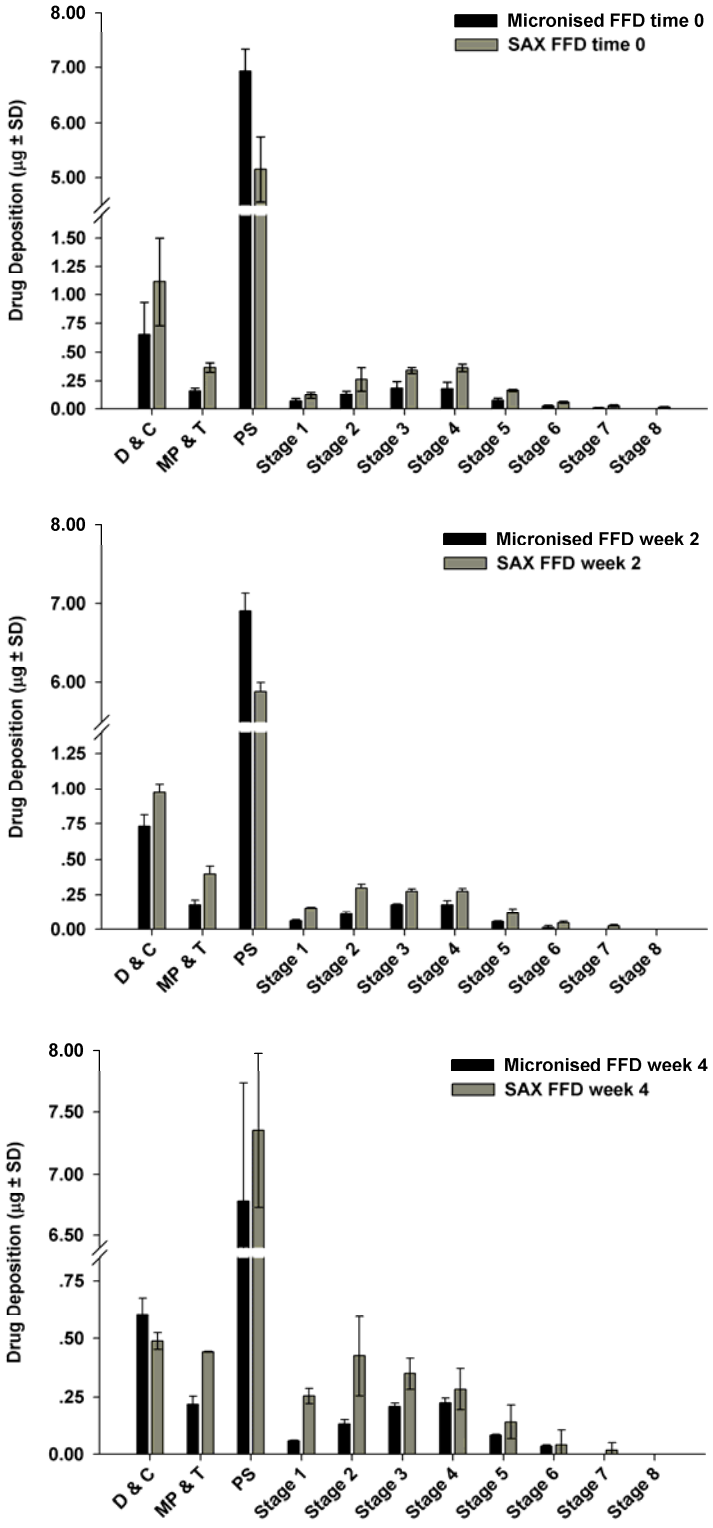

Figure 6.10: NGI deposition per capsule of FFD aerosolised from the combination formulations of micronised Bud:FFD (36:1) compared with SAX-produced Bud:FFD (36:1) at 25˚C/75% RH as a function of storage time (week 0, 2 and 4)

Upon aerosolisation of the micronised Bud/FFD formulation at the initial time-point, the ED of budesonide was significantly greater ($p<0.05$) than that of budesonide aerosolised from the SAX Bud/FFD formulation as shown by Figure 6.11. However, there was no statistical difference in the ED of FFD upon aerosolisation of either formulation. Upon storage at 25˚C and 75% RH for two and four weeks, the ED of budesonide and formoterol were not dramatically affected upon aerosolisation of both formulations. An exception to this observation was the slight but significant ($p<0.05$) increase in the ED of budesonide following aerosolisation of the SAX Bud/FFD formulation following storage at 25˚C and 75% RH for two and four weeks in comparison to the initial time-point. In addition, it is evident from Figure 6.11 that the ED of FFD increased following four week storage of the SAX Bud/FFD formulation at 25˚C and 75% RH.

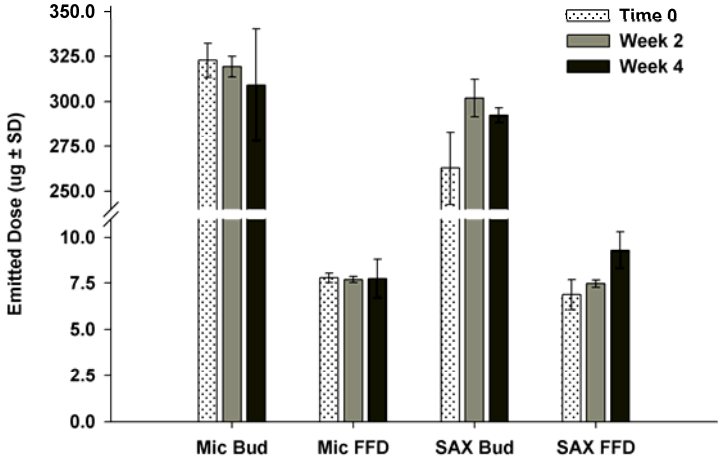

Figure 6.11: The emitted dose per capsule of micronised and SAX combination formulations stored at 25˚C/75% RH in different periods of time (week 0, 2 and 4)

The fine particle dose (FPD) of budesonide and formoterol following aersolisation of the micronised Bud/FFD and SAX Bud/FFD formulations are shown in Figure 6.12 before and after storage at 25˚C and 75% RH for two and four weeks. At the initial time-point, aerosolisation of the SAX Bud/FFD formulation resulted in significantly ($p<0.05$) greater FPD of budesonide (57.08 ± 0.91 µg) and formoterol (0.97 ± 0.06 µg) than the micronised Bud/FFD formulation [Bud (47.62 ± 2.75 µg) and FFD (0.48 ± 0.14 µg)]. Following aerosolisation of the SAX Bud/FFD formulation after storage at 25˚C and

75% RH for two weeks, the FPD of Bud (47.32 ± 2.24 µg) and FFD (0.74 ± 0.05 µg) were significantly higher ($p<0.05$) than FPD of Bud (32.58 ± 0.69 µg) and FFD (0.43 ± 0.04 µg) from the micronised Bud/FFD formulation. After storage at 25˚C and 75% RH for four weeks, there were no differences in the FPD of budesonide or formoterol following aerosolisation of either formulation as shown in Figure 6.12. However, it is evident from Figure 6.12 that whilst storage conditions did not affect the FPD of FFD from either formulation at 2 and 4 weeks, the FPD of budesonide from both formulations significantly ($p<0.05$) decreased.

Storage of the micronised Bud/FFD formulation for two weeks at 25˚C and 75% RH resulted in a significant ($p<0.05$) decrease in the FPD of Bud in comparison to the initial time-point. The decrease in the FPD of Bud on storage of the micronised Bud/FFD formulation was also seen upon aerosolisation of the SAX Bud/FFD formulation after storage. It is evident from Figure 6.12 that the FPD of Bud decreases following storage of the SAX Bud/FFD formulation for two and four weeks at 25˚C and 75% RH. Figure 6.12 also shows that storage of the micronised and SAX Bud/FFD formulations at 25˚C and 75% RH for two and four weeks resulted in no significant change in the FPD of FFD in comparison to the initial time-point.

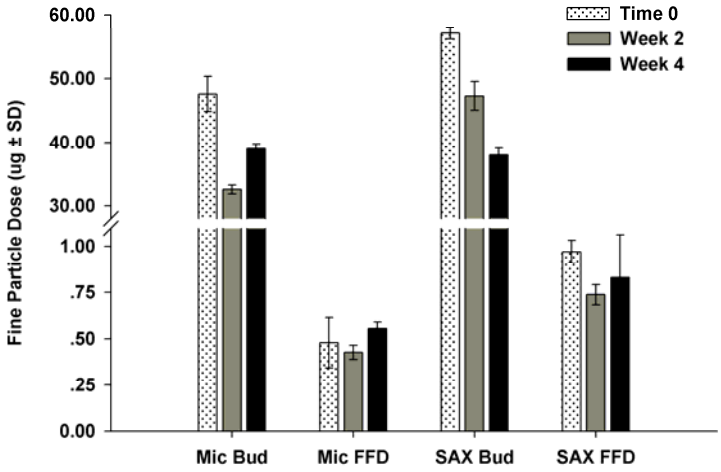

Figure 6.12: The fine particle dose per capsule of micronised and SAX combination formulations stored at 25˚C/75% RH in different periods of time (week 0, 2 and 4)

The percentage fine particle fraction of the emitted dose (FPF_{ED}) of budesonide and formoterol following aersolisation of the micronised Bud/FFD and SAX Bud/FFD formulations are shown in Figure 6.13 before and after storage at 25˚C and 75% RH for two and four weeks.

Upon aerosolisation of the SAX Bud/FFD formulation, the FPF_{ED} of budesonide and formoterol were 21.78 ± 1.40 % and 14.19 ± 0.92 %, respectively, which were significantly ($p<0.05$) greater than the FPF_{ED} of Bud (14.75 ± 0.63 %) and FFD (6.19 ± 1.87 %) following aerosolisation of the micronised Bud/FFD formulation.

Upon storage of both formulations at 25˚C and 75% RH for two weeks, the FPF_{ED} of budesonide (15.69 ± 0.85 %) and FFD (9.87 ± 0.64 %) upon aerosolisation of the SAX Bud/FFD were significantly higher ($p<0.05$) than FPF_{ED} of Bud (10.21 ± 0.24 %) and FFD (5.56 ± 0.60 %) following aerosolisation of the micronised Bud/FFD formulation. After storage of the formulations at 25˚C and 75% RH for four weeks, there were no significant differences in the FPF_{ED} of budesonide and formoterol following aerosolisation of both formulations. However, in comparison to the initial time-point the FPF_{ED} of budesonide decreased significantly ($p<0.05$) following aerosolisation of the micronised Bud/FFD and SAX Bud/FFD formulations following storage at 25˚C and 75% RH for two and four weeks. In contrast, the FPF_{ED} of formoterol was not affected following storage of the micronised Bud/FFD formulation, however, the FPF_{ED} of formoterol decreased significantly ($p<0.05$) following storage of the SAX Bud/FFD formulation at two and four weeks.

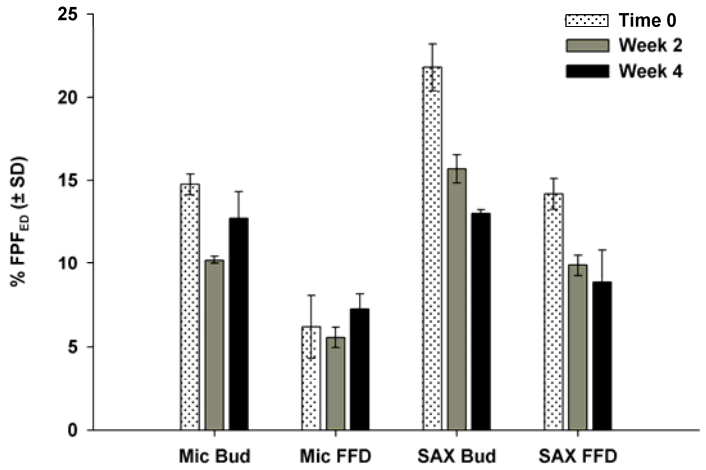

Figure 6.13: The fine particle fraction of emitted dose (FPF_{ED}) per capsule of micronised and SAX combination formulations stored at 25˚C/75% RH in different periods of time (week 0, 2 and 4)

The mean normalised mass ratios of Bud:FFD as a function of recovered dose deposited on stages 2 to 5 of the NGI following aerosolisation of both formulations at the initial time-point and following storage at 25˚C/75% RH for two and four weeks are shown in Figure 6.14. It is evident from Figure 6.14 that the ratios of Bud:FFD on stages 2 to 5 following aerosolisation of both micronised and SAX Bud/FFD formulations before and after storage are greater than one. These data suggest that deposition of both drugs were inconsistent and were not deposited in a uniform manner. However, Figure 6.14 shows that aerosolisation of the SAX Bud/FFD resulted in greater consistency in the delivery of both drugs on stage 2–5 than micronised Bud/FFD. This is further supported by Figure 6.14, which shows that the mass ratio of Bud:FFD following aerosolisation of the SAX Bud/FFD formulations were closer to one. Storage of the micronised Bud/FFD formulations at 25˚C/75% RH for two and four weeks resulted in significant variations in the mass ratio of Bud/FFD on stages 2–5, which may indicate towards significant under-and over dosing of either active. In contrast, the mass ratio of Bud:FFD on stages 2–5 remained more consistent following storage of the SAX Bud/FFD formulations at two and four weeks.

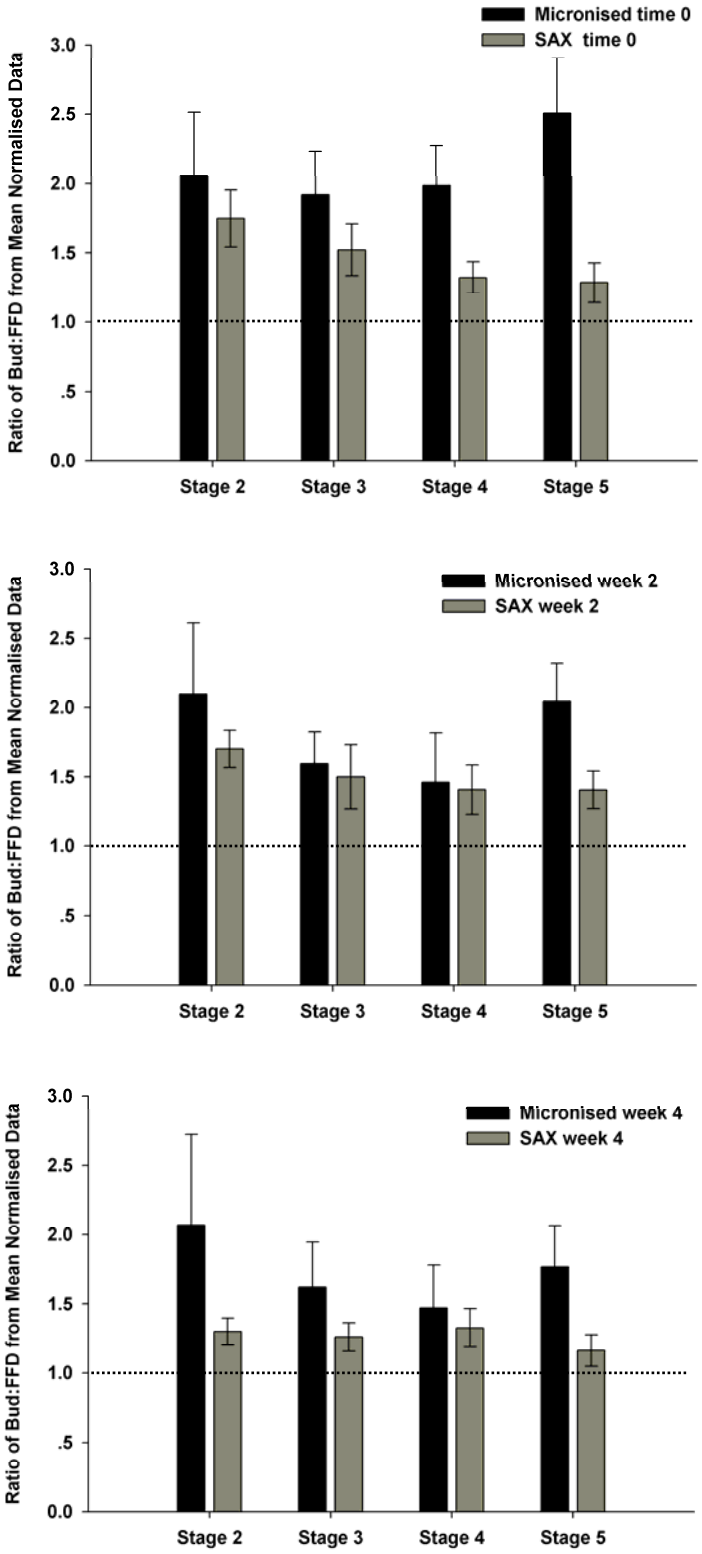

Figure 6.14: Ratios of Bud:FFD from mean normalised data of stage 2-5 of micronised Bud:FFD (36:1) compared with SAX-produced Bud:FFD (36:1) stored at 25˚C/75% RH for 0, 2 and 4 weeks

6.5.1.4 Study II: In-Vitro Performance of Bud-FFD Formulations at 40˚C/75% RH

The *in-vitro* inhalation performance of combination based DPI formulations comsisting of micronised Bud and FFD and combined SAX particles of Bud/FFD was investigated. In addition, the performance of both formulations was assessed following storage of the materials for 2 and 4 weeks at 40˚C/75% RH. The mean mass data of drug deposited per capsule on each stage of the NGI for both micronised Bud/FFD and SAX Bud/FFD formulations are shown in Table 6.3 along with the ED, FPD, FPF_{ED} and MMAD. Furthermore, the stage-by-stage deposition of both drugs before and after storage can be observed in Figure 6.15 and 6.16. These data suggest that upon aersolisation of the SAX Bud/FFD formulation, more budesonide and formoterol were delivered to the lower stages of the impactor than the formulation containing micronised budesonide and formoterol.

Table 6.3 (continued on next page): NGI deposition per capsule of drug aerosolised from the formulations of micronised Bud:FFD and SAX-produced Bud:FFD with ratio 36:1 stored at 40˚C/75% RH in different periods of time (week 0, 2 and 4).

Bud = budesonide; FFD = formoterol fumarate dihydrate

Formulations	***Mean Drug Deposition on Impactor Stages (µg ± SD)***											***Mean ED (µg ± SD)***	***Mean FPD (µg ± SD)***	***Mean FPF_{ED} (% ± SD)***	***MMAD (µm ± GSD)***
	D & C	**MP &T**	**PS**	**S1**	**S2**	**S3**	**S4**	**S5**	**S6**	**S7**	**MOC**				
Micronised Bud at week 0	49.39 ± 10.84	12.38 ± 2.01	245.91 ± 6.31	4.79 ± 0.59	11.98 ± 0.55	16.09 ± 0.62	16.10 ± 2.71	8.34 ± 0.41	3.40 ± 0.28	2.31 ± 0.42	1.37 ± 0.23	322.69 ± 9.34	47.62 ± 2.75	14.75 ± 0.63	2.60 ± 2.50
Micronised FFD at week 0	0.65 ± 0.28	0.16 ± 0.02	6.93 ± 0.40	0.07 ± 0.02	0.13 ± 0.03	0.19 ± 0.06	0.18 ± 0.06	0.07 ± 0.02	0.02 ± 0.01	0.01 ± 0.01	0.00 ± 0.00	7.77 ± 0.25	0.48 ± 0.14	6.19 ± 1.87	3.20 ± 2.00
SAX-produced Bud at week 0	66.92 ± 13.04	23.29 ± 0.68	154.86 ± 14.75	8.94 ± 0.74	18.73 ± 4.67	21.59 ± 0.87	19.88 ± 0.70	8.84 ± 0.48	2.86 ± 0.91	2.49 ± 0.14	1.44 ± 0.17	262.89 ± 20.23	57.08 ± 0.91	21.78 ± 1.40	3.00 ± 2.60
SAX-produced FFD at week 0	1.11 ± 0.39	0.37 ± 0.04	5.15 ± 0.59	0.12 ± 0.03	0.26 ± 0.10	0.34 ± 0.03	0.36 ± 0.03	0.17 ± 0.01	0.06 ± 0.01	0.03 ± 0.01	0.01 ± 0.01	6.88 ± 0.81	0.97 ± 0.06	14.19 ± 0.92	2.90 ± 2.40
Micronised Bud at week 2	45.23 ± 9.32	15.73 ± 2.92	253.55 ± 18.83	5.12 ± 0.76	9.98 ± 1.38	11.15 ± 1.49	10.02 ± 1.24	4.16 ± 0.70	1.77 ± 0.67	0.94 ± 0.50	0.53 ± 0.18	312.94 ± 25.83	28.56 ± 4.30	9.09 ± 0.66	3.20 ± 2.50
Micronised FFD at week 2	1.09 ± 0.40	0.19 ± 0.03	6.15 ± 0.48	0.06 ± 0.02	0.11 ± 0.02	0.18 ± 0.03	0.19 ± 0.02	0.07 ± 0.01	0.00 ± 0.00	0.00 ± 0.00	0.00 ± 0.00	6.95 ± 0.60	0.44 ± 0.06	6.25 ± 0.42	3.60 ± 1.80
SAX-produced Bud at week 2	51.66 ± 6.15	30.49 ± 5.96	172.03 ± 32.88	9.58 ± 1.28	18.62 ± 1.83	15.36 ± 0.88	11.78 ± 1.69	5.27 ± 0.56	2.32 ± 0.46	0.97 ± 0.43	0.51 ± 0.20	266.94 ± 43.10	36.22 ± 3.09	13.70 ± 1.42	3.80 ± 2.50
SAX-produced FFD at week 2	0.61 ± 0.04	0.41 ± 0.08	4.76 ± 0.65	0.13 ± 0.01	0.25 ± 0.03	0.20 ± 0.01	0.15 ± 0.01	0.06 ± 0.02	0.02 ± 0.02	0.00 ± 0.00	0.00 ± 0.00	5.97 ± 0.74	0.42 ± 0.03	7.17 ± 1.08	4.10 ± 1.90

Table 6.3 (continued from previous page): NGI deposition per capsule of drug aerosolised from the formulations of micronised Bud:FFD and SAX-produced Bud:FFD with ratio 36:1 stored at 40˚C/75% RH in different periods of time (week 0, 2 and 4).

Bud = budesonide; FFD = formoterol fumarate dihydrate

Formulations	***Mean Drug Deposition on Impactor Stages (µg ± SD)***											***Mean ED (µg ± SD)***	***Mean FPD (µg ± SD)***	***Mean FPF_{ED} (% ± SD)***	***MMAD (µm ± GSD)***
	D & C	**MP &T**	**PS**	**S1**	**S2**	**S3**	**S4**	**S5**	**S6**	**S7**	**MOC**				
Micronised Bud at week 4	40.29 ± 4.39	16.68 ± 0.48	267.17 ± 0.76	5.49 ± 0.44	9.79 ± 0.29	10.29 ± 0.51	8.36 ± 0.73	3.98 ± 0.47	1.45 ± 0.15	0.61 ± 0.09	0.27 ± 0.02	324.08 ± 1.35	24.96 ± 0.78	7.70 ± 0.21	3.50 ± 2.40
Micronised FFD at week 4	0.45 ± 0.23	0.17 ± 0.02	5.90 ± 0.23	0.05 ± 0.01	0.10 ± 0.02	0.14 ± 0.01	0.14 ± 0.04	0.06 ± 0.01	0.00 ± 0.00	0.00 ± 0.00	0.00 ± 0.00	6.56 ± 0.24	0.34 ± 0.06	5.17 ± 1.00	3.70 ± 1.80
SAX-produced Bud at week 4	47.62 ± 6.01	27.23 ± 1.16	201.55 ± 17.23	9.60 ± 1.76	14.99 ± 2.78	11.21 ± 1.78	8.75 ± 1.35	3.40 ± 1.14	1.54 ± 0.24	0.66 ± 0.28	0.31 ± 0.08	279.24 ± 23.08	25.87 ± 4.46	9.24 ± 1.15	4.30 ± 2.60
SAX-produced FFD at week 4	0.34 ± 0.19	0.29 ± 0.06	4.65 ± 0.49	0.09 ± 0.02	0.15 ± 0.02	0.10 ± 0.03	0.07 ± 0.01	0.04 ± 0.01	0.00 ± 0.00	0.00 ± 0.00	0.00 ± 0.00	5.39 ± 0.53	0.21 ± 0.03	3.96 ± 0.69	4.90 ± 1.90

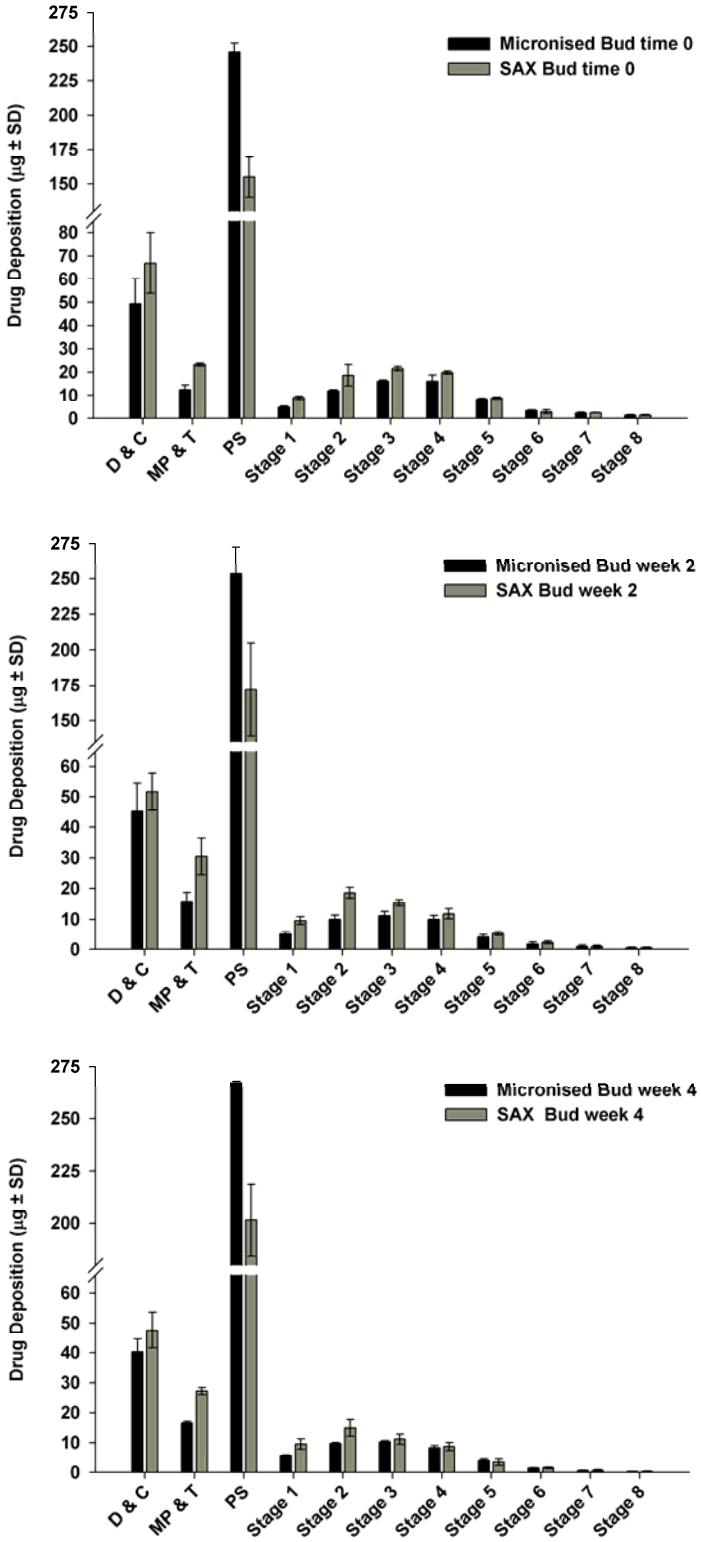

Figure 6.15: NGI deposition per capsule of Bud aerosolised from the combination formulations of micronised Bud:FFD (36:1) compared with SAX-produced Bud:FFD (36:1) at 40˚C/75% RH in different periods of time (week 0, 2 and 4)

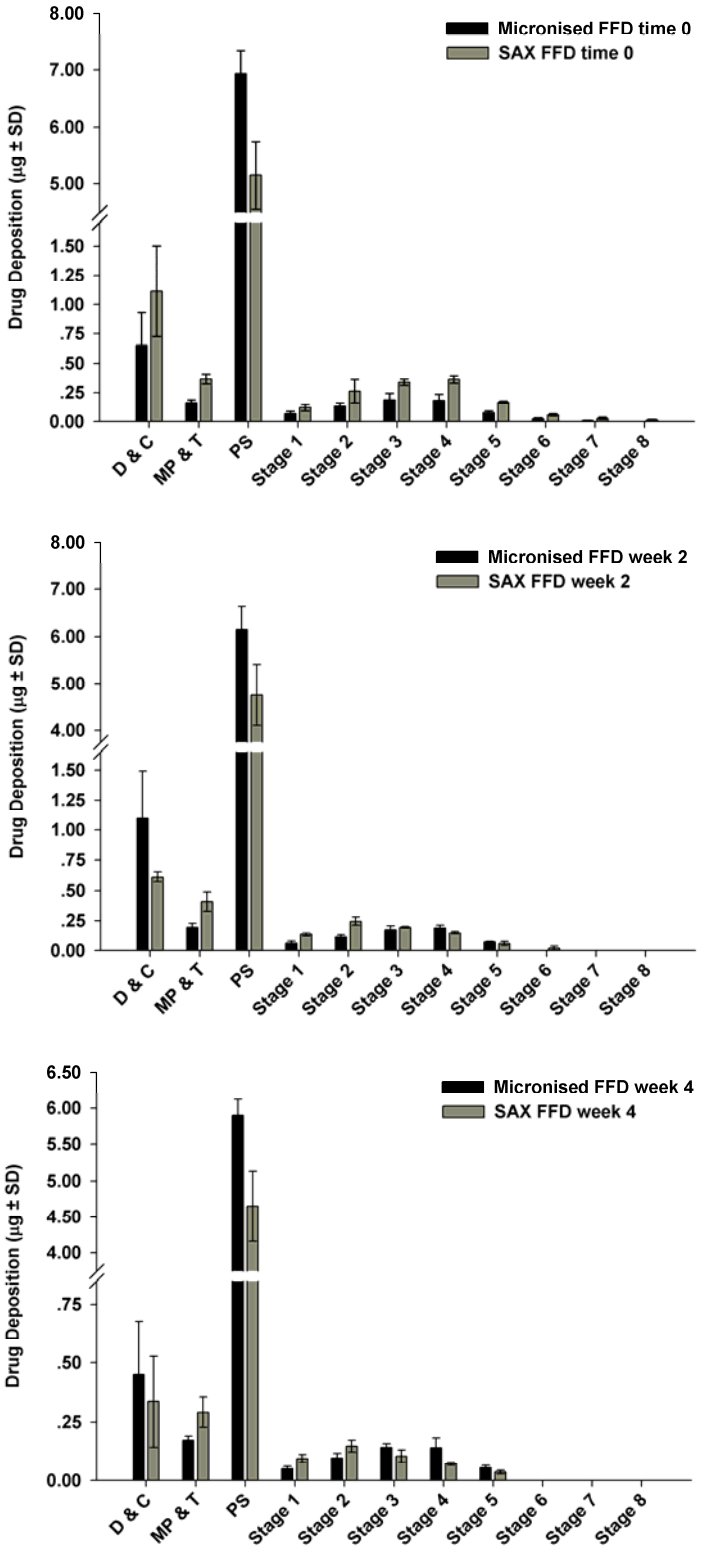

Figure 6.16: NGI deposition per capsule of FFD aerosolised from the combination formulations of micronised Bud:FFD (36:1) compared with SAX-produced Bud:FFD (36:1) upon processing and storage at 40˚C/75% RH for 2 and 4 weeks

Upon storage of the micronised and SAX Bud/FFD formulations at 40˚C and 75% RH for two and four weeks, the ED of Bud were not affected as shown by Figure 6.17. Following storage of the formulations for four weeks under the same conditions, the ED of FFD decreased significantly ($p<0.05$) in comparison to the initial time-point.

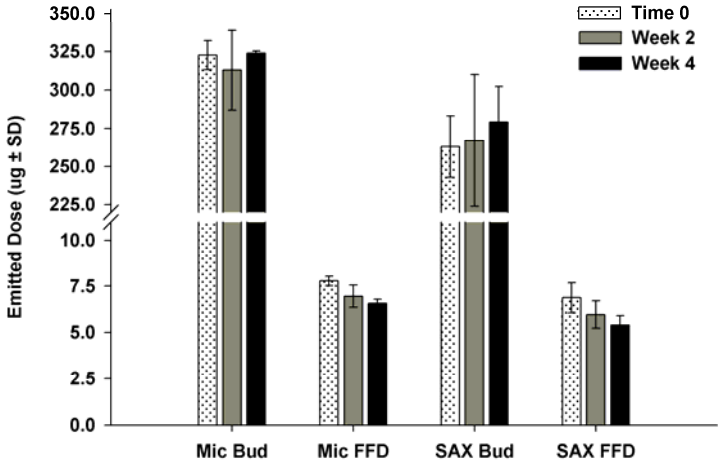

Figure 6.17: The emitted dose per capsule of micronised and SAX combination formulations stored at 40˚C/75% RH in different periods of time (week 0, 2 and 4)

The fine particle dose (FPD) of budesonide and formoterol following aersolisation of the micronised Bud/FFD and SAX Bud/FFD formulations are shown in Figure 6.18 before and after storage at 40˚C and 75% RH for two and four weeks.

After storage at 40˚C and 75% RH for two and four weeks, there were significant ($p<0.05$) differences in the FPD of budesonide following aerosolisation of both the micronised and SAX Bud/FFD formulation as shown in Figure 6.18. However, it is evident from Figure 6.18 that whilst storage conditions did not significantly affect the FPD of FFD following storage of the micronised Bud/FFD formulation at either formulation at 2 and 4 weeks, the FPD of SAX produced FFD decreased significantly ($p<0.05$) upon storage.

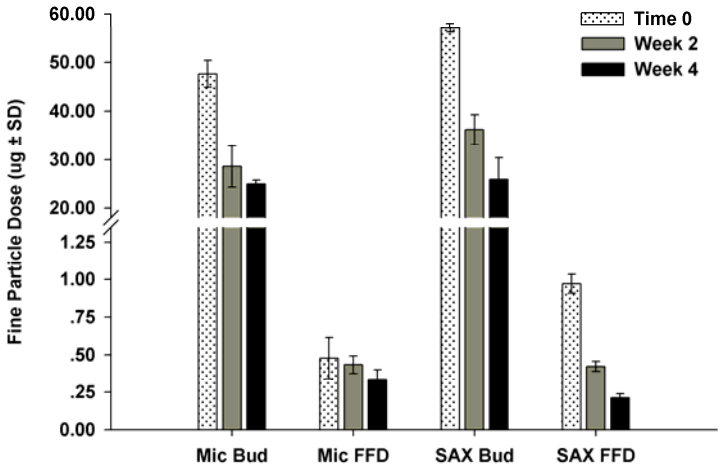

Figure 6.18: The fine particle dose per capsule of micronised and SAX combination formulations stored at 40˚C/75% RH in different periods of time (week 0, 2 and 4)

The percentage fine particle fraction of the emitted dose (FPF_{ED}) of budesonide and formoterol following aerosolisation of the micronised Bud/FFD and SAX Bud/FFD formulations are shown in Figure 6.19 following storage at 40˚C and 75% RH for two and four weeks.

Upon storage of the micronised and SAX Bud/FFD formulations at 40˚C and 75% RH for two and four weeks, the FPF_{ED} of budesonide decreased significantly ($p<0.05$) in comparison to the respective initial time-points. In contrast, the FPF_{ED} of formoterol was not affected following storage of the micronised Bud/FFD formulation, however, the FPF_{ED} of formoterol decreased significantly ($p<0.05$) following storage of the SAX Bud/FFD formulation at two and four weeks.

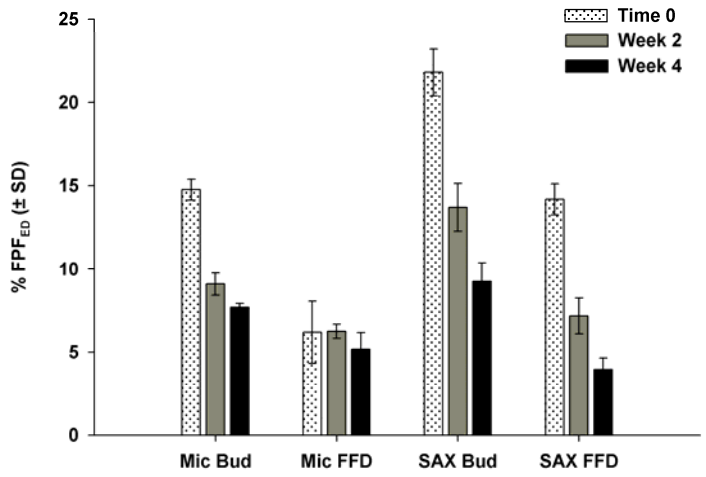

Figure 6.19: The fine particle fraction of emitted dose (FPF_{ED}) per capsule of micronised and SAX combination formulations stored at 40˚C/75% RH in different periods of time (week 0, 2 and 4)

The mean normalised mass ratios of Bud:FFD as a function of recovered dose deposited on stages 2 to 5 of the NGI following aerosolisation of both formulations at the initial time-point and following storage at 40˚C/75% RH for two and four weeks are shown in Figure 6.20. It is evident from Figure 6.20 that the ratios of Bud:FFD on stages 2 to 5 following aerosolisation of both micronised and SAX Bud/FFD formulations before and after storage at 40˚C and 75% RH were similar to those observed in Figure 6.14 following storage at 25˚C and 75% RH. Storage of the micronised Bud/FFD formulation at 40˚C/75% RH for two and four weeks resulted in significant variations in the mass ratio of Bud/FFD on stages 2–5, which may indicate towards significant under-and over dosing of either active. In contrast, the mass ratio of Bud:FFD on stages 2–5 remained more consistent following storage of the SAX Bud/FFD formulations.

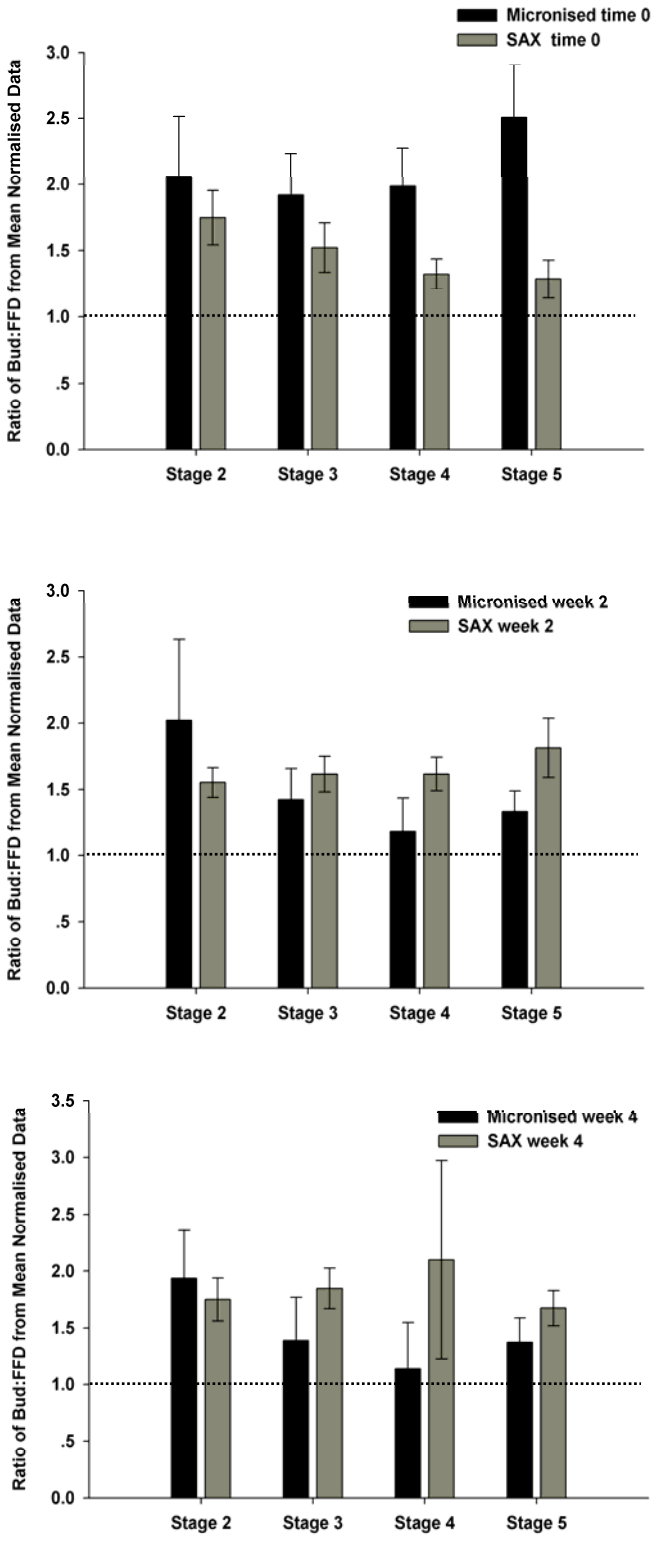

Figure 6.20: Ratios of Bud:FFD from mean normalised data on stage 2-5 delivery of micronised Bud:FFD (36:1) compared with SAX-produced Bud:FFD (36:1) before and upon storage at 40˚C/75% RH for 2 and 4 weeks

6.5.2 Discussion

In this study, the SAX approach was successfully implemented in the fabrication of low-dose FFD in combination with Bud, which was suitable for pulmonary drug delivery.

In order to assess the *in-vitro* performance of the SAX engineered combination particles of Bud/FFD, two formulations of the SAX-produced Bud/FFD and physical mixture of Bud/FFD were formulated. At the initial time point, the FPF_{ED} of Bud and FFD from a formulation containing SAX-produced Bud/FFD were significantly ($p<0.05$) greater than micronised Bud/FFD. These results suggest that the morphology of the SAX Bud/FFD particles may have aided greater delivery of the actives owing to lower surface contact area and therefore lower adhesion to components of the formulation.

The mass ratio data of Bud:FFD as normalised as a function of recovered dose on stages 2 to 5 following aerosolisation of the micronised and SAX formulations were greater than one. These data suggest that though both actives were being delivered to the lower stages of the impactor, they were delivered independently of each other. However, in comparison to the micronised Bud/FFD formulation, the mass ratio of Bud:FFD on stages 2–5 following aerosolisation of the SAX Bud/FFD formulation was more consistent. The performance of the SAX Bud/FFD formulation suggests that both actives were within one geometric particle. This feature of the formulation containing SAX Bud/FFD particles is critical to the clinical efficacy observed with the SMART approach to asthma therapy, because significant variations in the delivery of both actives as observed with the formulation containing micronised Bud/FDD may lead to significant under or overdosing situations.

Upon storage of the SAX Bud/FFD formulation under the different environmental conditions, data resulted in a significant decrease in the FPD and FPF_{ED} of both actives ($P<0.05$). This was also observed for the micronised Bud/FFD formulation, but only in relation to the FPD and FPF_{ED} of budesonide and not formoterol. Such data suggest that one or more components of the SAX Bud/FFD particles may have remained in the metastable state and may not have crystallised during processing by SAX, which would render the material susceptible to dynamic transformations that would affect product performance on storage. However, dynamic vapour sorption studies suggested that the SAX Bud/FFD particles were stable on exposure to elevated humidity and did not

indicate any signs of physical transformations. These data are also supported by DSC and XRPD studies.

It is interesting to note that whilst the performance of micronised Bud was affected upon storage the performance of micronised FFD was not. In contrast, both the performance of Bud and FFD decreased significantly following storage of formulations containing SAX Bud/FFD particles. One possible explanation for this trend may be that as the SAX particles contain both drugs in one individual particle, failure in the delivery of one of the actives will also affect the performance of the other. In the case of the SAX Bud/FFD formulation, the particles contain more budesonide than FFD, therefore, a drop in the performance of budesonide will also result in a significant decrease in the delivery of FFD. In contrast, the micronised formulation contains both drugs in a physical mixture. Therefore, the drop in performance of micronised budesonide will be independent of micronised FFD.

6.6 Conclusions

The SAX process may be utilised to produce individual particulates of two active ingredients, which will effectively allow the delivery of combination medicaments containing low doses of one or more actives. Combination particles of Bud/FFD were successfully fabricated with desired surface properties, which enabled greater delivery of both actives to the lower stages of the impactor, in comparison to formulations containing physical mixtures of micronised forms of the actives. Furthermore, the delivery of both actives as combined SAX particles resulted in consistent delivery of both actives across the lower stages of the impactor. However, as both actives are present in one particle, the delivery of both actives is sensitive to change on storage.

Chapter 7: General Conclusions and Further work

7.1 Introduction

The objective of pharmaceutical engineering of inhalation dosage forms is the generation of a drug product that enable the delivery of medicines efficiently and effectively to the human airways. Currently, the processing of these dosage forms remains highly empirical, which corresponds with high failure rates of these drug products during development and manufacturing. The primary source of dry powder inhaler (DPI) formulation failure is the lack of control on key physicochemical properties of the active(s), which can be related to the process of micronisation that is used to generate respirable particles. We propose that to control the specific performance and stability properties of DPI dosage forms, the central design principle in DPI manufacturing must focus on tailoring the mesoscopic design of particle interfaces to enable careful control of particle-particle interactions and therefore, drug product performance.

This principle must be taken one-step further with respect to combined inhalation products, which are significantly more complicated than binary formulations. As asthma and COPD are two-component conditions of the airways, the most effective treatment for reducing smooth muscle dysfunction and inflammation is to use combined therapy of long acting β_2-agonist (LABA) and corticosteroid (ICS) together in order to illicit significant clinical advantages. It has been demonstrated that addition of a long-acting β_2-agonist (LABA) to an inhaled corticosteroid (ICS) is superior to ICS alone in achieving asthma control (Matz, Emmett et al., 2001). Furthermore, there is evidence to suggest that patients with COPD may also benefit from combined inhalation therapy with ICS and LABA (Calverley, Pauwels et al., 2003).

The improved clinical outcome on therapy on combined inhalation therapy with ICS and LABA is reported to be as a result of synergistic actions of LABA and ICS at the cellular, receptor and molecular level (Theophilus, Moore et al., 2006). The opportunity for synergistic action is enhanced by co-deposition of both particles on the same cells of the airways. Administration of the two drugs by a single inhaler would lead to an increased chance for co-deposition compared with administration via two separate inhalers. However, current combined inhalation products are subject to a greater

variability in dose delivery of each active, which may be perpetuated as a function of product storage conditions (Taki, Zeng et al., 2006). Hence, there is a requirement of processes that may enable production of combination inhaled products that will allow both drugs to be delivered more effectively and independently of dose variations.

7.2 Summary

Following physical characterisation of the materials utilised in the study, the development of the SAX process in the lab-scale size was successfully achieved by controlling many factors involved in the SAX system. Many factors, including pressure, solvents, non-solvents and temperatures, had a significant effect on properties of resultant materials. As a result, a laboratory SAX system was produced that enabled the formation of small scale batches of SAX material with a significant level of control and manipulation.

The SAX process was applied as a single step droplet-to-particle operation to process drug particles for delivery to the respiratory tract. The SAX process was used to engineer crystalline drug particles and the result found that it was possible to modify crystalline particles of budesonide with suitable properties for the inhaled drug. Moreover, budesonide SAX particles were found to outperform micronised budesonide particles as determined by *in-vitro* performance testing. Furthermore, porous/hollow crystalline particles of budesonide with geometric diameter of 8–10 µm were produced, which were found to possess an aerodynamic diameter between 2–4 µm. These particles possessed the same delivery efficiency as micronised drug products.

The SAX process was also used to produce individual particulates of two active ingredients, to allow effective delivery of combination medicaments independently of dose variations of the actives. All physicochemical characterisation demonstrated that the SAX-produced combined particles of FP and SX were successfully co-processed into individual particles with crystalline properties. Additionally, *in-vitro* performance studies strongly confirmed that all SAX FP/SX formulations delivered both drugs consistently and independently of dose variations to the lower stages of the impactor even after storage of the formulations at accelerated stability conditions.

In addition, low-dose combined drug particles of Bud and FFD were produced *via* the SAX system. For the combination of low-dose drugs, it has been demonstrated that the FPF_{ED} of Bud and FFD from SAX-produced Bud/FFD formulation was significantly ($p<0.05$) greater than a micronised Bud/FFD formulation. However, the mass ratio of Bud:FFD across stages 2 – 5 was not close to 1 when either formulation was aerosolised. However, the SAX combination Bud/FFD particles were more consistent in the delivery of both actives than micronised. Under stability conditions, the performance of the SAX Bud/FFD particles did decrease, which may be related to the fact that performance of both actives are affected by one another, therefore, changes in one active may affect the delivery of the other after storage.

This approach, however, presents itself as novel means to produce inhaled combination dosage forms which may lead to enhanced clinical efficacy.

7.3 General Conclusions

In conclusion, it is evident from the work presented that the SAX process has been succesfully utilised in modifying the surface morphology of crystalline particles suitable for pulmonary drug delivery. The SAX process has been successfully developed by controlling all crucial factors which were involved in the system. Furthermore, the process has been successfully employed to engineer drug particles, with optimum properties for delivery to the lungs. Moreover, *in-vitro* performance SAX-produced formulation was significantly greater than the micronised formulation. Consequently, the SAX process was progressively utilised to produce individual particles of two active ingredients which would allow the delivery of combination medicaments effectively and independently of dose variation. All physical characterisation revealed that the SAX-combined particles were co-processed into individual particles with the crystalline properties. Additionally, the *in-vitro* performance study strongly confirmed that all SAX combined formulations with high-dose ratio, stored in different conditions and periods of time had the higher FPF_{ED} than micronised formulations. However, for low dose ratio of the combination drugs, there was an inconsistent ratio between two combined drugs. This approach presents itself as a novel means to produce inhaled combination dosage forms for respiratory products.

7.4 Further Work

According to these data presented in the thesis, the SAX process shows significant promise for generating single and, also, combination particles for delivery to the lungs. In Chapter 4, budesonide was used as a model drug for particle engineering *via* the SAX system, these particles were found to confer some functionality that affected drug product performance. A future development of this approach would be to engineer SAX particles *in-situ* with excipient particles to enable the one-step production of DPI formulations. This approach may involve either atomisation of a solution that contained both drug and excipient, however, such approach may be hampered by incompatibilities of a universal solvent to solubilise both drug and excipient. However, further work in this area may result in the development of a continuous processing route, which may improve the quality and efficiency of DPI drug product manufacturing.

From Chapter 5 and 6, it can be seen that the particle engineering *via* the SAX process leads to an important opportunity to generate individual particulates of two active ingredients, which will allow the delivery of combination medicaments effectively and independently of dose variation. The high-dose combination particles produced from the SAX process were successfully co-processed into individual particles with the crystalline properties. As conditions such as COPD are multi-factorial, a further development of this approach may investigate the potential of the SAX process to generate particles with multiple actives in one particulate. It would be beneficial to design the work by adding another essential drug to generate triple drug particles in order to formulate the pulmonary dosage form to help prevent COPD and asthma patients for the long-term treatment.

References

Abbas,A., Srour,M., Tang,P., Chiouc,H., Chan,H.K., Romagnoli,J.A., 2007. Sonocrystallisation of sodium chloride particles for inhalation. Chemical Engineering Science, 62, 2445-2453.

Adi,H., Traini,D., Chan,H.K., Young,P.M., 2008. The influence of drug morphology on the aerosolisation efficiency of dry powder inhaler formulations. Journal of Pharmaceutical Sciences, 97, 2780-2788.

Adolfsson,A., Olsson,H., Nystrom,C., 1997. Effect of particle size and compaction load on interparticulate bonding structure for some pharmaceutical materials studied by compaction and strength characterisation in butanol. European Journal of Pharmaceutics and Biopharmaceutics, 44, 243-251.

Ambarkhane,A.V., Pincott,K., Buckton,G., 2005. The use of inverse gas chromatography and gravimetric vapour sorption to study transitions in amorphous lactose. International Journal of Pharmaceutics, 294, 129-135.

Andronis,V., Yoshioka,M., Zografi,G., 1997. Effects of sorbed water on the crystallization of indomethacin from the amorphous state. Journal of Pharmaceutical Sciences, 86, 346-351.

Ankerst,J., 2005. Combination inhalers containing inhaled corticosteroids and long-acting beta(2)-agonists: Improved clinical efficacy and dosing options in patients with asthma. Journal of Asthma, 42, 715-724.

Asgharian,B., Anjilvel,S., 1994. Inertial and Gravitational Deposition of Particles in A Square Cross-Section Bifurcating Airway. Aerosol Science and Technology, 20, 177-193.

Autumn,K., Sitti,M., Liang,Y.C.A., Peattie,A.M., Hansen,W.R., Sponberg,S., Kenny,T.W., Fearing,R., Israelachvili,J.N., Full,R.J., 2002. Evidence for van der Waals adhesion in gecko setae. Proceedings of the National Academy of Sciences of the United States of America, 99, 12252-12256.

Balashazy,I., Hofmann,W., 1993. Particle Deposition in Airway Bifurcations .1. Inspiratory Flow. Journal of Aerosol Science, 24, 745-772.

Baraniuk,J.N., Ali,M., Brody,D., Maniscalco,J., Gaumond,E., Fitzgerald,T., Wong,G., Yuta,A., Mak,J.C.W., Barnes,P.J., Bascom,R., Troost,T., 1997. Glucocorticoids induce beta(2)-adrenergic receptor function in human nasal mucosa. American Journal of Respiratory and Critical Care Medicine, 155, 704-710.

Barnes,P.J., Chung,K.F., Page,C.P., 1998. Inflammatory mediators of asthma: an update. Pharmacology Reviews, 50, 515-596.

Barnes,P.J., 2002. Scientific rationale for inhaled combination therapy with long-acting beta(2)-agonists and corticosteroids. European Respiratory Journal, 19, 182-191.

Barnes,P.J., Shapiro,S.D., Pauwels,R.A., 2003. Chronic obstructive pulmonary disease: molecular and cellular mechanisms. European Respiratory Journal, 22, 672-688.

Barnes,P.J., 2004. Mediators of chronic obstructive pulmonary disease. Pharmacology Reviews, 56, 515-548.

Barnes,P.J., 2007. Chronic obstructive pulmonary disease: A growing but neglected global epidemic. Plos Medicine, 4, 779-780.

Barnes,P.J., 2008. Immunology of asthma and chronic obstructive pulmonary disease. Nature Reviews Immunology, 8, 183-192.

Bascom,R., Bromberg,P.A., Costa,D.A., Devlin,R., Dockery,D.W., Frampton,M.W., Lambert,W., Samet,J.M., Speizer,F.E., Utell,M., 1996. Health effects of outdoor air pollution. American Journal of Respiratory and Critical Care Medicine, 153, 3-50.

Bateman,E.D., Britton,M., Carrillo,J., Almeida,J., Wixon,C., 1998. Salmeterol/fluticasone combination inhaler - A new, effective and well tolerated treatment for asthma. Clinical Drug Investigation, 16, 193-201.

Beach,S., Latham,D., Sidgwick,C., Hanna,M., York,P., 1999. Control of the physical form of salmeterol xinafoate. Organic Process Research & Development, 3, 370-376.

Begat,P., Morton,D.A.V., Staniforth,J.N., Price,R., 2004. The cohesive-adhesive balances in dry powder inhaler formulations I: Direct quantification by atomic force microscopy. Pharmaceutical Research, 21, 1591-1597.

Begat,P., Young,P.M., Edge,S., Kaerger,J.S., Price,R., 2003. The effect of mechanical processing on surface stability of pharmaceutical powders: Visualization by atomic force microscopy. Journal of Pharmaceutical Sciences, 92, 611-620.

Bell,J.H., Hartley,P.S., Cox,J.S.G., 1971. Dry Powder Aerosols .1. New Powder Inhalation Device. Journal of Pharmaceutical Sciences, 60, 1559-1564.

Berkeley,T.E., 1912. Solubility and supersolubility from the osmotic standpoint. Philosophical Magazine, 24, 254-268.

Bergmann,K.C., Lindemann,L., Braun,R., Steinkamp,G., 2004. Salmeterol/fluticasone propionate (50/250 mcg) combination is superior to double dose fluticasone (500 mcg) for the treatment of symptomatic moderate asthma. Swiss Medical Weekly, 134, 50-58.

Berry,J., Kline,L.C., Hart,J.L., Sequeira,J., 2003. Influence of the storage orientation on the aerodynamic particle size of a suspension metered dose inhaler containing propellant HFA-227. Drug Development and Industrial Pharmacy, 29, 631-639.

Biddiscombe,M.F., Melchor,R., Mak,V.H., Marriot,R.J., 1987. Lung deposition of salbutamol directly labeled with technetium-99m, delivered by pMDI and DPI. International Journal of Pharmaceutics, 91, 111-121.

Bisgaard,H., Le Roux,P., Bjamer,D., Dymek,A., Vermeulen,J.H., Hultquist,C., 2006. Budesonide/formoterol maintenance plus reliever therapy - A new strategy in pediatric asthma. Chest, 130, 1733-1743.

Bosquillon,C., Lombry,C., Preat,V., Vanbever,R., 2001. Comparison of particle sizing techniques in the case of inhalation dry powders. Journal of Pharmaceutical Sciences, 90, 2032-2041.

Bosquillon,C., Rouxhet,P.G., Ahimou,F., Simon,D., Culot,C., Preat,V., Vanbever,R., 2004. Aerosolization properties, surface composition and physical state of spray-dried protein powders. Journal of Controlled Release, 99, 357-367.

Botsaris,G.D., 1976. Secondary nucleation: A review. In: Mullins,J.W. (Ed.), Plenum Press, New York, USA.

Boucher,R.C., 1994. State of Art: Human airway ion transport. American Journal of Respiartory Care Medicine, 150, 271-593.

Bousquet,J., Dahk,R., Khalteev,N., 2007. Global alliance against chronic respiratory diseases. Allergy, 62, 216-223.

Braithwaite, P and Williams, S. Inhaler. Innovata Biomed Ltd. [US6,845,772 B], 1-8. 25-12-2005.

Brittain,H.G., Bogdanowich,S.J., Bugay,D.E., Devincentis,J., Lewen,G., Newman,A.W., 1991. Physical characterisation of pharmaceutical solids. Pharmaceutical Research, 8, 963-973.

Brittain,H.G., 1997. Spectral methods for the characterization of polymorphs and solvates. Journal of Pharmaceutical Sciences, 86, 405-412.

Brittain,H.G., Bogdanowich,S.J., Bugay,D.E., Devincentis,J., Lewen,G., Newman,A.W., 1991. Physical characterisation of pharmaceutical solids. Pharmaceutical Research, 8, 963-973.

Broadhead,J., Rouan,S.K.E., Rhodes,C.T., 1992. The spray drying of pharmaceuticals. Drug Development and Industrial Pharmacy, 18, 1169-1206.

Buckton,G., Darcy,P., 1996. Water mobility in amorphous lactose below and close to the glass transition temperature. International Journal of Pharmaceutics, 136, 141-146.

Buckton,G., 1997. Characterisation of small changes in the physical properties of powders of significance for dry powder inhaler formulations. Advanced Drug Delivery Reviews, 26, 17-27.

Buckton,G., Darcey,P., 1999. Assessment of disorder in crystalline powders - a review of analytical techniques and their application. International Journal of Pharmaceutics, 179, 141-158.

Burton,W.K., Cabrera,N., 1951. The growth of crystals and the equilibrium structure of their surfaces. Philiosphical Translations A, 299, 299-320.

Byron,P.R., Patton,J.S., 1994. Drug-delivery via the respiratory-tract. Journal of Aerosol Medicine-Deposition Clearance and Effects in the Lung, 7, 49-75.

Byron,P.R., Peart,J., Staniforth,J.N., 1997. Aerosol electrostatics .1. Properties of fine powders before and after aerosolization by dry powder inhalers. Pharmaceutical Research, 14, 698-705.

Calverley,P., Pauwels,R., Vestbo,J., Jones,P., Pride,N., Gulsvik,A., Anderson,J., Maden,C., Tristan,S.G., 2003. Combined salmeterol and fluticasone in the treatment of chronic obstructive pulmonary disease: a randomised controlled trial. Lancet, 361, 449-456.

Calverley,P.M.A., Anderson,J.A., Celli,B., Ferguson,G.T., Jenkins,C., Jones,P.W., Yates,J.C., Vestbo,J., Calverley,P.M.A., Anderson,J.A., Celli,B., Ferguson,G.T., Jenkins,C., Jones,P.W., Knobil,K., Yates,J.C., Vestbo,J., Cherniack,R., Similowski,T., Cleland,J., Whitehead,A., Wise,R., McGarvey,L., John,M., 2007. Salmeterol and fluticasone propionate and survival in chronic obstructive pulmonary disease. New England Journal of Medicine, 356, 775-789.

Campbell,L.M., Szafranski,W., 2002. Budesonide/formoterol in a single inhaler (Symbicort((R))) reduces severe exacerbations in patients with moderate to severe COPD. Thorax, 57.

Castellanos,A., 2005. The relationship between attractive interparticle forces and bulk behaviour in dry and uncharged fine powders. Advances in Physics, 54, 263-376.

Cazzola,M., Ando,F., Santus,P., Ruggeri,P., Di Marco,F., Sanduzzi,A., D'Amato,M., 2007. A pilot study to assess the effects of combining fluticasone propionate/salmeterol and tiotropium on the airflow obstruction of patients with severe-to-very severe COPD. Pulmonary Pharmacology & Therapeutics, 20, 556-561.

Cazzola,M., Testi,R., Matera,M.G., 2002. Clinical pharmacokinetics of salmeterol. Clinical Pharmacokinetics, 41, 19-30.

Chawla,A., Taylor,K.M.G., Newton,J.M., Johnson,M.C.R., 1994. Production of spray-dried salbutamol sulfate for use in dry powder aerosol formulation. International Journal of Pharmaceutics, 108, 233-240.

Chew,N.Y.K., Chan,H.K., 2001. Use of solid corrugated particles to enhance powder aerosol performance. Pharmaceutical Research, 18, 1570-1577.

Chiou,H., Li,L., Hu,T.T., Chan,H.K., Chen,J.F., Yun,J., 2007. Production of salbutamol sulfate for inhalation by high-gravity controlled antisolvent precipitation. International Journal of Pharmaceutics, 331, 93-98.

Clark,A.R., Egan,M., 1994. Modeling the Deposition of Inhaled Powdered Drug Aerosols. Journal of Aerosol Science, 25, 175-186.

Clarke,A.R., 1995. Medical Aerosol Inhalers: Past, Present and Future. Aerosol Science and Technology, 23, 374-391.

Cline,D., Dalby,R., 2002. Predicting the quality of powders for inhalation from surface energy and area. Pharmaceutical Research, 19, 1274-1277.

Coulomb,A., 1785. Memoires de l'Acaďmie Royale des Sciences, 4, 569.

Crowder,T.M., Hickey,A., 2006. Powder specific active dispersion for generation of pharmaceutical aerosols. International Journal of Pharmaceutics, 327, 65-72.

Crowder,T.M., Rosati,J.A., Schroeter,J.D., Hickey,A.J., Martonen,T.B., 2002. Fundamental effects of particle morphology on lung delivery: Predictions of Stokes' law and the particular relevance to dry powder inhaler formulation and development. Pharmaceutical Research, 19, 239-245.

Dalby,R., Spallek,M., Voshaar,T., 2004. A review of the development of Respimat(R) Soft Mist(TM) Inhaler. International Journal of Pharmaceutics, 283, 1-9.

Dalby,R., Suman,J., 2003. Inhalation therapy: technological milestones in asthma treatment. Advanced Drug Delivery Reviews, 55, 779-791.

Danesh,A., Chen,X., 2000. Polymorphic discrimination using atomic force microscopy: Distinguishing between two polymorphs of the drug cimetidine. Langmuir, 16, 866-870.

Davey,R., Garside,J., 2000. From molecules to crystallizers. Oxford University Press, Oxford, UK.

Davis, B. The winner's cirlce. Pharmaceutical Technology Europe 20[9], 86-92. 2008.

de Boer,A.H., Gjaltema,D., Hagedoorn,P., Schaller,M., Witt,W., Frijlink,H.W., 2002. Design and application of a new modular adapter for laser diffraction characterization of inhalation aerosols. International Journal of Pharmaceutics, 249, 233-245.

de Boer,A.H., Hagedoorn,P., Frijlink,H.W., 2003. The choice of a compressor for the aerosolisation of tobramyicn (TOBI**)** with the PARI LC PLUS resusable nebuliser. International Journal of Pharmaceutics, 268, 59-69.

Dean,T.P., Dai,Y., Shute,J.K., Church,M.K., Warner,J.O., 1993. Interleukin-8 Concentrations Are Elevated in Bronchoalveolar Lavage, Sputum, and Sera of Children with Cystic-Fibrosis. Pediatric Research, 34, 159-161.

Deryaguin,B.V., Krotova,N.A., Smilga,V.P., 1978. Adhesion of Solids. Consultants Bureau, New York.

Dransfield,M.T., Bailey,W.C., 2004. Fluticasone propionate/salmeterol for the treatment of chronic-obstructive pulmonary disease. Expert Opinion on Pharmacotherapy, 5, 1815-1826.

Duddu,S.P., Sisk,S.A., Walter,Y.H., Tarara,T.E., Trimble,K.R., Clark,A.R., Eldon,M.A., Elton,R.C., Pickford,M., Hirst,P.H., Newman,S.P., Weers,J.G., 2002. Improved lung delivery from a passive dry powder inhaler using an engineered PulmoSphere (R) powder. Pharmaceutical Research, 19, 689-695.

Dunbar,C.A., Morgan,B., Van Oort,M., Hickey,A.J., 2000. A comparison of dry powder inhaler dose delivery characteristics using a power criterion. Journal of Pharmaceutical Science and Technology, 54, 478-484.

Duncanhewitt,W.C., Grant,D.J.W., 1986. True density and thermal expansivity of pharmaceutical Solids - Comparison of methods and assessment of crystallinity. International Journal of Pharmaceutics, 28, 75-84.

Eckert,C.A., Knutson,B.L., Debenedetti,P.G., 1996. Supercritical fluids as solvents for chemical and materials processing. Nature, 383, 313-318.

Edge,S., Kibbe,A., Kussendrager,K.D., 2005. Lactose Monohydrate. In: Rowe,R.C., Sheskey,P.J., Owen,S.C. (Eds.), Pharmaceutical Press, London, 389-395.

Edge,S., Muller,S., Price,R., Shur,J., 2008. Factors affecting defining the quality and functionality of excipients used in the manufacture of of dry powder inhaler products. Drug Development and Industrial Pharmacy, 34, 966-973.

Edwards,D.A., Hanes,J., Caponetti,G., Hrkach,J., BenJebria,A., Eskew,M.L., Mintzes,J., Deaver,D., Lotan,N., Langer,R., 1997. Large porous particles for pulmonary drug delivery. Science, 276, 1868-1871.

El-Sabawi,D., Price,R., Edge,S., Young,P.M., 2006. Novel temperature controlled surface dissolution of excipient particles for carrier based dry powder inhaler formulations. Drug Development and Industrial Pharmacy, 32, 243-251.

Feeley,J.C., York,P., Sumby,B., Dicks,H., 1998. Determination of surface properties and flow characterisation of salbutamol sulphate, before and after micronisation. International Journal of Pharmaceutics, 172, 89-96.

Fields, M. R. Inhaler. [2,581,182], 1-5. 1950. United States of America.

Frank,F.C., 1949. The influence of dislocations on crystal growth. Discussions of the Faraday Society, 5, 48-54.

Fuller,K.N.G., Tabor,D., 1975. Effect of Surface-Roughness on Adhesion of Elastic Solids. Proceedings of the Royal Society of London Series A-Mathematical Physical and Engineering Sciences, 345, 327-342.

Ganderton,D., 1992. The generation of respirable cloud from coarse powder aggregates. Journal of Biopharmaceutical Science, 3, 101-105.

Garcia-Contreras,L., Hickey,A.J., 2003. Aerosol treatment of cystic fibrosis. Critical Reviews in Therapeutic Drug Carrier Systems, 20, 317-356.

Greening,A.P., Ind,P.W., Northfield,M., Shaw,G., 1994. Added Salmeterol Versus Higher-Dose Corticosteroid in Asthma Patients with Symptoms on Existing Inhaled Corticosteroid. Lancet, 344, 219-224.

Guchardi,R., Frei,M., John,E., Kaerger,J.S., 2008. Influence of fine lactose and magnesium stearate on low dose dry powder inhaler formulations. International Journal of Pharmaceutics, 348, 10-17.

Gurney,J.W., 1991. Cross-Sectional Physiology of the Lung. Radiology, 178, 1-10.

Halbert,R., Natoli,J.L., Gano,A., Badamgarav,E., Buist,A.S., Mannino,D.M., 2006. Global burden of COPD: systematic review and meta-analysis. European Respiratory Journal, 28, 523-532.

Hamaker,H.C., 1937. London-van der Waals forces attraction between spherical particles. Physica (Utrecht), 4, 1058-1072.

Hancock,B.C., Shamblin,S.L., Zografi,G., 1995. Molecular mobility of amorphous pharmaceutical solids below their glass-transition temperatures. Pharmaceutical Research, 12, 799-806.

Hancock,B.C., Zografi,G., 1994. The relationship between the glass-transition temperature and the water-content of amorphous pharmaceutical Solids. Pharmaceutical Research, 11, 471-477.

Hannemann,L.A., 1999. What is new in asthma: New dry powder inhalers. Pediatric Health Care, 13, 159-165.

Harris,D., 2007. Testing Inhalers. Pharmaceutical Technology Europe, 11, 11.

Hartman,P., Perdok,W.G., 1955. On the relations between structure and morphology of crystals. Acta Crystallographica, 8, 49-52.

Helgesson, P., Jennings, D., and Nelson, C. Inhalation devices. [6,892,728 B2], 1-38. 2005.

Hem,S.L., 1967. The effect of ultrasonic vibrations on crystallization processes. Ultrasonics, 5, 202-207.

Hersey,J.A., 1975. Ordered mixing: a new concept in powder mixing practise. Powder Technology, 11, 41-44.

Heyder,J., Gebhart,J., Rudolf,G., Schiller,C.F., Stahlhofen,W., 1986. Depoistion of particles in the human respiratory tract in the size range 0.005-15mM. Journal of Aerosol Science, 17, 811-825.

Hickey,A.J., Dunbar,C.A., 1997. A new millenium for inhaler technology. Pharmaceutical Technology, 21, 116-125.

Hickey,A.J., Mansour,H.M., Telko,M.J., Xu,Z., Smyth,H.D.C., Mulder,T., McLean,R., Langridge,J., Papadopoulos,D., 2007. Physical characterization of component particles included in dry powder inhalers. I. Strategy review and static characteristics. Journal of Pharmaceutical Sciences, 96, 1282-1301.

Hiestand,E.N., 1966. Powders: Particle-particle interactions. Journal of Pharmaceutical Sciences, 55, 1325-1344.

Hofmann,W., Sturm,R., Winkler-Heil,R., Pawlak,E., 2003. Stochastic model of ultrafine particle deposition and clearance in the human respiratory tract. Radiation Protection Dosimetry, 105, 77-80.

Holgate,S.T., 2008. Pathogenesis of asthma. Clinical and Experimental Allergy, 38, 872-897.

Holgate,S.T., 2007. Epithelium dysfunction in asthma. Journal of Allergy and Clinical Immunology, 120, 1233-1246.

Holgate,S.T., Davies,D.E., Powell,R.M., Howarth,P.H., Haitchi,H.M., Holloway,J., 2007. Local genetic and environmental factors in asthma disease pathogenesis: chronicity and persistence mechanisms. European Respiratory Journal, 29, 793-803.

Holgate,S.T., Polosao,R., 2008. Treatment strategies for allergy and asthma. Nature Reviews Immunology, 8, 218-230.

Jayasing,S.S., Pilpel,N., Harwood,C.F., 1970. Effect of Temperature and Compression on Cohesive Properties of Particulate Solids. Materials Science and Engineering, 5, 287.

Jeffery,P.K., 1997. Airway mucose: Secretory cells, mucus and mucin genes. European Respiratory Journal, 10, 1655-1662.

Johnson,K.L., 1998. Mechanics of adhesion. Tribology International, 31, 413-418.

Johnson,K.L., 1996. Continuum mechanics modeling of adhesion and friction. Langmuir, 12, 4510-4513.

Johnson,K.L., Kendall,K., Roberts,A.D., 1971. Surface energy and the contact of elastic solids. Proceedings of the Royal Society of London. Series A, Mathematical and Physical Sciences, 324, 301-313.

Johnson,M., 2002. Combination therapy for asthma: Complementary effects of long-acting B2-agonists and corticosteroids. Current Opinion in Allergy and Clinical Immunology, 15, 16-22.

Jones,M.D., Harris,H., Hooton,J.C., Shur,J., King,G.S., Mathoulin,C.A., Nichol,K., Smith,T.L., Dawson,M.L., Ferrie,A.R., Price,R., 2008. An investigation into the relationship between carrier-based dry powder inhalation performance and formulation cohesive-adhesive force balances. European Journal of Pharmaceutics and Biopharmaceutics, 69, 496-507.

Jones,M.D., Young,P.M., Traini,D., Shur,J., Edge,S., Price,R., 2008. The use of atomic force microscopy to study the conditioning of micronised budesonide. International Journal of Pharmaceutics, 357, 314-317.

Jung,J., Perrut,M., 2001. Particle design using supercritical fluids: Literature and patent survey. Journal of Supercritical Fluids, 20, 179-219.

Kaerger,J.S., Price,R., 2004. Processing of spherical crystalline particles via a novel solution atomization and crystallization by sonication (SAXS) technique. Pharmaceutical Research, 21, 372-381.

Kajimoto,O., 1999. Solvation in supercritical fluids: Its effects on energy transfer and chemical reactions. Chemical Reviews, 99, 355-389.

Kawashima,Y., Serigano,T., Hino,T., Yamamoto,H., Takeuchi,H., 1998. Design of inhalation dry powder of pranlukast hydrate to improve dispersibility by the surface modification with light anhydrous silicic acid (AEROSIL 200). International Journal of Pharmaceutics, 173, 243-251.

Keating,G.M., McCormack,P.L., 2007. Salmeterol/fluticasone propionate: A review of its use in the treatment of chronic obstructive pulmonary disease. Drugs, 67, 2383-2406.

Knowles,M.R., Boucher,R.C., 2002. Mucus clearance as a primary innate defense mechanism for mammalian airways. Journal of Clinical Investigation, 109, 571-577.

Krekel,J., Polke,R., 1992. Quality assurance in process-development. Chemie-Ingenieur Technik, 64, 528-535.

Krishnan,S., Busnaina,A.A., Rimai,D.S., Demejo,L.P., 1994. The Adhesion-Induced Deformation and the Removal of Submicrometer Particles. Journal of Adhesion Science and Technology, 8, 1357-1370.

Krupp,H., 1967. Particle adhesion theory and experiment. Advanced Colloid Interface, 1, 111-239.

Krycer,I., Hersey,J.A., 1981. Detection of mechanical activation during the milling of lactose monohydrate. International Journal of Pharmaceutical Technical Product Manufacturing, 2, 55-56.

Kunkel,S.L., Standiford,T., Kasahara,K., Strieter,R.M., 1991. Interleukin-8 (Il-8) - the Major Neutrophil Chemotactic Factor in the Lung. Experimental Lung Research, 17, 17-23.

Lalor,C.B., Hickey,A.J., 1996. Pharmaceutical aerosols for delivery of drugs to the lungs. In: Collbeck,I. (Ed.), Blackie Academic & Professionals, London.

Laudise,R.A., 1970. The growth of single crystals. 2nd Ed., Prentice-Hall, Englewood Cliffs, USA.

Leuenberger,H., Plitzko,M., Puchkov,M., 2006. Spray freeze drying in a fluidized bed at normal and low pressure. Drying Technology, 24, 711-719.

Li,H.Y., Neill,H., Innocent,R., Seville,P., Williamson,I., Birchall,J.C., 2003. Enhanced dispersibility and deposition of spray-dried powders for pulmonary gene therapy. Journal of Drug Targeting, 11, 425-432.

Li,H.Y., Seville,P.C., Williamson,I.J., Birchall,J.C., 2005. The use of amino acids to enhance the aerosolisation of spray-dried powders for pulmonary gene therapy. Journal of Gene Medicine, 7, 343-353.

Lifshitz,E.M., 1955. Journal of Experimental Theoretical Physics, 29, 94.

Lippmann,M., Yeates,D.B., Albert,R.E., 1980. Deposition, Retention, and Clearance of Inhaled Particles. British Journal of Industrial Medicine, 37, 337-362.

Lopez,A.D., Mathers,C., 2006. Measuring the global burden of disease and epidemiological transitions: 2002-2030. Annals of Tropical Medicine and Parasitology, 100, 481-499.

Lorimer,J.P., Mason,T.J., 1987. Sonochemistry Part 1-The Physical Aspects. Chemical Society Reviews, 16, 239-274.

Louey,M.D., Van Oort,M., Hickey,A.J., 2006. Standardised entrainment tubes for the evaluation of pharmaceutical dry powder dispersion. Journal of Aerosol Science, 37, 1520-1531.

Maa,Y.F., Nguyen,P.A., Sweeney,T., Shire,S.J., Hsu,C.C., 1999. Protein inhalation powders: Spray drying vs spray freeze drying. Pharmaceutical Research, 16, 249-254.

Malcolmson,R.J., Embleton,J.K., 1998. Dry powder formulations for pulmonary delivery. Pharmaceutical Science Technology Today, 1, 394-398.

Mannino,D.M., Buist,A.S., 2007. Global burden of COPD: risk factors, prevalence, and future trends. Lancet, 370, 765-773.

Marple,V.A., Roberts,D.L., Romay,F.J., Miller,N.C., Truman,K.G., Holroyd,M.J., Mitchell,J.P., Hochrainer,D., 2003. Next generation pharmaceutical impactor (A new impactor for pharmaceutical inhaler testing). Part I: Design. Journal of Aerosol Medicine-Deposition Clearance and Effects in the Lung, 16, 283-299.

Martonen,T.B., Katz,I., 1993. Deposition Patterns of Polydisperse Aerosols Within Human Lungs. Journal of Aerosol Medicine-Deposition Clearance and Effects in the Lung, 6, 251-274.

Martonen,T.B., Katz,I., Fults,K., Hickey,A.J., 1992. Use of Analytically Defined Estimates of Aerosol Respirable Fraction to Predict Lung Deposition Patterns. Pharmaceutical Research, 9, 1634-1639.

Masoli,M., Fabian,D., Holt,S., Beasley,R., 2004. The global burden of asthma: executive summary of the GINA dissemination committee report. Allergy, 59, 496-478.

Masters,K., 1985. Spray Drying Handbook. 4th Edition Ed., Longman Scientific & Technical, New York.

Matz,J., Emmett,A., Rickard,K., Kalberg,C., 2001. Addition of salmeterol to low-dose fluticasone versus higher-dose fluticasone: An analysis of asthma exacerbations. Journal of Allergy and Clinical Immunology, 107, 783-789.

McDonald,K.J., Martin,G.P., 2000. Transition to CFC-free metered dose inhalers - into the new millennium. International Journal of Pharmaceutics, 201, 89-107.

McFarlane,J.S., Tabor,D., 1950. Adhesion of solids and the effect of surface films. Proceedings of the Royal Society of London. Series A, Mathematical and Physical Sciences, 202, 224-243.

Mcmurry,P.H., Rader,D.J., 1985. Aerosol Wall Losses in Electrically Charged Chambers. Aerosol Science and Technology, 4, 249-268.

Michael,Y., Snowden,M.J., Chowdhry,B.Z., Ashurst,I.C., vies-Cutting,C.J., Riley,T., 2001. Characterisation of the aggregation behaviour in a salmeterol and fluticasone propionate inhalation aerosol system. International Journal of Pharmaceutics, 221, 165-174.

Mie,G., 1908. Contributions to the optics of diffuse media. Annals of Physics, 25, 377-445.

Miller-Larsson,A., Selroos,O., 2006. Advances in asthma and COPD treatment: Combination therapy with inhaled corticosteroids and long-acting beta(2)-agonists. Current Pharmaceutical Design, 12, 3261-3279.

Morrison,F.A., 1974. Inertial impaction in stagnation flow. Journal of Aerosol Science, 5, 241-250.

Mullins,J.W., 1992. Crystallization. 4th Ed., Butterworth-Heinemann, Oxford, UK.

Mumenthaler,M., Leuenberger,H., 1991. Atmospheric Spray-Freeze Drying - A Suitable Alternative in Freeze-Drying Technology. International Journal of Pharmaceutics, 72, 97-110.

Myerson,A.S., 2002. Handbook of industrial crystallization. Butterworth-Heinemann, Woburn, MA, USA.

Nelson,H.S., 2005. Combination therapy of long-acting beta agonists and inhaled corticosteroids in the management of chronic asthma. Current Allergy and Asthma Reports, 5, 123-129.

Nelson,H.S., Chapman,K.R., Pyke,S.D., Johnson,M., Pritchard,J.N., 2003. Enhanced synergy between fluticasone propionate and salmeterol inhaled from a single inhaler versus separate inhalers. Journal of Allergy and Clinical Immunology, 112, 29-36.

Newman,S.P., Busse,W.W., 2002. Evolution of dry powder inhaler design, formulation, and performance. Respiratory Medicine, 96, 293-304.

Newman,S.P., Moren,F., Trofast,E., Talaee,N., Clarke,S.W., 1991. Terabutaline sulphate Turbuhaler: effect of inhaled flow rate on drug deposition and efficacy. International Journal of Pharmaceutics, 74, 209-213.

Nickerson,T.A., 1974. Fundamentals of diary chemistry. 2nd Ed., Avi Publishing Co.Inc, Westport, USA.

Nowak,N., Kakade,P.P., Annapragada,A.V., 2003. Computational fluid dynamics simulation of airflow and aerosol deposition in human lungs. Annals of Biomedical Engineering, 31, 374-390.

O'Byrne,P.M., Bisgaard,H., Godard,P.P., Pistolesi,M., Palmqvist,M., Zhu,Y.J., Ekstrom,T., Bateman,E.D., 2005. Budesonide/formoterol combination therapy as both maintenance and reliever medication in asthma. American Journal of Respiratory and Critical Care Medicine, 171, 129-136.

Onsager,L., Samaras,N.T., 1934. The surface tension of Debye-Huckel electrolytes. The Journal of Chemical Physics, 2, 528-536.

Palakodaty,S., York,P., Pritchard,J., 1998. Supercritical fluid processing of materials from aqueous solutions: The application of SEDS to lactose as a model substance. Pharmaceutical Research, 15, 1835-1843.

Park,S.H., Lee,K.W., 2000. Lognormal size distribution theory for deposition of polydisperse aerosol particles. Nuclear Science and Engineering, 135, 288-295.

Pasquali,I., Bettini,R., Giordano,F., 2006. Solid-state chemistry and particle engineering with supercritical fluids in pharmaceutics. European Journal of Pharmaceutical Sciences, 27, 299-310.

Patton,J.S., 1996. Mechanisms of macromolecule absorption by the lungs. Advanced Drug Delivery Reviews, 19, 3-36.

Pauwels,R., Newman,S., Borgstrom,L., 1997. Airway deposition and airway effects of antiasthma drugs delivered from metered-dose inhalers. European Respiratory Journal, 10, 2127-2138.

Pauwels,R.A., Buist,A.S., Calverley,P.M., Jenkins,C.R., Hurd,S.S., 2001. Global strategy for the diagnosis, management, and prevention of chronic obstructive pulmonary disease. NHLBI/WHO Global Initiative for Chronic Obstructive Pulmonary Lung Disease (GOLD) Workshop summary. American Journal of Respiartory Care Medicine, 163, 1256-1276.

Pauwels,R.A., Sears,M.R., Campbell,M., Villasante,C., Huang,S., Lindh,A., Petermann,W., Aubier,M., Schwabe,G., Bengtsson,T., 2003. Formoterol as relief medication in asthma: a worldwide safety and effectiveness trial. European Respiratory Journal, 22, 787-794.

Pauwels,R.A., Rabe,K.F., 2004. Burden and clinical features of chronic obstructive pulmonary disease (COPD). Lancet, 364, 613-620.

Pearce,N., it-Khaled,N., Beasley,R., Mallol,J., Keil,U., Mitchell,E., Robertson,C., 2007. Worldwide trends in the prevalence of asthma symptoms: phase III of the International Study of Asthma and Allergies in Childhood (ISAAC). Thorax, 62, 757-765.

Peukert,W., 2005. General concepts in nanoparticle technology and their possible implication on cultural science and philosophy. Powder Technology, 158, 133-140.

Pfeiffer-Brodka,K., Langguth,P., Graf,P., Haeusler,H., 2003. Influence of mechanical activation on the physical stability of salbutamol sulphate. European Journal of Pharmaceutics and Biopharmaceutics, 56, 393-400.

Price,R., Young,P.M., Edge,S., Staniforth,J.N., 2002. The influence of relative humidity on particulate interactions in carrier-based dry powder inhaler formulations. International Journal of Pharmaceutics, 246, 47-59.

Price,R., Young,P.M., 2005. On the physical transformations of processed pharmaceutical solids. Micron, 36, 519-524.

Price,R., Edge,S., 2007. Developments in particle engineering processes for pharmaceutical drug delivery systems. Pharmaceutical Technology Europe, 19, 33-36.

Rumpf,H., 1967. Uber die eigenschaften von nutzstauben. Staub Reinhalt. Luft, 27, 3-13.

Prime,D., Atkins,P.J., Slater,A., Sumby,B., 1997. Review of dry powder inhalers. Advanced Drug Delivery Reviews, 26, 51-58.

Rasenack,N., Steckel,H., Muller,B.W., 2004. Preparation of microcrystals by in situ micronization. Powder Technology, 143-144, 291-296.

Richards,J., Hirst,P., Pitcairn,G., Mahashabde,S., Abramowitz,W., Nolting,A., Newman,S.P., 2001. Deposition and pharmacokinetics of flunisolide delivered from pressurized inhalers containing non-CFC and CFC propellants. Journal of Aerosol Medicine-Deposition Clearance and Effects in the Lung, 14, 197-208.

Rogers,T.L., Nelsen,A.C., Sarkari,M., Young,T.J., Johnston,K.P., Williams,R.O., 2003. Enhanced aqueous dissolution of a poorly water soluble drug by novel particle engineering technology: Spray-freezing into liquid with atmospheric freeze-drying. Pharmaceutical Research, 20, 485-493.

Ruecroft,G., Hipkiss,D., Ly,T., Maxted,N., Cains,P.W., 2005. Sonocrystallization: The use of ultrasound for improved industrial crystallization. Organic Process Research & Development, 9, 923-932.

Ruecroft,G., 2007. Power ultrasound and particle engineering - Crystals for drug delivery and formulation. Chimica Oggi-Chemistry Today, 25, 12-14.

Salekigerhardt,A., Ahlneck,C., Zografi,G., 1994. Assessment of disorder in crystalline solids. International Journal of Pharmaceutics, 101, 237-247.

Savage,P.E., Gopalan,S., Mizan,T.I., Martino,C.J., Brock,E.E., 1995. Reactions at Supercritical Conditions - Applications and Fundamentals. Aiche Journal, 41, 1723-1778.

Seville,P.C., Kellaway,I.W., Birchall,J.C., 2002. Preparation of dry powder dispersions for non-viral gene detivery by freeze-drying and spray-drying. Journal of Gene Medicine, 4, 428-437.

Shekunov,B.Y., York,P., 2000. Crystallization processes in pharmaceutical technology and drug delivery design. Journal of Crystal Growth, 211, 122-136.

Shekunov,B.Y., Feeley,J.C., Chow,A.H.L., Tong,H.H.Y., York,P., 2003. Aerosolisation behaviour of micronised and supercritically-processed powders. Journal of Aerosol Science, 34, 553-568.

Shekunov,B.Y., Chattopadhyay,P., Tong,H.H.Y., Chow,A.H.L., 2007. Particle size analysis in pharmaceutics: Principles, methods and applications. Pharmaceutical Research, 24, 203-227.

Shur,J., Harris,H., Jones,M.D., Kaerger,J.S., Price,R., 2008. The role of fines in the modification of the fluidization and dispersion mechanism within dry powder inhaler formulations. Pharmaceutical Research, 25, 1931-1940.

Shur,J., Nevell,T.G., Shute,J.K., Smith,J.R., 2008. The spray drying of unfractionated heparin: Optimization of the operating parameters. Drug Development and Industrial Pharmacy, 34, 559-568.

Shute,J.K., Vrugt,B., Lindley,I.J.D., Holgate,S.T., Bron,A., Aalbers,R., Djukanovic,R., 1997. Free and complexed interleukin-8 in blood and bronchial mucosa in asthma. American Journal of Respiratory and Critical Care Medicine, 155, 1877-1883.

Sievers,R.E., Milewski,P.D., Sellers,S.P., Miles,B.A., Korte,B.J., Kusek,K.D., Clark,G.S., Mioskowski,B., Villa,J.A., 2000. Supercritical and near-critical carbon dioxide assisted low-temperature bubble drying. Industrial & Engineering Chemistry Research, 39, 4831-4836.

Sin,D.D., Man,S.F.P., 2007. Do chronic inhaled steroids alone or in combination with a bronchodilator prolong life in chronic obstructive pulmonary disease patients? Current Opinion in Pulmonary Medicine, 13, 90-97.

Smith,I.J., Parry-Billings,M., 2003. The inhalers of the future? A review of dry powder devices on the market today. Pulm. Pharmacol. Ther., 16, 79-95.

Smyth,H., Hickey,A.J., Brace,G., Barbour,T., Gallion,J., Grove,J., 2006. Spray pattern analysis for metered dose inhalers I: Orifice size, particle size, and droplet motion correlations. Drug Development and Industrial Pharmacy, 32, 1033-1041.

Sobolev,V.V., 1989. The effect of cavitation on crystallization of metal in the process of ultrasonic treatment of a melt. Russian Metallagy, 5, 45-52.

Staniforth,J.N., Rees,J.E., 1982. Electrostatic charge interactions in ordered powder mixes. Journal of Pharmacy and Pharmaceutical Sciences, 34, 69-76.

Steckel,H., Rasenack,N., Muller,B.W., 2003. In-situ micronization of disodium cromoglycate for pulmonary delivery. European Journal of Pharmaceutics, 55, 173-180.

Steckel,H., Pichert,L., Muller,B.W., 2004. Influence of process parameters in the ASES process on particle properties of budesonide for pulmonary delivery. European Journal of Pharmaceutics and Biopharmaceutics, 57, 507-512.

Stempel,D.A., Stoloff,S.W., Rosenzweig,J.R.C., Stanford,R.H., Ryskina,K.L., Legorreta,A.P., 2005. Adherence to asthma controller medication regimens. Respiratory Medicine, 99, 1263-1267.

Stokes,G.G., 1908. Mathematical and physical papers. Astrophysical Journal, 23, 173.

Strickland-Constable,R.F., 1968. Kinetics and mechanisms of crystallization. 2nd Ed., Academic Press, New York, USA.

Suryabarayanan,R., 1995. X-ray powder diffractometry. In: Brittain,H.G. (Ed.), Marcel Dekker, New York, 187-221.

Tabor,D., 1976. Surface forces and surface interactions. Journal of Colloid and Interface Science, 58, 1-13.

Taki,M., Zeng,X.M., Oliver,M., Marriott,C., Martin,G.P., 2006. A comparison of the in-vitro deposition profiles of drugs from a combination dry powder inhaler (DIPI) using the Next Generation Impactor (NGI). Journal of Pharmacy and Pharmacology, 58, A65.

Taulbee,D.B., Yu,C.P., 1975. Theory of Aerosol Deposition in Human Respiratory-Tract. Journal of Applied Physiology, 38, 77-85.

Telko,M., Hickey,A.J., 2005. Dry powder inhaler formulations. Respiratory Care, 50, 1209-1227.

Theophilus,A., Moore,A., Prime,D., Rossomanno,S., Whitcher,B., Chrystyn,H., 2006. Co-deposition of salmeterol and fluticasone propionate by a combination inhaler. International Journal of Pharmaceutics, 313, 14-22.

Thibert,R., Tawashi,R., 1999. Micronization of Pharmaceutical Solids. Microspheres, Microcapsules & Liposomes; Ed. Reza Arshady, Vo1: Preparation & Chemical Applications, 327.

Ticehurst,M.D., Rowe,R.C., York,P., 1994. Determination of the surface-properties of two batches of salbutamol sulfate by inverse gas-chromatography. International Journal of Pharmaceutics, 111, 241-249.

Tiddens,H.A.W.M., 2004. Inhaled antibiotics. Pediatric Pulmonology, 92-94.

Timsina,M.P., Martin,G.P., Marriott,C., Ganderton,D., Yianneskis,M., 1994. Drug-Delivery to the Respiratory-Tract Using Dry Powder Inhalers. International Journal of Pharmaceutics, 101, 1-13.

Tong,H.H.Y., Shekunov,B.Y., York,P., Chow,A.H.L., 2003. Thermal analysis of trace levels of polymorphic impurity in salmeterol xinafoate samples. Pharmaceutical Research, 20, 1423-1429.

Tsuda,A., Butler,J.P., Fredberg,J.J., 1994a. Effects of Alveolated Duct Structure on Aerosol Kinetics .1. Diffusional Deposition in the Absence of Gravity. Journal of Applied Physiology, 76, 2497-2509.

Tsuda,A., Butler,J.P., Fredberg,J.J., 1994b. Effects of Alveolated Duct Structure on Aerosol Kinetics .2. Gravitational Sedimentation and Inertial Impaction. Journal of Applied Physiology, 76, 2510-2516.

Usmani,O.S., Ito,K., Maneechotesuwan,K., Ito,M., Johnson,M., Barnes,P.J., Adcock,I.M., 2005. Glucocorticoid receptor nuclear translocation in airway cells after inhaled combination therapy. American Journal of Respiratory and Critical Care Medicine, 172, 704-712.

Valverde,J.M., Ramos,A., Castellanos,A., Watson,P.K., 1998. The tensile strength of cohesive powders and its relationship to consolidation, free volume and cohesivity. Powder Technology, 97, 237-245.

Vidgren,M.T., Karkkainen,A., Karjalainen,P., Paronen,T.P., 1987. A Novel Labeling Method for Measuring the Deposition of Drug Particles in the Respiratory-Tract. International Journal of Pharmaceutics, 37, 239-244.

Virchow,J.C., Crompton,G.K., Dal Negro,R., Pedersen,S., Magnan,A., Seidenbergf,J., Barnes,P.J., 2008. Importance of inhaler devices in the management of airway disease. Respiratory Medicine, 102, 10-19.

Visser,J., 1995. Particle adhesion and removal: a review. Particulate Science and Technology, 13, 169-196.

Vogel,L., Peukert,W., 2004. Determination of material properties relevant to grinding by practicable labscale milling tests. International Journal of Mineral Processing, 74, S329-S338.

Wallin,A., Sue-Chu,M., Bjermer,L., Ward,J., Sandstrom,T., Lindberg,A., Lundback,B., Djukanovic,R., Holgate,S., Wilson,S., 2003. Effect of inhaled fluticasone with and without salmeterol on airway inflammation in asthma. Journal of Allergy and Clinical Immunology, 112, 72-78.

Wendlandt,W.W., 1986. Thermal Analysis. 3rd Edition Ed., John Wiley & Sons, New York.

Westmeier,R., Steckel,H., 2008. Combination particles containing salmeterol xinafoate and fluticasone propionate: Formulation and aerodynamic assessment. Journal of Pharmaceutical Sciences, 97, 2299-2310.

World Health Organisation. Global surveillance, prevention and control of chronic respiratory diseases: a comprehensive approach. Bousquet, J. and Khalteev, N. WF 140, 1-155. 2007.

Yeomans,A.H., Rogers,E.E., Ball,W.H., 1949. Deposition of Aerosol Particles. Journal of Economic Entomology, 42, 591-596.

York,P., 1999. Strategies for particle design using supercritical fluid technologies. Pharmaceutical Science Technology Today, 2, 430-440.

Young,P.M., Price,R., Lewis,D., Edge,S., Traini,D., 2003a. Under pressure: predicting pressurized metered dose inhaler interactions using the atomic force microscope. Journal of Colloid and Interface Science, 262, 298-302.

Young,P.M., Price,R., Tobyn,M.J., Buttrum,M., Dey,F., 2003b. Effect of humidity on aerosolization of micronized drugs. Drug Development and Industrial Pharmacy, 29, 959-966.

Young,S.W., 1911. Mechanical stimulus to crystallization in supercooled liquids. Journal of the American Chemical Society, 33, 148-162.

Yu,L., 2001. Amorphous pharmaceutical solids: preparation, characterization and stabilization. Advanced Drug Delivery Reviews, 48, 27-42.

Zeng,X.M., Martin,G.P., Marriott,C., 2001. Particulate Interaction in Dry Powder Formulations for Inhalation. Taylor & Francis, London.

Zetterstrom,O., Buhl,R., Mellem,H., Perpina,M., Hedman,J., O'Neill,S., Ekstrom,T., 2001. Improved asthma control with budesonide/formoterol in a single inhaler, compared with budesonide alone. European Respiratory Journal, 18, 262-268.